

## PUBLISHER :



### Address of Publisher & Editor's Office :

GDAŃSK UNIVERSITY  
OF TECHNOLOGY  
Faculty  
of Ocean Engineering  
& Ship Technology

ul. Narutowicza 11/12  
80-952 Gdańsk, POLAND  
tel.: +48 58 347 13 66  
fax : +48 58 341 13 66  
e-mail : office.pmr@pg.gda.pl

Account number :  
**BANK ZACHODNI WBK S.A.**  
I Oddział w Gdańsku  
41 1090 1098 0000 0000 0901 5569

### Editorial Staff :

**Kazimierz Kempa** Editor in Chief  
e-mail : kkempa@pg.gda.pl

**Przemysław Wierzychowski** Scientific Editor  
e-mail : e.wierzychowski@chello.pl

**Jan Michalski** Editor for review matters  
e-mail : janmi@pg.gda.pl

**Tadeusz Borzęcki** Editor for international relations  
e-mail : tador@pg.gda.pl

**Piotr Bzura** Managing Editor  
e-mail : pbzura@pg.gda.pl

**Cezary Spigarski** Computer Design  
e-mail : biuro@oficynamorska.pl

Domestic price :  
single issue : 20 zł

Prices for abroad :  
single issue :  
- in Europe EURO 15  
- overseas US\$ 20

ISSN 1233-2585



## POLISH MARITIME RESEARCH

*in internet*

[www.bg.pg.gda.pl/pmr/pmr.php](http://www.bg.pg.gda.pl/pmr/pmr.php)



## POLISH MARITIME RESEARCH

No 2(56) 2008 Vol 15

## CONTENTS

- 3 **TOMASZ CEPOWSKI**  
*Determination of optimum hull form  
for passenger car ferry with regard to its sea-keeping  
qualities and additional resistance in waves*
- 12 **HENRYK JARZYNA**  
*How to divide the global resistance change  
into the components related to the pushing propeller  
and the pulling propeller of the double-ended ship*
- 15 **TOMASZ ABRAMOWSKI**  
*Application of artificial neural networks to assessment  
of ship manoeuvrability qualities*
- 22 **JANUSZ KOLENDA**  
*Modification of Hooke's law  
for multiaxial stress in viscoelastic solids*
- 26 **KAROL NIKLAS**  
*Search for optimum geometry of selected  
steel sandwich panel joints*
- 32 **M. BEHZAD, A. EBRAHIMI, A. MEGHDARI**  
*A new continuous model for flexural vibration  
analysis of a cracked beam*
- 40 **LESŁAW KYZIOŁ**  
*Determining strength of the modified wood*
- 46 **ZBIGNIEW KORCZEWSKI**  
*Contemporary diagnostic methods for ship engines:  
a report on scientific research activity  
of Polish Naval Academy in this field*
- 59 **STANISŁAW POLANOWSKI**  
*Determination of location of Top Dead Centre  
and compression ratio value on the basis  
of ship engine indicator diagram*
- 65 **JERZY GIRTLEK**  
*A probabilistic concept of load assessment  
of self-ignition engines*
- 71 **ANDRZEJ MIELEWCZYK**  
*A discrete model of the plate heat exchanger*
- 77 **MIROŚLAW WOŁOSZYN**  
*Detection of ferromagnetic objects  
in local magnetic anomaly of the Baltic Sea*

The papers published in this issue have been reviewed by:  
Assoc. Prof. M. Czech ; Prof. J. Girtler ; Prof. F. Grabski  
Prof. K. Jakubiuk ; Prof. T. Koronowicz ;  
Assoc. Prof. J. Kozak ; Prof. T. Szelangiewicz  
Prof. K. Wierzychowski

# Editorial

---

POLISH MARITIME RESEARCH is a scientific journal of worldwide circulation. The journal appears as a quarterly four times a year. The first issue of it was published in September 1994. Its main aim is to present original, innovative scientific ideas and Research & Development achievements in the field of :

## **Engineering, Computing & Technology, Mechanical Engineering,**

which could find applications in the broad domain of maritime economy. Hence there are published papers which concern methods of the designing, manufacturing and operating processes of such technical objects and devices as : ships, port equipment, ocean engineering units, underwater vehicles and equipment as well as harbour facilities, with accounting for marine environment protection.

The Editors of POLISH MARITIME RESEARCH make also efforts to present problems dealing with education of engineers and scientific and teaching personnel. As a rule, the basic papers are supplemented by information on conferences , important scientific events as well as cooperation in carrying out international scientific research projects.

## Scientific Board

---

Chairman : Prof. **JERZY GIRTLEK** - Gdańsk University of Technology, Poland

Vice-chairman : Prof. **ANTONI JANKOWSKI** - Institute of Aeronautics, Poland

Vice-chairman : Prof. **MIROSLAW L. WYSZYŃSKI** - University of Birmingham, United Kingdom

---

Dr **POUL ANDERSEN**  
Technical University  
of Denmark  
Denmark

Prof. **STANISŁAW GUCMA**  
Maritime University of Szczecin  
Poland

Prof. **YASUHIKO OHTA**  
Nagoya Institute of Technology  
Japan

Dr **MEHMET ATILAR**  
University of Newcastle  
United Kingdom

Prof. **ANTONI ISKRA**  
Poznań University  
of Technology  
Poland

**Prof. ANTONI K. OPPENHEIM**  
University of California  
Berkeley, CA  
USA

Prof. **GÖRAN BARK**  
Chalmers University  
of Technology  
Sweden

Prof. **JAN KICIŃSKI**  
Institute of Fluid-Flow Machinery  
of PAFci  
Poland

Prof. **KRZYSZTOF ROSOCHOWICZ**  
Gdańsk University  
of Technology  
Poland

Prof. **SERGEY BARSUKOV**  
Army Institute of Odessa  
Ukraine

Prof. **ZYGMUNT KITOWSKI**  
Naval University  
Poland

Dr **YOSHIO SATO**  
National Traffic Safety  
and Environment Laboratory  
Japan

Prof. **MUSTAFA BAYHAN**  
Süleyman Demirel University  
Turkey

Prof. **JAN KULCZYK**  
Wrocław University of Technology  
Poland

Prof. **KLAUS SCHIER**  
University of Applied Sciences  
Germany

Prof. **MAREK DZIDA**  
Gdańsk University  
of Technology  
Poland

Prof. **NICOS LADOMMATOS**  
University College London  
United Kingdom

Prof. **FREDERICK STERN**  
University of Iowa,  
IA, USA

Prof. **ODD M. FALTINSEN**  
Norwegian University  
of Science and Technology  
Norway

Prof. **JÓZEF LISOWSKI**  
Gdynia Maritime University  
Poland

Prof. **JÓZEF SZALA**  
Bydgoszcz University  
of Technology and Agriculture  
Poland

Prof. **PATRICK V. FARRELL**  
University of Wisconsin  
Madison, WI  
USA

Prof. **JERZY MATUSIAK**  
Helsinki University  
of Technology  
Finland

Prof. **TADEUSZ SZELANGIEWICZ**  
Technical University  
of Szczecin  
Poland

Prof. **WOLFGANG FRICKE**  
Technical University  
Hamburg-Harburg  
Germany

Prof. **EUGEN NEGRUS**  
University of Bucharest  
Romania

Prof. **WITALIJ SZCZAGIN**  
State Technical University  
of Kaliningrad  
Russia

Prof. **BORIS TIKHOMIROV**  
State Marine University  
of St. Petersburg  
Russia

Prof. **DRACOS VASSALOS**  
University of Glasgow  
and Strathclyde  
United Kingdom

# Determination of optimum hull form for passenger car ferry with regard to its sea-keeping qualities and additional resistance in waves

Tomasz Cepowski, Ph. D.  
Szczecin Maritime University

## ABSTRACT



*This paper presents a method which makes it possible to determine optimum hull form of passenger car ferry with regard to selected sea-keeping qualities and additional resistance in waves. In the first phase of investigations a hull form characterized by the highest qualities was selected from the list of similar ships. Next, its optimum dimension ratios were determined. Design criteria were formulated by using a method based on deterministic scenarios, but objective functions of partial targets were determined in the form of artificial neural networks. To select the best design variants elements of fuzzy logic were used, that made it possible a.o. to show merits of the design by means of linguistic variables. Such approach made it possible to find the best hull form and its dimensions from the point of view of all considered criteria simultaneously.*

**Keywords:** sea-keeping qualities, roll-on-roll-off ferry ship, rolling, transverse accelerations, vertical accelerations, motion sickness index, additional resistance in waves, ship hull form, ship design parameters, artificial neural networks, fuzzy logic.

## INTRODUCTION

In the ship design process design solutions complying both with economic criteria and technical constraints, are searched for. The economic criteria contain a set of ship owner's requirements to which can belong a.o. ship service speed of a significant impact on ship operation profitability on a given shipping route. As the ship is often operated in heavy weather conditions the reaching of its assumed service speed depends a.o. on its additional resistance in waves. And, for certain types of ships, e.g. passenger car ferries, their non-susceptibility to weather conditions, i.e. the so called good sea-keeping qualities, constitutes a more - and- more important technical limitation. The additional ship resistance in waves and good sea-keeping qualities are strongly dependent on ship's hull form and dimensions. Therefore modeling the ship qualities should be performed already in the preliminary ship design stage. Selection of a non-suitable hull form and dimensions of a ship irreversibly worsens its design merits and any change of dimensions of a built ship is economically unprofitable. In [1, 3] a method which makes it possible to take into account the ship sea-keeping qualities and additional ship resistance in waves in the phase of parametric design, is presented. As a result of the research, optimum values of ship dimensions and certain global coefficients characterizing hull form of a ro-ro ferry ship were determined. However the aim of the research presented in this paper was to model a geometrically described hull form and to determine an optimum hull form with regard

to its sea-keeping qualities and additional resistance in waves. The obtained results are presented with the use of an example design task.

## DESIGN TASK

In the research the following design tasks were formulated: to find such hull form of the ro-ro ferry, which minimizes values of the design criteria at fulfilled assumed constraints for the passenger car ferry sailing in heavy weather conditions.

In the design task the following were assumed:

❖ ship design parameters describing its hull form, considered independent variables:

- ◆ L/B
- ◆ B/d
- ◆ CB
- ◆ CWL

where: L, B, d – ship length, breadth and draught, respectively, CB – block coefficient of underwater part of hull, CWL – waterplane coefficient;

❖ constraints:

- ◆ theoretical displacement  $V = 13723 \text{ m}^3$
- ◆ range of L/B : from 5.17 to 6.74
- ◆ range of B/d : from 3.22 to 4.46
- ◆ range of CB : from 0.6 to 0.64
- ◆ range of CWL : from 0.8 to 0.85
- ◆ the initial transverse metacentric height  $GM = 1 \text{ m}$

## METHOD

To solve the problem was elaborated a method consisted of the two phases:

1. On the basis of the list of similar ships - determination of alternative design variants and selection of the best one (Fig. 1)

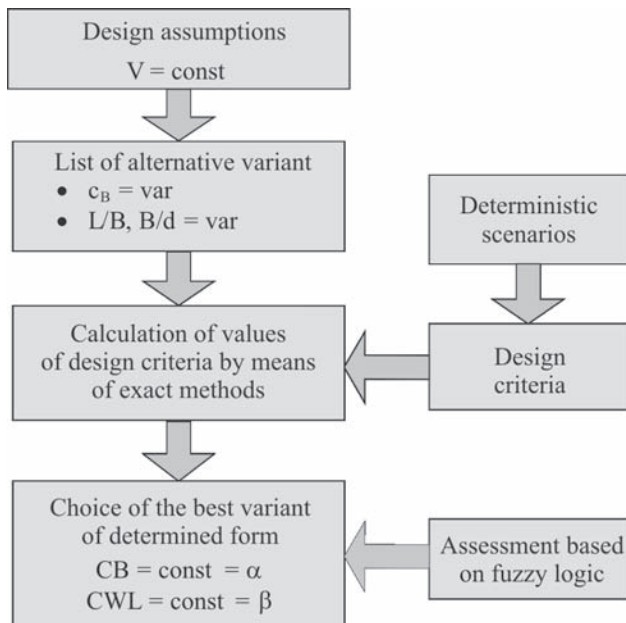


Fig. 1. Algorithm showing the 1<sup>st</sup> phase of the research

2. On the basis of the best hull form variant selected in the 1<sup>st</sup> phase – selection of the optimum ratios of ferry ship dimensions (Fig. 2).

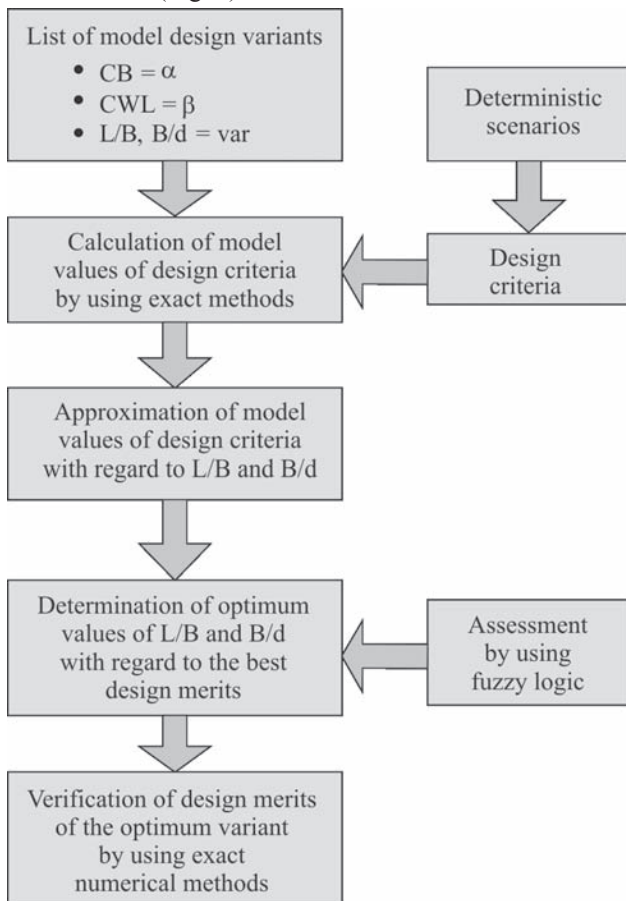


Fig. 2. Algorithm showing the 2<sup>nd</sup> phase of the research

The assessment process of design variants carried out in both research phases was based on the below given design criteria.

## DESIGN CRITERIA

One of the crucial design problems of ro-ro ferries is to ensure appropriate damage stability. The ship stability criteria being in force are rather far from taking into account the complex physical phenomena associated with ship hydromechanics, and they are based first of all on physical parameters calculated for a ship in still water conditions. Hence the application of design criteria inadequate to the conditions in which the ship operates does not ensure a sufficient level of safety. The IMO has initiated efforts aimed at undertaking a research on elaboration of new standards for ship stability assessment. One of the ways to solve the problem is elaboration of methods for investigating the intensity of ship rolling motion (e.g. [12]) or probability of ship capsizing (e.g. [10]). In the case of ro-ro ferry ships such investigations are aimed at elaboration and improvement of simulation models of sinking process of damaged ferry in given conditions (acc. [8]). The example models are presented in [13, 15]. The above referred research makes it possible to simulate ferry sinking process however any design criteria have not yet evolved from that.

The design criteria assumed in this research are to an extent associated with the above mentioned recommendations, as they are based on statistical values of ship response in waves. For their formulation a method based on deterministic scenarios [16], was used, hence the following scenarios were assumed:

**Scenario no. 1:** the design ferry sails with the speed  $v = 15$  kn in the statistical heavy weather conditions (the significant wave height of 3 m, the characteristic wave period in the range from 3s to 18 s.), the ship encounters the wave from the most unfavourable directions.

**Scenario no. 2:** the designed ferry is in the following damage state : its side plating amidships has been broken at the level of car deck, the disabled ship is in the statistical heavy weather conditions (the significant wave height of 3 m, the characteristic wave period in the range from 3s to 18 s.), the ship heads the wave at the encounter angle  $\beta = 120^\circ$  (where:  $180^\circ$  – head wave,  $0^\circ$  – following wave).

Such approach made it possible to formulate the following design criteria:

For Scenario no. 1:

1. As-small-as-possible value of the motion sickness index MSI (acc. ISO 2631/3), [9] for the wave encounter angle  $\beta = 120^\circ$
2. As-small-as-possible value of the additional ship resistance in waves R, for  $\beta = 180^\circ$
3. As-small-as-possible significant value of the roll angle  $\varphi$ , for  $\beta = 30^\circ$
4. As-small-as-possible value of the transverse accelerations at the car deck,  $a_t$ , acc. [16], in the point P2 in Fig. 3, for  $\beta = 30^\circ$
5. As-small-as-possible value of the vertical accelerations at the car deck,  $a_v$ , acc. [16], in the point P2 in Fig. 3.

For Scenario no. 2:

6. As-low-as-possible number of events of flooding the car deck in the place of broken side plating,  $L_{GW}$ , for the wave encounter angle  $\beta = 120^\circ$ , in the point P1 in Fig. 3.

Fulfilment of the criteria no. 1, 3, 5 ensures an appropriate voyage comfort for passengers, moreover the criterion no. 3

ensures safety of ship stability, resulting from a lower intensity of ship rolling motions. Fulfilment of the criterion no. 4 leads to a lower hazard due to possible shift of vehicles on the car deck. Fulfilment of the criterion no. 6 can lower a number of flooding events of the car deck due to broken side plating, and thus decrease mass of the water flooded on the deck, that can make sinking time of the ship longer. And, fulfilment of the criterion no. 2 can lower a decrease of ship speed in waves, and thus operational costs due to lower fuel consumption.

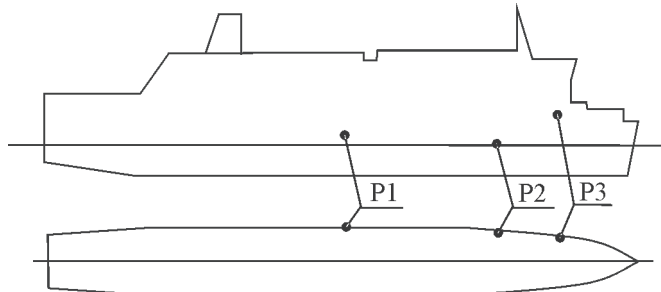


**Fig. 3.** The coordinates of the points P1, P2, P3 for which the following quantities were calculated: number of car deck flooding events – in the point P1 ( $0.5L, 0.49B, d+1m$ ), transverse accelerations – in the point P2 ( $0.75L, 0.45B, d$ ), vertical accelerations – in the point P3 ( $0.8L, 0.32B, 2d$ ), where:  $L$  – ship length,  $B$  – ship breadth,  $d$  – ship draught

### THE 1<sup>st</sup> PHASE OF THE RESEARCH

The 1<sup>st</sup> phase of the research was aimed at the finding - on the basis of the list of alternative variants – a hull form of the best merits. In the investigations were used eight ro-ro ferries whose dimensions and hull forms are presented in Tab. 1 and Fig. 4.

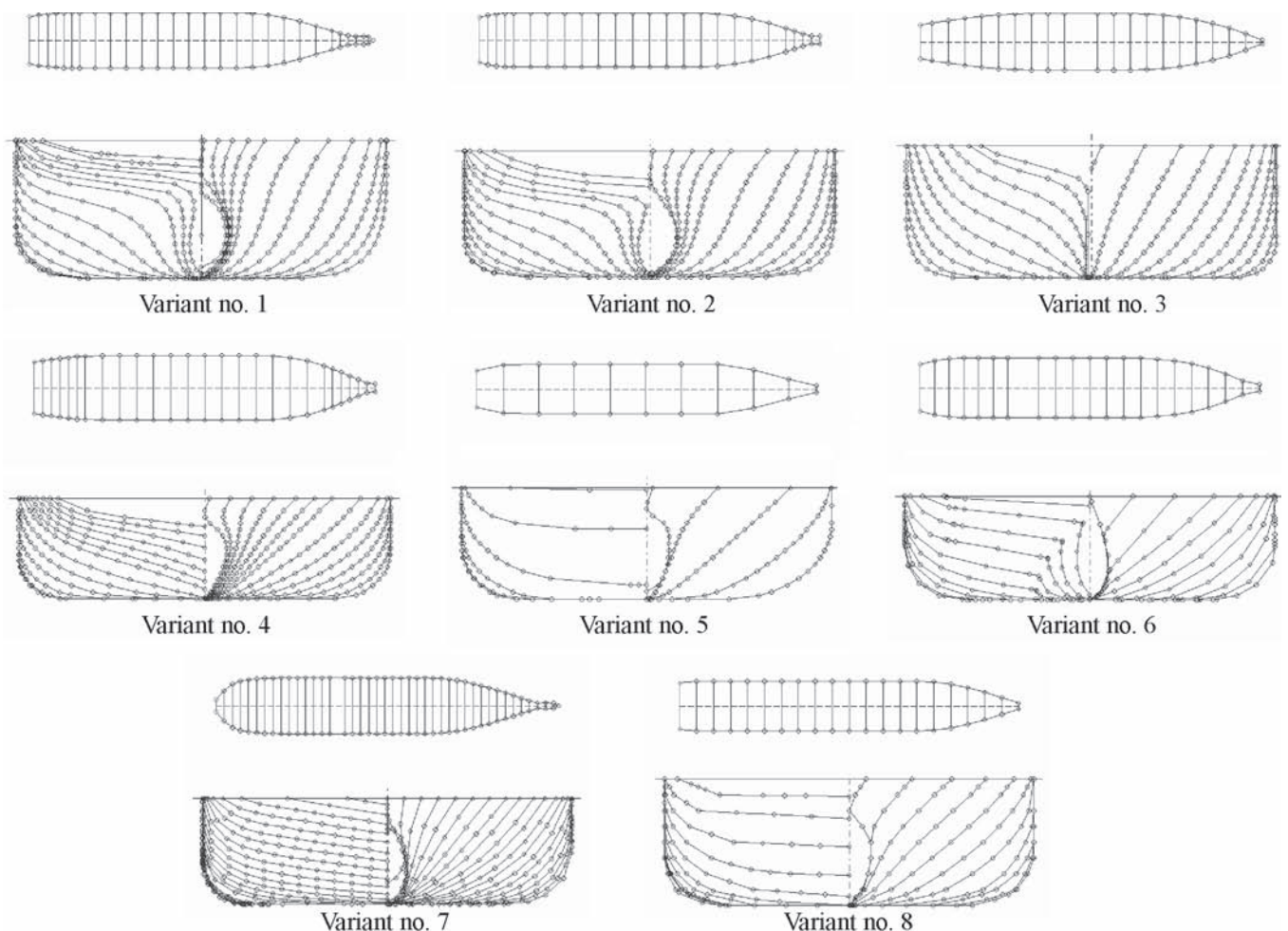


**Fig. 4.** Hull forms of alternative design variants of ro-ro ferry,  $V = 13723 \text{ m}^3$ ,  $CB, L/B, B/d = \text{var}$

**Tab. 1.** List of alternative design variants,  $V = 13723 \text{ m}^3$ ,  $CB, L/B, B/d = \text{var}$

Design variants	CB	CWL	L/B	B/d
Variant no. 1	0.599	0.809	5.68	3.22
Variant no. 2	0.644	0.828	6.17	3.58
Variant no. 3	0.637	0.811	5.71	3.40
Variant no. 4	0.616	0.828	5.17	4.46
Variant no. 5	0.620	0.831	6.74	3.90
Variant no. 6	0.634	0.852	5.57	3.77
Variant no. 7	0.626	0.850	5.64	3.5
Variant no. 8	0.610	0.804	6.74	4.04

For each of the design variants given in Tab. 1 statistical values of the assumed design criteria were calculated. The conventional ITTC wave spectrum was assumed. The calculations were carried out by means of the exact numerical methods included in the SEAWAY software based on the theory of two-dimensional flow. For calculation of hydrodynamic coefficients the Frank's method was applied [5]. The accuracy tests of the SEAWAY's software, presented in [9], have shown that its calculation accuracy is high. For calculations of the additional ship resistance in waves the Gerritsma-Beukelman method was used [6].

To the investigations were applied such values of the design criteria which reached their maxima in the assumed statistical wave conditions (i.e. the significant wave height equal to 3 m, the characteristic wave period within the range from 3s to 18 s.). It enabled to eliminate influence of the wave parameters on ship responses and to lower the number of independent variables in the design task in question. The results of calculations are presented in Tab. 2.

**Tab. 2.** Values of the design criteria used in the 1<sup>st</sup> phase of the research, where: MSI – motion sickness index,  $a_t$  – transverse acceleration at the car deck,  $a_v$  – vertical accelerations,  $\varphi$  – significant amplitude of ship rolling, R – additional ship resistance in waves,  $L_{GW}$  – hourly number of car deck flooding events in the place of broken side plating

Design variants	MSI [%]	$\varphi$ [°]	$a_v$ [m/s <sup>2</sup> ]	$a_t$ [m/s <sup>2</sup> ]	R [kN]	$L_{GW}$ [1/h]
Variant no. 1	49.1	7.79	2.14	1.33	195.8	267.5
Variant no. 2	37.8	6.50	2.02	1.11	165.1	285.4
Variant no. 3	35.9	2.16	2.00	0.60	163.6	271.9
Variant no. 4	16.6	4.32	1.77	0.73	187.9	285.1
Variant no. 5	24.4	7.70	1.87	1.31	178.2	283.4
Variant no. 6	20.9	9.13	1.83	1.56	176.6	285.5
Variant no. 7	30.4	8.00	1.94	1.36	174.0	289.9
Variant no. 8	17.7	6.08	1.78	1.04	148.3	278.9

In the further part of the research the best design variant was selected with the use of a method based on fuzzy logic elements.

### APPLICATION OF FUZZY LOGIC ELEMENTS TO SELECTION OF THE BEST DESIGN SOLUTION

Fuzzy logic finds its application wherever the use of classic logic creates a problem consisted in difficulty of mathematical description of a process or when to calculate or select variables for solving a problem is not possible. In the design problem in question fuzzy logic was used as an element which aids to assess quality of a design variant (of low, mean or high merits) and to decide on choice of the best design (of the best merits).

In the 1<sup>st</sup> research phase the set of solutions given in Tab. 2 was fuzzyfied with the use of the attribution function described by the Eq. (1):

$$\mu(x_i) = \begin{cases} 1 & \text{for } x_i \geq \alpha_{2(i)} \\ 0 & \text{for } x_i \leq \alpha_{1(i)} \\ \frac{x_i - \alpha_{1(i)}}{\alpha_{2(i)} - \alpha_{1(i)}} & \text{for } \alpha_{1(i)} < x_i < \alpha_{2(i)} \end{cases} \quad (1)$$

where:

$\mu(x_i)$  – value of attribution function for i-th design criterion (i = MSI,  $\varphi$ ,  $a_v$ ,  $a_t$ , R,  $L_{GW}$ )

$x_i$  – value of i-th design criterion (from Tab. 2)

$\alpha_{1(i)}$ ,  $\alpha_{2(i)}$  – threshold values acc. Tab. 3.

The graphical form of the function (1) as well as its linguistic interpretation is presented in Fig. 5; and, values of the coefficients  $\alpha_{1(i)}$ ,  $\alpha_{2(i)}$  are given in Tab. 3.

**Tab. 3.** Values of the coefficients  $\alpha_{1(i)}$  and  $\alpha_{2(i)}$  for the design criteria: MSI – motion sickness index,  $a_t$  – transverse acceleration at the car deck,  $a_v$  – vertical accelerations,  $\varphi$  – significant amplitude of ship rolling, R – additional ship resistance in waves,  $L_{GW}$  – hourly number of car deck flooding events in the sector of broken side plating

	MSI [%]	$\varphi$ [°]	$a_v$ [m/s <sup>2</sup> ]	$a_t$ [m/s <sup>2</sup> ]	R [kN]	$L_{GW}$ [1/h]
$\alpha_{1(i)}$	27.43	4.48	1.89	0.92	164.13	274.97
$\alpha_{2(i)}$	38.27	6.81	2.02	1.24	179.97	282.43

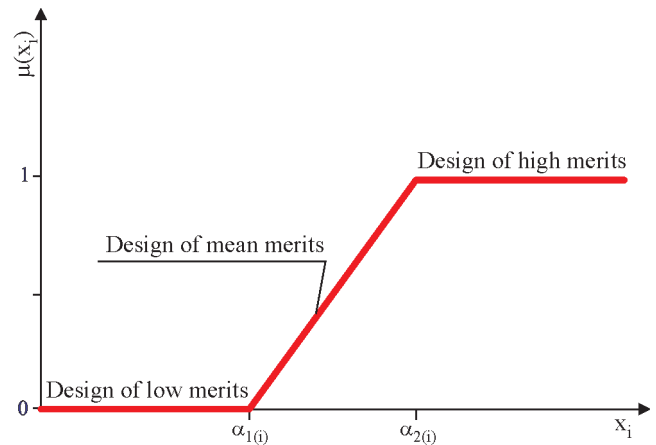


**Fig. 5.** Attribution function acc. Eq. (1)

Next, assessment of the design solutions fuzzyfied with the use of Eq. (1) was performed. To assess design quality the minimizing operator MIN was applied in accordance with Eq. (2):

$$\text{MIN} = \text{MIN}(\mu(\text{MSI}), \mu(\text{R}), \mu(\varphi), \mu(a_t), \mu(a_v), \mu(L_{GW})) \quad (2)$$

where:

MIN – minimizing operator

$\mu(\text{MSI}), \mu(\text{R}), \mu(\varphi), \mu(a_t), \mu(a_v), \mu(L_{GW})$  – attribution function of the design criteria: MSI – motion sickness index,  $a_t$  – transverse acceleration at the car deck,  $a_v$  – vertical accelerations,  $\varphi$  – significant amplitude of ship rolling, R – additional ship resistance in waves,  $L_{GW}$  – hourly number of car deck flooding events in the place of broken side plating, respectively.

The values of the MIN operator as well as attribution function of the design criteria are given in Tab. 4 and Fig. 6.

**Tab. 4.** The values of the MIN operator as well as attribution function of the design criteria: MSI – motion sickness index,  $a_t$  – transverse acceleration at the car deck,  $a_v$  – vertical accelerations,  $\varphi$  – significant amplitude of ship rolling, R – additional ship resistance in waves,  $L_{GW}$  – hourly number of car deck flooding events in the place of broken side plating

Variants	$\mu(\text{MSI})$	$\mu(\varphi)$	$\mu(a_v)$	$\mu(a_t)$	$\mu(\text{R})$	$\mu(L_{GW})$	MIN
Variant no. 1	0.000	0.000	0.000	0.000	0.000	1.000	0.000
Variant no. 2	0.043	0.132	0.000	0.406	0.939	0.000	0.000
Variant no. 3	0.218	1.000	0.135	1.000	1.000	1.000	0.135
Variant no. 4	1.000	1.000	1.000	1.000	0.000	0.000	0.000
Variant no. 5	1.000	0.000	1.000	0.000	0.112	0.000	0.000
Variant no. 6	1.000	0.000	1.000	0.000	0.213	0.000	0.000
Variant no. 7	0.726	0.000	0.622	0.000	0.377	0.000	0.000
Variant no. 8	1.000	0.313	1.000	0.625	1.000	0.473	0.313

From Tab. 4 and Fig. 6 it results that variant no. 8 is of the best merits.

**Fig. 6.** Values of the MIN operator and attribution functions of the design variants

## THE 2<sup>nd</sup> PHASE OF THE RESEARCH

The 2<sup>nd</sup> phase was aimed at determination of optimum design parameters of the ro-ro ferry under the following assumptions:

- $L/B = \text{var}$
- $B/d = \text{var}$

at the determined hull form complying with Variant no. 8, i.e.:

- $CB = 0.64$
- $CWL = 0.801$

as well as the earlier accepted design assumptions.

In the 1<sup>st</sup> step a model set of design variants was elaborated and values of the design criteria were calculated. The same assumptions, calculation method and design criteria as in the 1<sup>st</sup> phase, were used. The calculation results are presented in Tab. 5.

Next, approximations of values of the dependent variables were elaborated depending on the independent variables. The

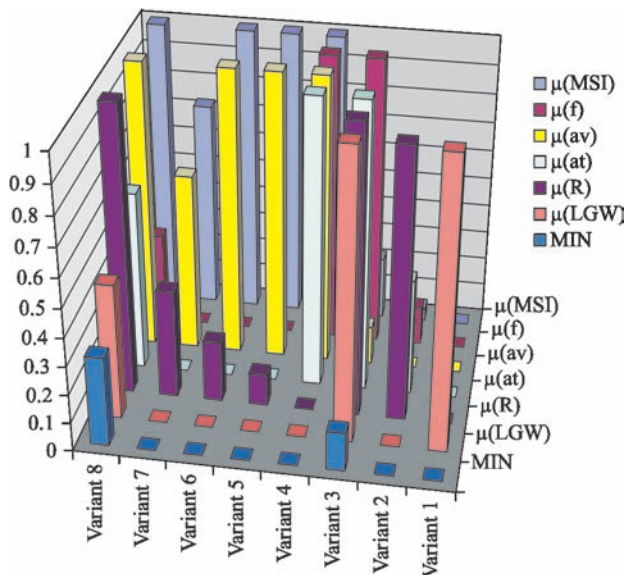


Fig. 6. Values of the MIN operator and attribution functions of the design variants

Tab. 5. The model set of independent variables and dependent ones assumed in the design task of  $CB = 0,64$ ,  $CWL = 0,801$ , where:  $L$  – ship length,  $B$  – ship breadth,  $d$  – ship draught,  $MSI$  – motion sickness index,  $a_v$  – transverse acceleration at the car deck,  $a_v$  – vertical accelerations,  $\varphi$  – significant amplitude of ship rolling,  $R$  – additional ship resistance in waves,  $L_{GW}$  – hourly number of car deck flooding events in the place of broken side plating

Variants	Independent variables		Dependent variables					
	$L/B$ [-]	$B/d$ [-]	$MSI$ [%]	$\varphi$ [°]	$a_v$ [ $m/s^2$ ]	$a_v$ [ $m/s^2$ ]	$R$ [kN]	$L_{GW}$ [1/h]
Variant no.1	6.75	3.60	8.6	8.37	1.65	1.43	215.0	243.1
Variant no.2	4.11	3.53	24.6	12.06	1.88	2.06	224.9	264.2
Variant no.3	4.99	3.53	35.3	10.02	1.99	1.72	207.6	280.4
Variant no.4	5.87	3.53	35.9	7.13	2.00	1.22	176.7	285.5
Variant no.5	6.75	3.53	29.0	5.66	1.92	0.97	147.1	278.9
Variant no.6	3.23	3.22	8.2	8.20	1.64	1.41	206.0	236.9
Variant no.7	4.11	3.22	26.2	10.34	1.90	1.77	223.1	256.7
Variant no.8	4.99	3.22	40.6	9.88	2.05	1.70	212.9	275.0
Variant no.9	5.87	3.22	43.7	7.11	2.08	1.22	183.0	285.2
Variant no.10	6.75	3.22	38.4	5.52	2.02	0.95	150.7	282.4
Variant no.11	3.23	3.84	8.7	9.13	1.65	1.56	220.8	247.4
Variant no.12	4.11	3.84	100.0	12.87	13.70	2.20	225.9	269.2
Variant no.13	4.99	3.84	30.0	9.84	1.94	1.69	203.1	282.9
Variant no.14	5.87	3.84	28.8	7.11	1.92	1.22	171.9	284.0
Variant no.15	6.75	3.84	21.2	5.82	1.83	1.00	150.7	278.7
Variant no.16	3.23	4.15	8.5	10.59	1.64	1.80	226.8	250.3
Variant no.17	4.11	4.15	20.4	13.68	1.82	2.34	226.2	271.8
Variant no.18	4.99	4.15	25.3	9.57	1.88	1.63	200.1	282.6
Variant no.19	5.87	4.15	22.8	7.15	1.85	1.22	170.6	281.1
Variant no.20	6.75	4.15	15.8	6.23	1.75	1.07	149.3	279.2
Variant no.21	3.23	4.46	8.0	12.16	1.63	2.07	230.6	252.7
Variant no.22	4.11	4.46	17.9	14.14	1.79	2.41	225.4	274.6
Variant no.23	4.99	4.46	21.3	9.47	1.83	1.61	199.8	282.4
Variant no.24	5.87	4.46	17.8	7.24	1.78	1.23	171.4	277.9
Variant no.25	6.75	4.46	11.3	6.63	1.68	1.13	153.9	278.2

approximations were obtained by means of the artificial neural networks of MLP type (Multi Layer Perceptron) and presented with the use of Eqs. (3), (4), (5), (6), (7) and (8):

$$MSI = \frac{\left( \frac{1}{1 + e^{-(L/B, B/d) \times S + P} \times A - B} \right) \times C - \alpha_0}{\alpha_2} - \alpha_1 \quad (3)$$

where:

MSI – motion sickness index [%]; L – ship length; B – ship breadth; d – ship draught;

A – matrix of weighing factors:

$$\begin{bmatrix} -0.311 & 0.921 & -0.694 & 5.134 & 2.302 & -1.432 & -3.048 & -3.136 & 0.695 & 0.098 & -0.090 \\ 0.957 & 2.041 & 0.917 & 2.913 & 1.206 & -0.194 & -0.191 & -1.058 & 0.459 & -0.254 & 0.123 \end{bmatrix}$$

S – matrix of coefficients:

$$\begin{bmatrix} 0.284 & 0 \\ 0 & 0.806 \end{bmatrix}$$

B – vector of threshold values:

$$[-0.271 \quad -1.606 \quad -0.124 \quad -1.718 \quad -0.701 \quad 0.526 \quad 0.322 \quad -3.638 \quad -0.342 \quad -0.260 \quad -0.704]$$

C – column vector of weighing factors:

$$[-0.955 \quad -1.137 \quad -0.771 \quad 2.374 \quad 0.855 \quad -1.171 \quad -1.886 \quad 1.953 \quad 0.008 \quad -0.537 \quad -0.535]$$

P – vector of translation values: [-0.918 -2.597]

$\alpha_0, \alpha_1, \alpha_2$  – coefficients of the values:  $\alpha_0 = 0.8, \alpha_1 = -0.245, \alpha_2 = 0.031$

$$R = \frac{\left( \frac{1}{1 + e^{-(L/B, B/d) \times S + P} \times A - B} \right) \times C - \alpha_0}{\alpha_2} - \alpha_1 \quad (4)$$

where:

R – additional ship resistance in waves, [kN]

A – matrix of values of weighing factors:

$$\begin{bmatrix} -0.533 & -2.682 & 4.015 & 0.886 & -3.133 \\ 0.065 & -0.252 & 1.285 & 1.316 & -0.798 \end{bmatrix}$$

B – vector of threshold values: [-0.466 0.249 2.501 1.186 -2.844]

C – column vector of values of weighing factors: [-0.350 -2.402 -1.706 1.705 1.517]

$\alpha_0, \alpha_1, \alpha_2$  – coefficient of the values:  $\alpha_0 = -0.32, \alpha_1 = -1.846, \alpha_2 = 0.013$

$$\varphi = \frac{\left( \frac{1}{1 + e^{-(L/B, B/d) \times S + P} \times A - B} \right) \times C - \alpha_0}{\alpha_2} - \alpha_1 \quad (5)$$

where:

$\varphi$  – significant roll amplitude [°]

A – matrix of values of weighing factors:

$$\begin{bmatrix} 3.869 & 5.902 \\ 0.798 & 0.478 \end{bmatrix}$$

B – vector of threshold values: [0.530 2.873]

C – column vector of values of weighing factors: [3.143 -2.295]

$\alpha_0, \alpha_1, \alpha_2$  – coefficients of the values:  $\alpha_0 = 0.798, \alpha_1 = -0.677, \alpha_2 = 0.123$

$$a_v = \frac{\left( \frac{1}{1 + e^{-(L/B, B/d) \times S + P} \times A - B} \right) \times C - \alpha_0}{\alpha_2} - \alpha_1 \quad (6)$$

where:

$a_v$  – vertical accelerations [m/s<sup>2</sup>],

A – matrix of values of weighing factors:

$$\begin{bmatrix} 1.76 & 0.38 & 2.19 & 0.58 & -0.92 & 0.89 & 0.19 & 0.50 & -0.21 & -0.14 & 0.70 & 0.88 & 0.11 & 0.47 & 3.88 & -1.57 \\ 0.12 & -0.40 & 0.12 & 1.02 & 0.25 & -0.84 & 0.98 & -0.29 & -1.12 & -0.14 & 0.95 & -0.30 & 0.48 & -0.11 & 1.18 & -0.32 \end{bmatrix}$$

B – vector of threshold values:

$$[-0.85 \ -0.71 \ -0.62 \ 0.15 \ 0.86 \ -0.27 \ -0.61 \ -0.89 \ 0.34 \ 0.05 \ 0.60 \ 0.17 \ 0.39 \ -0.32 \ 0.60 \ -1.51]$$

C – column vector of values of weighing factors:

$$[0.78 \ -0.48 \ 1.02 \ -0.46 \ -0.77 \ -0.61 \ -1.54 \ -0.41 \ 0.79 \ 0.08 \ -1.62 \ -0.73 \ -0.46 \ -0.51 \ 2.74 \ 1.75]$$

$\alpha_0, \alpha_1, \alpha_2$  – coefficients of the values:  $\alpha_0 = 0.157, \alpha_1 = -3.727, \alpha_2 = 2.272$

$$a_t = \frac{\left( \frac{1}{1 + e^{-((L/B, B/d) \times S + P) \times A - B}} \times C - \alpha_0 \right) - \alpha_1}{\alpha_2} \quad (7)$$

where:

$a_t$  – transverse accelerations at the car deck, [m/s<sup>2</sup>]

A – matrix of values of weighing factors:

$$\begin{bmatrix} 3.862 & -6.941 \\ 1.672 & -1.839 \end{bmatrix}$$

B – vector of threshold values: [ 2.487 -4.718 ]

C – column vector of values of weighing factors: [ 2.662 2.562 ]

$\alpha_0, \alpha_1, \alpha_2$  – coefficients of the values :  $\alpha_0 = 2.449, \alpha_1 = -0.674, \alpha_2 = 0.694$

$$L_{GW} = \frac{\left( \frac{1}{1 + e^{-((L/B, B/d) \times S + P) \times A - B}} \times C - \alpha_0 \right) - \alpha_1}{\alpha_2} \quad (8)$$

where:

$a_v$  – vertical accelerations, [m/s<sup>2</sup>]

A – matrix of values of weighing factors:

$$\begin{bmatrix} 0.108 & -0.507 & -0.278 & -0.658 & 2.414 & -3.652 & -1.223 & 1.756 & 0.941 & -0.748 & -0.307 & 1.202 & 0.724 & 0.666 \\ 0.363 & 0.154 & 0.064 & 0.538 & 0.079 & -0.409 & -0.370 & 0.887 & -0.521 & -0.856 & 0.533 & 0.346 & -0.174 & 0.424 \end{bmatrix}$$

B – vector of threshold values:

$$[-1.007 \ 0.932 \ 0.823 \ 0.421 \ -1.062 \ -0.243 \ 0.616 \ -0.895 \ 0.089 \ -0.700 \ -0.185 \ 0.486 \ -0.241 \ -0.286]$$

C – column vector of values of weighing factors:

$$[-0.781 \ 0.436 \ 0.698 \ 0.581 \ 1.399 \ -2.512 \ -0.344 \ 1.135 \ -0.733 \ 0.997 \ 0.285 \ -1.148 \ -0.661 \ -0.698]$$

$\alpha_0, \alpha_1, \alpha_2$  – coefficients of the values:  $\alpha_0 = -0.446, \alpha_1 = -4.874, \alpha_2 = 0.021$

In Tab. 6. the above mentioned networks are described and their selected statistical parameters are given. From the data it results that the functions (3), (4), (5), (6), (7) and (8) have a simple structure and high accuracy.

**Tab. 6.** Structure and selected statistical parameters of the elaborated neural networks

Variable	Neural network structure	Correlation coefficient R	Mean square error RMS	
			of learning	of validation
MSI	2x11x1	0.998	1.40	0.57
$\varphi$	2x2x1	0.984	0.38	0.46
R	2x5x1	0.999	1.55	1.20
$a_t$	2x2x1	0.997	0.09	0.04
$a_v$	2x16x1	0.999	0.08	0.04
$L_{GW}$	2x14x1	0.999	1.28	0.64

In the further part of the research a hull form of the passenger car ferry was searched for with regard to the assumed criteria. To solve the problem the functions (2), (3), (4), (5), (6) and (7) were used.

In searching for a design solution which satisfies the assumed criteria the methods of one –criterial and multi-criterial optimization can be applied. However the main drawback of the methods is that they inform only where an optimum is located and they do not provide any information on a form of objective function, hence there is no certainty that the obtained solution is global optimum [4]. Number of possible combinations is relatively small as in the design task in question only two dependent variables of a rather small variability range appear. Therefore in order to determine an optimum solution the set of all possible design solutions was taken into account. For calculations the following increments of the design parameters were assumed:

$$\Rightarrow \Delta L/B = 0.01$$

$$\Rightarrow \Delta B/d = 0.01$$

The calculation results were analyzed in the same way as in the 1<sup>st</sup> phase of the research. To this end all design solutions were fuzzified by means of Eq. (1) and for their assessment the minimizing operator MIN acc. Eq. (2) was applied.

From the performed investigations it results that the best solution was obtained for the following values of the design parameters :

$$\Rightarrow L/B = 6.72 \div 6.75$$

$$\Rightarrow B/d = 3.57 \div 3.80$$

The value of the t-norm MIN for the above given solutions is presented in Fig. 7. Among them the design variant of  $L/B = 6.75$  and  $B/d = 3.60$  appears the best one. The optimum hull form of the ro-ro ferry is shown in Fig. 8.

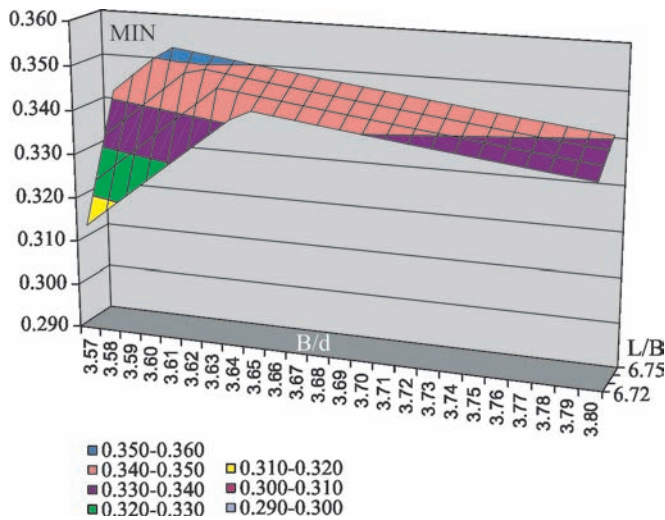


Fig. 7. Values of the t-norm MIN for the best design solutions,  $CB = 0.64$ ,  $CWL = 0.801$ ,  $L/B = 6.72 \div 6.75$ ,  $B/d = 3.57 \div 3.80$

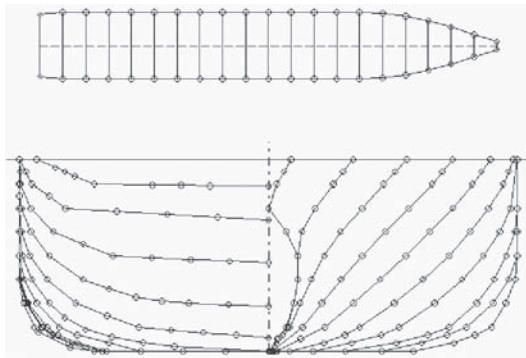


Fig. 8. The optimum hull form of the ro-ro ferry,  $V = 13723 \text{ m}^3$ ,  $CB = 0.64$ ,  $CWL = 0.801$ ,  $L/B = 6.75$  i  $B/d = 3.60$

To verify the result, values of the design criteria for the above given variant were determined (by using exact numerical methods) and then compared with the approximate ones. The results are shown in Tab. 7.

Tab. 7. Verification of the values of the design criteria for the optimum design variant, where:  $MSI$  – motion sickness index,  $a_t$  – transverse acceleration at the car deck,  $a_v$  – vertical accelerations,  $\varphi$  – significant amplitude of ship rolling,  $R$  – additional ship resistance in waves,  $L_{GW}$  – hourly number of car deck flooding events in the place of broken side plating

Method	MSI [%]	$\varphi$ [°]	$a_v$ [ $\text{m/s}^2$ ]	$a_t$ [ $\text{m/s}^2$ ]	R [kN]	$L_{GW}$ [1/h]
Approximation	29.3	5.99	1.90	0.98	147	278.5
Exact	27.3	5.69	1.90	0.98	147	279.8

## CONCLUSIONS

- In this paper a method which makes it possible to determine exact hull form of optimum ro-ro ferry with regard to many criteria, namely:
  - ✦ motion sickness index
  - ✦ rolling
  - ✦ transverse accelerations at the car deck

- ✦ vertical accelerations
- ✦ water flooding onto the car deck in the place of broken side plating
- ✦ additional ship resistance in waves, has been presented.

- The elaborated method is partly based on exact numerical calculations and partly on approximations obtained with the use of artificial neural networks. To assess the design merits the method based on deterministic scenarios was applied, and decision as to the choice of the best solution was based on fuzzy logic elements. It made it possible to present design merits in the form of linguistic variables and to find a design variant being a compromise between partial targets.
- The optimum hull form of the ferry, resulting from the approximation, was verified by means of exact numerical methods. As results from Tab. 7 the elaborated approximations appear very accurate, that can speak for that the design in question possesses appropriate (compromise) merits with regard to all partial criteria.
- The presented approximations may be used to design analyses (e.g. acc. [1]) or as objective functions in other optimization methods of ship design parameters.
- The presented approach, due to the fuzzy logic elements applied to the assessing of design variant merits, makes it possible to simplify a multi-criterial design problem to that one-criterial. In such case several partial criteria can be represented by a single criterion, e.g. the t – norm minimizing operator, and solutions for which it reaches maximum can be searched for. Such approach may be used a.o. in optimization methods based on genetic algorithms.

## BIBLIOGRAPHY

1. Cepowski T.: *Approximation of the index for assessing ships sea-keeping performance on the basis of ship design parameters*. Polish Maritime Research, No 3(53), Vol 14, 2007
2. Cepowski T.: *Modeling the additional ship resistance in waves by means of ship hull form parameters* (in Polish), (submitted to 2007 Transcomp Conference), 2007
3. Cepowski T.: *Modeling design parameters of passenger car ferry with regard to selected sea-keeping qualities and additional ship resistance in waves*, (to be published in Polish Maritime Research journal)
4. Chądzyński W.: *Elements of contemporary design methods of floating objects* (in Polish). Scientific Reports of Szczecin University of Technology (Prace Naukowe Politechniki Szczecińskiej), Department of Ocean Engineering and Marine Systems' Designing, Szczecin 2001
5. Frank W.: *Oscillation of Cylinders in or below the Free Surface of Deep Fluids*, Technical Report 2375, Naval Ship Research and Development Centre, Washington DC, U.S.A., 1967
6. Gerritsma, J. and Beukelman, W.: *Analysis of the Resistance Increase in Waves of a Fast Cargo-ship*. International Shipbuilding Progress, 18(217), 1972
7. Goldberg D.E.: *Genetic Algorithms in Search, Optimization, and Machine Learning*, published by Pearson Education, Inc, 1989
8. ITC : *Recommended Procedures and Guidelines, Model Tests on Damage Stability in Waves*, 7.5-02, 07-04.2, 2005
9. Journée J.M.J. : *Verification and Validation of Ship Motions Program SEAWAY*. Report1213a, Delft University of Technology, The Netherlands, 2001
10. Kobylński L.: *Goal-based stability standards*, Proceedings of the 9th International Ship Stability Workshop, Germanischer Lloyd Operating 24/7, Hamburg 2007

11. Lasdon, L.S., Waren, A.D.: *Generalized reduced gradient software for linearly and nonlinearly constrained problems*, in: Greenberg, H.J., (Ed.) *Design and Implementation of Optimization Software*. Sijthoff and Noordhoff, Holland, 1978
12. Ogawa Y.: *An examination for the numerical simulation of parametric roll in head and bow seas*, Proceedings of the 9<sup>th</sup> International Ship Stability Workshop, Germanischer Lloyd Operating 24/7, Hamburg 2007
13. Pawłowski M.: *Subdivision and damage stability of ships*. Foundation for Promotion of Shipbuilding Industry and Maritime Economy (Fundacja Promocji Przemysłu Okrętowego i Gospodarki Morskiej), Gdańsk 2004
14. Riola J.M., M.Garcia de Arboleya: *Habitability and personal space in seakeeping behaviour*, Journal of Maritime Research, Vol III, No 1, 2006
15. Spanos D., Papanikolaou A.: *On the Time to Capsize of a Damaged RoRo/Passenger Ship in Waves*, Proceedings of the 9<sup>th</sup> International Ship Stability Workshop, Germanischer Lloyd Operating 24/7, Hamburg 2007
16. Szozda Z.: *A Concept of Ship Stability Criteria Based on Cargo Shift Caused by Rolling due to Gust*, Scientific Reports (Zeszyty Naukowe) No. 2(74), Szczecin Maritime Academy, 2004

**CONTACT WITH THE AUTHOR**

Tomasz Cepowski, Ph. D.  
 Institute of Marine Navigation,  
 Maritime University of Szczecin  
 Wały Chrobrego 1/2  
 70-500 Szczecin, POLAND  
 e-mail : cepowski@am.szczecin.pl



Photo: C. Spigarski

# How to divide the global resistance change into the components related to the pushing propeller and the pulling propeller of the double-ended ship

Henryk Jarzyna, Prof.

## ABSTRACT



The division of the global resistance change  $\Delta R_{R+D}$  due to the simultaneous action of the pushing (SR) and pulling (SD) screw propellers into the components  $\Delta R_R$  and  $\Delta R_D$  can be done by taking into account two different procedures and different hypothetical assumptions given in the form of the division coefficients  $(A_j)_R$  and  $(A_j)_D$ , the same in each procedure.

In the procedure no 1:  $\Delta R_R = \Delta R_{R+D}(A_j)$  and  $\Delta R_D = \Delta R_{R+D}(A_j)_{Dj}$

In the procedure no 2:  $\Delta R_R = T_R - (R_0 - F_D)(A_j)_R$  and  $\Delta R_D = T_D - (R_0 - F_D)(A_j)_D$

Two necessary conditions were formulated to be fulfilled when selection of the coefficients  $(A_j)_R$  and  $(A_j)_D$  is done. The results of the analysis are univocal. Among the possible division coefficients only one pair of them fulfills the formulated conditions. This pair is:

$$(A_1)_R = \frac{T_R}{T_{R+D}} \text{ and } (A_1)_D = \frac{T_D}{T_{R+D}}$$

**Keywords:** self propulsion tests, double-ended ships, resistance change due to propeller action.

## INTRODUCTION

In model self propulsion tests, among other problems, the model resistance changes due to propeller action can be investigated. In the case of a ship with the pushing screw propeller (SR) the procedure of determination of the ship hull resistance change is well known from the ITTC Recommendation:

$$\Delta R = T - (R_0 - F_D) \quad (1)$$

where:

- $\Delta R$  - ship hull resistance change
- $R_0$  - ship hull resistance when towed (from resistance test)
- $T$  - screw propeller thrust (measured)
- $F_D$  - additional towing force (calculated)

In special cases, e.g. double ended ferry fitted with pushing, SR, and pulling, SD, screw propellers being in simultaneous action the determination of the global resistance change can be performed according to the known ITTC Recommendations:

$$\Delta R_{R+D} = T_R + T_D - (R_0 - F_D) = T_{R+D} - (R_0 - F_D) \quad (2)$$

where:

- $T_R, T_D$  - thrust of SR and SD screw propellers (measured values)
- $R_0$  - ship hull resistance when towed (from resistance test)

- $F_D$  - additional towing force (calculated)
- $\Delta R_{R+D}$  - global ship resistance change due to simultaneous action of SR and SD propellers.

The mentioned ITTC Recommendations do not give any instruction related to the necessary procedure of dividing the global resistance increase  $\Delta R_{R+D}$  into the components  $\Delta R_R$  and  $\Delta R_D$  due to the both screw propellers SR and SD. Additional hypothetical assumptions are to be proposed to form this dividing procedure.

In this paper an analysis of the possible hypothetical assumptions is given from the point of view of the necessary conditions formulated by the author.

## POSSIBLE PROCEDURES AND HYPOTHESES

The division of the global resistance change  $\Delta R_{R+D}$  due to the simultaneous action of the pushing screw propeller SR and the pulling screw propeller SD into the components  $\Delta R_R$  and  $\Delta R_D$  can be done by taking into account two different procedures and different hypothetical assumptions, the same in each procedure.

Two possible procedures are evident from the formal twofold notation of the division way.

The first procedure ( $i = 1$ ) makes direct use of the components  $\Delta R_R$  and  $\Delta R_D$  which are combined with the division coefficients  $(A_j)_R$  and  $(A_j)_D$  in the form:

$$\Delta R_R = \Delta R_{R+D}(A_j)_R \quad (3)$$

$$\Delta R_D = \Delta R_{R+D}(A_j)_D$$

The second procedure ( $i = 2$ ) refers to the notation of global resistance change in the form (2):

$$\Delta R_{R+D} = T_{R+D} - (R_0 - F_D)$$

and makes use of the similar notation related to the components  $\Delta R_R$  and  $\Delta R_D$ :

$$\Delta R_R = T_R - (R_0 - F_D)_R \quad (4)$$

$$\Delta R_D = T_D - (R_0 - F_D)_D$$

where  $(R_0 - F_D)_R$  and  $(R_0 - F_D)_D$  are connected with the same division coefficients  $(A_j)_R$  and  $(A_j)_D$  in the form:

$$(R_0 - F_D)_R = (R_0 - F_D)(A_j)_R \quad (5)$$

$$(R_0 - F_D)_D = (R_0 - F_D)(A_j)_D$$

giving:

$$\Delta R_R = T_R - (R_0 - F_D)(A_j)_R \quad (6)$$

$$\Delta R_D = T_D - (R_0 - F_D)(A_j)_D$$

The form of the division coefficients  $(A_j)_R$  and  $(A_j)_D$  is limited to a fraction of the component thrust  $T_R$ ,  $T_D$  or the component  $P_{DR}$ ,  $P_{DD}$  and global thrust or power. All measured values ( $T_R$ ,  $T_D$ ,  $T_{R+D}$ ,  $T_{R+0}$ ,  $T_{0+D}$ ,  $P_{DR}$ ,  $P_{DD}$ ,  $P_{D(R+D)}$ ,  $P_{D(R+0)}$ ,  $P_{D(0+D)}$ ) are gained from the three possible types of self propulsion tests:

- Test No 1 - the basic test with SR and SD screw propellers in simultaneous action, where:  $T_R$ ,  $T_D$ ,  $T_{R+D}$ ,  $P_{DR}$ ,  $P_{DD}$ ,  $P_{D(R+D)}$  - measured values.
- Test No 2 - the auxiliary test with SR screw propeller only, where:  $T_{R+0}$ ,  $P_{D(R+0)}$  - measured values.
- Test No 3 - the auxiliary test with SD screw propeller only, where:  $T_{0+D}$ ,  $P_{D(0+D)}$  - measured values.

The different analyzed hypotheses in the form of the division coefficients  $(A_j)_R$  and  $(A_j)_D$  are given in Tab.1, distinguished by the indices  $j$ , (from  $j = 1$  to  $j = 6$ ).

Tab. 1. Possible division coefficients  $(A_j)_R$  and  $(A_j)_D$

	$(A_j)_R$	$(A_j)_D$
<b>j = 1 thrust ratio</b>	$\frac{T_R}{T_{D+R}}$	$\frac{T_D}{T_{D+R}}$
<b>j = 2 thrust ratio</b>	$\frac{T_R}{T_{0+R}}$	$\frac{T_D}{T_{D+0}}$
<b>j = 3 power ratio</b>	$\frac{P_{DR}}{P_D}$	$\frac{P_{DD}}{P_D}$
<b>j = 4 power ratio</b>	$\frac{P_{DR}}{P_{D(0+R)}}$	$\frac{P_{DD}}{P_{D(D+0)}}$
<b>j = 5 thrust ratio</b>	$\frac{T_R}{T_m}$	$\frac{T_D}{T_m}$
<b>j = 6 power ratio</b>	$\frac{P_{DR}}{P_{Dm}}$	$\frac{P_{DD}}{P_{Dm}}$

## THE NECESSARY REQUIREMENTS TO BE MET

From the division coefficients given in Tab. 1 these are to be selected which satisfy two necessary conditions formulated by the author.

### Condition No 1:

The sum of the components  $\Delta R_R$  and  $\Delta R_D$  calculated by help of the division coefficients  $(A_j)_R$  and  $(A_j)_D$  is to be equal to the measured global value  $\Delta R_{R+D}$ :

$$\Delta R_R + \Delta R_D = \Delta R_{R+D} \quad (7)$$

### Condition No 2:

The component  $\Delta R_R$  and  $\Delta R_D$  calculated by help of the of the division coefficients  $(A_j)_R$  and  $(A_j)_D$  - in each of the procedures ( $i=1$  and  $i=2$ ) - are to be respectively equal to:

$$\Delta R_{R1} = \Delta R_{R2} \quad (8)$$

$$\Delta R_{D1} = \Delta R_{D2}$$

### Theorem No 1:

The division coefficients  $(A_j)_R$  and  $(A_j)_D$  fulfill the necessary condition No 1 then and only then when the sum of these coefficients is equal to one:

$$(A_j)_R + (A_j)_D = 1 \quad (9)$$

Proof: Condition No 1 realized in procedure No 1 takes the form:

$$\begin{aligned} \Delta R_{R1} + \Delta R_{D1} &= \Delta R_{R+D}(A_j)_R + \Delta R_{R+D}(A_j)_D = \\ &= \Delta R_{R+D}[(A_j)_R + (A_j)_D] \end{aligned} \quad (10)$$

The right hand side of this notation is equal to:  $\Delta R_{R+D}$  only then if  $[(A_j)_R + (A_j)_D] = 1$

Condition No 1 realized in procedure No 2 takes the form:

$$\begin{aligned} \Delta R_{R2} + \Delta R_{D2} &= T_R - (R_0 - F_D)_R + T_D - (R_0 - F_D)_D = \\ &= T_R - (R_0 - F_D)(A_j)_R + T_D - (R_0 - F_D)(A_j)_D = \\ &= T_R + T_D - (R_0 - F_D)[(A_j)_R + (A_j)_D] \end{aligned} \quad (11)$$

The right hand side of this notation is equal to  $\Delta R_{R+D}$  only then if:  $[(A_j)_R + (A_j)_D] = 1$  because  $T_R + T_D - (R_0 - F_D) = T_{R+D} - (R_0 - F_D) = \Delta R_{R+D}$ .

### Theorem No 2:

The division coefficients  $(A_j)_R$  and  $(A_j)_D$  fulfill the necessary condition No 2 then and only then if:

$$(A_j)_R = \frac{T_R}{T_{R+D}} \quad \text{and} \quad (A_j)_D = \frac{T_D}{T_{R+D}} \quad (12)$$

Proof: If  $\Delta R_R$  is calculated in each of the procedures ( $i = 1$  and  $i = 2$ ) then one has:

- in procedure No 1:

$$\Delta R_{R1} = \Delta R_{R+D}(A_j)_R \quad (13)$$

- in procedure No 2:

$$\Delta R_{R2} = T_R - (R_0 - F_D)(A_j)_R \quad (14)$$

and if both the values are equalized according to the condition No 2 then one receives:

$$\Delta R_{R+D}(A_j)_R = T_R - (R_0 - F_D)(A_j)_R \quad (15)$$

$$[\Delta R_{R+D} + (R_0 - F_D)](A_j)_R = T_R \quad (16)$$

$$T_{R+D}(A_j)_R = T_R \quad (17)$$

$$(A_j)_R = \frac{T_R}{T_{R+D}} \quad (18)$$

If  $\Delta R_D$  is calculated in each of the procedures ( $i = 1, i = 2$ ) then one has:

- in procedure No 1:

$$\Delta R_{D1} = \Delta R_{R+D} (A_j)_D \quad (19)$$

- in procedure No 2:

$$\Delta R_{D2} = T_D - (R_0 - F_D)(A_j)_D \quad (20)$$

and if both the values are equalized according to the condition No 2 then one receives:

$$\Delta R_{R+D} (A_j)_D = T_D - (R_0 - F_D)(A_j)_D \quad (21)$$

$$[\Delta R_{R+D} + (R_0 - F_D)](A_j)_D = T_D \quad (22)$$

$$(A_j)_D = \frac{T_D}{T_{R+D}} \quad (23)$$

The necessary condition No 2 with the demand that results of the division should be the same in both the procedures, leads to the statement that the division coefficient must be univocally defined as follows:

$$(A_1)_R = \frac{T_R}{T_{R+D}} \quad ; \quad (A_1)_D = \frac{T_D}{T_{R+D}} \quad (24)$$

Both the coefficients fulfill simultaneously the condition No 1.

## CONCLUSIONS

- Among the division coefficients given in Tab. 1, only one pair:

$$(A_1)_R = \frac{T_R}{T_{R+D}} \quad ; \quad (A_1)_D = \frac{T_D}{T_{R+D}} \quad (25)$$

fulfills unconditionally both the necessary conditions: condition No 1:

$$(A_1)_R + (A_1)_D = 1 \quad (26)$$

condition No 2:  $\Delta R_{R11} = \Delta R_{R21}$

$$\Delta R_{D11} = \Delta R_{D21} \quad (27)$$

- The division coefficients  $(A_3)_R$  and  $(A_3)_D$ , given in Tab. 1 for  $j = 3$ , and related to the power:

$$(A_3)_R = \frac{P_{DR}}{P_{D(R+D)}} \quad ; \quad (A_3)_D = \frac{P_{DD}}{P_{D(R+D)}} \quad (28)$$

fulfill the condition no 1:

$$(A_3)_R + (A_3)_D = 1 \quad (29)$$

but they do not fulfill the condition No 2 in general:

$$\Delta R_{R13} \neq \Delta R_{R23} \quad (30)$$

$$\Delta R_{D13} \neq \Delta R_{D23}$$

unless the efficiencies of the screw propellers SR and SD are equal to each other because in this special case only the following is true:

$$\frac{P_{DR}}{P_{D(R+D)}} = \frac{T_R}{T_{R+D}} \quad \text{and} \quad \frac{P_{DD}}{P_{D(R+D)}} = \frac{T_D}{T_{R+D}} \quad (31)$$

- The simplicity of the first procedure makes it generally preferred in practical application.

## NOMENCLATURE

$F_D$	– the additional towing force
$F_{DR}, F_{DD}$	– the parts of $F_D$ being under the influence of the SR and SD propeller, respectively
$P_D$	– the total delivered power
$P_{D(0+R)}$	– the power of the SR propeller only being in action
$P_{D(D+0)}$	– the power of the SD propeller only being in action
$P_{DR}, P_{DD}$	– the power of the SR and SD propeller, respectively, being in simultaneous action
$P_{Dm}$	– the algebraic mean value: $P_{Dm} = \frac{P_{D(0+R)} + P_{D(D+0)}}{2}$
$R$	– the hull resistance when propelled
$R_0$	– the hull resistance when towed
$R_{D+R}$	– the hull resistance when propelled by the SR and SD propellers
$R_{0+R}$	– the hull resistance when propelled by the SR propeller only
$R_{D+0}$	– the hull resistance when propelled by the SD propeller only
$R_{0R}, R_{0D}$	– the parts of $R_0$ being under the influence of the SR and SD propeller, respectively
$\Delta R$	– the resistance increase due to the propeller action
$\Delta R_{D+R}$	– the resistance increase due to the simultaneous action of the SR and SD propeller
$\Delta R_{0+R}$	– the resistance increase due to the SR propeller only being in action
$\Delta R_{D+0}$	– the resistance increase due to the SD propeller only being in action
$\Delta R_R, \Delta R_D$	– the resistance increase due to the SR and SD propeller, respectively, being in simultaneous action
SD	– the pulling screw propeller
SR	– the pushing screw propeller
$T_{D+R}$	– the thrust of the SD and SR propeller being in simultaneous action
$T_{0+R}$	– the thrust of the SR propeller only being in action
$T_{D+0}$	– the thrust of the SD propeller only being in action
$T_R, T_D$	– the thrust of the SR and SD propeller, respectively, being in simultaneous action
$T_m$	– the algebraic mean value: $T_m = \frac{T_{0+R} + T_{D+0}}{2}$

## Acronyms

ITTC – International Towing Tank Conference.

## BIBLIOGRAPHY

1. Jarzyna H.: *Interaction of Ship Hull and Propeller* (in Polish), Monograph, Fluid Flow Machinery, Ossolineum Publishing House, Vol.14., Wrocław 1993
2. Jarzyna H.: *Some Problems of the Model Self Propulsion Tests* (in Polish), Monograph, Fluid Flow Machinery, Ossolineum Publishing House, Vol.26, Wrocław 2002
4. Jarzyna H., Tuskowska T.: *Ship Power Prediction Methods Based on a General Definition of the Equivalent Open-Water Screw Propeller*, Monograph, IFFM Publishers, Gdańsk 2002
5. Jarzyna H.: *Selection of the Most Suitable Method to Split the Resistance Increment into Components Related to Individual Propellers of Double-Ended Ferry*. Archives of Civil and Mechanical Engineering, Vol VII, No 3, Wrocław 2007
6. Proceedings of ITTC: *Reports of the Performance Committee to 15-th ITTC-1978; 16-th ITTC-1981; 17-th ITTC-1984; 18-th ITTC-1987; 19-th ITTC-1990; 20-th ITTC-1993*

# Application of artificial neural networks to assessment of ship manoeuvrability qualities

Tomasz Abramowski, Ph. D.  
Szczecin University of Technology

## ABSTRACT



*This paper presents an attempt to applying neural networks for assessment of parameters of standard manoeuvrability tests, i.e. circulation test and zig-zag test. Methodological approach to application of neural networks as well as applied network structures and neuron activation functions are generally presented. Also, results of simulations performed by means of the elaborated networks are given in comparison with test cases selected at random. In order to analyze and reveal general trends, correlation relationships between results from network simulations and test cases were calculated and are presented as well.*

**Keywords:** neural networks, ship manoeuvrability qualities

## INTRODUCTION

One of the elements subjected to hydromechanical analysis during ship design are its manoeuvrability qualities. In 2002 IMO adopted its MSC.137(76) resolution on "Standards for ship manoeuvrability" which imposed relevant requirements on manoeuvrability parameters of new ships. Therefore it seems reasonable to elaborate tools for assessing such qualities. In this work a method based on application of neural networks was proposed. Such networks have been already used for similar purposes. Clausen *et al.* [3] proposed to use neural networks to determine ship main dimensions in preliminary design stage. Koushan [7, 9] presented possible approximations of propeller-generated pressures and rudder forces, by using neural networks. Cepowski [2] applied the method in question to assessment of ship sea-keeping qualities.

In this work were analyzed possible application of neural networks to two typical manoeuvres performed during sea trials of single propeller ship, namely : the circulation test with ship rudder laid right by 35° and the 10°/10° zig-zag test . The choice of the tests was conditioned by the fact of their standardization in IMO regulations. The presented work was aimed at elaboration of a method making it possible to perform multi-variant, simultaneous analysis of design solutions without necessity of multiple repetition of calculations by means of a simulator.

To simulate and form the networks the MATLAB environment with application of the Neural Network Toolbox

package was used [9]. A dynamic simulator being a part of Tribon Initial Design software was used as a source of learning data. The Tribon System is based on numerical solving the well-known differential equations of two-dimensional motion of ship:

$$\begin{aligned} (m + m_x)(\ddot{u} - v\omega - X_G \omega^2) &= X_H + X_P + X_R + X_E \\ (m + m_y)(\ddot{v} - u\omega - X_G \dot{\omega}) &= Y_H + Y_R + Y_E \\ (I_z + J_z)\dot{\omega} + mX_G(\dot{v} + u\omega) &= N_H + N_R + N_E \end{aligned} \quad (1)$$

The right-hand sides of the equations represent the inertial terms including added masses, and their left-hand sides – the hydrodynamic forces : acting on ship hull –  $(X_H, Y_H, N_H)$ , on propeller –  $(X_P)$ , on rudder –  $(X_R, Y_R, N_R)$ , as well as due to such disturbances as wind and wave –  $(X_E, Y_E, N_E)$ . Despite the learning data were supplemented by available sea trial results, their prevailing part was provided by the simulator. Hence the elaborated networks can be considered to be a simplified algebraic form of the Eqs. (1).

The full set of network learning and testing data comprised 260 cases having systematically changeable parameters. The set was divided in random into the learning set which took part in the process of calculation of network weighing factors and which comprised 230 cases, and the testing set which served solely to assess network quality and which did not take part in learning process and comprised 30 cases. The analysis of parameters in question covered the data presented in Tab.1.

Tab.1. Variability range of parameters of analyzed ships

Parameter	Maximum value	Minimum value
$L_{pp}$ [m]	260.0	90.0
$B$ [m]	50.0	12.0
$T$ [m]	15.0	4.6
$C_B$ [-]	0.85	0.6
$L_{pp}/B$ [-]	7.9	4.1
$B/T$ [-]	6.0	2.2
$L_{pp}/T$ [-]	29.8	14.1

The propeller pitch ratio  $P/D$  was equal to 1 for all learning cases. The learning data relate to manoeuvres executed in water of unlimited depth. For both the manoeuvres the same rate of laying the rudder, equal to  $2^\circ/s$ , was assumed.

The input data were normalized within the interval (1,-1) in accordance with the following relationship:

$$y = \frac{(y_{max} - y_{min}) \cdot (x - x_{min})}{(x_{max} - x_{min}) + y_{min}} \quad (2)$$

where:

- $y_{max}, y_{min}$  - assumed limits of normalization interval, in the considered case:  $y_{max} = 1, y_{min} = -1$
- $x_{min}$  - minimum value in a given row of data,
- $x_{max}$  - maximum value in a given row of data.

For all elaborated networks one neuron activation function was applied. It has the following form:

$$\text{tansig}(x_i) = \frac{2}{(1 + e^{-2 \cdot x_i}) - 1} \quad (3)$$

where:

- $x_i$  - input value.

The run of the applied activation function is shown in Fig. 1.

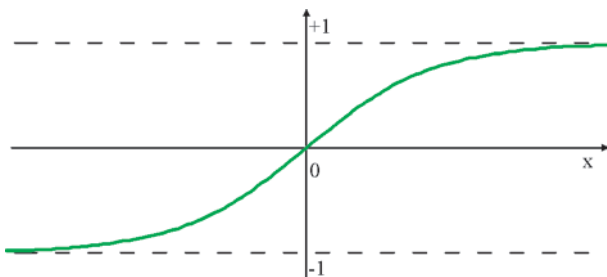


Fig. 1. The applied neuron activation (saturation) function.

## ARTIFICIAL NEURAL NETWORKS

There is no commonly accepted, unambiguous definition of artificial neural network (SSN). It can be said that the SSNs are an attempt to connect human brain possibilities of parallel processing with speed and precision of computer processors. Such connection provides, to the networks, capability of learning, memorizing, calling and comparing the nonlinear, multi-dimensional structures of data in order to interpolate and extrapolate them appropriately. The traditionally applied modelling methods consist in collecting data and attempting to combine them into known physical, chemical or mechanical relationships. In such case to linearize mathematical models is necessary to make them simpler for analyzing. The method based on neural networks consists in an attempt to understand

a modeled system as an entity of relations occurring within its structure and it searches all linear and nonlinear relations which can influence its operation. Some neural networks constitute models of biological neural structures, but the other ones do not. However historically, most inspirations in the field of neural networks come from a desire of creating an artificial system capable of executing complex, possibly 'intelligent' calculations similar to those regularly done by human brain.

Neural network structure is comprised of several processing units capable of mutual communicating by means of connections having different weighing factors. Generally, not every neural network has its structure similar to that shown in Fig. 2., which consists of the following elements:

- ★ Input layer – used for receiving and processing external signals,
- ★ Hidden layers (or only one layer)- whose signals remain within the network,
- ★ Output layer – used for sending signals outside.

Each layer can be composed of several single neurons, and number of neurons in input and output layers is determined by a kind of task to be solved (number of variables and results).

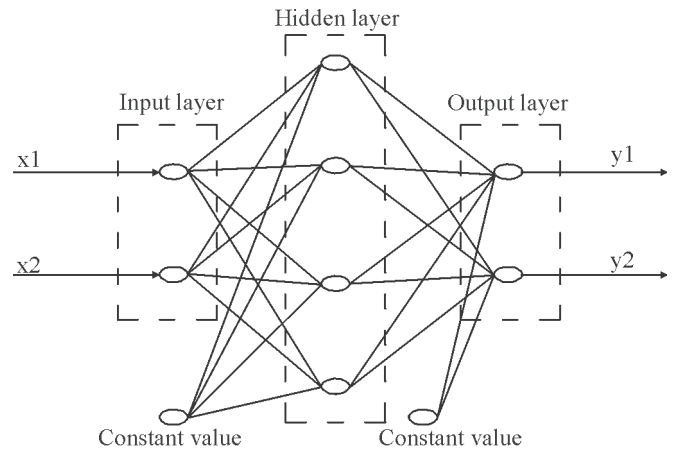


Fig. 2. Example structure of neural network

Neurons of particular layers can be additionally connected with external elements which serve as constant values and improve effectiveness of network learning process. In order to clearly present the operational principle of neural networks, making use of idea of a single neuron is most effective (Fig. 3):

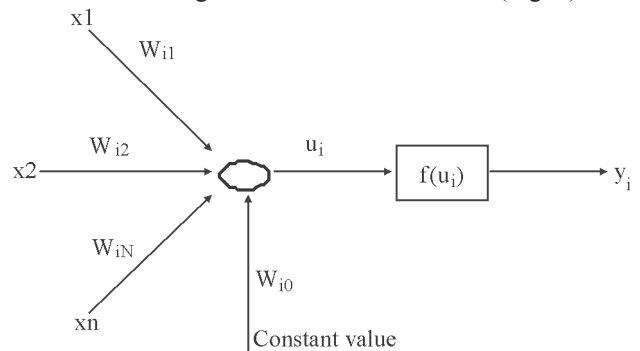


Fig. 3. Single neuron.

Calculation of the output value  $y_i$  for a single neuron is performed in accordance with the following relationship:

$$y_i = F \left( \sum_{j=1}^N W_{ij} \cdot x_j + W_{i0} \right) \quad (4)$$

where:

- $F$  - applied activation function

- $W_i$  - weighing factors for particular connections
- $x_i$  - input value
- $\dot{W}_{i0}$  - constant values attributed to particular connections.

For given constant values and weighing factors it is easy to generalize the above presented relationship for an arbitrary number of layers and number of neurons in a given layer by using linear algebraic equations. The basic task in applying neural networks is to calculate constant values and weighing factors for a given network structure. The task is realized during learning process. The often used learning method is that called back-propagation one, applied in this work and presented in detail by Osowski [11].

The first operation in the learning process is to prepare two sequences of data : learning one and verifying one. The learning sequence constitutes a set of such data which relatively exactly characterize a given problem. A single portion of the data is called the learning vector. It contains the input vector, i.e. the input data delivered to network input points, and output vector, i.e. the data expected to be generated by the network at its output points. After processing the input vector, the teacher compares the obtained values and expected ones and informs the network on whether the response is correct or not, if not – on how large error of the response resulted. The error is then propagated within the network but in the opposite sequence than that of the input vector (i.e. from output layer to input one) and on its basis an appropriate correction of weighing factors is introduced to each neuron in order to obtain a lower response error as a result of the repeated processing of the same input vector. Such procedure is repeated again and again until the error generated by the network is lower than that assumed. Then the successive input vector is delivered to the network input points and the described operations are repeated. After processing the entire learning sequence (called the epoch) the error for the epoch is calculated and the entire cycle is repeated until the error drops under its allowable value. As mentioned above, the SSNs show certain tolerance for discontinuities, random disturbances or even small shortages in the learning set. It just results from their capability of generalizing the knowledge.

The verification process of network operation follows the learning process. In this moment it is important to put in the network some specimens not coming from the training set, in order to check if the network is capable of effective generalizing the learned task. To this end is used the verifying sequence which has the same features as the learning one, i.e. its data characterize the problem exactly and exact responses are known. However it is important to select the data which have not been used earlier for learning. This way the verifying sequence is presented, however the difference is that errors generated in the process are not propagated back but only number of correct responses is recorded and on this basis the statement is made if the network in question satisfies imposed requirements i.e. to which extent it has been learned.

The initial weighing factors with which a given network starts learning, are numbers generated at random. After learning process it is always favourable to repeat all the procedure beginning from generation of initial weighing factors, in order to check the obtained results.

In the case of large networks and learning sequences consisted of many thousands of learning vectors, number of calculations to be executed during all the learning cycle is gigantic, hence time-consuming. Also, it does not happen that a network is correctly built at once but always it becomes a result of many trials and errors. Moreover it can be never guaranteed that even a correct network does not come to a local minimum instead to continue finding global one. Therefore

algorithms realizing the SSNs are fitted with mechanisms which make it possible to control speed and quality of learning. These are the so called learning and momentum coefficients. They influence steepness of activation function and control speed of influence of change of weighing factors on learning process.

## CALCULATIONS FOR CIRCULATION TESTS

To simulate the circulation manoeuvre a network of 9x12x7 structure was elaborated. The input values to the network (arguments) were in turn the following : the ship length between perpendiculars,  $L_{pp}$ , ship breadth  $B$ , ship draught  $T$ , block coefficient of ship hull underwater part,  $C_B$ , longitudinal position of ship centre of gravity,  $L_{CG}$ , propeller diameter  $D$ , ship speed at the beginning of the circulation manoeuvre,  $V_{APP}$ , rudder aspect ratio  $\lambda$  and the total rudder area  $A_R$ .

The neural network outputs were the following : transverse and head translations (transfer and advance) at ship course change by  $90^\circ$ , tactical diameter of circulation and head translation for the course change by  $180^\circ$ , steady circulation diameter, total decrease of ship speed at course change by  $360^\circ$ ,  $V/V_{APP}$  as well as the drift angle  $\beta$  during steady circulation.

The elaborated structure is presented in Fig. 4.

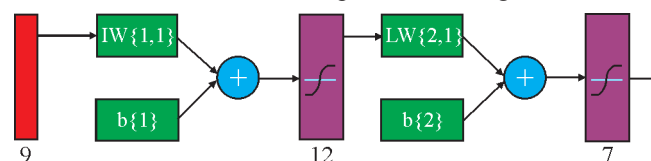


Fig. 4. Neural network for circulation manoeuvre

In Fig. 5 the run of the network learning process is shown. It can be observed that after about 300 epochs of learning the network did not exhibit any further improvement of approximation quality.

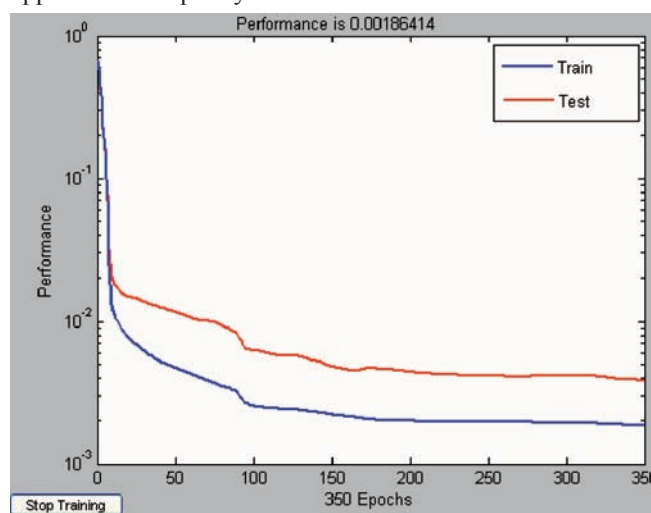


Fig. 5. Run of network learning process for circulation manoeuvre

The simulation of the manoeuvre was performed on the basis of a case selected from the testing set. The results of the simulation compared with the expected values are presented in Fig. 6.

It can be observed that for the course angle change by  $90^\circ$  the network error is of the order of the ship breadth. In the case of the course angle change by  $180^\circ$  the error is somewhat smaller - equal to about a half of the ship breadth. The drift angle at steady circulation is of a similar order. The difference of diameters at steady circulation is almost imperceptible. For purposes of this presentation one case characterized by the greatest errors was selected out of 30 testing ones.

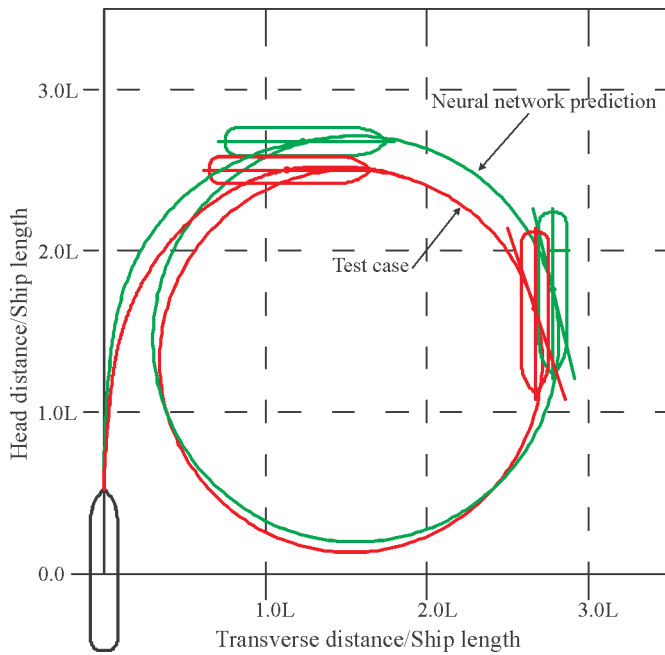


Fig. 6. Results of simulation of neural network for circulation manoeuvre

In Fig. 7. is presented the correlation between the drift angle values determined by means of neural networks and its

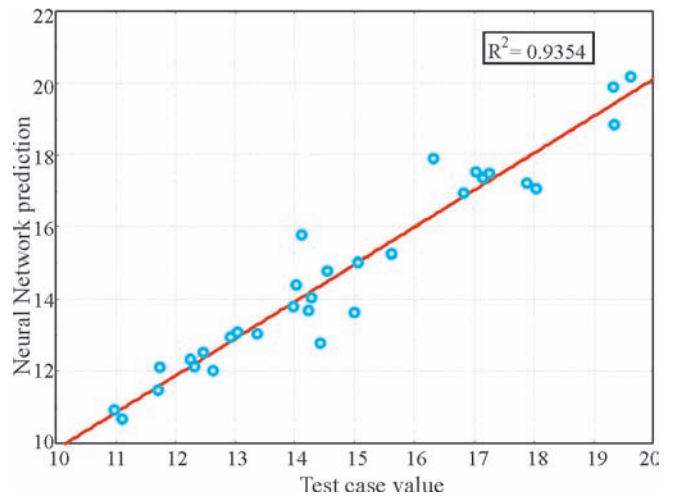


Fig. 7. Correlation between values of the drift angle at steady circulation, obtained from the network, and relevant testing values.

testing values, and in Fig. 8 – the correlation of values of the head translation at the course change by 90°.

Example results of network prediction values compared with relevant testing ones are shown in Tab. 2. The values concerning the translations (distances) are related to the ship length. Apart from the tests of correlation between results obtained from the network and testing cases, also capability

Tab. 2. Example simulation quality of neural network used for assessment of circulation parameters

	Course change	Parameter	Values							
	Testing values	90°	Advance/L [-]	3.12	3.27	3.77	3.70	3.69	3.40	2.69
Transfer/L [-]			1.54	1.67	1.98	1.89	2.01	1.62	1.19	1.29
180°		Tactical diameter [-]	3.34	3.58	4.19	3.99	4.38	3.52	2.62	2.82
		Advance/L [-]	1.90	2.13	2.34	2.30	2.15	2.35	1.96	2.10
Steady circulation		Diameter [-]	2.62	2.32	2.86	2.64	3.34	2.31	1.65	1.92
		V/Vapp [-]	0.53	0.38	0.44	0.42	0.56	0.37	0.33	0.41
	Drift angle [°]	13.13	15.29	12.96	14.50	12.34	17.42	18.91	16.96	
Neural network	90°	Advance/L [-]	3.09	3.23	3.71	3.6	3.74	3.38	2.74	2.92
		Transfer/L [-]	1.47	1.65	1.94	1.88	2.03	1.62	1.22	1.3
	180°	Tactical diameter [-]	3.21	3.57	4.12	4.01	4.41	3.55	2.67	2.85
		Advance/L [-]	1.99	2.09	2.32	2.29	2.19	2.32	1.99	2.06
	Steady circulation	Diameter [-]	2.63	2.34	2.86	2.7	3.31	2.38	1.62	1.96
		V/Vapp [-]	0.55	0.38	0.46	0.43	0.55	0.39	0.33	0.43
Drift angle [°]		13.06	15.63	12.95	13.97	12.25	17.13	19.34	16.84	
Relative error in [%] of a given value			1	1	2	3	1	1	2	7
			5	1	2	1	1	0	3	1
			4	0	2	0	1	1	2	1
			5	2	1	1	2	1	1	2
			0	1	0	2	1	3	2	2
			4	1	5	1	2	5	1	4
			1	2	0	4	1	2	2	1

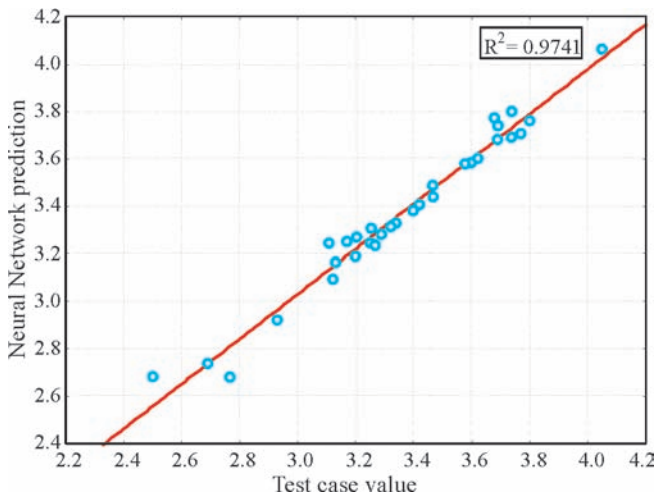


Fig. 8. Correlation between values of the head translation at the course change by 90°, obtained from the network, and relevant testing values.

of the elaborated networks, related to modeling the general trends of circulation parameters, was analyzed. In Fig. 9 is presented an example of the testing of influence of the ship hull block coefficient  $C_B$  on circulation parameters by using the elaborated networks.

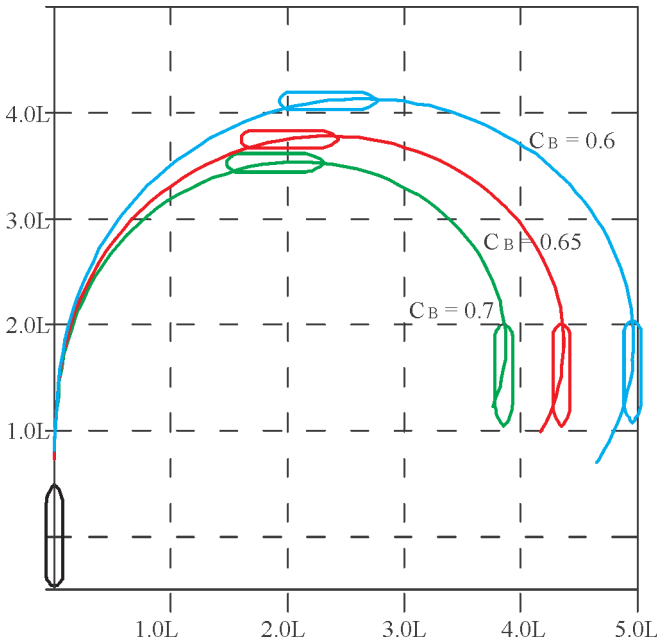


Fig. 9. Testing of the trend representing capability of the elaborated networks. Influence of ship hull block coefficient.

### CALCULATIONS FOR ZIG-ZAG TESTS

To simulate the zig-zag test the network of 9 x 11 x 5 structure was elaborated. Inputs to the network were identical as for the circulation test. It was the following parameters: duration time of the course change by 10° (initial turning time),  $t_a$ ; 1st and 2nd overshoot angle,  $\Delta\psi_1, \Delta\psi_2$ ; 1st and 2nd time to check yaw (time of rudder inertia angle),  $t_1, t_2$ . The network structure is shown in Fig. 10. The run of the network learning process is shown in Fig. 11. The learning process was terminated after 600 epochs.

In Fig. 12 are presented results of the zig-zag test simulation compared with those of the test case. Errors in representing particular time values and overshoot angles are contained within a few percent interval of relevant values. In Fig. 13 and 14 is

presented correlation between the test values for the 1st and 2nd overshoot angle and the relevant values approximated by the neural network.

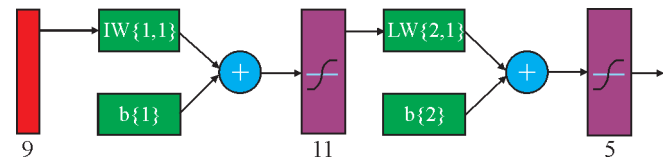


Fig. 10. Neural network for simulation of zig-zag test

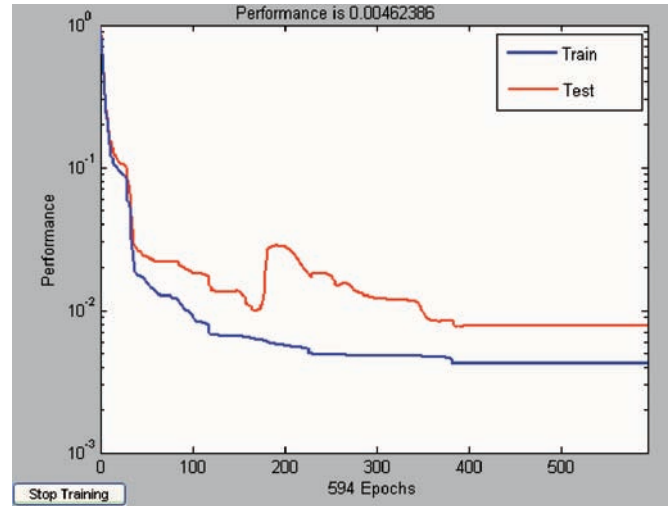


Fig. 11. Run of learning process of the network for zig-zag test

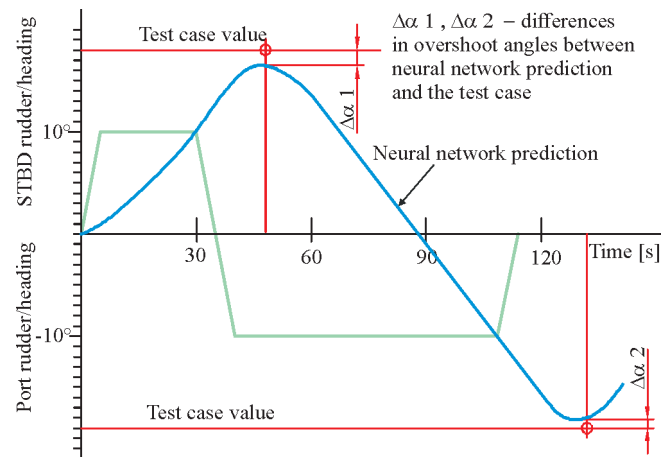


Fig. 12. Results of zig-zag test simulation by using the neural network

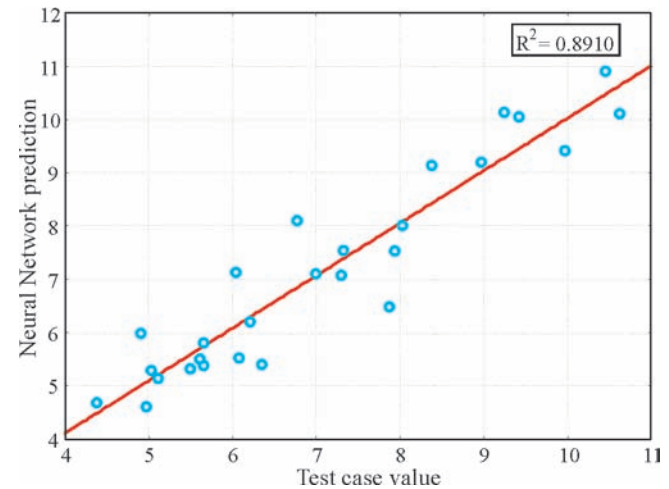


Fig. 13. Approximation quality of the neural network, based on the correlation for the 1st overshoot angle

The example results of the zig-zag test prediction, compared with relevant test values are given in Tab. 3. The obtained prediction quality is somewhat worse than that in the case of simulation of circulation manoeuvre.

Tab. 3. Example simulation quality of the neural network used for assessment of zig-zag test parameters

Test values	Parameter	Values							
	1 <sup>st</sup> overshoot angle. $\Delta\psi_1$ [°]	7.87	7.30	6.05	7.33	6.21	11.45	8.38	5.66
2 <sup>nd</sup> overshoot angle. $\Delta\psi_2$ [°]	9.12	10.49	8.78	10.76	8.44	13.36	11.69	6.68	
Initial Turning Time. $t_a$ [s]	32.00	38.00	62.00	36.00	38.00	28.00	34.00	32.00	
1 <sup>st</sup> Time to check yaw. $t_1$ [s]	18.00	24.00	34.00	24.00	20.00	22.00	26.00	16.00	
2 <sup>nd</sup> Time to check yaw. $t_2$ [s]	20.00	28.00	42.00	28.00	22.00	24.00	30.00	16.00	
Neural network	1 <sup>st</sup> overshoot angle. $\Delta\psi_1$ [°]	6.50	7.06	7.13	7.55	6.21	9.56	9.16	5.39
	2 <sup>nd</sup> overshoot angle. $\Delta\psi_2$ [°]	8.22	10.23	9.08	9.97	8.10	13.54	12.96	6.54
	Initial Turning Time. $t_a$ [s]	30.00	38.00	58.00	37.00	37.00	28.00	33.00	33.00
	1 <sup>st</sup> Time to check yaw. $t_1$ [s]	16.00	24.00	34.00	23.00	20.00	20.00	24.00	15.00
	2 <sup>nd</sup> Time to check yaw. $t_2$ [s]	18.00	28.00	40.00	27.00	22.00	24.00	28.00	16.00
Relative error in [%] of a given value:		21	3	15	3	0	20	9	5
		11	3	3	8	4	1	10	2
		6	0	7	2	3	1	3	3
		13	2	1	4	0	9	8	8
		12	0	5	5	2	1	7	0

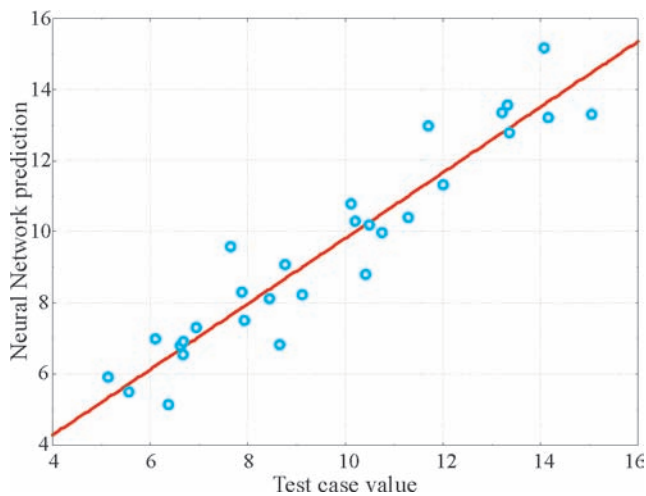


Fig. 14. Approximation quality of the neural network, based on the correlation for the 2nd overshoot angle

## CONCLUSIONS

- The presented method makes it possible to simultaneously determine parameters of analyzed manoeuvres depending on design parameters of ship. The presented correlation diagrams show that the networks correctly recognize trends and that the obtained results are not accidental.
- The simulation quality for circulation manoeuvre is a little better than that for zig-zag test, though it would be possible to improve the simulation quality by supplementing the learning set.
- It should be highlighted that the presented method is not aimed at improving ship motion modeling quality but only at improving and adjusting the existing algorithms to demands of design process.
- The presented neural networks are capable of exact interpolating however their capability in extrapolating have not been sufficiently recognized so far, hence during application of the method any results obtained for values of the ship parameters being beyond their intervals given in Tab. 1, should be considered very cautiously.
- However from another side the traditional manoeuvrability simulators make as a rule use of regression relationships to determine force coefficients. The method in question makes it possible to continue research in the presented direction, e.g. by taking into account corrections associated with water depth, ship trim or application of multi-propeller propulsion systems.
- It is also possible to use neural network for dynamic simulation of manoeuvre; in this case for a given ship as
- Essence of the presented method consists in its possible applications to optimization and multi-criterial automatic design of ships. A difficulty in applying traditional manoeuvrability simulators is their low capability of fast and simultaneous analyzing many design solutions within a similar time interval. This is the feature which must characterize optimization algorithms. Sometimes the feature is more desirable than a high accuracy of results achieved at the expense of large time consumption. In the case of optimization algorithms it is necessary first of all to distinguish a better solution from worse one.

network inputs would be used its kinematic parameters at a given time instant  $t$  together with taking into account instantaneous position of rudder and screw propeller setting, and network outputs – kinematic parameters after a given time interval  $\Delta t$ .

- Certainly further investigations on the method would be carried out in the direction of bettering the learning data by supplementing them by results from real sea trials, and with a view of presenting example optimization results.

## BIBLIOGRAPHY

1. Abramowski T.: *Application of Artificial Neural Networks for Determination of Propeller's Crash-ahead, Crash-back and Backing Performance*, Ship Technology Research, Vol.48, No.4, November 2001
2. Cepowski T.: *Optimization of transport ship design parameters with a view of its sea-keeping qualities* (in Polish), Doctor thesis, Szczecin University of Technology, Szczecin 2002
3. Clausen H.B., Lutzen M., Friis-Hansen A., Bjerneboe N.: *Bayesian and Neural Networks for Preliminary Ship Design*. Marine Technology, vol. 38, no. 4, October 2001
4. IMO Resolution, *Standards for ship manoeuvrability*. MSC.137(76), adopted on 4 December 2002
5. Inoue S., Hirano M., Kijama M., Takashina: *A practical calculation method of ship manoeuvring motion*, Int. Shipbuilding Progress, vol. 28, no 325, 1981
6. McClelland, J., and D. Rumelhart: *Explorations in Parallel Distributed Processing*, MIT Press, Cambridge 1988
7. Koushan, K.: *Prediction of propeller induced pressure pulses using artificial neural networks*, 1st Int. Conf. Computer Applications and Information Technology in the Maritime Industries, Potsdam 2000
8. Koushan K., Mesbahi E.: *Empirical Prediction Methods for Rudder Forces of a Novel Integrated Propeller-Rudder System*, Proc. OCEANS'98, Nice 1998
9. Demuth H., Beale M., Hagan M.: *Matlab User's Guide: Neural Network Toolbox 5*. The MathWorks, 2007
10. Mesbahi E., Atlar M.: *Artificial neural networks: applications in marine design and modelling*, 1st Int. Conf. Computer Applications and Information Technology in the Maritime Industries, Potsdam 2000
11. Osowski, S.: *Neural networks in algorithmic form* (in Polish). Scientific Technical Publishing House (WNT), 1996
12. Tadeusiewicz R.: *Neural networks* (in Polish). Academic Publishing House (Akademicka Oficyna Wydawnicza), Warszawa 1993
13. Sha O.P., Ray T., Gokarn R.P.: *An artificial neural network model for preliminary ship design*, ICCAS 94, 8th Int. Conf. on Comp. Applications in Shipbuilding, Bremen 1994

---

## CONTACT WITH THE AUTHOR

Tomasz Abramowski, Ph. D.  
 Faculty of Marine Technology,  
 Szczecin University of Technology  
 Al. Piastów 41  
 71-065 Szczecin, POLAND  
 e-mail: tomasz.abramowski@ps.pl



Photo: C. Spigarski

# Modification of Hooke's law for multiaxial stress in viscoelastic solids

Janusz Kolenda, Prof.  
Naval Academy of Gdynia

## ABSTRACT



*On the basis of Hooke's law for multiaxial stress in elastic solids, similar relationships for viscoelastic materials are considered. It is assumed that the material is homogeneous and isotropic, and that the Kelvin-Voigt's model is applicable to normal strain components. An analogous model is also taken for shear strain components. It is shown that the ratio of coefficients of viscous damping of normal and shear strain components is equal to the ratio of Young modulus and shear modulus. As a result, the modified Hooke's law for multiaxial stress in viscoelastic materials has been formulated which includes three material constants: Young modulus, Poisson's ratio and coefficient of viscous damping of normal strain.*

**Keywords:** Hooke's law, viscoelastic material, Kelvin-Voigt's model, multiaxial loading

## INTRODUCTION

For the purpose of solving physical problems considered in the present paper, it is assumed that an engineering detail is made of a homogeneous isotropic metal and loaded below the yield point. The elastic behaviour of a particular homogeneous, isotropic metal at a given temperature is completely defined by the Young modulus and the Poisson's ratio [1, 2]. However, even in the region below the proportional limit metals are not perfectly elastic. If a load is suddenly applied and then maintained constant, a small amount of "creep" will always be observed [1]. This creep is due to anelastic strain which may arise from any of several sources, such as the presence of grain boundaries, twin boundaries, or slip bands, the diffusion of interstitial solute atoms and the phenomenon of magnetostriction. Particular attention is focused on anelastic strain in the vibration theory of continuous systems [3, 4]. To exemplify the problem, let us mention that contrary to free vibrations of perfectly elastic systems where the principle of energy conservation may be assumed, in reality the initial energy of isolated vibrating systems diminishes with time as a result of energy dissipation caused by damping properties of structural materials. This phenomenon is very complex but there are several approximate models of anelastic materials and damping mechanisms which are simple enough to be accepted in practice, for instance the Kelvin-Voigt's model (spring and dashpot in parallel) and hysteretic damping [3-6]. In the present paper, the Kelvin-Voigt's model is applied to viscoelastic materials under three-dimensional loads. The second part of this paper, to be published separately, will be devoted to the applications of relationships contained herein, with an emphasis made on the behaviour of viscoelastic solids under multiaxial loads and dissipation energy.

## HOOKE'S LAW

When structures, machines, and engineering details are in service, they are usually subjected to surface forces or body forces (inertial, gravitational, or electromagnetic) that cause combined stresses in their elements. To completely define an element, it is necessary to specify the components of the stress tensor represented by the array:

$$\mathbf{T} = \begin{bmatrix} \sigma_x & \tau_{yx} & \tau_{zx} \\ \tau_{xy} & \sigma_y & \tau_{zy} \\ \tau_{xz} & \tau_{yz} & \sigma_z \end{bmatrix} \quad (1)$$

where  $\sigma$  are the normal stress components and  $\tau$  are the shear stress components on three orthogonal planes passing through the point. If surface couples and body couples may be ignored, the number of independent stress components reduces from nine to six since then  $\tau_{xy} = \tau_{yx}$ ,  $\tau_{yz} = \tau_{zy}$ , and  $\tau_{zx} = \tau_{xz}$ . Consequently, deformation produced by stress components can be completely specified by six strain components: normal ones  $\epsilon_x$ ,  $\epsilon_y$ ,  $\epsilon_z$  and shear ones  $\gamma_{xy}$ ,  $\gamma_{yz}$ ,  $\gamma_{zx}$ . The Hooke's law states that in elastic solids between these components the following relations hold [7, 8]:

$$\begin{aligned} E\epsilon_x &= \sigma_x - \nu(\sigma_y + \sigma_z) \\ E\epsilon_y &= \sigma_y - \nu(\sigma_x + \sigma_z) \\ E\epsilon_z &= \sigma_z - \nu(\sigma_x + \sigma_y) \\ G\gamma_{xy} &= \tau_{xy} \\ G\gamma_{yz} &= \tau_{yz} \\ G\gamma_{zx} &= \tau_{zx} \end{aligned} \quad (2)$$

Here E is the Young modulus,  $\nu$  is the Poisson's ratio, and:

$$G = \frac{E}{2(1+\nu)} \quad (3)$$

is the shear modulus.

For any combination of loads, there exist at any point three orthogonal planes upon which only normal stress components act. These are the principal stresses, designated in declining order of magnitude:  $\sigma_1$ ,  $\sigma_2$ , and  $\sigma_3$ . Therefore, for the particular case where x, y and z are the principal directions, Eqs (2) yield:

$$\begin{aligned} E\varepsilon_1 &= \sigma_1 - \nu(\sigma_2 + \sigma_3) \\ E\varepsilon_2 &= \sigma_2 - \nu(\sigma_1 + \sigma_3) \\ E\varepsilon_3 &= \sigma_3 - \nu(\sigma_1 + \sigma_2) \\ \gamma_{12} &= \gamma_{23} = \gamma_{31} = 0 \end{aligned} \quad (4)$$

From Mohr's stress and strain circles [7, 8] it follows that the maximum shear stress and the maximum shear strain are:

$$\tau = 0.5(\sigma_1 - \sigma_3) \quad (5)$$

$$\gamma = 2\varepsilon_1 \quad (6)$$

The relationship between  $\tau$  and  $\gamma$  reads:

$$G\gamma = \tau \quad (7)$$

For the given stress state that:

$$\sigma_1 = -\sigma_3, \sigma_2 = 0 \quad (8)$$

one gets:

$$E\varepsilon_1 = \sigma_1 - \nu(0 - \sigma_1) = \sigma_1(1 + \nu) \quad (9)$$

$$\tau = \sigma_1 \quad (10)$$

## HOOKE'S LAW FOR VISCOELASTIC MATERIALS

Let us consider what happens to a long rod of homogeneous isotropic material if a tensile force is applied to the end of the rod in the direction x parallel to its length. Of course, this rod will exhibit a uniform tensile strain  $\varepsilon_x$  produced by the stress  $\sigma_x$ .

For elastic state:

$$E\varepsilon_x = \sigma_x \quad (11)$$

Also, it will be observed that the fractional change in diameter is proportional to the axial strain and such that:

$$\varepsilon_y = -\nu\varepsilon_x, \varepsilon_z = -\nu\varepsilon_x \quad (12)$$

If the force and, consequently, the stress  $\sigma_x$  is time-dependent:

$$\sigma_x = \sigma_x(t) \quad (13)$$

it is assumed that Eqs (12) are also valid, i.e.:

$$\varepsilon_y(t) = -\nu\varepsilon_x(t), \varepsilon_z(t) = -\nu\varepsilon_x(t) \quad (14)$$

Differentiation of Eqs (14) with respect to time gives:

$$\dot{\varepsilon}_y(t) = -\nu\dot{\varepsilon}_x(t), \dot{\varepsilon}_z(t) = -\nu\dot{\varepsilon}_x(t) \quad (15)$$

In order to account for viscoelastic properties of the rod in this case by means of the Kelvin-Voigt's model, Eqs (11) and (12) must be replaced by:

$$E\varepsilon_x + \eta\dot{\varepsilon}_x = \sigma_x \quad (16)$$

$$\varepsilon_y = -\nu_a\varepsilon_x, \varepsilon_z = -\nu_a\varepsilon_x \quad (17)$$

where  $\eta$  is the coefficient of viscous damping of normal strain, and [9]:

$$\nu_a = \nu_e + \nu_s + \nu_c \quad (18)$$

In Eq. (18),  $\nu_a$  is the Poisson's ratio in the case of anelastic strain,  $\nu_e$  is related to elastic deformations,  $\nu_s$  is caused by microslips, and  $\nu_c$  reflects the influence of microcracks. If the load is such that the solid remains in elastic state, then:

$$\nu_a = \nu_e = \nu, \nu_s = \nu_c = 0 \quad (19)$$

Since experiments show that Eq. (19) corresponds very closely to the behaviour of many solids under small loads [9], in what follows Eqs (12), (14) and (15) will be applied.

Now we shall compute the normal strain in the x-direction caused by normal stresses in the y- and z-directions, where x, y and z are any three mutually perpendicular directions.

For the strain due to  $\sigma_y$  one gets analogously to Eq. (16):

$$E\varepsilon_y + \eta\dot{\varepsilon}_y = \sigma_y \quad (20)$$

Thus:

$$\nu E\varepsilon_y + \nu\eta\dot{\varepsilon}_y = \nu\sigma_y \quad (21)$$

But in this case:

$$\varepsilon_x = -\nu\varepsilon_y, \dot{\varepsilon}_x = -\nu\dot{\varepsilon}_y \quad (22)$$

so that:

$$E\varepsilon_x + \eta\dot{\varepsilon}_x = -\nu\sigma_y \quad (23)$$

Similarly, for the stress in the z-direction one obtains:

$$E\varepsilon_x + \eta\dot{\varepsilon}_x = -\nu\sigma_z \quad (24)$$

Eqs (16), (23) and (24) are linear. These equations and principle of superposition lead to the following equation for the strain in x-direction:

$$E\varepsilon_x + \eta\dot{\varepsilon}_x = \sigma_x - \nu(\sigma_y + \sigma_z) \quad (25)$$

Equations for the strains in the other directions can be found in the same way.

When x, y and z are the principal directions, Eq. (25) becomes:

$$E\varepsilon_1 + \eta\dot{\varepsilon}_1 = \sigma_1 - \nu(\sigma_2 + \sigma_3) \quad (26)$$

For the stress state described by equations:

$$\sigma_1(t) = -\sigma_3(t), \sigma_2 = 0 \quad (27)$$

we have from Eq. (26):

$$E\varepsilon_1 + \eta\dot{\varepsilon}_1 = \sigma_1(1 + \nu) \quad (28)$$

Now let us assume that for viscoelastic solids loaded below the yield point, the maximum shear stress and strain can be expressed by Eqs (5) and (6), determined for elastic solids.

Differentiation of Eq. (6) with respect to time yields

$$\dot{\gamma} = 2\dot{\varepsilon}_1 \quad (29)$$

Analogously to Eq. (16) for normal strain component, for viscoelastic materials and shear strain component instead of Eq. (7) one can write [3, 4]:

$$G\gamma + \lambda\dot{\gamma} = \tau \quad (30)$$

where  $\lambda$  is the coefficient of viscous damping of the shear strain.

By Eq. (28):

$$2E\varepsilon_1 + 2\eta\dot{\varepsilon}_1 = 2\sigma_1(1 + \nu) \quad (31)$$

Through Eqs (6), (10) and (29), Eq. (31) takes on the form:

$$E\gamma + \eta\dot{\gamma} = 2\tau(1 + \nu) \quad (32)$$

that is:

$$G\gamma + \frac{\eta}{2(1 + \nu)}\dot{\gamma} = \tau \quad (33)$$

From comparison of Eqs (30) and (33) it is seen that:

$$\lambda = \frac{\eta}{2(1 + \nu)} \quad (34)$$

Summarizing, the modified Hooke's law for multiaxial stress in viscoelastic solids can be expressed as:

$$\begin{aligned} E\varepsilon_x + \eta\dot{\varepsilon}_x &= \sigma_x - \nu(\sigma_y + \sigma_z) \\ E\varepsilon_y + \eta\dot{\varepsilon}_y &= \sigma_y - \nu(\sigma_x + \sigma_z) \\ E\varepsilon_z + \eta\dot{\varepsilon}_z &= \sigma_z - \nu(\sigma_x + \sigma_y) \\ G\gamma_{xy} + \lambda\dot{\gamma}_{xy} &= \tau_{xy} \\ G\gamma_{yz} + \lambda\dot{\gamma}_{yz} &= \tau_{yz} \\ G\gamma_{zx} + \lambda\dot{\gamma}_{zx} &= \tau_{zx} \end{aligned} \quad (35)$$

where:

$$G = \frac{E}{2(1 + \nu)}, \quad \lambda = \frac{\eta}{2(1 + \nu)} \quad (36)$$

Another derivation of Eqs (34) and (35) can be found in [10].

Eqs (35) can be rewritten in the following alternative forms:

$$\begin{aligned} E\varepsilon_x + \eta\dot{\varepsilon}_x &= \sigma_x - \nu(\sigma_y + \sigma_z) \\ E\varepsilon_y + \eta\dot{\varepsilon}_y &= \sigma_y - \nu(\sigma_x + \sigma_z) \\ E\varepsilon_z + \eta\dot{\varepsilon}_z &= \sigma_z - \nu(\sigma_x + \sigma_y) \\ E\gamma_{xy} + \eta\dot{\gamma}_{xy} &= 2(1 + \nu)\tau_{xy} \\ E\gamma_{yz} + \eta\dot{\gamma}_{yz} &= 2(1 + \nu)\tau_{yz} \\ E\gamma_{zx} + \eta\dot{\gamma}_{zx} &= 2(1 + \nu)\tau_{zx} \end{aligned} \quad (37)$$

or

$$\begin{aligned} \sigma_x &= \frac{(1 - \nu)(E\varepsilon_x + \eta\dot{\varepsilon}_x) + \nu[E(\varepsilon_y + \varepsilon_z) + \eta(\dot{\varepsilon}_y + \dot{\varepsilon}_z)]}{(1 + \nu)(1 - 2\nu)} \\ \sigma_y &= \frac{(1 - \nu)(E\varepsilon_y + \eta\dot{\varepsilon}_y) + \nu[E(\varepsilon_x + \varepsilon_z) + \eta(\dot{\varepsilon}_x + \dot{\varepsilon}_z)]}{(1 + \nu)(1 - 2\nu)} \\ \sigma_z &= \frac{(1 - \nu)(E\varepsilon_z + \eta\dot{\varepsilon}_z) + \nu[E(\varepsilon_x + \varepsilon_y) + \eta(\dot{\varepsilon}_x + \dot{\varepsilon}_y)]}{(1 + \nu)(1 - 2\nu)} \\ \tau_{xy} &= \frac{E\gamma_{xy} + \eta\dot{\gamma}_{xy}}{2(1 + \nu)} \\ \tau_{yz} &= \frac{E\gamma_{yz} + \eta\dot{\gamma}_{yz}}{2(1 + \nu)} \\ \tau_{zx} &= \frac{E\gamma_{zx} + \eta\dot{\gamma}_{zx}}{2(1 + \nu)} \end{aligned} \quad (38)$$

When x, y and z are the principal directions with respects to stress, Eqs (37) become:

$$\begin{aligned} E\varepsilon_1 + \eta\dot{\varepsilon}_1 &= \sigma_1 - \nu(\sigma_2 + \sigma_3) \\ E\varepsilon_2 + \eta\dot{\varepsilon}_2 &= \sigma_2 - \nu(\sigma_1 + \sigma_3) \\ E\varepsilon_3 + \eta\dot{\varepsilon}_3 &= \sigma_3 - \nu(\sigma_1 + \sigma_2) \\ E\gamma_{12} + \eta\dot{\gamma}_{12} &= 0 \\ E\gamma_{23} + \eta\dot{\gamma}_{23} &= 0 \\ E\gamma_{31} + \eta\dot{\gamma}_{31} &= 0 \end{aligned} \quad (39)$$

It means that, contrary to the stress-strain relations (4) in perfectly elastic solids, viscoelastic materials subjected to normal stress components may exhibit not only normal but also shear strain components (for instance after removal of a shear load).

Eqs (35) and (37) through (39) present the modified stress-strain relations in viscoelastic solids under triaxial load conditions. In what follows those in simpler load cases are listed.

Plane stress ( $\sigma_z = \tau_{yz} = \tau_{zx} = 0$ )

$$\begin{aligned} E\varepsilon_x + \eta\dot{\varepsilon}_x &= \sigma_x - \nu\sigma_y \\ E\varepsilon_y + \eta\dot{\varepsilon}_y &= \sigma_y - \nu\sigma_x \\ E\varepsilon_z + \eta\dot{\varepsilon}_z &= -\nu(\sigma_x + \sigma_y) \\ E\gamma_{xy} + \eta\dot{\gamma}_{xy} &= 2(1 + \nu)\tau_{xy} \\ E\gamma_{yz} + \eta\dot{\gamma}_{yz} &= 0 \\ E\gamma_{zx} + \eta\dot{\gamma}_{zx} &= 0 \end{aligned} \quad (40)$$

and

$$\begin{aligned} \sigma_x &= \frac{E\varepsilon_x + \eta\dot{\varepsilon}_x + \nu(E\varepsilon_y + \eta\dot{\varepsilon}_y)}{1 - \nu^2} \\ \sigma_y &= \frac{E\varepsilon_y + \eta\dot{\varepsilon}_y + \nu(E\varepsilon_x + \eta\dot{\varepsilon}_x)}{1 - \nu^2} \\ \tau_{xy} &= \frac{E\gamma_{xy} + \eta\dot{\gamma}_{xy}}{2(1 + \nu)} \end{aligned} \quad (41)$$

Plane stress ( $\varepsilon_z = \gamma_{yz} = \gamma_{zx} = 0$ )

$$\begin{aligned} E\varepsilon_x + \eta\dot{\varepsilon}_x &= (1 + \nu)[\sigma_x(1 - \nu) - \nu\sigma_y] \\ E\varepsilon_y + \eta\dot{\varepsilon}_y &= (1 + \nu)[\sigma_y(1 - \nu) - \nu\sigma_x] \\ E\gamma_{xy} + \eta\dot{\gamma}_{xy} &= 2(1 + \nu)\tau_{xy} \\ \text{and} \\ \sigma_x &= \frac{(1 - \nu)(E\varepsilon_x + \eta\dot{\varepsilon}_x) + \nu(E\varepsilon_y + \eta\dot{\varepsilon}_y)}{(1 + \nu)(1 - 2\nu)} \\ \sigma_y &= \frac{(1 - \nu)(E\varepsilon_y + \eta\dot{\varepsilon}_y) + \nu(E\varepsilon_x + \eta\dot{\varepsilon}_x)}{(1 + \nu)(1 - 2\nu)} \\ \sigma_z &= \frac{\nu[E(\varepsilon_x + \varepsilon_y) + \eta(\dot{\varepsilon}_x + \dot{\varepsilon}_y)]}{(1 + \nu)(1 - 2\nu)} = \nu(\sigma_x + \sigma_y) \\ \tau_{xy} &= \frac{E\gamma_{xy} + \eta\dot{\gamma}_{xy}}{2(1 + \nu)} \end{aligned} \quad (42)$$

### Uniaxial stress ( $\sigma_z \neq 0$ )

$$\begin{aligned} E\varepsilon_x + \eta\dot{\varepsilon}_x &= \sigma_x \\ E\varepsilon_y + \eta\dot{\varepsilon}_y &= -\nu\sigma_x \\ E\varepsilon_z + \eta\dot{\varepsilon}_z &= -\nu\sigma_x \\ E\gamma_{xy} + \eta\dot{\gamma}_{xy} &= 0 \\ E\gamma_{yz} + \eta\dot{\gamma}_{yz} &= 0 \\ E\gamma_{zx} + \eta\dot{\gamma}_{zx} &= 0 \end{aligned} \quad (44)$$

and

$$\sigma_x = E\varepsilon_x + \eta\dot{\varepsilon}_x \quad (45)$$

### Shear stress ( $\tau_{xy} \neq 0$ )

$$\begin{aligned} E\varepsilon_x + \eta\dot{\varepsilon}_x &= 0 \\ E\varepsilon_y + \eta\dot{\varepsilon}_y &= 0 \\ E\varepsilon_z + \eta\dot{\varepsilon}_z &= 0 \\ E\gamma_{xy} + \eta\dot{\gamma}_{xy} &= 2(1+\nu)\tau_{xy} \\ E\gamma_{yz} + \eta\dot{\gamma}_{yz} &= 0 \\ E\gamma_{zx} + \eta\dot{\gamma}_{zx} &= 0 \end{aligned} \quad (46)$$

and

$$\tau_{xy} = \frac{E\gamma_{xy} + \eta\dot{\gamma}_{xy}}{2(1+\nu)} \quad (47)$$

As it is seen, the two-parameter Kelvin-Voigt's model of viscoelastic materials leads to relatively simple stress-strain relations. The stress-strain relations based on the three-parameter model of viscoelastic materials (spring and Maxwell's model in parallel) are given in [11].

## CONCLUSIONS

- The Hooke's law for multiaxial stress in elastic solids has been modified to account for damping properties of real materials.
- The Kelvin-Voigt's model for viscoelastic materials has been applied to normal and shear strain components.
- The viscoelastic behaviour of a homogeneous, isotropic material at a given temperature is completely defined by Young modulus  $E$ , Poisson's ratio  $\nu$  and coefficient  $\eta$  of viscous damping of normal strain.
- The aforementioned constants can be determined in a uniaxial test.

○ It is shown that

$$\frac{\eta}{\lambda} = \frac{E}{G} = 2(1+\nu) \quad (48)$$

where  $G$  is the shear modulus and  $\lambda$  is the coefficient of viscous damping of shear strain.

## NOMENCLATURE

$E$	– Young modulus
$G$	– shear modulus
$t$	– time
$x, y, z$	– three mutually perpendicular directions
$\gamma$	– shear strain component
$\varepsilon$	– normal strain component
$\eta$	– coefficient of viscous damping of normal strain
$\lambda$	– coefficient of viscous damping of shear strain
$\nu$	– Poisson's ratio
$\sigma$	– normal stress
$\tau$	– shear stress
1, 2, 3	– principal directions

## BIBLIOGRAPHY

1. Lubahn J.D., Felgar R.P.: *Plasticity and Creep of Metals*. J. Wiley & Sons, New York, 1961
2. Nowacki W.: *Theory of Elasticity* (in Polish). PWN, Warszawa, 1971
3. Panovko J.G.: *Internal Friction at Vibrations of Elastic Systems* (in Russian). Fizmatgiz, Moscow, 1960
4. Giergiel J.: *Damping of Mechanical Vibrations* (in Polish). PWN, Warszawa, 1990
5. Nashif A.D., Johnes D.I.G., Henderson J.P.: *Vibration Damping*. J. Wiley & Sons, New York, 1985
6. Blake A. (Ed.): *Handbook of Mechanics, Materials, and Structures*. J. Wiley & Sons, New York, 1985
7. Jakubowicz A., Orłóś Z.: *Strength of Materials* (in Polish). WNT, Warszawa, 1996
8. Haslach H.W., Jr., Armstrong R.W.: *Deformable Bodies and Their Material Behaviour*. J. Wiley & Sons, 2004
9. Kuzmenko W.A.: *New schemes of deformation of solids* (in Russian). Izd. Naukova Dumka, Kiev, 1973
10. Nyashin Y., Likhov V., Kolenda J.: *On the stress-strain relations in viscoelastic solids*. Marine Technology Transactions, Vol. 18, 2007, to be printed
11. Pisarenko G. S., Lebedev A. A.: *Resistance of Materials to Deformation and Failure in Complex Stress State* (in Russian). Izd. Naukova Dumka, Kiev, 1969.

## CONTACT WITH THE AUTHOR

Prof. Janusz Kolenda  
Mechanic-Electric Faculty,  
Polish Naval Academy  
Śmidowicza 69  
81-103 Gdynia POLAND  
phone : +48 58 626 27 89

# Search for optimum geometry of selected steel sandwich panel joints

Karol Niklas, MS.c.  
Gdańsk University of Technology

## ABSTRACT



*Application of steel sandwich panels to ship structures requires many problems to be solved. Joints between the panels as well as those between the panels and other structures is one of the more difficult problems associated with the structures in question. This paper presents the searching for process of optimum geometry of a panel-to-panel joint of longitudinal arrangement, performed by means of the ANSYS software. A configuration was searched for of parameters which can ensure as-low-as possible values of geometrical stress concentration coefficients at acceptable mass and deformations of the structure. Analysis of the obtained results made it possible to propose the optimum geometry of the considered joint.*

**Keywords:** steel sandwich panels, connection, optimization

## INTRODUCTION

Ship structures are evolving with time. The need for increasing ship reliability, lifetime and safety results mainly from economic motivations. Along with increasing prices of steel and fuels, which exert high impact on decisions made in shipbuilding industry, one of the main impulses accelerating development of new, better structures is a tendency to make the shipbuilding time shorter and, at the same time, the time between its inspections and repairs longer. The pressure towards shortening the shipbuilding time is so high that shipyards have been transformed in sort of assembly factory of ship sections produced in smaller specialised cooperating plants. The next factor which is becoming more and more important in decision-making in the shipbuilding industry is ecological safety. The need for protection against ecological disasters provoked by ship accidents (collisions, groundings) was the main motivation for designing two-skin hulls. The development of the already existing structures is mainly done by evolution - structure improvement based on many-years' experience gained by the Classification Societies. In successive regulations higher and higher requirements are formulated (especially those concerning the ecology), with an intention to reduce the risk relating to ship operation. Along with the improvement of classical ship structure, the investigations are in progress over completely new structures which can be used as ship components. A list of these new structures includes steel sandwich panels, which reveal extremely favourable bending resistance and stiffness in relation to mass.

## STEEL SANDWICH PANELS

Briefly speaking, the sandwich panels are two-skin structures revealing favourable stiffness and bending resistance in relation to mass. A concept of multi-layer structures has been well known for years and is in common use in building of plastic watercraft (laminated-foam-laminated, for instance). Employing advantageous multi-layer structures in shipbuilding was stopped for decades by technological problems (deformations generated during welding of extremely thin plates to their stiffeners, among others). And only recently the development of laser welding technology has made it possible to produce steel sandwich panels (Fig. 1).

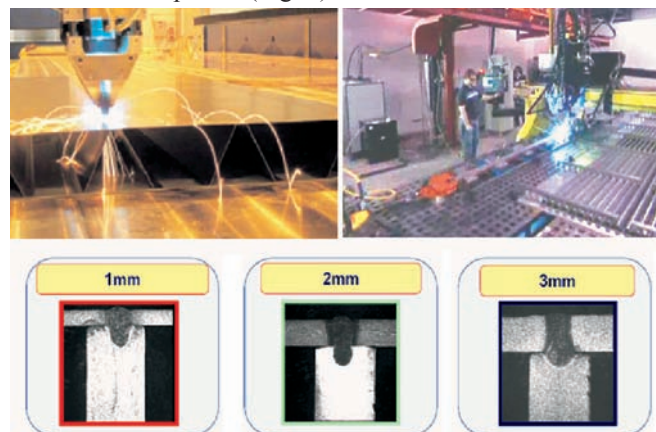


Fig. 1. Industrial production of steel sandwich panels [4]

The laser welding technology was introduced to the industry about ten years ago. The need, having its origin in economic motivations, to reduce the mass of the structure is so high that it compensates high costs of laser welding.

But before making full use of the advantages offered by the steel sandwich panels, some problems concerning their application are to be solved. In particular, problems which stop their use as carrying elements of a structure concern [1, 2, 3]:

- ★ strength
- ★ fatigue
- ★ fire and acoustic insulation
- ★ transmission of vibrations
- ★ reaction to dynamic and point loads
- ★ corrosion resistance

The use of sandwich panels in ship structures also requires analysing issues referring to the presence of cables and pipelines, communication holes, repairs of damages, operating control and utilisation. A separate group of problems, of high significance for the final shape of the structure, are joints between the panels, and between the panels and the classical structure.

## SELECTED PANEL JOINTS

Joints between panels or between a panel and the classical structure are difficult problems affecting practical application of the panels. Solving a number of minor problems concerning these joints is a basic condition for their future use as components of larger structures. There are a variety of types of joints, including, for instance, panel-panel or panel-classic structure joints, cross-joints, panel height reduction, and panel-support joint. One of more common constructional centres in the panel structure is the front panel-panel joint in longitudinal arrangement, in which the welds which link the panels are parallel to the direction of the stiffenings, see Fig. 2.

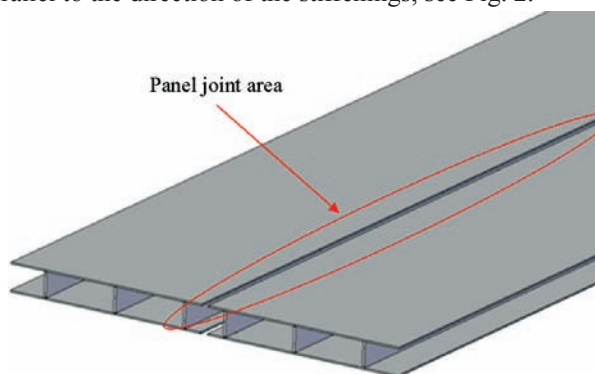


Fig. 2. Positions of I-core panels in longitudinal arrangement.

Numerous ways of execution of these joints are proposed. Sample (but not only possible) solutions are shown in Fig. 3. Individual proposals of these joints differ by mass, expected stiffness, cost, and time of execution. Within the framework of preliminary studies, two panel joints were selected for further examination from the point of view of technological realisability. In the assessment a number of factors were taken into account including: number of welds, preparing edges for welding, width of groove, assembly tolerance, ability to cut edges after fitting, fixing elements during the assembly, access to places be welded, smoothness of the joint, ability to prefabricate, and expected after-welding deformations. As a result, the joints which turned out most favourable from the point of view of technological realisability were those making use of cover plates and rectangular profiles, see Figs 3c and 3b.

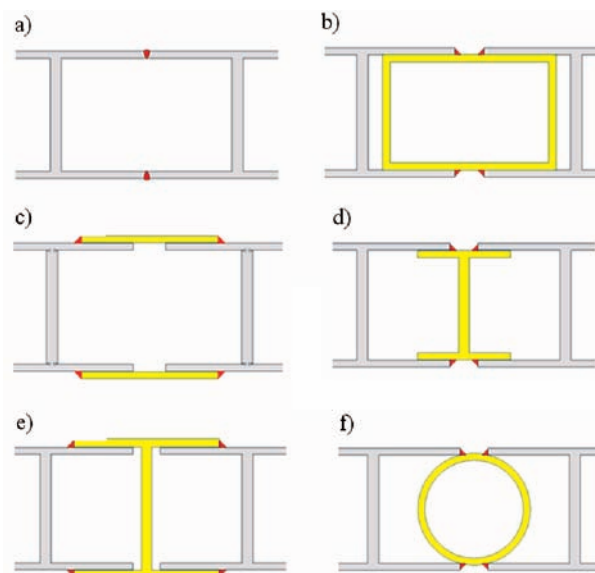


Fig. 3. Proposed joints

## SEARCH FOR OPTIMUM GEOMETRY OF THE SELECTED JOINTS

To assess strength-to-mass ratios of the selected joint geometries, reduced stresses were calculated, using the Finite Element Method (FEM), in the joints loaded with stretching and compressing forces acting in the direction perpendicular to the joint.

The geometry of the selected joints was described using parameters shown in Fig. 4, in which the adopted coordinate system and the symmetry plane are marked as well. It was assumed that the joined panels have the same geometry. Because of repeatability of the joint structures, the “distance from panel end to first stiffener” parameter takes the value of  $\frac{1}{4}$  or  $\frac{1}{2}$  of the distance between the stiffeners. The parametric description was formulated in order to search for such a configuration of parameters for which the joint reveals the lowest coefficient of geometric concentration at relatively small mass and deformation. The reduced Mises stresses were used as the measure of joint’s ability to carry the load (stretching or compressing force). The preferential criterion of joint evaluation was the stress, at an acceptable mass of the joint (up to 10% of panel mass). If, for some configurations of parameters, joints revealing similar stresses were obtained, the joint with smaller mass was selected. Two load conditions were assumed, which were stretching and compression in the panel plane.

## NUMERICAL MODELS OF THE JOINTS

The calculations were performed in ANSYS environment. The assumed symmetry of the geometry and load, Fig. 5, has made it possible to analyse  $\frac{1}{4}$  of the model, which considerably speeded up the calculations. To compensate possible effect of panel deflection on the operation of the joint, loads were applied at a distance equal to 2.5 distances between the stiffeners. Writing the geometry in the parametric form provided opportunities for performing a large series of calculations with changing combinations of parameters, without the necessity to build a new model for each combination. The modelling was done using the PLANE183 element – a plane solid-type element with the square shape function. The models had a carefully selected regular grid consisting of about 15 thousand elements. The side length of an individual element was approximately

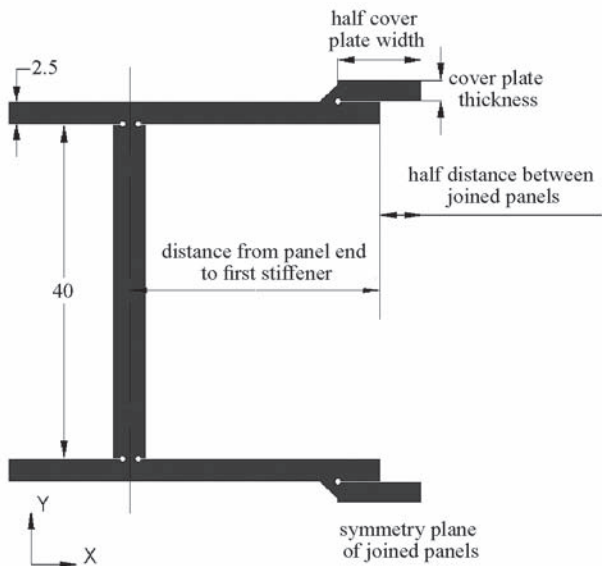
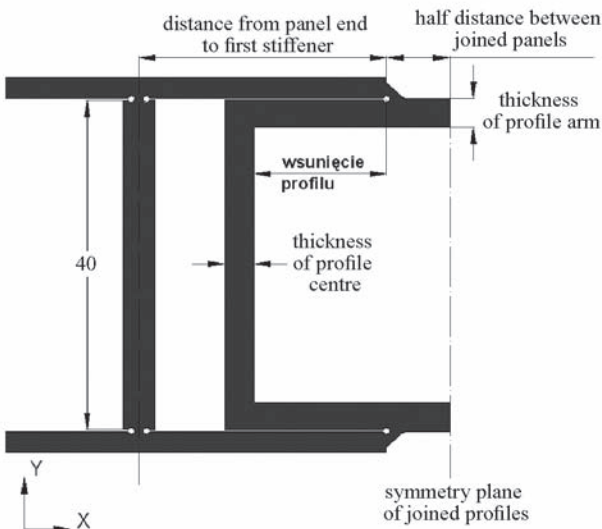


Fig. 4. Parameters describing the geometry of selected joints



equal to 0.1mm. The steel material constants were assumed for the isotropic model:  $E = 2e^5$  MPa and  $\nu = 0.3$ .

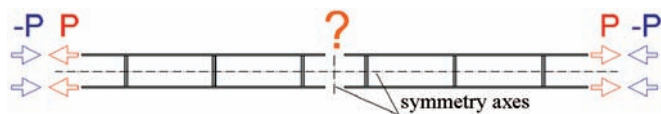


Fig. 5. Panel loaded with stretching force (P) and compressing force (-P).



Fig. 6. Calculation model with assumed boundary conditions.

A sample model of the joint is given in Fig. 6, along with the applied boundary conditions and load. During numerical modelling of sandwich type structures, the most difficult and the most questionable model elements are laser welds. The technology of welding the stiffeners to the plating assumes laser welding from outside. Specific nature of the laser-welded joints is the reason why some gaps form between the stiffeners and the plating (their dimension in the discussed panel structures can approximately reach 0.1mm). In the ending areas of the welds technological notches are localised, which, when geometrically

modelled in the numerical model, would lead to unrealistic, excessively high concentration of stresses [5, 6, 7, 8, 9]. For the computer model to reflect the real laser joints in a most realistic way, so-called circular concentrators are introduced to replace the welds in those places, see Fig. 7. These concentrators create geometric smoothing of the notches in the form of circles with specially selected dimensions and positions [8, 10, 11, 12]. Of extremely high importance in weld modelling is taking into account different nature of laser weld operation compared to a joint made using a traditional technology. The laser weld are characteristic of three operation stages [1]: 1 – rotation of the joined elements; 2 – contact of the plating with the stiffener; 3 – common displacement of the plating and the stiffener in the same direction, but with the load carried by a much smaller cross-section than in classically welded structures. In order to control the nature of weld operation, relevantly defined “contact regions” have been introduced at selected stiffener edges.

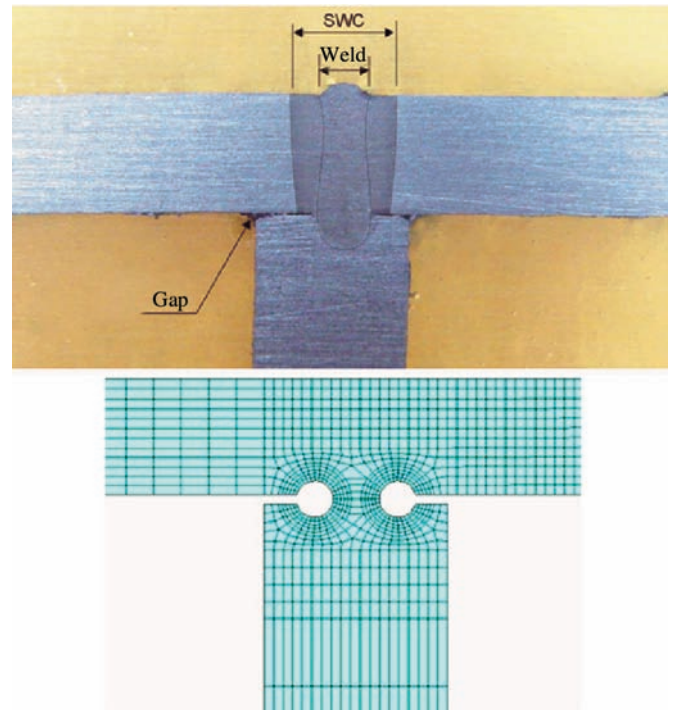


Fig. 7. Laser welded joint [1] and the FEM model.

## RESULTS

To make the interpretation easier, the results of calculations are presented in the form of diagrams. In these diagrams the vertical axis represents the geometric concentration coefficient  $K_g$ , calculated as the ratio of the maximum of the reduced Mises stress to the nominal stress. On the horizontal axes, different variable parameters describing the geometry of the joints are shown. Each configuration of parameters is represented by one point in the diagram. A huge volume of results has made it possible to build a surface which illustrates the effect of particular parameters on stress concentration. These surfaces were smoothed using the distance-weighted smallest square method, for which the calculations were done by the code “Statistica”. The data discussed in the article solely refer to stresses.

Fig. 8 presents the results concerning the joint making use of cover plates. When increasing the “half cover plate width” parameter the stress concentration decreases and reaches a local minimum for 20-30mm. Further increasing of the plate width results in stress increase by about 40% in the vicinity of the first stiffener. Within the parameter range of 10-40 mm the

deformations in the y-axis direction increase for stretching load and decrease for compression. When the width of the cover plate exceeds the distance to the first stiffener (40-50 mm), the Mises stresses rapidly decrease. Deformations in the y-axis direction within this range decrease for the cover plate thickness of 2.5 and 3 mm, and reach a local minimum for 50 mm, but increase for the cover plate thickness of 2 mm. More detailed analysis of the effect of particular parameters on stress and deformation of the joint has made it possible to select the most favourable configuration of parameters. The optimal configuration of parameters for the panel joints having the “distance from panel end to first stiffener” parameter equal to  $\frac{1}{4}$  turned out to be the joint with the cover plate thickness equal to 2.5 mm and the parameter “half cover plate width” equal to 50 mm.

Diagram of geometric concentration stress coefficient  $K_g$  for cover plate panel joint with the distance from panel end to first stiffener equal to  $\frac{1}{4}$

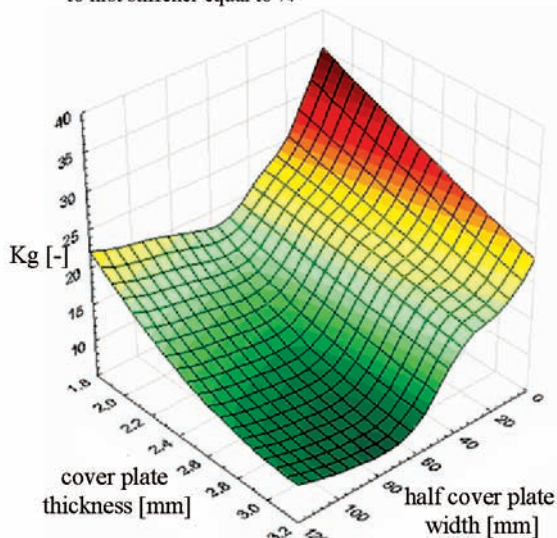


Diagram of geometric concentration stress coefficient  $K_g$  for cover plate panel joint with the distance from panel end to first stiffener equal to  $\frac{1}{2}$

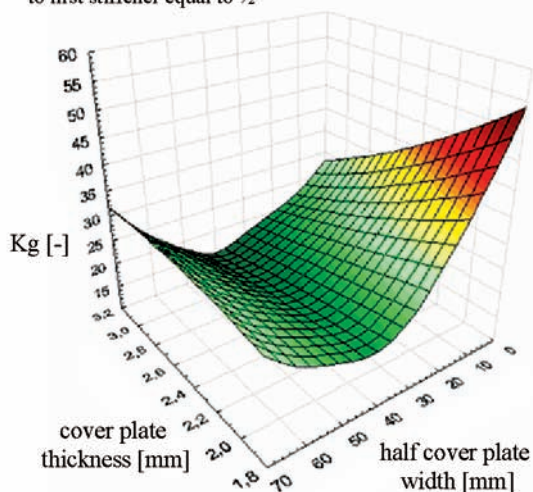


Fig. 8. Geometric concentration coefficient as a function of geometric parameters of the cover plate joint - stretching

For the cover plate panel joints with the “distance from panel end to first stiffener” parameter equal to  $\frac{1}{2}$ , the maximal values of the reduced Mises stresses their reach minima in the vicinity of the parameter value equal to 40 mm for all cover plate thickness cases when changing the “half cover plate width” parameter. Largest deformations are observed for the parameter equal to 30 mm when compressing. When compared to the  $\frac{1}{4}$  case, panel joints with the “distance from panel end to

first stiffener” parameter equal to  $\frac{1}{2}$  reveal five times as large deformations in the y-axis direction during compression, at a comparable level of the maximum Mises stresses. The optimal configuration of parameters of the analysed joint is the cover plate joint with cover plate thickness equal to 3 mm and the “half cover plate width” parameter equal to 40 mm.

Diagram of geometric concentration stress coefficient  $K_g$  for rectangular profile panel joint with the distance from panel end to first stiffener equal to  $\frac{1}{4}$

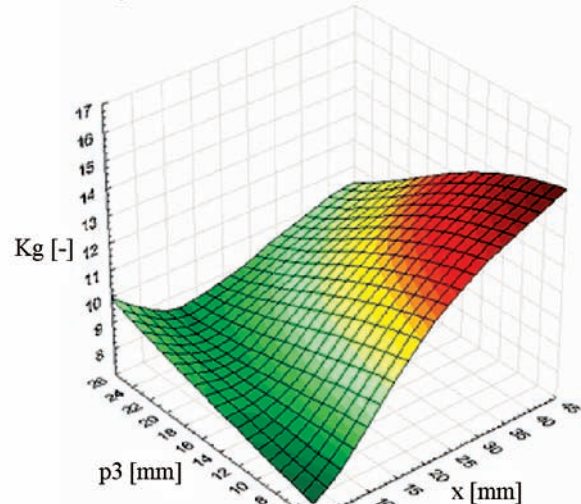


Diagram of geometric concentration stress coefficient  $K_g$  for cover plate panel joint with the distance from panel end to first stiffener equal to  $\frac{1}{4}$ .  $K_g[-]$  = distance weighted smallest square smoothing

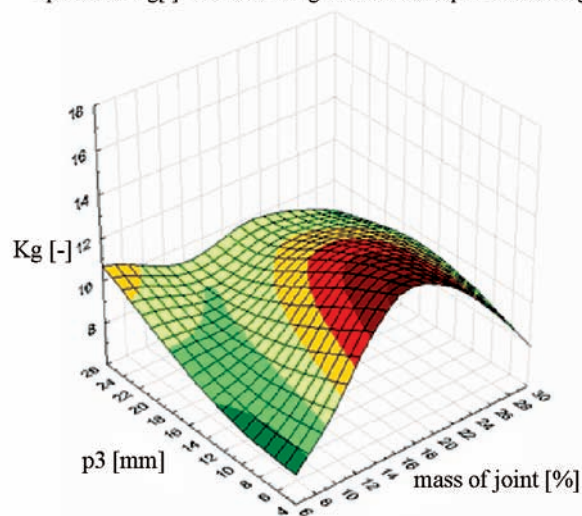


Fig. 9. Geometric concentration coefficient as a function of geometric parameters and mass of the rectangular profile joint - stretching

For rectangular profile panel joints with the “distance from panel end to first stiffener” parameter equal to  $\frac{1}{4}$ , the maximal values of the reduced Mises stresses and deformations in the y-axis direction depend much less on whether the joint is stretched or compresses than it was observed for the cover plate joints, Fig. 9. For small values of parameter  $p_3$  (profile insertion) the difference between deformations in the x-axis and y-axis directions are visibly smaller than for the cover plate joints, but when the profile insertion increases these differences also increase (still remaining much smaller than for the cover plate joints). After comparing stresses and corresponding masses of particular joints we can see that for the same mass the maximum reduced Mises stresses change nearly by twice when changing the parameters. Also at the same stress level, changing parameters can result in mass change by as much as 20%. The optimum configuration of parameters is a joint with the gap

$x = 3.25$  mm, profile thickness equal to 3 mm and profile insertion equal to 5 mm. This joint reveals the lower stress level at the mass equal to 9% of panel mass. Moreover, the deformations for these parameters also are the smallest.

Diagram of geometric concentration stress coefficient  $K_g$  for rectangular profile panel joint with the distance from panel end to first stiffener equal to  $\frac{1}{2}$ . Distance weighted smallest square smoothing

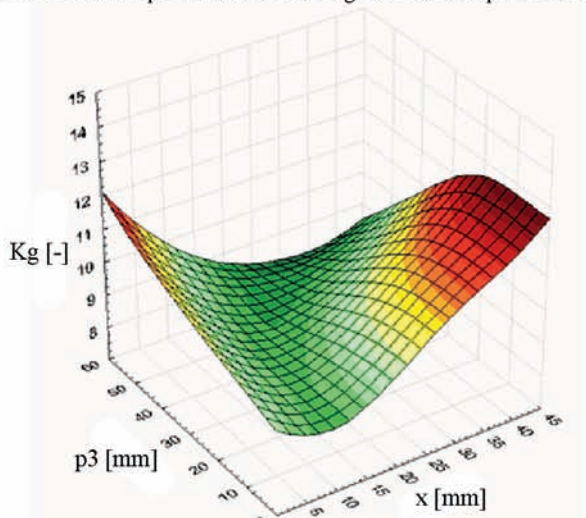


Diagram of geometric concentration stress coefficient  $K_g$  for cover plate panel joint with the distance from panel end to first stiffener equal to  $\frac{1}{4}$ . Distance weighted smallest square smoothing

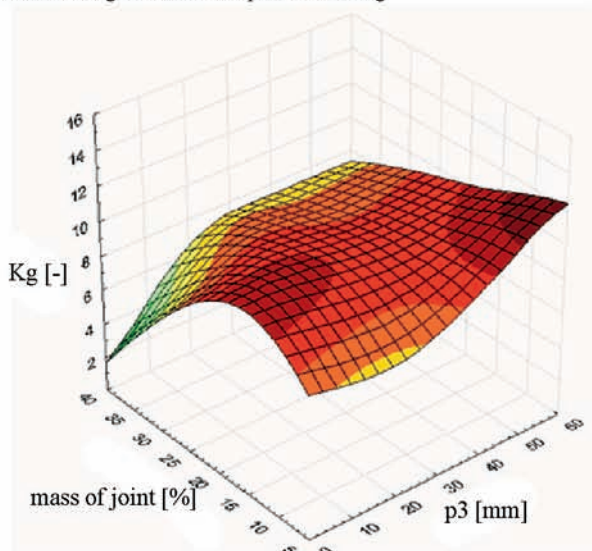


Fig. 10. Geometric concentration coefficient as a function of geometric parameters and mass of the rectangular profile joint - stretching

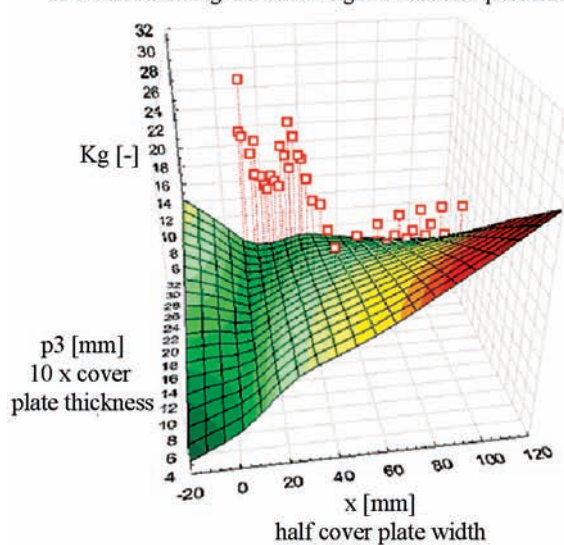
The results obtained for the rectangular profile panel joints with the “distance from panel end to first stiffener” parameter equal to  $\frac{1}{2}$  are given in Fig. 10. The optimal configuration of parameters is the joint with the gap  $x = 5$  mm between the joined panels, profile thickness equal to 2.5 mm and profile insertion equal to 5 mm. This joint reveals the lower stress level at the mass of joint equal to 8% of the panel mass.

The analysis of the above results makes it possible to formulate some summarising conclusions and compare the two examined types of joint: the cover plate joint and the rectangular profile joint, Fig. 11.

The cover plate panel joint reveals much higher geometric concentration coefficients. Although it has solution intervals characterised by much smaller mass, maximum stresses in those intervals reach several times as high levels as those observed in the rectangular profile joints. Also the maximum deformations are much smaller for the rectangular profile joints. To sum up,

at comparable masses of the both joints (within the ranges of their optimal parameters) the rectangular profile joint secures much lower stresses and deformations, in particular in the y-axis direction.

Comparison diagram of cover plate and rectangular profile joints. Panel joints with the distance from panel end to first stiffener equal to  $\frac{1}{4}$  for stretching. Distance weighted smallest square smoothing



Comparison diagram of cover plate and rectangular profile joints. Panel joints with the distance from panel end to first stiffener equal to  $\frac{1}{2}$  for stretching. Distance weighted smallest square smoothing

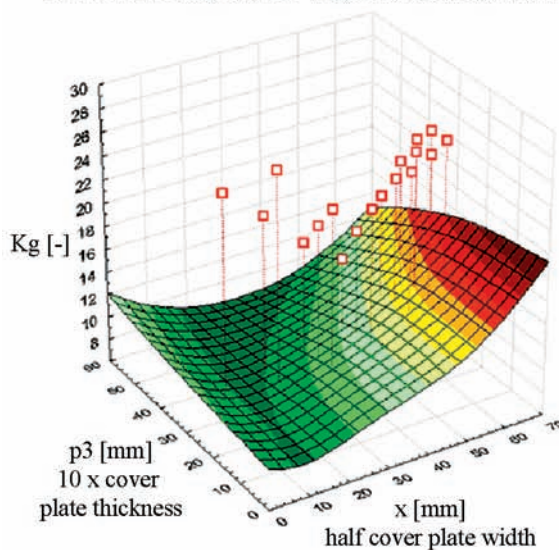


Fig. 11. Comparing the cover plate joint (points) and the rectangular profile joint (surface)

The final solution of the panel-panel heading joints in longitudinal arrangement is the rectangular profile joint shown in Fig. 12.

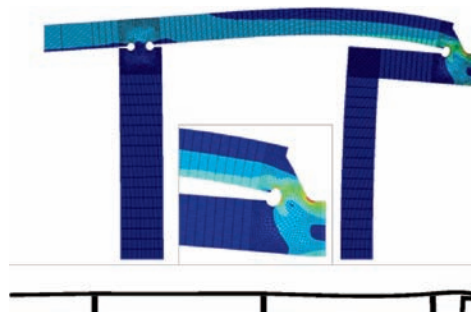


Fig. 12. Patterns of reduced Mises stresses and deformations (in 600:1 scale) for the optimum design (compression).

## SUMMARY AND CONCLUSIONS

- The development of ship structures, dictated by strong economic factors, leads to better and better solutions. At the same time, concepts are formulated to replace fragments of classical ship structure by new-type elements. New solutions which can lead to remarkable reduction in mass and production time of the ship are steel sandwich panels. At present they cannot be used as ship bearers, because of the lack of relevant regulations of Classification Societies. But the economic pressure is so high that it forces increasing the use of panels in ship constructions. The panels are used for building between-decks, systems of ramps, decks of river vessels, balconies on passenger ships, stairways, and/or partition walls. Shipyards are becoming more and more similar to assembly factories using prefabricated elements produced by smaller specialised plants. This approach considerably reduces costs and, what is more important, the production time, which for numerous shipyards may be a decisive factor on the present-day competing market.
- Certainly, new solutions bring new problems, which also are to be solved for the steel sandwich panels. One of basic problems refers to the joints between the panels, and between the panels and the classical ship structure. Statistically, the most frequently used type of joint is the panel-panel heading joint in the longitudinal arrangement. From among frequently proposed solutions of this joint two types were selected taking into account technological realisability, which were the cover plate joint and the rectangular profile joint. Parametric models were worked out for these two joints. A solution was searched which would secure relatively low coefficients of geometric concentration at small mass and acceptable deformation. The analysis of the obtained results made it possible to suggest the optimum joint geometry.
- Steel sandwich panels seem to grow in importance. They are likely to take a special place in the production of mega-yachts, the demand for which is enormously high, as their production making use of plastics is highly uneconomical.

## BIBLIOGRAPHY

1. Janusz Kozak: *Problems in assessing selected strength characteristics of steel two-skin ship structures*. Publishers of the Gdansk University of Technology, Gdańsk 2005, (in Polish)
2. Romanoff J., Kujala P.: *The Optimum Design for Steel Sandwich Panels Filled with Polymeric Foams*. Proc. of 6th Int. Conf. on Fast Sea Transportation, Vol. 3, Southampton, 2001
3. Noury P., Hayman B., McGeorge D., Weitzenbock J.: *Lightweight Construction for Advanced Shipbuilding – Recent Development*. DNV internal report, 2002
4. Internet: <http://sandwich.balport.com>, <http://www.plsystems.us>, <http://www.visotekinc.com>, <http://sandwich.balport.com>, <http://akseli.tekes.fi>
5. Report No 01 on test of steel SANDWICH panels. Project: *Application of Steel Sandwich Panels into Ship Structure EUREKA E! 3074 (ASPIS)*. Gdansk University of Technology, Faculty of Ocean Engineering and Ship Technology, Internal report No. 01/2004, 2004, (in Polish)
6. Report No. 07 on tests of steel SANDWICH panels. Project: *Application of Steel Sandwich Panels into Ship Structure EUREKA E! 3074 (ASPIS)*. Gdansk University of Technology, Faculty of Ocean Engineering and Ship Technology, Internal report No. 07/2004, 2004 (in Polish).
7. Synthesis report test results. Project: *Advanced Steel Sandwich Structures, Vth EC Framework Program SANDWICH*, Internal report D44, 2003
8. *Sandwich design principles and prototype designs*, Pentti Kujala, internal/ confidential document.
9. Kozak J.: *Strength Tests of Steel Sandwich Panel*. PRADS 2004
10. Kujala P., Klanac A.: *Analytical and Numerical Analyses of All Steel Sandwich Panels Under Uniform Pressure Load*. Design 2002, Vol. 2, Dubrovnik, 2002
11. Allen H.G.: *The analysis and design of structural sandwich panels*. Pergamon Press, 1969
12. *FEM analysis of a single SANDWICH panel*. Project ASPIS - EUREKA E!3074 (in Polish). Gdansk University of Technology, Faculty of Ocean Engineering and Ship Technology, Internal report, 2004.

### CONTACT WITH THE AUTHOR

Karol Niklas, MS.c.  
Faculty of Ocean Engineering  
and Ship Technology  
Gdansk University of Technology  
Narutowicza 11/12  
80-952 Gdansk, POLAND  
e-mail: k.niklas@pg.gda.pl

# A new continuous model for flexural vibration analysis of a cracked beam

M. Behzad, A. Ebrahimi, A. Meghdari  
Sharif University of Technology

## ABSTRACT

*In this paper a new continuous model for vibration analysis of a beam with an open edge crack is presented. A quasi-linear displacement field is suggested for the beam and the strain and stress fields are calculated. The equation of motion of the beam is calculated using the Hamilton principle. The calculated equation of motion is solved with a modified weighted residual method and the natural frequencies and mode shapes are obtained. The results are compared with those obtained by finite element method and an excellent agreement has been observed. The presented model is a simple and accurate method for analysis of the cracked beam behavior near or far from the crack tip.*

**Keywords:** vibration, crack, beam, natural frequency, mode shape, weighted residual

## INTRODUCTION

Fatigue and cracks are important subjects in industrial machineries which can lead to catastrophic failures in certain conditions. The importance of the early detection of the cracks takes researchers to study various aspects of the behavior of a structure defected by cracks. One of these aspects is the vibration of cracked structures. Crack development in a system changes the vibration behavior. With measurement and analysis of these vibrations the cracks can be identified well in advance and appropriate actions can be taken to prevent more damage to the system.

The vibration behavior of cracked structures has been investigated by many researchers. Dimarogonas presented a review on the topic of vibration of cracked structures [1]. His review contains vibration of cracked rotors, bars, beams, plates, pipes, blades and shells. Two more literature reviews are also available on the dynamic behavior of cracked rotors by Wauer and Gasch [2, 3].

Cracked beam is one of the structural elements which has been studied by researchers. There exist three methods for vibration modeling of cracked beams: discrete models with local flexibility model for crack, continuous models with local flexibility model for crack and continuous models with continuous model for crack.

For the first time, Dimarogonas suggested the local flexibility method for modeling the crack [4]. He assumed the crack to be a rotational spring between two healthy parts of the beam. The stiffness of this spring obtained from the concept of J-integral in fracture mechanics. This local flexibility idea has

been followed by several researchers till now. Some researchers modeled two healthy half beams discretely and added the flexibility of the rotational spring to the flexibility matrix of the system [5,6]. While others modeled two healthy half beams continuously and used appropriate boundary conditions for each part to link them through the rotational spring [7,8]. Some other researchers are tried to modify and improve the local flexibility model of the crack by adding one or two linear springs beside the rotational one [9]. These methods have also been extended for beams with more than one crack [10-12]. The local flexibility model for the crack is a simple approach and has a relative good result in finding fundamental natural frequency of a cracked beam. However this method offers no solutions for finding the stress at the crack area under the dynamic loads, mode shapes in free vibrations and operational deformed shape in forced vibrations.

Another approach to vibration analysis of cracked beams is continuous modeling of the crack. Christides and Barr developed a continuous theory for vibration of a uniform Euler-Bernoulli beam containing one or more pairs of symmetric cracks [13]. They suggested some modifications on the familiar stress field of a normal Euler-Bernoulli beam in order to consider the crack effect. The differential equation of motion and corresponding boundary conditions are given as the results. However in their model two different and incompatible assumptions have been made for displacement and strain fields. Although the accuracy of the results in finding the natural frequencies is acceptable for some applications their model is not still reliable for more accurate analyses such as stress analysis near the crack tip under dynamic loading and mode shape analysis. In addition the

resulted partial differential equation is complex and dependent on some constants which are unknown and must be calculated by correlating the analytically obtained results with those calculated by finite element in each case. Several researchers followed the Christides and Barr approach by modifying their method and gained some improvements [14-18]. However there still exists the inconsistency between strain and displacement fields which causes inaccuracy of the results especially in mode shapes and stress analysis.

In this paper a new continuous approach for vibration analysis of cracked beams has been presented. The crack is assumed to be an open edge crack. A bilinear displacement field has been suggested for the cracked beam and the strain and stress fields have been calculated. The differential equation of motion of the cracked beam has been obtained using the Hamilton principle. This partial differential equation has been solved with special numerical algorithm based on Galerkin projection method. The required constant needed in this model can be obtained using fracture mechanics. The results of this study are compared with the finite element results for verification.

## MAIN IDEA AND ASSUMPTIONS

The basic assumption in the Euler-Bernoulli bending theory for beams is that the plane sections of beam which are perpendicular to the neutral axis remain plane and perpendicular to the neutral axis after deformation. In the presence of an edge crack, the planes will not remain plane after deformation particularly at the vicinity of the crack due to a shear stress near the crack tip which leads to warping in plane sections. Thus at the vicinity of the crack the displacement field is completely nonlinear. For the planes far from the crack tip, the warping will be smaller and the displacement field can be assumed linear. In order to have a better sense of the bending in a cracked beam, a real model has been produced in this research and the mid span crack behavior under a pure bending moment can be seen in Fig. 1. The beam is made from a linear elastic material with low modulus of elasticity and a U-shape notch at the mid-span as a crack.

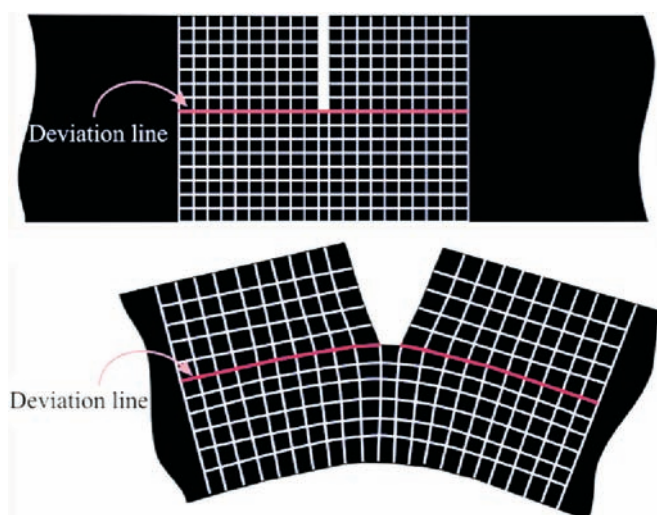


Fig. 1. A linear elastic cracked beam subjected to pure bending

Near the crack area the plane sections will no longer remain plane. With a good approximation it can be supposed that each plane section turns into two straight planes after deformation. The horizontal line passing through the crack tip is called “deviation line” in this research which is shown in Fig. 1. Each straight plane section turns into two planes with

different slopes one beneath and the other above the deviation line. The slope difference between these two planes decreases while the distance from the crack increases. These two straight planes connect to each other through a nonlinear part near the deviation line.

In order to find the stress, strain and deformation functions for a cracked beam in flexural vibrations a bilinear displacement field for the beam has been suggested in this research. In fact it is assumed that each plane section turns into two straight planes after deformation. The essential assumptions used in this research can be listed as follows:

- ★ the beam is slender and prismatic
- ★ the crack is considered to be an open edge notch
- ★ the deformations are supposed to be small
- ★ the plane strain assumption has been used in this research. Consequently the displacements along y-axis have been neglected
- ★ the stresses are small enough and the crack does not grow.

## DISPLACEMENT FIELD

On the base of the above assumptions and explanations, the following displacement field is introduced for a cracked beam in flexural vibrations:

$$\begin{cases} w = w(x, t) \\ v = 0 \\ u(x, z, t) = u_0(x, t) - z\psi(x, t) + \Delta(x, z, t)h(z) \end{cases} \quad (1)$$

In which  $u$ ,  $v$ ,  $w$  are the displacement components along  $x$ ,  $y$  and  $z$  axes.  $u_0(x, t)$  is the longitudinal displacement of the deviation line along the  $x$ -axis and  $\psi(x, t)$  is the slope of the plane sections below the deviation line. In an Euler-Bernoulli beam theory by neglecting the shear stress effect one has  $\psi(x, t) = w_x(x, t)$ . In a cracked beam the shear stress near the crack tip cannot be ignored thus  $\psi(x, t)$  is different from  $w_x(x, t)$ . However far from the crack the shearing stress decreases gradually and  $\psi(x, t)$  tends to be equal to  $w_x(x, t)$   $h(z)$  is the unit step function which is equal to zero for  $z \leq 0$  and 1 for  $z > 0$ . Accordingly the term  $w_x(x, t)h(z)$  can be considered as the extra displacement of the plane sections above the deviation line. Fig. 2 shows these parameters graphically.

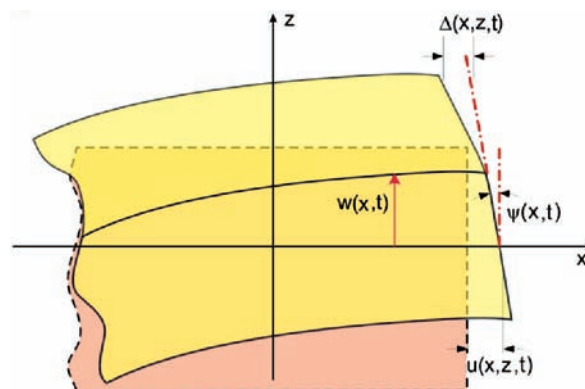


Fig. 2. Deformation field definition of a cracked beam

The additional displacement of the plane section above the deviation line has its maximum value at the crack faces and decreases gradually with distance from the crack tip. This additional displacement is a nonlinear and complex variable with respect to  $x$ . Here in this research an exponential regime has been assumed for the function  $\Delta(x, z, t)$  along the  $x$ -axis as follows:

$$\Delta(x, z, t) = \varphi(z, t) \cdot e^{-\alpha \frac{|x-x_c|}{d}} \operatorname{sgn}(x-x_c) \quad (2)$$

In equation (2)  $\alpha$  is a dimensionless exponential decay rate which will be obtained later in this paper,  $x_c$  is the crack position,  $d$  is the depth of the beam and  $\operatorname{sgn}(x-x_c)$  is the sign function which is -1 for  $x < x_c$  and +1 for  $x > x_c$ . The application of sign function is due to the fact that the additional displacement function has a discontinuity at the position of the crack and the sign of its value changes when passing through the crack tip.

In order to find  $\varphi(x, t)$ , zero normal stress condition at the crack faces can be used. The normal strain function can be found using equation (2):

$$\varepsilon_x = u_{,x} = u_{0,x} - z\psi_{,x} - \frac{\alpha}{d} \varphi(z, t) e^{-\alpha \frac{|x-x_c|}{d}} h(z) \quad (3)$$

In which the subscript  $,x$  denotes the partial derivative with respect to  $x$ . The normal stress at the crack faces should be zero so one has:

$$\varphi(z, t) = \frac{d}{\alpha} (u_{0,x}(x_c, t) - z\psi_{,x}(x_c, t)) \quad (4)$$

To avoid discontinuity at the crack tip and considering the nonlinearity at the crack tip, the function  $\varphi(x, t)$  is modified in this paper as follows:

$$\varphi(z, t) = \frac{d}{\alpha} \left( u_{0,x}(x_c, t) - u_{0,x}(x_c, t) e^{-\beta \frac{z}{d}} - z\psi_{,x}(x_c, t) \right) \quad (5)$$

In equation (5)  $\beta$  is a dimensionless parameter and will be discussed later in this paper.

### EQUATION OF MOTION

Now the strain field can be extracted from the displacement field. The only nonzero components of the stress field are  $\varepsilon_x$  and  $\gamma_{xy}$  as follows:

$$\begin{cases} \varepsilon_x = u_{,x} = u_{0,x} - z\psi_{,x} - \left( u_{0,x}(x_c, t) - u_{0,x}(x_c, t) e^{-\beta \frac{z}{d}} - z\psi_{,x}(x_c, t) \right) h(z) e^{-\alpha \frac{|x-x_c|}{d}} \\ \gamma_{xy} = \frac{1}{2} (w_{,x} + u_{,z}) = \frac{1}{2} \left( w_{,x} - \psi + \left( \frac{\beta}{\alpha} u_{0,x}(x_c, t) e^{-\beta \frac{z}{d}} - \frac{d}{\alpha} \psi_{,x}(x_c, t) \right) e^{-\alpha \frac{|x-x_c|}{d}} \operatorname{sgn}(x-x_c) \right) \end{cases} \quad (6)$$

The normal stress energy of the beam can be obtained using the following relation:

$$V = \frac{1}{2} \int_V \sigma_{xx} \varepsilon_{xx} dV = \frac{1}{2} E \int_V \varepsilon_{xx}^2 dV \quad (7)$$

In which  $V$  is the normal strain energy function,  $V$  is the volume of the beam and  $E$  is the modulus of elasticity.

In this research the cracked beam is assumed to be slender. So the Euler-Bernoulli assumption can be used and one can neglect the shear strain energy in compare with the normal strain energy. Similar to a normal Euler-Bernoulli beam the average shear strain in each cross section can be assumed to be zero. So the following relation can be hold:

$$\int_A \gamma_{xy} dA = 0 \quad (8)$$

The kinetic energy of the cracked beam can be also calculated as follows:

$$T = \frac{1}{2} \int_V \rho w_{,t}^2 dV \quad (9)$$

In equation (9) similar to the Euler-Bernoulli beam theory the rotational moment of inertia has been neglected. Using the Hamilton principle one has:

$$\delta \int_{t_0}^{t_1} (T - V) dt = 0 \quad (10)$$

Now using equations (6) to (10) and performing appropriate calculations the following equations can be obtained:

$$\begin{cases} u_{0,x} = \bar{z} \psi_{,x} + k_3 \bar{z}_h \psi_{,x}(x_c, t) e^{-\alpha \frac{|x-x_c|}{d}} \\ \psi_{,x} = w_{,xx} + k_5 w_{,xx}(x_c, t) e^{-\alpha \frac{|x-x_c|}{d}} \end{cases} \quad (11)$$

In equation (11)  $\bar{z}$  is the vertical coordinate of the centroid of the cross section and  $\bar{z}_h$  is the vertical coordinate of the centroid of the healthy part of the cross section as shown in Fig. 3. The parameters  $k_3$  and  $k_5$  are geometrical dimensionless constants defined in equation (13).

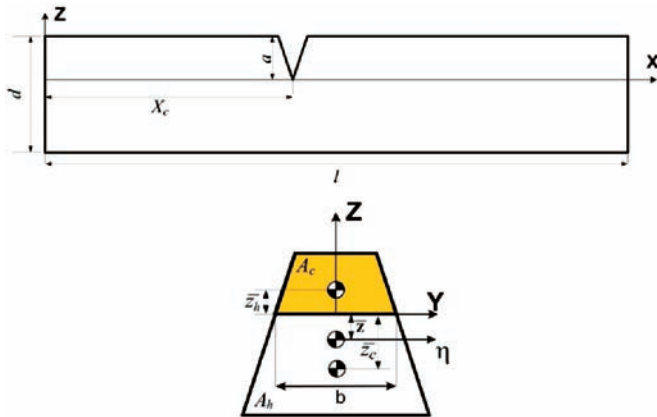


Fig. 3. A cracked beam parameter definition

And finally the equation of motion for free vibrations of a cracked slender beam can be obtained as follows:

$$\frac{\partial^2}{\partial x^2} EI_\eta \left( w_{,xx} + \kappa w_{,xx}(x_c, t) e^{-\alpha \frac{|x-x_c|}{d}} \right) + \rho A w_{,tt} = 0 \quad (12)$$

In equations (11) and (12) the parameters  $k_{1-6}$  and  $\kappa$  are geometrical dimensionless constants which can be defined as follows:

$$\left\{ \begin{aligned} k_1 &= \frac{1}{A_c} \int_{A_c} e^{-\beta \frac{z}{d}} dA \\ k_2 &= \frac{A_h}{A_h + k_1 A_c} \\ k_3 &= \frac{A_c}{A} \left( k_2 - k_1 k_2 - \frac{\bar{z}_c}{\bar{z}_h} \right) \\ k_4 &= \frac{Ad}{A_h d + \beta k_1 k_2 \bar{z}_h A_c} \\ k_5 &= \frac{A_c}{A} k_4 \left( 1 - \frac{\beta}{d} k_1 k_2 \bar{z}_h \right) \\ k_6 &= \frac{1}{A_c \bar{z}_c} \int_{A_c} z e^{-\beta \frac{z}{d}} dA \\ \kappa &= k_5 - \frac{k_3 k_4 A \bar{z}_c \bar{z}_h}{I_\eta} + \frac{k_4}{I_\eta} \left( k_2 A_c \bar{z}_c \bar{z}_h (1 - k_6) - I_{c_y} \right) \end{aligned} \right. \quad (13)$$

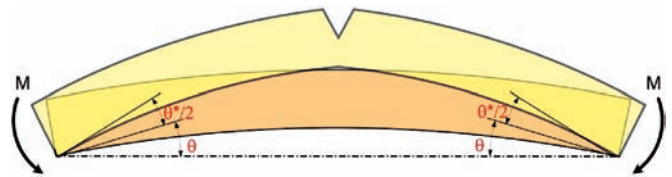
Where  $A$  is the cross section area of the beam,  $A_c$  is the area of the crack face,  $I_{c_y}$  is the moment of inertia of the crack face about  $y$ -axis and  $I_\eta$  is the moment of inertia of the cross section about the horizontal axis passing through the centroid of the cross section  $\eta$ .

The equation (12) is the main result of this investigation. In a normal beam the geometrical parameter  $\kappa$  is zero and hence equation (12) results in the Euler-Bernoulli beam equation for slender beams. The dimensionless exponential decay rates

$(\alpha, \beta)$  are the only factors which has not been discussed yet. In the next section the parameters  $\alpha$  and  $\beta$  are calculated.

## EXPONENTIAL DECAY RATES $\alpha$ AND $\beta$ CALCULATION

When a pair of bending moments  $M$  are applied to the



cracked beam an additional relative rotation  $\theta^*$  will exist between two ends of the beam due to the crack as shown in Fig. 4.

Fig. 4. Additional remote point rotation of a cracked beam

It can be shown that for a cracked beam under pure bending equation (12) will turn into the following form:

$$\frac{d^2 w}{dx^2} = \frac{M}{EI_\eta} \left( 1 - \frac{\kappa}{1 + \kappa} e^{-\alpha \frac{|x-x_c|}{d}} \right) \quad (14)$$

Solving equation (14) will result in the load-deflection relation of a cracked beam under static pure bending. The results are as follows:

$$w = \begin{cases} \frac{M}{EI_\eta} \left( \frac{x^2}{2} + c_1 x + c_2 - \frac{d^2}{\alpha^2} \cdot \frac{\kappa}{1 + \kappa} e^{\alpha \frac{x-x_c}{d}} \right) & x \leq x_c \\ \frac{M}{EI_\eta} \left( \frac{x^2}{2} + c_3 x + c_4 - \frac{d^2}{\alpha^2} \cdot \frac{\kappa}{1 + \kappa} e^{-\alpha \frac{x-x_c}{d}} \right) & x > x_c \end{cases} \quad (15)$$

In which the constants  $c_1, c_2, c_3$  and  $c_4$  will be as follows:

$$\left\{ \begin{aligned} c_2 &= \frac{d^2}{\alpha^2} \cdot \frac{\kappa}{1 + \kappa} e^{-\alpha \frac{x_c}{d}} \\ c_4 &= c_2 + 2x_c \frac{d}{\alpha} \cdot \frac{\kappa}{1 + \kappa} \\ c_3 &= -\frac{l}{2} - \frac{c_4}{l} + \frac{1}{l} \cdot \frac{d^2}{\alpha^2} \cdot \frac{\kappa}{1 + \kappa} e^{-\alpha \frac{l-x_c}{d}} \\ c_1 &= c_3 + 2 \frac{d}{\alpha} \cdot \frac{\kappa}{1 + \kappa} \end{aligned} \right. \quad (16)$$

Now using equation (15) one can obtain the additional remote point rotation  $\theta^*$  as follows:

$$\begin{aligned} \theta^* &= (\theta_{cracked}(0) - \theta(0)) - (\theta_{cracked}(l) - \theta(l)) = \\ &= -\frac{2M}{EI_\eta} \frac{d}{\alpha} \cdot \frac{\kappa}{1 + \kappa} \end{aligned} \quad (17)$$

In equation (17) the parameter  $\kappa$  is a function of  $\beta$ . However comparing the finite element results with those obtained by this model shows that the parameter  $\beta$  has a very large value and accordingly it can be assumed that the parameter  $\beta$  is infinity. So in equation (17) one can substitute  $\kappa$  with  $\lim_{\beta \rightarrow \infty} \kappa$ .

On the other hand the additional remote point rotation  $\theta^*$  has been obtained by empirical methods as follows [19]:

$$\theta^* = \frac{2Md}{E(1-\nu^2)I_\eta} \left( \frac{a}{d} \right)^2 \left( 5.93 - 19.69 \left( \frac{a}{d} \right) + 37.1 \left( \frac{a}{d} \right)^2 - 35.8 \left( \frac{a}{d} \right)^3 + 13.1 \left( \frac{a}{d} \right)^4 \right) \quad (18)$$

Equating the right hand sides of (17) and (18) will result in parameter  $\alpha$  values as presented in Fig. 5.

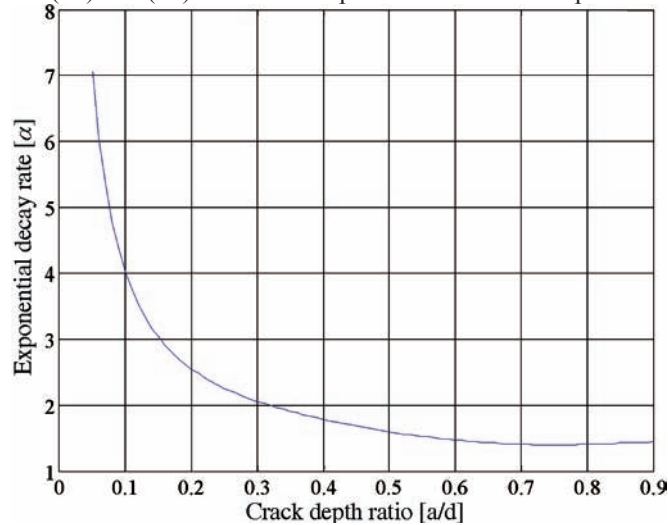


Fig. 5. Exponential decay rate  $\alpha$  versus crack depth ratio  $a/d$

In the next section the partial differential equation (12) has been solved and the natural frequencies and mode shapes have been calculated.

## EIGEN SOLUTION

In order to find the natural frequencies and mode shapes of a cracked beam, the equation of motion presented in equation (12) must be solved. However this equation cannot be solved analytically and a numerical method must be used. It can be assumed that the solution is a harmonic function so one has:

$$w(x, t) = X(x)e^{i\omega t} \quad (19)$$

In which  $\omega$  is the natural frequency of the beam. Substituting equation (19) into (12) and assuming  $EI_\eta$  to be constant along the beam the following eigenvalue problem will be resulted:

$$\frac{d^2}{dx^2} \left( X'' + \kappa X''(x_c) e^{-\alpha \frac{|x-x_c|}{d}} \right) - \frac{\rho A}{EI_\eta} \omega^2 X = 0 \quad (20)$$

Equation (20) has a special form and contains a singular function and depends on the value of the solution at the crack position. These anomalies prevent one to use the normal weighted residual solution for this Sturm-Liouville problem. In a normal Sturm-Liouville problem one can easily consider the function  $X$  to be in the form of  $\sum c_i S_i(x)$  in which  $S_i(x)$  are the shape functions which satisfy the physical boundary conditions. However in this research the results show that such an approach will lead to divergence of the results. Since the function  $e^{-\alpha \frac{|x-x_c|}{d}}$  in equation (20) is not a smooth function it seems that the solution specially for larger crack depth ratio tends to have large derivatives near the crack tip. Accordingly extracting the value of  $X''(x_c)$  from  $X$  by derivation can lead to large fluctuations in the results and divergence. In order to avoid the divergence problem the function  $X''$  and the value of  $X''(x_c)$  is not extracted from  $X$  by direct derivation. Instead the  $X''$  is discretised independently from  $X$  and then a constraint equation provided to link  $X''$  to  $X$ .

Considering the above discussion the following relations can be written:

$$\begin{cases} X'' + \kappa X''(x_c) e^{-\alpha \frac{|x-x_c|}{d}} = \sum_{i=1}^N c_i S_i(x) \\ X = \sum_{i=1}^N c'_i S_i(x) \end{cases} \quad (21)$$

In which  $c_i$  and  $c'_i$  are two independent set of constants and functions  $S_i(x)$  are the shape functions which must satisfy the physical boundary conditions. Substituting equation (21) into (20) and multiplying two sides of the equation by  $S_j(x)$  then integrating along the length of the beam one has:

$$\sum_{i=1}^N c_i \int_0^l S_i''(x) S_j(x) dx - \frac{\rho A}{EI_\eta} \omega^2 \sum_{i=1}^N c'_i \int_0^l S_i(x) S_j(x) dx = 0 \quad j = 1, 2, \dots, N \quad (22)$$

Or in the matrix form:

$$\left[ K_{ij} \right] [c_i] - \frac{\rho A}{EI_\eta} \omega^2 \left[ P_{ij} \right] [c_i] = 0, \quad K_{ij} = \int_0^l S_i''(x) S_j(x) dx, \quad P_{ij} = \int_0^l S_i(x) S_j(x) dx \quad (23)$$

On the other hand from equations (23) the following relation can be obtained:

$$\sum_{i=1}^N c_i' S_i''(x) = \frac{1}{1+\kappa} \sum_{i=1}^N c_i S_i(x) \quad (24)$$

Multiplying two sides of equation (24) by  $S_j(x)$ , integrating along the length of the beam and writing the equations in the matrix form one has:

$$\left[ c_i' \right] = \left[ Q_{ij} \right]^{-1} \left[ R_{ij} \right] [c_i], \quad Q_{ij} = \int_0^l S_i''(x) S_j(x) dx, \quad R_{ij} = \frac{1}{1+\kappa} \int_0^l S_i(x) S_j(x) dx \quad (25)$$

Substituting equation (25) into (23) the following equation will be resulted:

$$\left( \left[ K_{ij} \right] - \frac{\rho A}{EI_\eta} \omega^2 \left[ M_{ij} \right] \right) [c_i] = 0, \quad \left[ M_{ij} \right] = \left[ P_{ij} \right] \left[ Q_{ij} \right]^{-1} \left[ R_{ij} \right] \quad (26)$$

The natural frequencies and corresponding mode shapes for the cracked beam can be calculated solving the matrix eigenvalue problem of equation (26). In the next section the results are presented for a simply supported beam with rectangular cross-section.

## RESULTS FOR A SIMPLY SUPPORTED BEAM WITH RECTANGULAR CROSS-SECTION

In this section the new approach has been applied for free vibration analysis of a simply supported slender prismatic cracked beam with rectangular cross-section. In such a beam the exponential decay rate  $\beta$  can be assumed to be infinity and the exponential decay rate  $\alpha$  can be calculated from equations (17) and (18). The geometrical factor  $\kappa$  and the exponential decay rate  $\alpha$  are as follows:

$$\kappa = \left( \frac{a}{d} \right) \left( \frac{a}{d} - 2 \right), \quad \alpha = \frac{-91 \left( \frac{a}{d} - 2 \right)}{593 \left( \frac{a}{d} \right) - 1969 \left( \frac{a}{d} \right)^2 + 3714 \left( \frac{a}{d} \right)^3 - 3584 \left( \frac{a}{d} \right)^4 + 1312 \left( \frac{a}{d} \right)^5} \quad (27)$$

In a simply supported cracked beam the shape functions  $S_i(x)$  can be assumed to be in the form of  $\sin(ix/l)$  which satisfy the physical boundary conditions. The natural frequency and mode shapes can be calculated using eigenvalue problem of (26). In this research the number of shape functions  $N$  is set to be 100. In order to generalize the results the natural frequencies of the cracked beam have been divided to the corresponding values for a normal beam. Figures (6), (7) and (8) show the fundamental, second and third natural frequency ratios of the cracked beam respectively. In figures (6) to (8) the natural frequency ratios have been plotted versus the crack depth ratio ( $a/d$ ) for several crack positions.

In figures (6) to (8) the results of finite element (FE) analysis are also presented for verification. The finite element results have been obtained using ANSYS software. In order to have an accurate and reliable model the PLANE183 singular element has been used in the cracked area [20]. This element is an 8-node quadratic solid singular element which specially designed for crack analysis. In this research a fine mesh has been used at the vicinity of the crack and dependency of the results to the mesh size has been checked. In all of the results there is a good agreement between analytical results and those obtained by FE analysis.

As it can be seen in figure (6) the reduction rate of the fundamental natural frequency has a direct relation with the position of the crack. This rate reduces for cracks which have more distance from the mid span of the beam. For the cracks at  $x_c/l = 0.1$  the fundamental natural frequency only drops nearly 1 percent when the crack reaches to the half of the beam

depth while for the cracks at the mid span this value is about 15 percent.

The dependency of the reduction of the natural frequency to the crack position is also seen in the first few natural frequencies. For the cracks at the mid span the second natural frequency remains nearly constant with the crack depth because this point coincides with the node of the second vibration mode of the beam.

Figures (9) to (11) show the first three normalized mode shapes for a cracked beam with  $a/d = 0.5$  and  $x_c/l = 0.1, 0.3, 0.5$ . Comparison of the analytic and finite element results in this set of figures shows the efficiency of the model presented in this research.

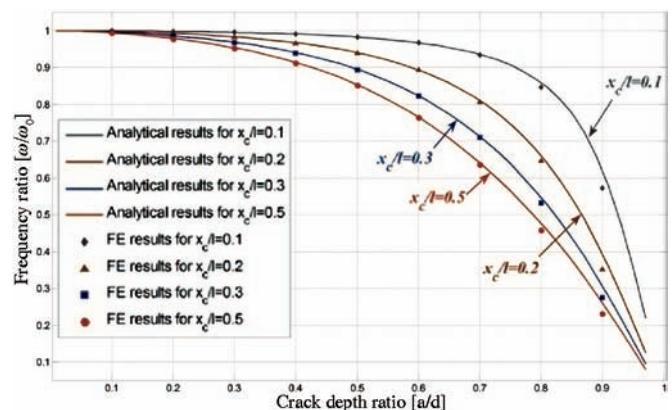


Fig. 6. Fundamental natural frequency ratio of a cracked beam versus crack depth ratio ( $a/d$ )

## CONCLUSIONS

- A new continuous theory for flexural vibration analysis of a beam with an edge crack has been introduced in this paper. The crack is assumed to be an open edge crack. A bilinear displacement field has been suggested for the beam and the strain and stress fields have been calculated. The extraction of the strain field from the displacement field is based on elasticity rules and hence the displacement and strain fields are completely compatible. The governing equation of motion has been obtained using the Hamilton principle. The required constants in this model are calculated from empirical formula in fracture mechanics. The equation of motion has been solved for natural frequencies and mode shapes using a special numerical algorithm presented in this paper.
- The analytical results have been compared with finite element results and an excellent agreement has been observed. The model is accurate for both natural frequencies and mode shapes calculations. Results show that for a simply supported beam the reduction of natural frequency is a function of crack depth ratio as well as the crack position.
- The presented model is a simple and accurate model which predicts the behavior of the cracked beam and its results are reliable near the crack tip and far from it. This model can be used for dynamic stress and strain calculations near the crack tip.

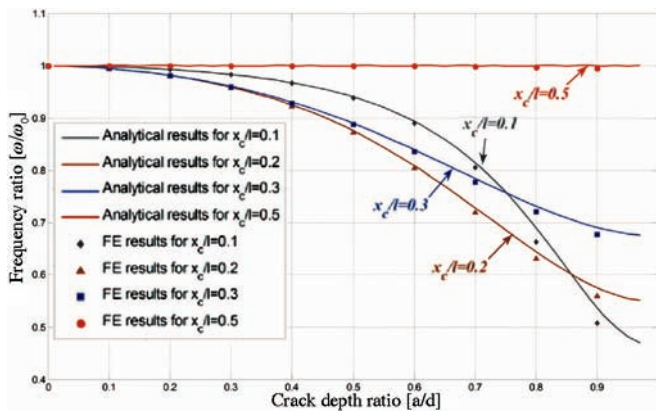


Fig. 7. Second natural frequency ratio of a cracked beam versus crack depth ratio ( $a/d$ )

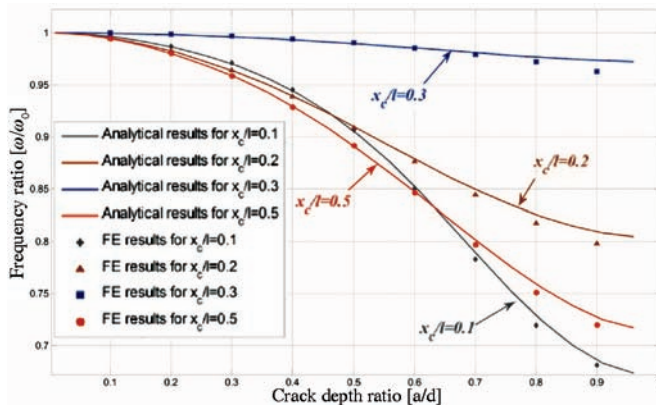


Fig. 8. Third natural frequency ratio of a cracked beam versus crack depth ratio ( $a/d$ )

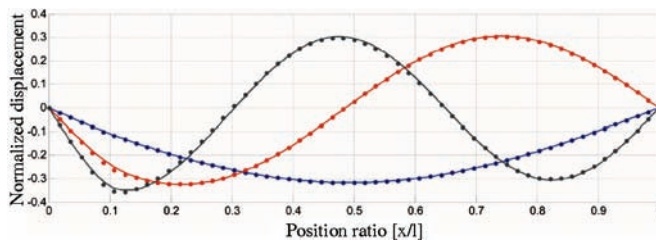


Fig. 9. First three normalized mode shapes of a cracked beam with  $x_c/l=0.1$  and  $a/d=0.5$  (—): Analytical results; (•••): Finite element results

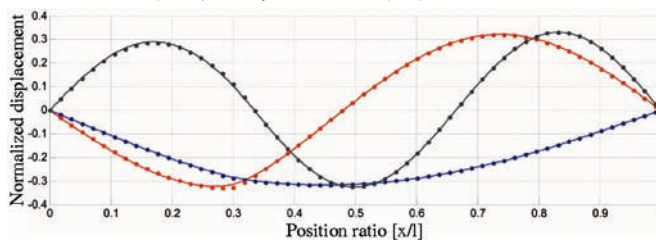


Fig. 10. First three normalized mode shapes of a cracked beam with  $x_c/l=0.3$  and  $a/d=0.5$  (—): Analytical results; (•••): Finite element results

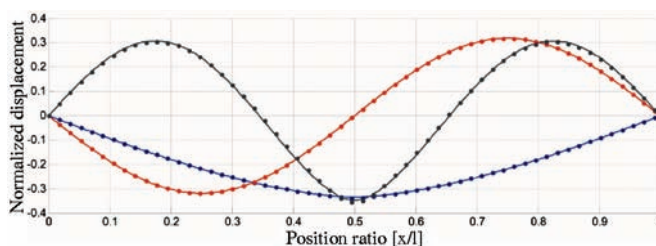


Fig. 11. First three normalized mode shapes of a cracked beam with  $x_c/l=0.5$  and  $a/d=0.5$  (—): Analytical results; (•••): Finite element results

## REFERENCES

1. Dimarogonas A. D.: *Vibration of cracked structures-A state of the art review*, Engineering Fracture Mechanics, Vol. 5, pp. 831-857, 1996
2. Wauer Jorg: *On the dynamics of cracked rotors: A literature survey*, Applied Mechanics Reviews, Vol. 43,1, pp. 13-17, 1990
3. Gasch R.: *A survey of the dynamic behavior of a simple rotating shaft with a transverse crack*, Journal of sound and vibration, Vol. 160(2), pp 313-332, 1993
4. Dimarogonas A. D., Paipetis S. A.: *Analytical methods in rotor dynamics*, London, Applied science publisher, 1983
5. Zheng D. Y., Fan S. C.: *Vibration and stability of cracked hollow-sectional beams*, Journal of sound and vibration, Vol. 267, pp. 933-954, 2003
6. Yanga J., Chena Y., Xiangc Y., Jiaa X. L.: *Free and forced vibration of cracked inhomogeneous beams under an axial force and a moving load*, Journal of Sound and Vibration 312, 166-181, 2008
7. Hai-Ping Lin: *Direct and inverse methods on free vibration analysis of simply supported beams with a crack*, Engineering structures, Vol. 26(4), pp. 427-436, 2004
8. Zheng D. Y., Fan S. C.: *Vibration and stability of cracked hollow-sectional beams*, Journal of sound and vibration, Vol. 267, pp. 933-954, 2003
9. Loyaa J. A., Rubiob L., Fernandez-Saeza J.: *Natural frequencies for bending vibrations of Timoshenko cracked beams*, Journal of Sound and Vibration 290, 640-653 2006
10. Orhan S.: *Analysis of free and forced vibration of a cracked cantilever beam*, NDT&E International 40, 443-450, 2007
11. Yang X. F., Swamidas A. S. J. and Seshadri R.: *Crack identification in vibrating beams using the energy method*, Journal of sound and vibration, Vol. 244(2), pp. 339-357, 2001
12. Jialai Wanga, Pizhong Qiaob: *Vibration of beams with arbitrary discontinuities and boundary conditions*, Journal of Sound and Vibration 308, 12-27, 2007.

13. Christides S., Barr A. D. S.: *One-dimensional theory of cracked Bernoulli-Euler beams*, Journal of mechanical science, Vol. 26(11/12), pp. 639-648, 1984
14. Shen M. H. H., Pierre C.: *Natural modes of Bernoulli-Euler beams with symmetric cracks*, Journal of sound and vibration, Vol. 138(1), pp. 115-134, 1990
15. Shen M. H. H., Pierre C.: *Free vibrations of beams with a single-edge crack*, Journal of sound and vibration, Vol. 170(2), pp. 237-259, 1994
16. Carneiro S. H. S., Inman D. J.: *Comments on the free vibration of beams with a single-edge crack*, Journal of sound and vibration, Vol. 244(4), pp. 729-737, 2001
17. Chondros T. G., Dimarogonas A. D. and Yao J.: *A continuous cracked beam vibration theory*, Journal of Sound and Vibration, Vol.215(1), pp. 17-34, 1998
18. Chondros T. G., Dimarogonas A. D. and Yao J.: *Vibration of a beam with breathing crack*, Journal of Sound and Vibration, Vol. 239(1), pp. 57-67, 2001
19. Tada H., Paris P. C. and Irvin G. R.: *The stress analysis of cracks handbook*. Hellertown, Pennsylvania: Del Research Corp., 1973.
20. ANSYS User's Manual for rev. 8, ANSYS Inc., 2004.

**CONTACT WITH THE AUTHORS**

M. Behzad, A. Ebrahimi, A. Meghdari  
 Mechanical Engineering Department,  
 Sharif University of Technology  
 11155-9567, Azadi Avenue,  
 Tehran, IRAN  
 email: m\_behzad@sharif.edu



The Ship Handling Research and Training Centre at Ilawa is owned by the Foundation for Safety of Navigation and Environment Protection, which is a joint venture between the Gdynia Maritime University, the Gdansk University of Technology and the City of Ilawa.

**Two main fields of activity of the Foundation are:**

- Training on ship handling. Since 1980 more than 2500 ship masters and pilots from 35 countries were trained at Ilawa Centre. The Foundation for Safety of Navigation and Environment Protection, being non-profit organisation is reinvesting all spare funds in new facilities and each year to the existing facilities new models and new training areas were added. Existing training models each year are also modernised, that's why at present the Centre represents a modern facility perfectly capable to perform training on ship handling of shipmasters, pilots and tug masters.
- Research on ship's manoeuvrability. Many experimental and theoretical research programmes covering different problems of manoeuvrability (including human effect, harbour and waterway design) are successfully realised at the Centre.

The Foundation possesses ISO 9001 quality certificate.

**Why training on ship handling?**

The safe handling of ships depends on many factors - on ship's manoeuvring characteristics, human factor (operator experience and skill, his behaviour in stressed situation, etc.), actual environmental conditions, and degree of water area restriction.

Results of analysis of CRG (collisions, rammings and groundings) casualties show that in one third of all the human error is involved, and the same amount of CRG casualties is attributed to the poor controllability of ships. Training on ship handling is largely recommended by IMO as one of the most effective method for improving the safety at sea. The goal of the above training is to gain theoretical and practical knowledge on ship handling in a wide number of different situations met in practice at sea.

For further information please contact:

**The Foundation for Safety of Navigation and Environment Protection**

Head office:  
 36, Chrzanowskiego street  
 80-278 GDAŃSK, POLAND  
 tel./fax: +48 (0) 58 341 59 19

Ship Handling Centre:  
 14-200 ILAWA-KAMIONKA, POLAND  
 tel./fax: +48 (0) 89 648 74 90  
 e-mail: office@ilawashiphhandling.com.pl  
 e-mail: office@portilawa.com

# Determining strength of the modified wood

Lesław Kyzioł,   
Polish Naval Academy in Gdynia

## ABSTRACT

*The article presents results of investigations of the effect of pinewood modification with methyl polymethacrylate on the anisotropy of its strength in complex stress conditions. The investigations aimed at determining the resistance of the examined wood to stretching, compression, stretching with shear, and compression with shear. For the investigations oriented on shear, shear with stretching, and shear with compression, a special specimen was prepared which differs by notch geometry from a typical Iosipescu specimen. A new test machine is described in the article, which is equipped with special specimen holders to perform investigations in complex stress conditions. Crack patterns recorded for the natural and modified wood are presented. For all tests, numerical FEM simulations were performed to obtain stress distributions inside the specimens. The calculated stress distributions were visualised as contour line projections for the natural and modified wood.*

**Keywords:** wood modification, wood-polymer composite, Iosipescu specimen, stress distribution in the specimen under load.

## INTRODUCTION

Numerous authors [5, 6, 10, 11] claim that the properties of the modified wood relating to its strength and deformation increase or decrease in proportion to the amount of the modifying substance.

All changes of mechanical properties of the wood exposed to the modification cannot be fully predicted without relevant experimental tests.

The goal of the reported activities was to determine the effect of pine whitewood modification of its strength anisotropy in complex stress conditions.

Wood is an orthotropic material revealing remarkably different strength characteristics depending on the anatomic direction. The literature makes distinction between three wood directions: longitudinal, tangential, and radial. The adopted

coordinate system is shown in Fig. 1 – the L axis is in the anatomic direction along the fibres, the R axis is in the radial direction, and the T axis is directed tangentially to the surfaces of particular fibre layers.

## COURSE OF INVESTIGATIONS

In order to examine the effort of the examined materials, tests were performed to determine wood resistance to stretching, compression, stretching with shear, and compression with shear. The shapes and dimensions of the specimens used for tests were taken from relevant standards [22–25].

The specimens were formed from a wooden square timber, seasoned in natural conditions in the temperature of  $295 \pm 2\text{K}$ . The average humidity of the specimens was equal to 8%. The tests were performed on natural wood specimens and those exposed to the modification process. The modification consisted in saturating the wood with the hydroquinone methyl ether modified methacrylate (MM), with further thermal polymerisation. The degree of specimen saturation with the monomer was controlled by adjusting the time during which the specimen was in the autoclave, in the way described in [21]. The modified wood with different contents of methyl polymethacrylate was marked, respectively, as K0.0, K0.35, K0.43, K0.48 and K0.56, where the numbers represent the number of kilograms of methyl polymethacrylate with respect to 1 kg of dry wood.

The stretching and compression tests were done on a universal test machine MTS-810.12, while the shear tests were performed on a machine designed and produced especially for

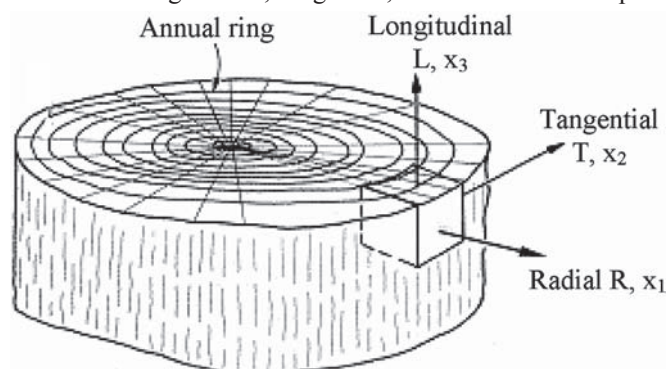


Fig. 1. Orientation of anatomic directions of the wood in rectangular coordinate system

this purpose [21]. Wood resistance to stretching, compression, and shear was determined based on the arithmetic mean of 6 to 10 specimens. The mean values and the statistic processing are discussed in [21]. The results of the mean value analysis are given in Table 1.

**Tab. 1.** Resistance limits to stretching, compression, and shear of natural and modified wood

Type of material	$R_{m\parallel}$ [MPa]	$R_{c\parallel}$ [MPa]	$R_{m\perp}$ [MPa]	$R_{c\perp}$ [MPa]	$R_t$ [MPa]
K0.0	95	55	4.5	8.5	22.10
K0.35	102	70	7	24	25.68
K0.43	110	80	8	26	26.50
K0.48	112	88	8.5	29	27.80
K0.56	118	98	9	32	30.20

where:  $R_{m\parallel}$  - resistance to stretching along fibres;  $R_{c\parallel}$  - resistance to compression along fibres;  $R_{m\perp}$  - resistance to stretching across fibres;  $R_{c\perp}$  - resistance to compression across fibres;  $R_t$  - shear resistance

### RESISTANCE OF THE MODIFIED WOOD TO IN-PLANE SHEAR

Prognosing strength of such composite layer structures as the wood is of vital importance in designs making use of this material. An important parameter which should be known in wood-based designs is wood resistance to in-plane shear. The literature sometimes gives contradictory data on the levels of wood resistance, which is not surprising [15]. The absence of reliable methods measuring material's resistance to in-plane shear results in little confidence in official design limitations, a consequence of which is taking into account excessive margins in design activities involving in-plane shear strength.

Methods of composite resistance investigations can be divided into tests making use of tubular specimens and plane specimens. Preparing wooden tubular specimens for investigations in complex load conditions is difficult due to the anatomic structure of the wood (annual rings), therefore in the reported case a decision was made to perform tests using plane specimens.

So far, a specimen which was found to be most useful, due to its shape, for composite tests is the Iosipescu specimen [4, 8, 9]. Attempts to adapt it to testing composites in plane stress conditions, following the method based on the Arcan instrument [4], were initiated by Broughton [7]. Its applicability for shear tests of various layer composites was confirmed by numerous investigation reports [1, 2, 13, 17÷19].

The failure of the Iosipescu specimen can be reached in the uniform stress conditions, although the presence of undesired transverse stress makes the interpretation of the shear resistance more complicated.

Below, assumptions are presented which refer to the measurement of the shear resistance of the composite Iosipescu specimens in the test bearing the name of the V method (ASTM D5379M:93). The definition of the shear resistance is, generally, not clear [14, 21]. For instance, for the same material Broughton [7] says about the "failure stress" equal to 58 MPa, while Morton [12] says about the "shear resistance" equal to 68 MPa. At the same time Adams [1] says about the "shear resistance" equal to 115 MPa for the same material and specimen, but another definition of the failure point [14, 15, 21].

When testing plane specimens we have to take into account that reaching the failure criterion generates the necessity for the appearance of shear. An important feature of the test is stress uniformity in the examined specimen area.



**Fig. 2.** a) modified Iosipescu specimen, b) specimen with summer wood upper layers, c) specimen with spring wood upper layers.  $\beta = 45^\circ$ ,  $g = 5$  mm - specimen thickness,  $b = 20$  mm - specimen width,  $p = 5$  mm - length of measuring section,  $L = 80$  mm - specimen length

Preliminary tests performed on a typical Iosipescu specimen (with an alternate system of layers, not always parallel to each other, sometimes twisted) have revealed that correct results cannot be obtained. During shear tests of this piece, it is not only the shearing stresses which are observed at the bottom of the notch. When the specimens are loaded with transverse load, their bending is observed, with the resultant normal stress generated by the bending moment. The wooden fibres are deformed (bent and stretched). Recognising the beginning of specimen failure is difficult [21].

Taking into account the experience gained by Iosipescu [8], a specimen was prepared which was then tested many times to reach the final shape and dimensions shown in Fig. 2. This specimen differs considerably from the typical Iosipescu piece by the notch geometry. Adopting such a specimen geometry is a result of long lasting experiments, numerical calculations and observations recorded during the tests. The depth of the notch with respect to the thickness of layers was selected in such a way that the beginning of the notch is at its edge [21].

The examined specimens had various configurations of softwood and hardwood layers. When preparing the specimens, care was taken that the wood layers were situated parallel to each other and had constant thickness along the specimen length.

There are test machines, produced in series, which are equipped with special holders for performing investigations in complex load conditions. However, due to high costs of these machines and specific nature of investigations, similar machines are frequently designed and produced individually in laboratories in which the investigations are performed.

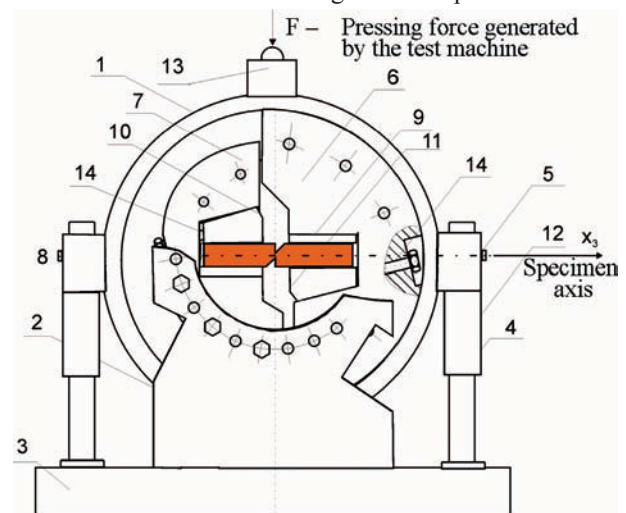


**Fig. 3.** Machine for generating plane stress distribution: 1 - casing; 2 - console; 3 - base; 4 - guide; 5 - pilot sleeve; 6 - right holder; 7 - left holder; 8 - insert for left holder jaw; 9 - insert for right holder jaw; 10 - left locking block; 11 - right locking block; 12 - guide sleeve; 13 -  $\phi 12$  ball and ball fixing; 14 - M6 bolt.

The designed and produced machine [21], shown in Fig. 3, has made it possible to generate the plane stress distribution, Fig. 2. Compared to a traditional test machine [7, 20], the position of the specimen axis with respect to the direction of

force  $F$  can be changed. As a result, depending on the specimen position angle with respect to the load direction, stretching or compression can be executed along with shear in the central part of the specimen.

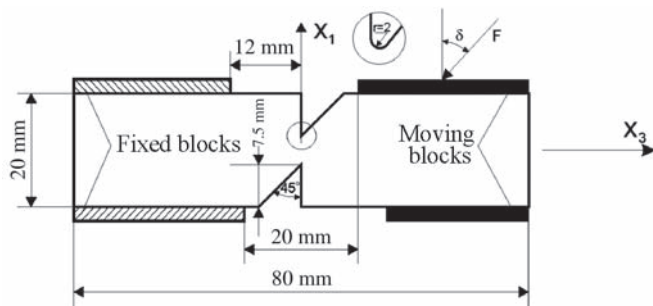


Fig. 4. Scheme of kinetic load of the specimen

The moving and fixed blocks are preliminary clamped in such a way that the  $F_{x_3}$  component of force  $F$  is smaller than the friction force between the blocks and the specimen. However, this clamping generates a preliminary stress. Taking this into account, the clamping force was selected experimentally at a level securing fulfilment of its function and, at the same time, not affecting considerably specimen's strength. Then the moving blocks were moved in the direction inclined at the angle  $\delta$  to the specimen axis. During the tests the value of force  $F$  was measured in relation to specimen displacement. When  $\delta = 0$ , the stress is close to pure shear. The test machine makes it possible to change the angle within the range  $-45 \div 45^\circ$ . Specimen stretching and compression in the direction of the  $x_3$  axis was done when the specimen was mounted directly in the machine jaws.

The scheme shown in Fig. 4 reveals some displacements of the upper blocks with respect to their lower counterparts. The scale of this displacement was set experimentally. It was large enough to generate united displacements at the contacting edges between the blocks and the specimen, which was of high significance for the operation of the FEM model used for the numerical stress analysis.

For  $\delta = 0$ , shear of the specimen is observed as provoked by the applied vertical displacement  $U_{x_3}$ , Fig. 4. The machine that loads the specimen records, via a relevant measuring instrument, the force along with the corresponding displacement. During specimen shear, the displacement  $U_{x_1}$  of the machine right-hand side, corresponding to force  $F = F_{x_1}^1$  is directed along the  $x_1$  axis. For negative (counterclockwise) specimen rotation angles in the test machine, see Fig. 3, force  $F$  generates shear  $F_t$  and compression  $F_c$  within the specimen, while for positive (clockwise) angles force  $F$  generates shear  $F_t$  and stretching  $F_m$ .

Fig. 5 shows a sample relation between the loads of the specimens made of natural and modified wood, and the holder displacements for  $\delta = 0^\circ$ . Numbers 1-4 denote successive crack stages of the specimen made of natural wood. The specimen failure does not take place immediately after the appearance of the first crack, as the arrangement of the wood layers with respect to the direction of force action changes at that moment. Further increase of load generates next cracks.

Some authors suggest that the final crack takes place, for plastics, in the uniform shear conditions. Unfortunately, no investigations were performed to verify this thesis [3, 7, 16]. Other authors propose to interpret the shear stress recorded at the appearance of final crack as the shear resistance.

Here, for both the natural and modified wood the shear resistance was assumed as that observed at the first crack of the specimen, Fig. 5 [21].

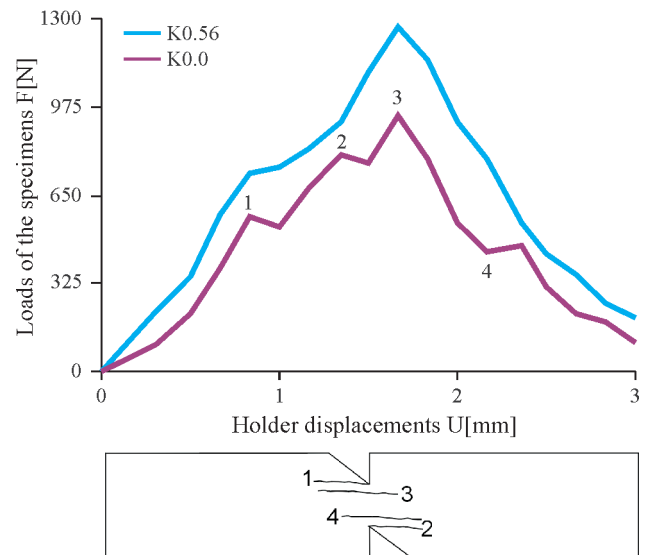


Fig. 5. Load - displacement curve with characteristic points of crack beginning (1, 2, 3, 4 - successive stages of specimen crack)

Fig. 6 shows crack patterns observed for the natural and modified wood. When exposed to load, the layers of the natural wood resembled significantly deformed "threads", and recording the time when the last layer is damaged was



Fig. 6. Specimen crack patterns: a) natural wood, b) composite D-PMM K0.35, c) composite D-PMM K0.56 (1, 2, 3, 4 - successive stages of wooden specimen crack)

difficult. Specimens of the modified wood revealed higher crack resistance. When the content of the polymer in the composite was higher, the material became more resistant to failure, Figs. 5 and 6c. The nature of crack of the modified wood K0.35 resembled an intermediate crack pattern between that observed for brittle and ductile material.

The above course of specimen crack referred to the case of shear. In a similar way, depending on the selected angle of specimen axis with respect to the direction of load, forces  $F$  were recorded assuming that the specimen resistance corresponds to the first crack (point 1 in Fig. 5). By changing the specimen position angle by  $15^\circ$  within the range  $-45^\circ$  to  $45^\circ$  the relation was obtained between the force  $F$  corresponding to the first crack and the angle  $\delta$ .

Fig. 7 shows loads of specimens made of natural and modified wood in relation to the angle  $\delta$  until the appearance of the first crack.

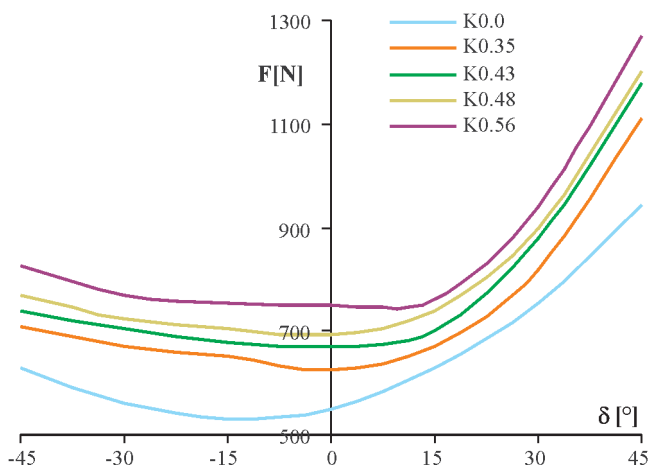


Fig. 7. Dependence of specimen load on the angle  $\delta$  until the appearance of the first crack  $\delta$  – specimen rotation angle with respect to the horizontal position

## ANALYSING TEST RESULTS

For all tests, FEM-based numerical simulations were performed to obtain stress distributions inside the pieces. In the calculation model the plane stress was assumed, and the discretisation was done in such a way that each layer of the soft and hard wood was modelled in the perpendicular direction by two nine-node elements. Physical properties of particular layers were described using a generalised Hooke law for orthotropic materials. Based on the obtained results, the flexibility matrices were determined for the soft and hard layers of the natural wood K0.0 and the modified wood K0.56 [21].

On average, the specimen consisted of seven softwood layers and eight hardwood layers, or the opposite. The ratio between the thicknesses of hardwood layers to softwood layers was approximately equal to 0.5. The depth of the notch with respect to the layers was selected in such a way that the beginning of the notch was at the edge of the layer and not in the middle of it. The layers were assumed to be situated parallel to each other and have constant thickness along specimen length. In the measuring section the top layer can be the either softwood or hardwood layer, Figs. 2b, c).

The specimen load was executed by moving the edges which were in contact with the moving blocks in the direction inclined by  $\delta$  to the specimen axis. When the force calculated from stresses for section  $x_3 = 0$  was equal to that measured, the obtained stress conditions were assumed as corresponding to specimen failure. Comparing edge displacements assumed in the calculations with the measured values made the basis for verification of the calculation model.

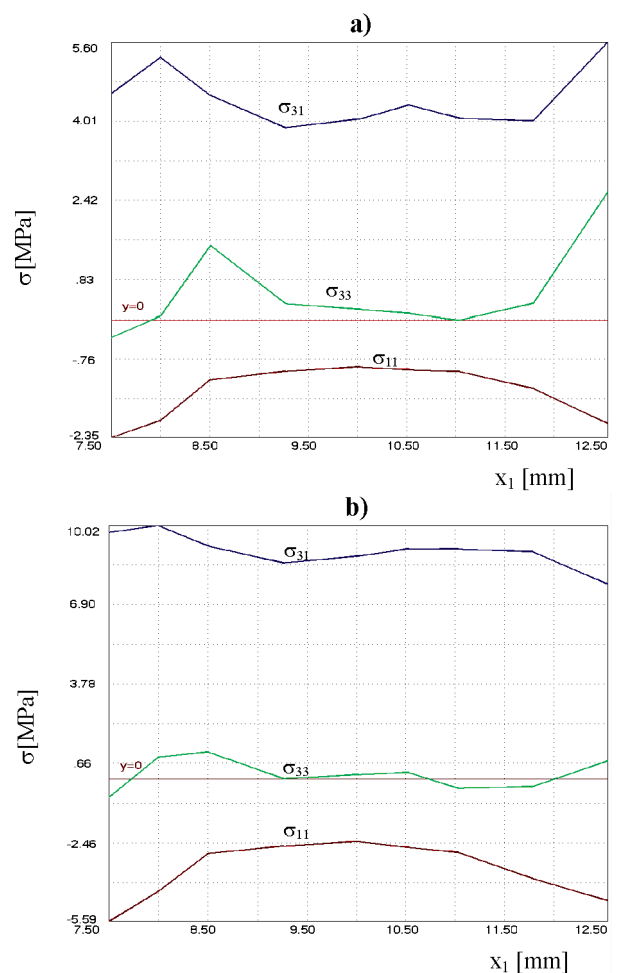


Fig. 8. Distribution of stresses in the measuring sections of the specimens made of: a) natural wood K0.0, b) modified wood K0.56 exposed to complex stress conditions for  $\delta = 0^\circ$

Fig. 8 presents stress distributions in the measuring sections of the specimens made of natural wood K0.0 and modified wood K0.56 for  $\delta = 0$ . Here, the shearing stresses  $\sigma_{31}$  take the highest values, while  $\sigma_{33}$  and  $\sigma_{11} = 0.25\sigma_{31}$  are close to zero. The stress distributions along the examined measuring sections of the specimens made of natural and modified wood differ between each other. For the natural wood, the saw-like shape of the diagram suggests the appearance of increased stresses in the hardwood with respect to those observed in the softwood. In the modified wood, on the other hand, the stress distribution is close to uniform, as elastic properties of the layers are similar to each other. Modifying the soft layers led to the “homogenisation” of the material, as a result of which the stress distribution curve is more uniform.

Figs 9 and 10 show, in the form of contour lines, the distributions of stress  $\sigma_{31}$  calculated using the FEM method for  $\delta = 0$  for natural and modified wood, respectively. The distribution of the tangential stress in the measuring section of the specimen made of natural wood, Fig. 9, reveals much higher effort of the hardwood than that of the softwood. Moreover, within the entire measuring section the material effort is more than twice as high as in the corresponding section of the modified wood, see Fig. 10. This effect is believed to have been caused by the “homogenisation” of the material in the hardwood layer direction [21].

For the specimen made of natural wood, stress distributions in the analysed section are shown Figs. 11a and b, while for the modified wood - in Figs. 11c and d. As can be noticed, the stresses for the two angles differ not only by a sign, but

also by an absolute value. These differences are much higher for the natural wood than for the modified wood. Similar differences in stress distributions in the measuring sections of the specimens made of wood K0.0 and K0.56 were recorded at complex load conditions for  $\delta = 90$  and  $\delta = -90$ . In the specimens exposed to load for  $\delta = 90$  and  $\delta = -90^\circ$  the dominating stresses  $\sigma_{33}$  are accompanied by limited stresses  $\sigma_{31}$  and negligible shear stresses. For the both cases ( $\delta = 90$

and  $\delta = -90^\circ$ ) the tests were performed on a universal test machine MTS 810.12.

The shear resistances and stress distributions were determined in complex load conditions (shear with stretching, and shear with compression) in the measuring sections of the specimens made of natural and modified wood. If the top layer in the measuring section was the hardwood layer, the stresses were higher than in case when the softwood layer was the top layer.

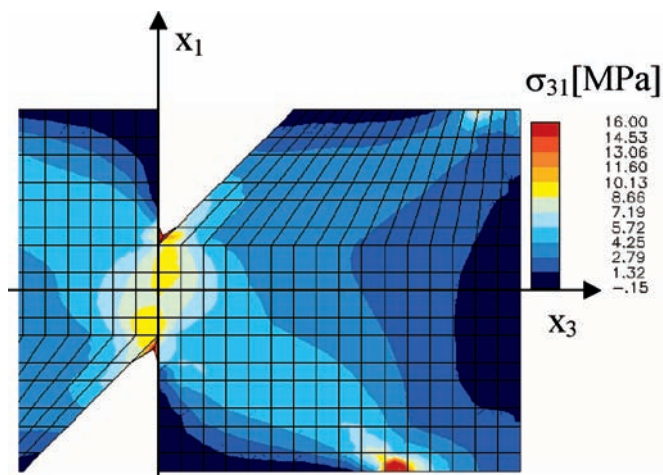


Fig. 9. Distribution of  $\sigma_{31}$  stress in selected natural wood specimen area

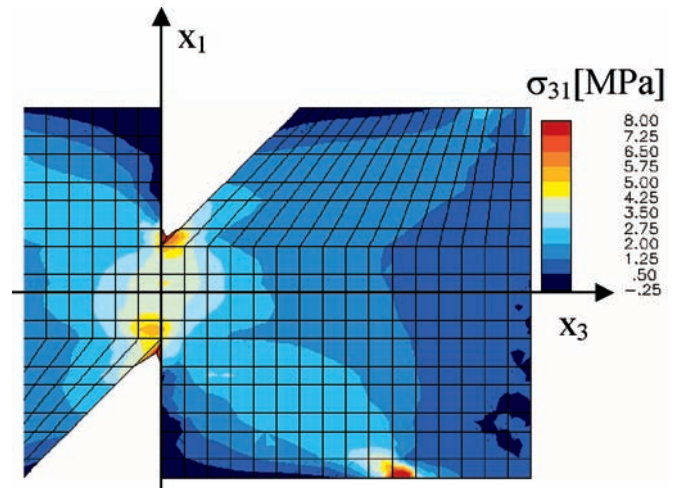


Fig. 10. Distribution of  $\sigma_{31}$  stress in selected modified wood specimen area

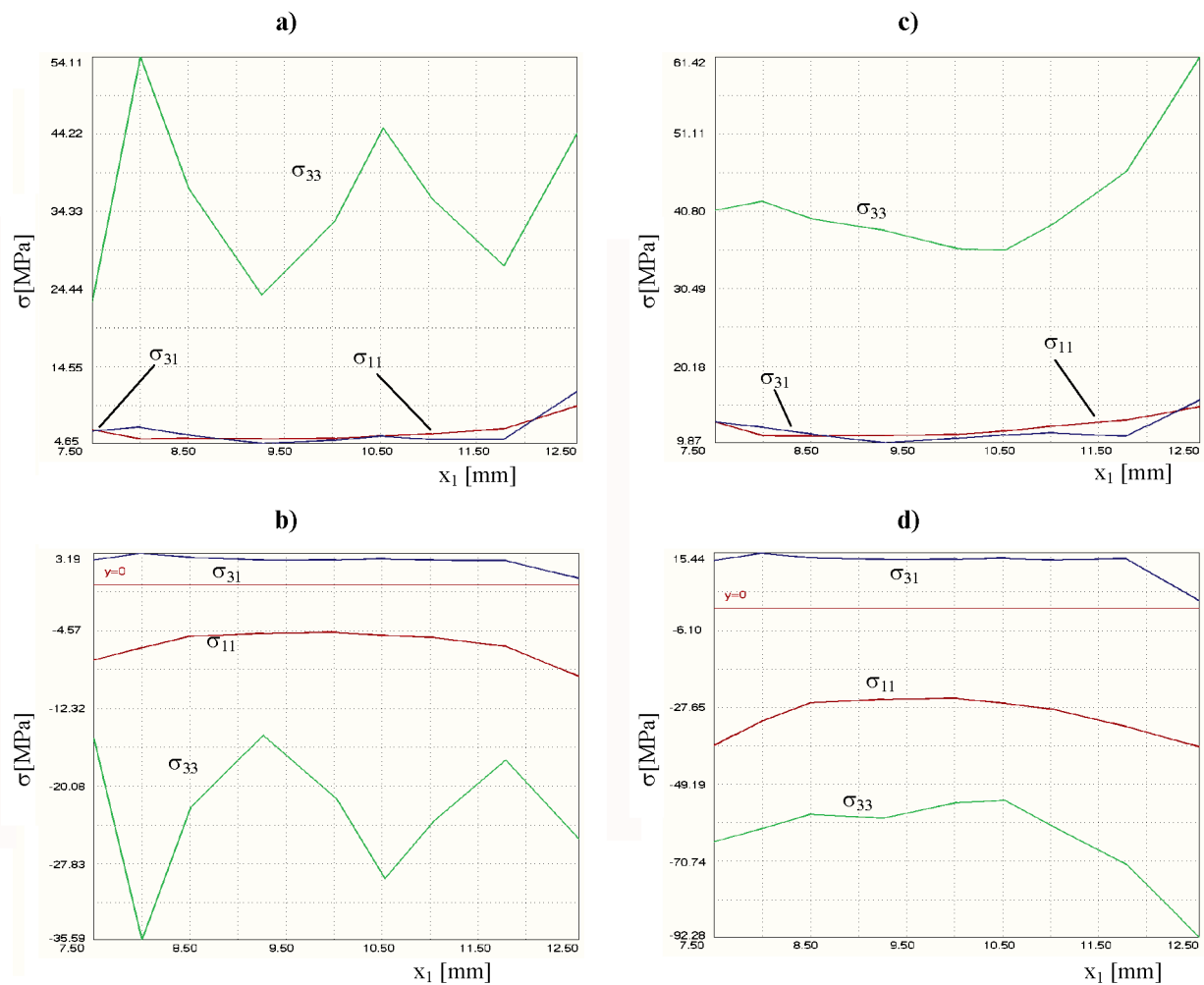


Fig. 11. Distribution of stresses in the measuring sections of specimens made of natural wood K0.0 at complex stress conditions for: a)  $\delta = 45^\circ$ , b)  $\delta = -45^\circ$  and modified wood K0.56 for: c)  $\delta = 45^\circ$ , d)  $\delta = -45^\circ$

## FINAL CONCLUSIONS

The performed tests have made it possible to formulate the following conclusions:

- When being compressed along the fibres, the effort of the modified wood can be nearly twice as high as for the natural wood. In case of compression across the fibres this ratio is even higher and can exceed 4. Also during stretching, remarkable increase of strength of the modified wood is observed.
- Stress distributions in specimens made of natural and modified wood and exposed to load reveal differences in levels and shapes. These differences are much higher for natural wood.
- When exposed to load, layers of the natural wood resembled significantly deformed “threads” and capturing the time when the last layer was damaged was difficult. The specimens made of modified wood revealed higher crack resistance. Increasing the content of polymer resulted in “homogenisation” of the wood structure, as a result of which the material became more resistant to failure.
- In the elements made of natural wood remarkable differences in the efforts of soft and layers were observed, while in the superficially modified wood the efforts of the soft and hard layers situated close to the surface were almost the same.
- In case of bent or twisted elements, a sufficient approach is to modify the wood only superficially. The softwood layers are strengthened and take over some part of the load from the hardwood layers. This way the stress distribution becomes more uniform.

## BIBLIOGRAPHY

1. Adams D.F., Lewis E.Q.: *Experimental strain analysis of the Iosipescu shear test specimen*. Exp. Mech., Vol. 35, No. 2, pp. 352-360, 1997
2. Adams D.F., Lewis E.Q.: *Experimental assessment of four composite material shear test methods*. J. Test. Evaluat. Vol. 25, No. 2, pp. 242-254, 1995
3. Adams D.F., Walrath D.F.: *Current status of the Iosipescu shear test*, J. Comp. Mat., Vol. 25, No. 1, pp. 494-506, 1987
4. Arcan M., Hashin Z., Voloshin A.: *A method to produce uniform plane-stress states with applications fiber-reinforced materials*. Exp. Mech., Vol. 18, pp. 141-145, 1984
5. Boding J., Goodman I.R.: *Prediction of elastic parameters for wood*, Wood Sci., Vol.5, No. 4, pp. 378-385, 1973
6. Boding J., Jayne B., A.: *Mechanics of wood and wood composites*, Van Nostrand Reinhold, New York, 1982
7. Broughton W.R., Kumosa M., Hill D.: *Analysis of the Iosipescu shear test applied to unidirectional carbon-fiber reinforced composites*, Comp. Science Tech., Vol. 38, pp. 299-325, 1990
8. Iosipescu N.: *New accurate procedure for single shear testing of metals*. J. Mater., Vol. 2, No. 3, pp. 537-566, 1967
9. Kumosa M., Hull D.: *Mixed – mode fracture of composites using Iosipescu shear test*. Int. J. Fracture, Vol. 35, pp. 83-102, 1987
10. Kyziol L.: *Modified wood – a promising material for shipbuilding*. Polish Maritime Research, pp. 6-10, 1999
11. Kyziol L., Kowalski S. J.: *Mechanical Properties of Modified Wood-IUTAM Symposium on Theoretical and Numerical Methods in Continuum Mechanics of Porous Materials*. University of Stuttgart, Germany, September 5-10, pp.221-229, 1999
12. Morton J., Ho H., Tsai M. Y., Farley G.: *An evaluation of the Iosipescu specimen for composite materials shear property measurement*. J. Compos. Mater., Vol. 26, pp. 708-750, 1992
13. Ochelski S.: *Critical evaluation of selected methods of composite investigations* (in Polish). WAT Bulletin, Year XLIX, No. 7, pp. 23-33, 2000
14. Pierron F., Vautrin A.: *Analyse de la rupture d'éprouvettes Iosipescu: application à la mesure de la résistance au cisaillement*. Ninth French Conference on Composite Materials, Vol.2, Saint-Etienne, 22-24 November, pp. 709-718, 1994
15. Pierron F., Vautrin A.: *Measurement of the in-plane shear strengths of unidirectional composites with the Iosipescu test*. Composites Science and Technology, Vol. 57, pp. 1653-1660, 1997
16. Pindera M.J. et al.: *A methodology for accurate shear characterization of unidirectional composites*. J. Compos. Mater., Vol. 21, pp. 1164-1185, 1987
17. Swanson S.R., Messick M., Tombes G.R.: *Comparison of torsion tube and Iosipescu in-plane shear test results for a carbon fibre reinforced epoxy composite*. Composites, Vol. 16, No. 3, pp. 178-183, 1985
18. Tarnopolskij Yu. M., Arnautov A.K., Kulkov V.L.: *Methods of determination of shear properties of textile composites*. Composites Part A, Vol. 30, pp. 879-885, 1999
19. Walrath D.E., Adams D.F.: *The Iosipescu shear test as applied to composite materials*. Ex. Mech. Vol.3, pp. 105-110, 1983
20. Wang Ch.H., Chalkley P.: *Plastic yielding of film adhesive under multiaxial stresses*. Inter. J. Adhesion Adhesives, Vol 20, pp. 155-164, 2000
21. Kyziol L.: *Analysing properties of the constructional wood superficially saturated with the MM polymer* (in Polish), Polish Naval Academy in Gdynia, No. 156 A, 2004
22. PN-79/D-04229. *Wood. Determining resistance to compression across fibres* (in Polish)
23. PN-81/D-04108. *Wood. Determining resistance to stretching across fibres* (in Polish)
24. PN-81/D-04107. *Wood. Determining resistance to stretching along fibres* (in Polish)
25. PN-79/D-04102. *Wood. Determining resistance to compression along fibres* (in Polish).

## CONTACT WITH THE AUTHOR

Lesław Kyziol, Rj .F.  
Faculty of Mechanical and Electrical Engineering  
Institute of Basic Engineering  
Polish Naval Academy in Gdynia  
Śmidowicza 69  
81-103 Gdynia, POLAND  
e-mail: L.Kyziol@amw.gdynia.pl

# Contemporary diagnostic methods for ship engines: a report on scientific research activity of Polish Naval Academy in this field

Zbigniew Korczewski,   
Polish Naval Academy

## ABSTRACT



*This paper devoted to ship combustion engine diagnostics, presents short characteristics of experimental test techniques applicable to state assessment of piston and gas turbine engines presently being in use in Polish Navy. Some metrological and organizational aspects of realization of necessary diagnostic tests as well as measurements of control parameters of engines of low susceptibility to control, were highlighted. Such engines are installed a.o. on board American origin frigates of Oliver Hazard Perry type as well as Norwegian origin submarines of Kobben type which have been recently incorporated into Polish Navy (i.e. General Electric turbine engines, Detroit Diesel and Mercedes Benz piston engines), as well as older engines of Russian production (Zorya turbine engines, Zvezda piston engines). Applicability of particular diagnostic methods was also assessed from the point of view of their effectiveness in identifying engine failures in conditions of its operation in ship power plant. Recently realized tests have made it possible to conduct operation of all piston and turbine engines used on board Polish Navy ships in accordance with their current technical state. On the average 120-130 diagnostic expertises are yearly issued, and the carried-out tests cover main functional systems of engines together with their control and safety subsystems.*

**Keywords:** marine diesel and gas turbine engines, technical diagnostics, base diagnostic system, operational examinations

## INTRODUCTION

Main research activity of the Institute of Ship Construction and Operation (IKiEO), Polish Naval Academy (AMW), is focused on the problems of diagnostics of ship combustion engines (both of piston and turbine kind). The activity has been developed continuously since 1982 owing to efforts of the following research teams: that dealing with turbine engines and supervised by Prof. Charchalis, A., that dealing with piston engines under supervision of Prof. Piaseczny, L., and Dr Polanowski, S., as well as that dealing with diagnostics of flow systems of turbine and piston engines under supervision of this author.

Introduction to Polish Navy, in recent years, driving engines of a new type of low susceptibility to control, makes it necessary to search for new, alternative diagnostic methods providing possibility of carrying out a complex assessment of technical state of the engines independently from very expensive servicing.

In this paper is described the range of scientific research undertaken in the Institute, which have been traditionally focused on the area of operation of ship machines and devices, including a.o. development of assessment methods of technical state of ship engines (and not only) being in service conditions on board a ship. Also, selected scientific problems dealing with

diagnostics of ship piston and turbine combustion engines, being recently under research in the Institute, are presented.

The below presented illustrative material was divided in two independent parts: the first –devoted to diagnostics of piston engines, the second– to diagnostics of turbine engines. The described “cuisine” of diagnostic techniques contains selected methods of diagnostic activity based on the following scope of measurements of:

- ★ Gasodynamic parameters of working medium, of high- and low variability,
- ★ Vibrations and their spectral and correlation analysis,
- ★ Metallic contamination in lubricating oil,
- ★ Torque,
- ★ Emission of toxic compounds contained in exhaust gases,
- ★ Parameters of supplied fuel,
- ★ As well as endoscopic examinations.

It should be added that a part of diagnostic instruments can be successfully applied to assessment of technical state both piston and turbine engines, e.g. an endoscopic set or gas analyzers. However procedures for realization of diagnostic tests are different as they are adjusted to a given type of engine, from case to case. A strategic aim of the presented diagnostic methods, continuously developed and modernized, is to bring them to practice of operation of ship engines installed on Polish

Navy ships and subjected to diagnostic survey in accordance with their current technical state.

## DIAGNOSTICS OF PISTON ENGINES – A HISTORICAL OUTLINE

Since 1982 in the Institute a series of scientific research investigations concerning the diagnosing of piston combustion engines has been realized. The undertaken scope of work has inspired actions leading to elaboration of effective and complex diagnostic methods applicable in service conditions of ship engine. A strategic aim was to pass to engine operation process in accordance with its technical state. As a result the “Basic diagnostic system” was implemented into the operational system of Polish Navy ships. Its concept and realization resulted from:

- \* the task project no. 148-39/C-SO/93.: „Basic system for diagnosing and predicting the technical state of piston combustion engines”,
  - \* the research project no. 9T12D00211.: „A method of diagnosing the main design systems of piston engines and compressors with application of analysis of vibration envelopes in the domain of crankshaft rotation angle”,
- realized by the team under supervision of Dr Polanowski. (Fig. 1).

Since 1992 have been systematically carried out diagnostic tests of piston engines of every type applied to propelling Polish Navy ships. Periodic assessment of technical state of the engines is realized by an experienced research team specialized in application of the newest methods of diagnosing in difficult conditions of ship operation. Realization of such tests is based on successive indication of engine cylinders during its steady operation under load within representative ranges.

With the use of special analyzers of fast-varying quantities [20] is carried out comparative, statistical and subject-matter analyses of developed indicator diagrams, runs of vibration accelerations generated by working mechanisms connected with cylinder system and transmitted to a measurement point on engine head, as well as runs of other quantities characterizing working processes in engine cylinders, recorded in the domain of crankshaft rotation angle. The so determined diagnostic measures: mean indicated pressure, indicated power, maximum combustion pressure and rate of cylinder pressure increase  $dp/da$  etc provide important information on overall technical state of constructional elements of combustion chamber. Results of the tests are used for analyzing trends, assessing changes in technical state of engines and preparing an operational decision.

The presently performed investigations make it possible to carry out, in accordance with the technical- state control procedure, operation of about 100 engines installed on board Polish Navy ships. On average, 75–80 expertises on technical state of the engines are yearly issued [21,23]. And, only those engines are subjected to the diagnostic control system which are fitted with indicator valves.

## ENDOSCOPIC DIAGNOSTICS

Novel ship engines are fitted with more and more perfect control – measurement systems to measure parameters characterizing their loading state. Despite that, from service practice are known cases of severe failures of engines, whose primary causes have not been found in a proper time, e.g. failures due to excessive vibration resulting from loss of stability of mechanical system and - in consequence - occurrence of a resonance.

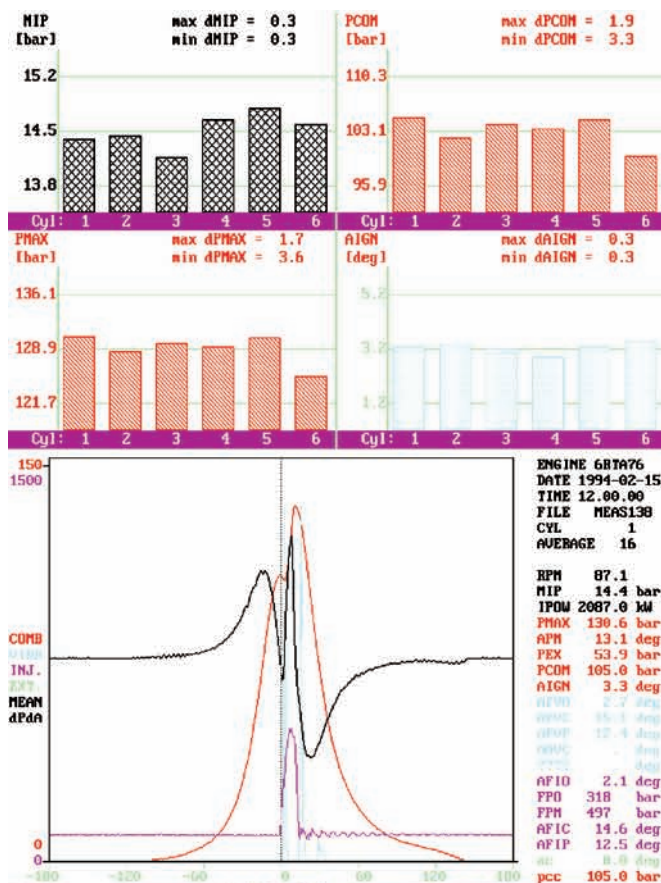


Fig. 1. The diagnostic team of Dr Polanowski at the stand for testing the cylinder systems of Henschel engines – cylinder pressure analyzer; example results of testing the engine combustion chamber

Difficulties in recognizing failures of ship combustion engines on the basis of thermal-gas-dynamic parameters characterizing working processes, are associated with proper interpretation of symptoms of a given failure. The symptoms are often identified as those arising from natural ageing process, contamination or wear of engine elements, determined by duration time of engine operation. In such cases external symptoms are usually concurrent and difficult for unambiguous determination. A special case forms the problem of analysis of diagnostic parameters for assessment of technical state (tightness) of the PRC system (Piston-Ring-Cylinder) of ship multi-cylinder piston engine deprived from possible application of cylinder indication. It often happens that trend curve of exhaust gas temperature changes only slightly deflects whereas piston head becomes burned through due to an injector failure. In such cases the only possibility to obtain any diagnosis of technical state of engine is ensured by visual inspection of its internal spaces with the use of endoscopes (elastic fibrescopes and stiff borescopes). In this non-invasive, very fast, inexpensive and unambiguous way all doubts bothering engine operator can be removed.

To operation process of ship combustion engines new diagnostic test methods are commonly introduced. Endoscopy which has been earlier used mainly for assessing technical state of flow part of turbine engines is dynamically developing and now it serves as a very useful and even indispensable tool for the diagnostic team of the Institute in its activity concerning piston engines especially those being in failure states or in the case of necessary prolongation of time interval between overhauls [23]. The team in question is equipped with the endoscopic set of OLYMPUS and STORZ firms (Fig.2).

The set is composed of three borescopes differing to each other with length of optic part, diameter and observation angle of diagnosed elements, namely: 90cm/8mm/90°, 30cm/4mm/0°, 30cm/10mm/120°. The latter one is especially useful in diagnosing combustion chambers and valve seats. The endoscopes show their high usefulness in hard accessible places of engine, e.g. combustion chambers - especially in the case when the disassembling of the head is difficult and time-consuming, in turbocharging system or internal spaces of mechanisms coupled with engine's crankshaft. In Fig. 2. a way of introducing the endoscope tip to internal space of piston engine, is presented. After disassembling the injector the endoscope makes it possible to assess technical state of piston head, cylinder liner surface and other subsystems mounted in it such as: spray nozzles of remaining injectors, inlet and outlet valves, start-up valves etc. The endoscopic inspection method plays special role in diagnosing the multi-block and multi-cylinder engines. For instance, in the engines of radial arrangement, of M503 type (having 42 cylinders) or M520 one (having 56 cylinders), installed in engine room, access to lower monoblocks and lower parts of reduction-reversible gear is very difficult. In the case of necessary overhauls, such engine together with the gear must be coupled out of propeller shaft, then heeled and lifted and sometimes even rotated inside the engine room so as to ensure access to the 1<sup>st</sup> or 7<sup>th</sup> cylinder block. From service practice it results that a fibrescope of a sufficiently long light pipe of optical system makes it possible to avoid such troubles and thus to save realization time of overhauls and their costs even by 25–30% [23].

Systematic endoscopic tests carried out in the frame of periodical maintenance surveys of ship engines operating in

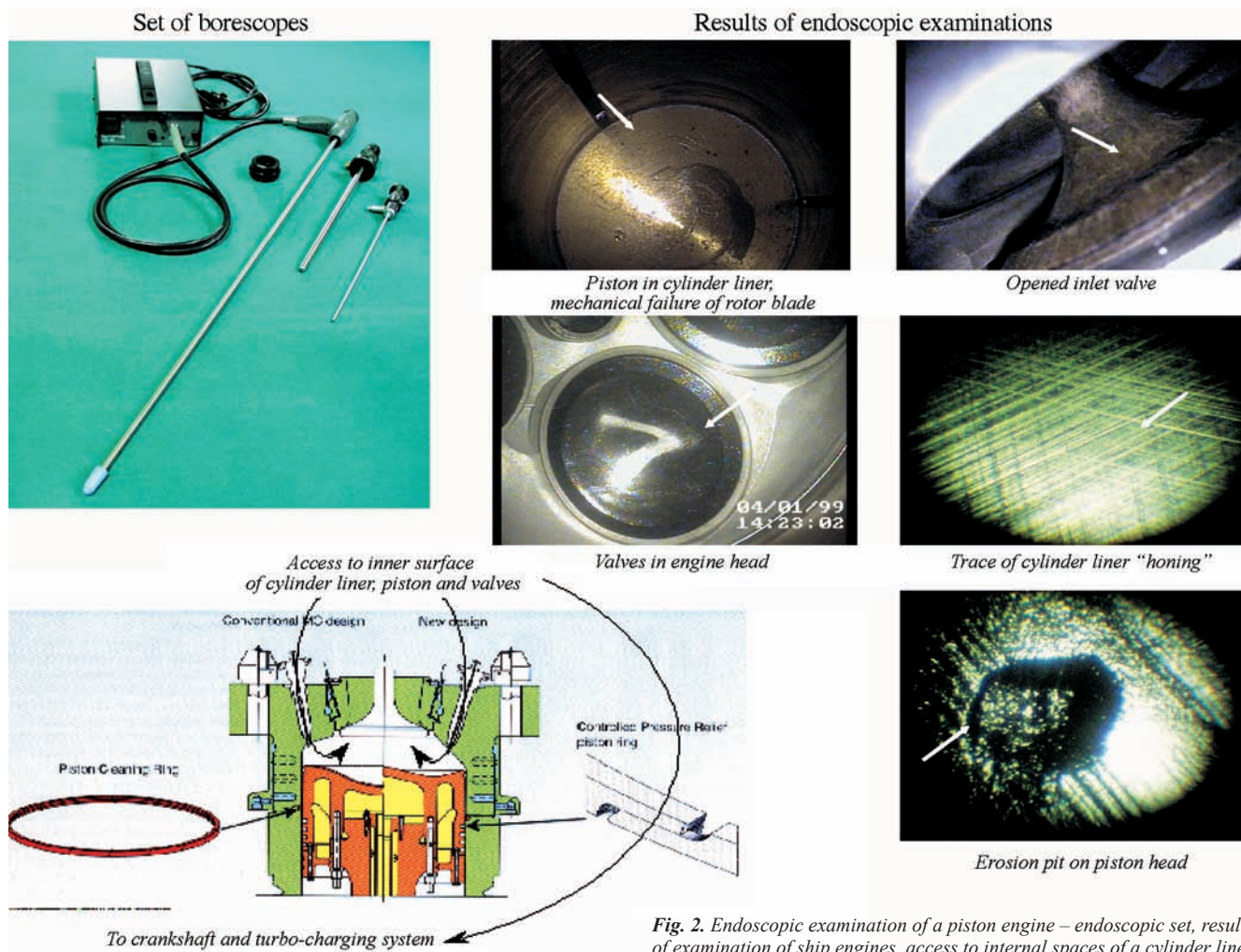


Fig. 2. Endoscopic examination of a piston engine – endoscopic set, results of examination of ship engines, access to internal spaces of a cylinder liner

Polish Navy have confirmed the high effectiveness of the method at relatively easy use of the testing instrumentation. As a result of such overhauls were disclosed many defects which – in the case of their further building-up - could highly endanger engine reliability. Selected defects of ship engines identified during endoscopic tests in service conditions have been systematically published in scientific journals, a.o. in [8,14,23].

## ALTERNATIVE METHODS FOR DIAGNOSING PISTON ENGINES

The scientific research work carried out in the Institute (under supervision of this author) is aimed at thorough modernization and further development of the so far functioning and proved diagnostic system by adding to it elements for controlling the main functional systems of engine (i.e. the piston-cylinder system, turbocharging system, fuel supply system as well as bearing system) in the situation when to assess technical state of engines not fitted with standard indicator valves becomes necessary. Just such engines (M401, Detroit Diesel and Mercedes Benz engines) are installed a.o. on the Polish Navy base trawlers of F207M type, American-origin frigates of Oliver Hazard Perry type and Norwegian-origin submarines of Kobben type, which have been lately incorporated to Polish Navy.

In the frame of realization of the following research projects:

- „Influence of adjustment of fuel supply system of ship piston combustion engine on spectrum of shaftline torsional vibrations ”,
- „Method of using measurements of cylinder internal pressure during idle operation to assessment of technical state of bearing system of ship piston combustion engine in service conditions”,
- „Diagnostic tests of supercharging system in the aspect of changes in combustion process occurring inside engine cylinder ”,
- „Research on influence of operational factors on performance and efficiency of propulsion systems of Polish Navy ships”,
- „Technical state assessment of ship engines of the series of AL, ASV and M520 types on the basis of measurement data collected by main propulsion monitoring systems of the ships of 206FM and 660 type”

was elaborated a number of new diagnostic stands which make it possible to indirectly assess the fuel combustion process in engine cylinders when their indication is not possible.

## DIAGNOSTICS OF TURBOCHARGING SYSTEMS

Turbocompressor constitutes a sensitive and – according to statistics - very unreliable element of four-stroke engine fitted with pulsatory supercharging system. Such situation results from specific operation conditions of ship engines, which are characterized by work at low and variable loads. It leads to an incomplete, and not quite thorough, fuel combustion in cylinders and further gas-dynamical and mechanical consequences of the phenomenon in the form of erosion, decreasing performance and lowering efficiency of turbocompressor, loss of stability of mechanical system, and at last to vibrations which generate accelerated wear of bearings and fatigue cracks of rotor's blades.

In diagnostic tests of pulsatory supercharging systems of ship engines it becomes necessary to identify run of changeability of being –at- disposal energy of pressure pulses

of exhaust gases delivered to turbocompressor during one working cycle. On the basis of measurements of instantaneous values of the ram pressure  $p_1^*$  and instantaneous values of the static pressure  $p_1, p_2$ , recorded at two control cuts, 1 and 2, of exhaust gas outlet channel, located at the distance  $L$  to each other – Fig.3, one determines the peak amplitude propagation velocity of exhaust gas pressure waves generated after opening successive outlet valves of engine cylinders. During next phase of the diagnostic reasoning, harmonic analysis of amplitude spectrum of exhaust gas pressure pulses in turbocompressor supply channel, is performed by means of the fast Fourier transform method [9,10,11].

For instance, from numerical data given in the form of time - frequency characteristics it can be observed which consequences result from elimination of one cylinder from operation: drop of the propagation velocity of exhaust gas pressure waves in turbocompressor supply channel as well as the unwanted concentration of amplitude spectrum of exhaust gas pressure pulses in the channel. In the amplitude spectrum, the fundamental frequency amplitude dominates that speaks about a significant unbalance of gas forces in engine cylinders, which makes destructive action on engine construction of unbalanced inertia forces generated by rotating and to-and-fro moving masses, increasing. The defined diagnostic measure in the form of the ratio of fundamental frequency amplitude and 3<sup>rd</sup> harmonic amplitude in vibration spectrum, for which trend analysis of changes of values is carried out during process of operation, makes it possible to assess technical state of elements of the PRC system, as well as of turbocharging system of the engine not fitted with standard indicator valves [11].

## DIAGNOSTICS OF FUEL SUPPLY SYSTEMS OF ENGINE

In the frame of the research project: „Influence of adjustment of fuel supply system of ship piston combustion engine on spectrum of shaftline torsional vibrations ” an original technical design was elaborated of a test stand for energy – orientated investigations of ship engines, for which an universal recorder of ship propulsion system performance and efficiency, based on measurements of fast-varying quantities, was built – Fig. 4 [2, 23]. In present, laboratory tests of the recorder are under way (on Sulzer 6AL20/24 engine), also it is tested in real conditions (on Sulzer 6AL25/30 main engine of H-5 tug). The tests cover simultaneous measuring and recording shaftline torsional vibrations and fuel consumption of both the engines. They are aimed at making assessment of influence of engine technical state changes on shaftline torsional vibration spectrum as well as fuel consumption. The experimental simulation consisted in disturbing the steady-state operation of engine by excluding its one cylinder from work. This way was simulated engine operation in the state of partial technical serviceability.

The recorded runs of ship shaftline torsional vibrations are subjected to spectral analysis with the use of the fast Fourier's transform (FFT) [2]. This way the diagnostic measures are determined for assessing technical state of engine cylinder systems and fuel supply system. An original set of methods for indirect assessing runs of gas-dynamic processes in cylinders, applicable also in diagnosing ship engines (and not only) in the case when direct measuring the pressure inside cylinders (due to lack of indicator valves) is not possible, is now in the final stage of elaboration. The set of the methods is scientifically investigated in the doctor thesis of M.Sc. Burski, St.

The achieved results encourage to continue further experimental tests on influence of regulation of fuel supply system and timing gear as well as changes in design structure

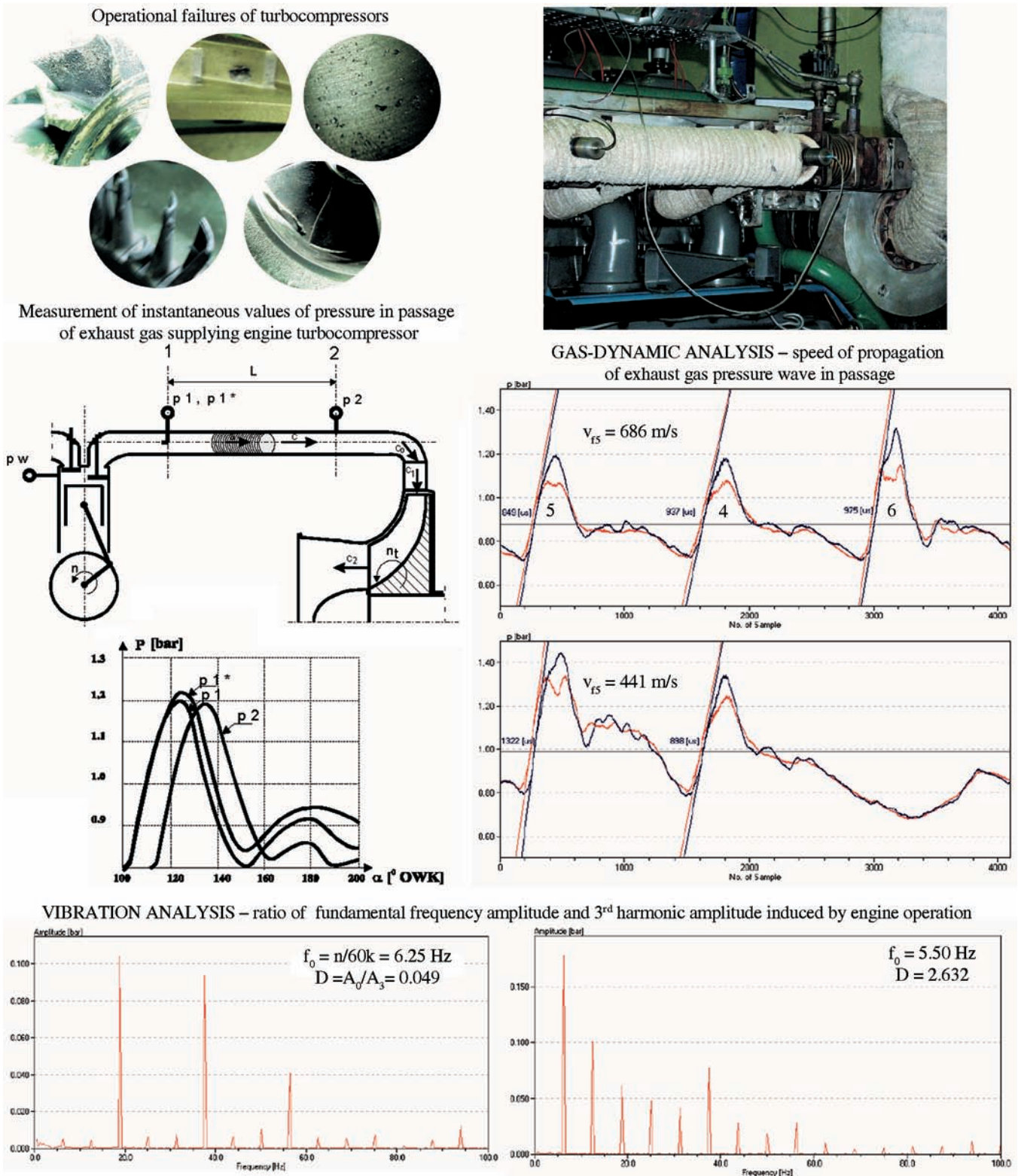


Fig. 3. The stand for the measuring of gas pressure pulses in exhaust gas system – results of diagnostic tests of turbocharging system

of turbine nozzle (i.e. simulation of contamination of blade passages) on the defined diagnostic measures.

### DIAGNOSTICS OF BEARING SYSTEMS

In the Institute is also under way an intensive research on the methods for technical state assessment of engine bearing system, based on the measuring of pressure inside cylinders under idle run. The research is aimed at finding a relationship between technical state changes of bearing system of piston of ship combustion engine (leading to its increased mechanical

losses), is based on indication of idle running engine at uncoupled driving unit.

Passive experimental investigations on the problem have been carried out in the frame of the doctor thesis of M.Sc. Wontk, L., since 1997 [23]. In present, in order to verify the proposed set of methods for diagnosing ship engines, active experiments on the laboratory engine where real defects of main and crankshaft bearings have been introduced, are under way. For realization of that phase of the research are used sets of bearing sleeves having wear of different kind and degree, dismantled from real objects out of service – Fig. 5.

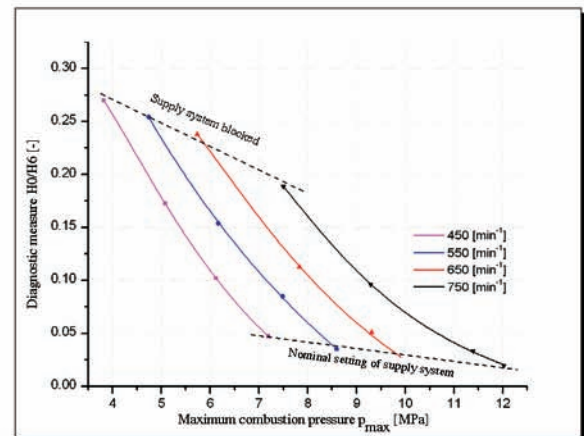
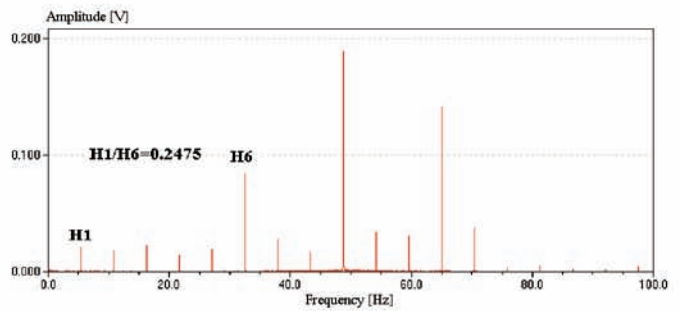
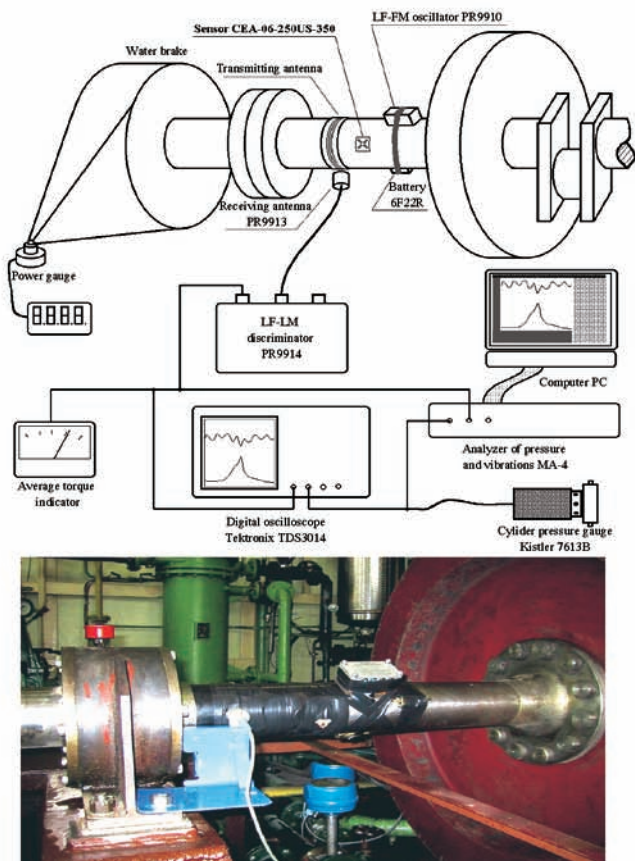


Fig. 4. The stand for measuring torsional vibrations of ship shaftlines – results of the indirect testing of runs of processes occurring inside cylinders

As the realized research results indicate, the idle-run indicated power constitutes a sensitive diagnostic parameters of engine. However it does not allow to unambiguously localize sources of increased mechanical losses but only to signalize their possible occurrence. Hence in order to unambiguously determine whether the changeable technical state of bearings is responsible for the increased mechanical losses it is necessary to verify the diagnostic tests by means of spectral tests of metallic particle content in lubricating oil. In present, a programme of preliminary tests aimed at proper choice of analytical models of copper and lead content is under elaboration.

## DIAGNOSTICS OF TURBINE ENGINES – A HISTORICAL OUTLINE

Since 1986 in the then Institute of Ship Construction and Operation, Polish Naval Academy, several scientific research projects on diagnosing ship gas turbine engines have been realized [3, 23]. Their scope of themes was inspired by the efforts leading to elaboration of effective diagnostic methods applicable in real service conditions on board a ship. A strategic aim was to pass to the operation process of engines in accordance with their technical state. As a result the “Basic diagnostic system” was implemented into the operational system of Polish Navy ships. Its concept and realization resulted from the following projects:

- The task project no. 148-23/S-SO/93: „Diagnostics of ship gas turbine engines”;
- The research projects:
  - ⇒ no. 9 T12D 008 11: „Technical state assessment of ship gas turbine engines on the basis of research on their dynamic features”;

- ⇒ no. 0 T00A 009 16: „Assessment methods of co-axiality of torque transmission elements of ship propulsion systems”;
- ⇒ no. 0 T00A 062 19: „Elaboration of a diagnostic system for ship gas turbine engines installed on the frigates being incorporated into Polish Navy”;
- ⇒ and also a dozen of tens of R&D projects and expertises financially supported by the State Committee for Scientific Research and Polish Navy.

The system which is continuously developed and modernized, contains several diagnostic stands which make it possible to perform a complex assessment of ship gas turbine engine (practically of an arbitrary configuration) as well as to elaborate a prediction of its further operation process. The system is equipped with special controlling and measuring instruments as well as analytical tools, which make it possible to perform diagnostic tests of engines during stopovers and sea trials of ships. [4,12,13].

In this chapter are presented short characteristics of experimental test techniques applied to assessment of technical state of General Electric LM-2500 engines and Zoria DR76 and DR77 engines, presently subjected to the diagnostic program in question [24]. Some metrological and organizational aspects of realization of necessary diagnostic tests as well as measurements of control parameters of gas turbine engine in steady states and transient ones (start-up, acceleration and deceleration) are also highlighted. Usefulness of particular diagnostic methods regarding their effectiveness in identifying engine operational unserviceability, has been assessed. In present, investigations are under way to make it possible to carry out engine operation process - in accordance with technical state - of all turbine engines being in use of Polish Navy. Each year, on average 14-16 expertises of engine

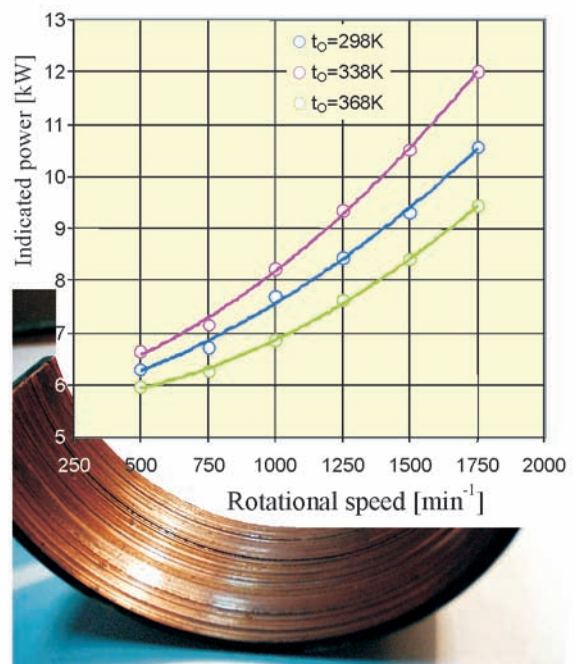
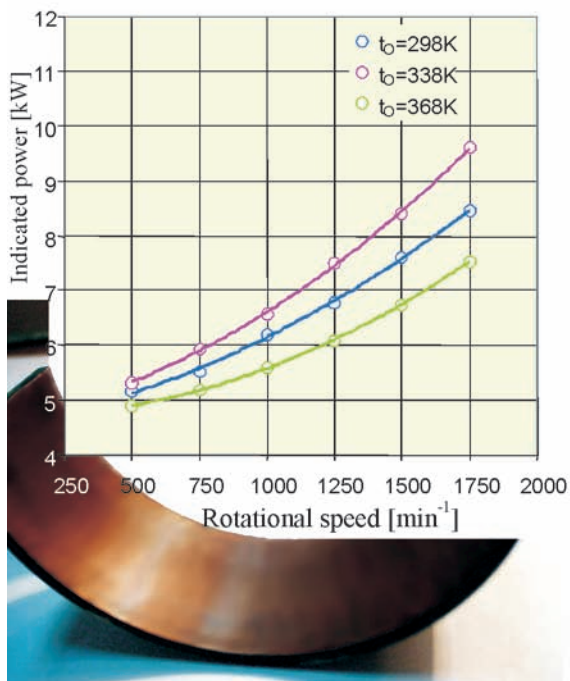
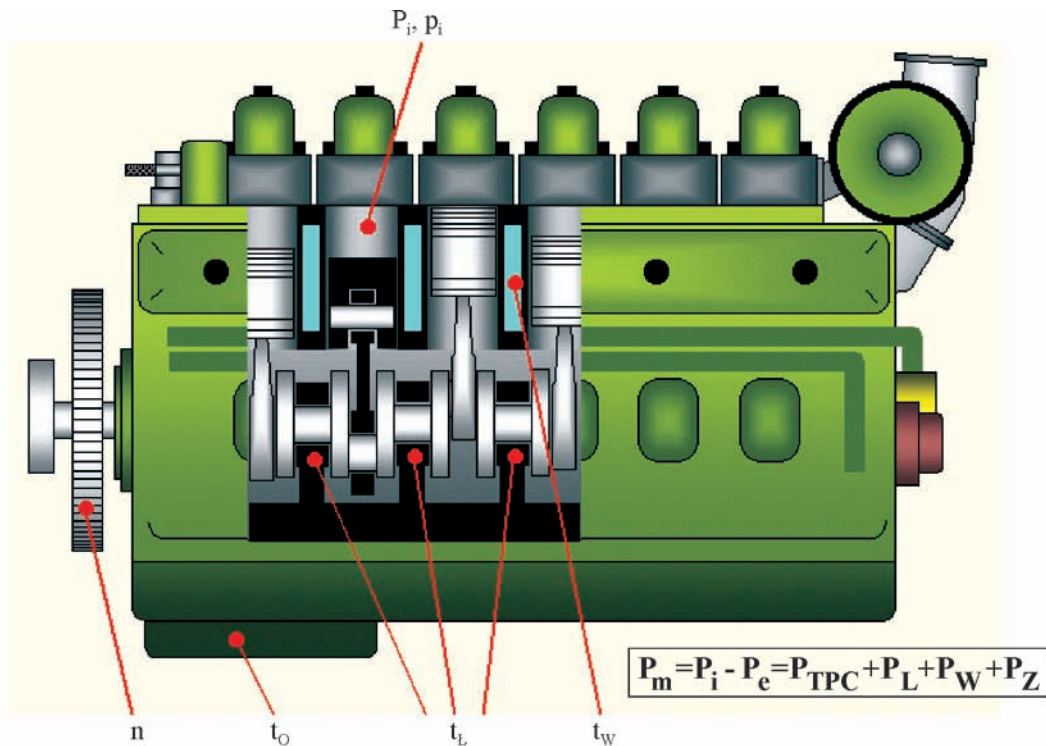


Fig. 5. The stand for the diagnosing of ship engine bearing system – results of tests of bearing sleeves.  
 $P_m$  – power of mechanical losses of engine,  $P_{TPC}$  – friction drag power lost in TPC (piston - piston rings - cylinder) system,  
 $P_L$  – friction drag power lost in bearing system,  $P_W$  – ventilation drag loss power,  
 $P_Z$  – friction drag power lost in mechanisms coupled with crankshaft and timing gear.

technical state are performed, on the basis of diagnostic tests of the main functional systems of the engines together with their control and safety devices [23].

### ENDOSCOPIC DIAGNOSTICS OF ENGINE FLOW PART

For endoscopic examinations of gas turbine engines is used an extended optical set which makes visual inspection and preparation of photographic documentation of internal elements of flow part of engine through inspection openings of abt. 5 mm in diameter, possible. For carrying out dimensional analysis of internal defects of engine elements, their visualization and

documentation in data base a Camedia C–2500L digital camera of OLYMPUS firm, is used. The camera is connected with a borescope or fibrescope by means of special links (adapters). Fig. 6. presents the endoscopic diagnostic set used in the basic diagnostic system of the Institute.

The borescopes of stiff lense system of various lengths make it possible to do observations within side sectors and head sector in a wide range of angles of view. The borescopes are very comfortable in use during visual inspection of edges of guide vanes and rotor blades. In order to overhaul all rotor blades the inspection should be connected with simultaneous turning the rotor by hand. Endoscopic examinations of ship engines are performed during preventive surveys once a year

at least, for current assessment of engine technical state, in the case when to extend the between-repair time period is necessary, as well as in the case of an increased vibration level, occurrence of metal particles in lubricating oil, jump deviations from trend curves of changes of exhaust gas temperature, excessive smoking, control of flow part washing effectiveness etc.

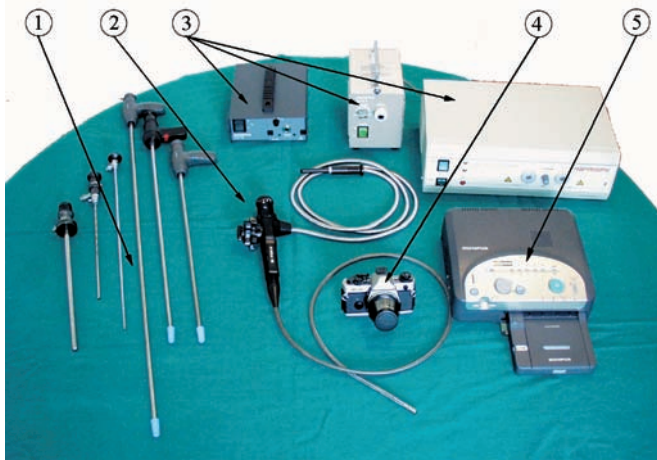


**Fig. 6.** The diagnostic set of OLYMPUS and STORZ firms:  
1 – set of borescopes, 2 – fibroscope, 3 – set of lighting sources,  
4 – digital camera, 5 – photoprinter

On the basis of multi-year endoscopic examinations of ship engines, the assessment methods of their technical state in service conditions were elaborated. They cover a necessary

scope and sequence of inspections of internal spaces, which make detecting the defects in particular constructional elements of engine's flow part, possible.

For each type of the engines used on Polish Navy ships detail manuals for performing the diagnostic examinations with the use of fibrescopes and borescopes, were prepared. In Fig. 7 and 8 example places for insertion of endoscope tips into flow part of turbine engines subjected to diagnostic survey, are presented. Selected defects of ship engines, identified during endoscopic examination in operation are presented in Fig. 9; they are systematically published in scientific journals, a.o. in [4, 8, 14].

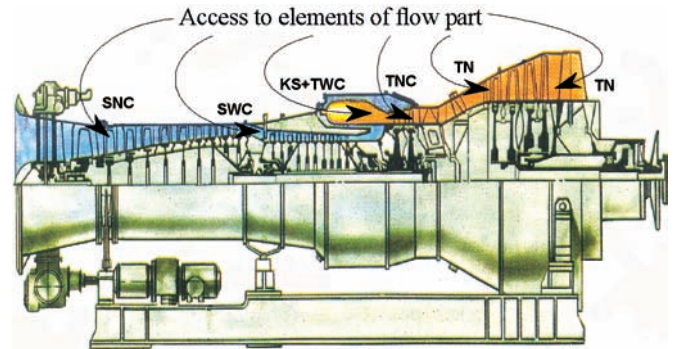


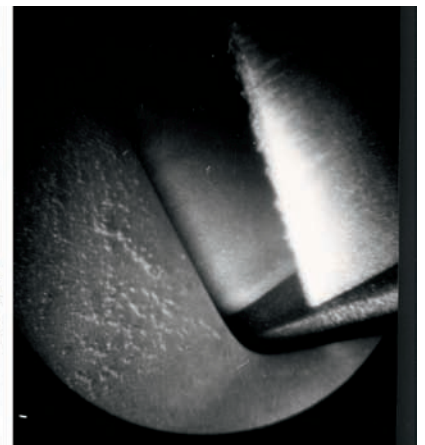
**Fig. 7.** Endoscopic examination of DR 76 and DR 77 gas turbine engines – access to their flow parts SNC – Low Pressure Compressor, SWC – High Pressure Compressor, KS – Combustion Chamber, TWC – High Pressure Turbine, TNC – Low Pressure Turbine, TN – Propulsion Turbine



*1st stage of gas generator turbine of LM-2500 engine – traces of erosion on rotor blade surface*



*6th stage of propulsion turbine of LM-2500 engine – traces of carbon deposit on rotor blade surface*



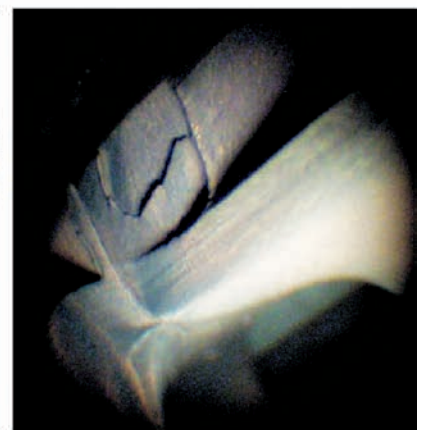
*1st stage of LP compressor of DR77 engine – contamination deposit on blade surfaces*



*9th stage of compressor of LM-2500 engine – dent and crack at the edge of attack of rotor blade*



*16th stage of compressor of LM-2500 engine – dent at the edge of attack of rotor blade*



*1st stage of HP turbine of DR76 engine – loss of material of blade plate*

**Fig. 9.** Defects in ship engines identified during endoscopic examinations

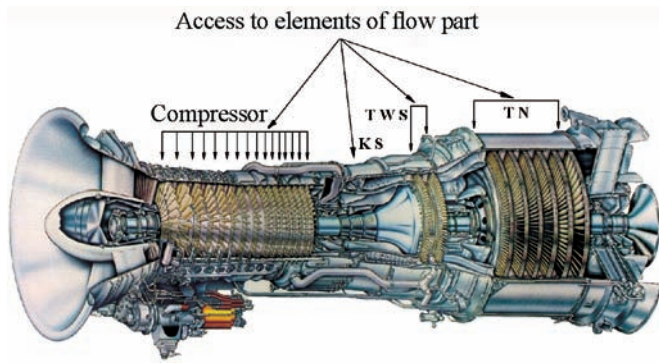
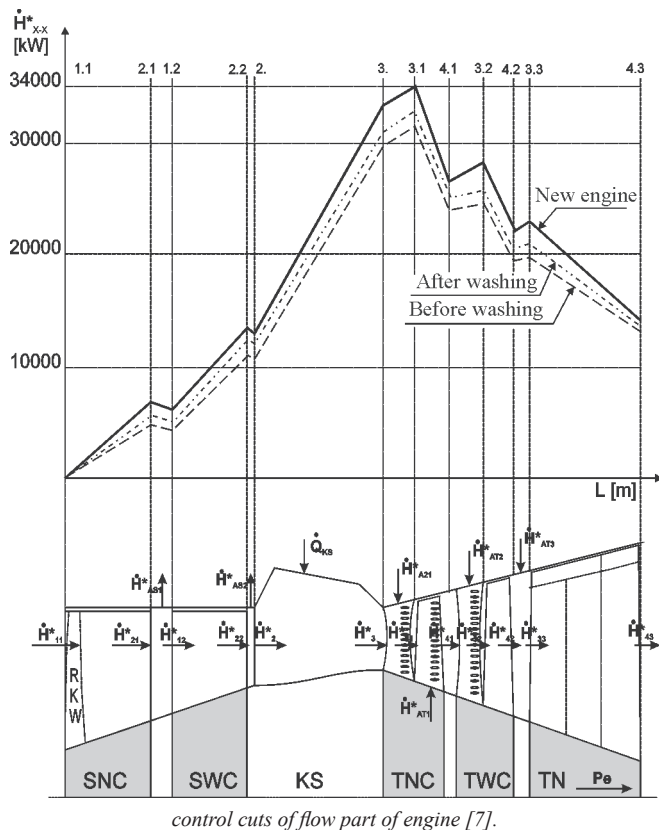


Fig. 8. Endoscopic examination of LM-2500 gas turbine engine – access to its flow part

### PARAMETRIC DIAGNOSTICS OF FLOW PART OF ENGINES

From statistical data gathered by ship engine producers as well as reliability analysis based on over-twenty-year lasting service experience from operation of engines installed on board Polish Navy ships it results that this is the flow part of engines which constitutes the most troublesome functional system of turbine engine and that the dominating unserviceability state is caused by different contaminations of blade passages of compressors and turbines [3, 4, 7]. During operation process of ship engines, is systematically performed assessment of their technical state in accordance with trend analysis of changes of energy characteristics of their flow parts [12]; this is the working medium entalpy flux distribution along flow passage,  $\dot{H}_{x-x}^* = f(L)$ , prepared for a given load range, usually of  $1.0 \dot{P}_{nom}^*$  (Fig. 10).

Fig. 10. Distribution of working medium entalpy flux in characteristic



control cuts of flow part of engine [7].

The so called degree of split of energy characteristics in particular control cuts of engine flow part, x-x, determined on the basis of measurements of thermal-gas-dynamic parameters of working medium, serves as the measure of the generalized

diagnostic parameter calculated by means of the following relation:

$$\Delta \dot{H}_{x-x}^* = \dot{H}_{x-x(pom)}^* - \dot{H}_{x-x(o)}^* \quad (1)$$

Another method of assessment of technical state of engine flow part consists in analysing its dynamic features. As a result of degradation of technical state of blade passages of compressors and turbines, inertia features of unsteady thermal and flow processes in engine are changed - and in consequence - also character of gas-dynamic interaction of its rotor units. The performed tests prove that a crucial diagnostic problem is the experimental determination of changeable capability of engine to cumulating and dispersing energy and substances in its mechanical and flow systems [13]. The so far performed efforts of the Institute's research team on the problem in question resulted in the monograph devoted to diagnostic use of acceleration and deceleration processes of multi-shaft engines, as well as in promotion of two doctors specialized in diagnostic investigations of starting-up processes of ship engines, namely: Dr Włoch, J. and Dr Pojawa, B. [13, 19, 22].

In present, in the Institute are under way research projects aimed at elaboration of a method for analytical determination of energy characteristics of engine flow passage, represented in the spatial coordinate frame of time and pivot angle of guide vanes of some first stages of compressor, considered to be the independent variables of occurring unsteady processes:  $\dot{H}_{x-x}^* = f(L, \tau, \alpha)$ .

The so arranged characteristics are used for assessment of changes of engine dynamic features for diagnostic purposes. In this case, an important difficulty is to measure a necessary number of control parameters with no delay and with required accuracy, as well as the necessity to model characteristics of the compressor of variable flow geometry, e.g. by using controlled guide vanes of its first stages – Fig. 11.

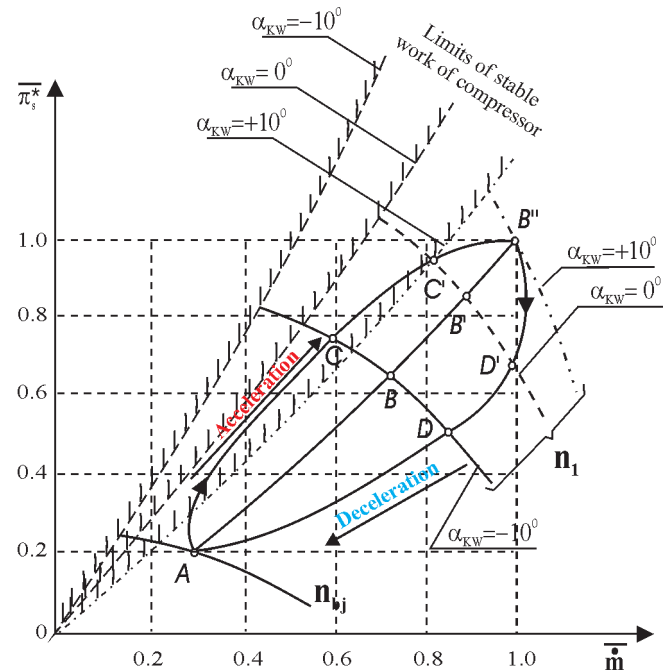


Fig. 11. Change of range of operation observed in compressor characteristics, caused by interaction of controlled guide vane; ABB'B'' – points of cooperation of the compressor with the network in steady states; ACC'B'' – points of cooperation of the compressor with the network during engine's acceleration; B'D'DA – points of cooperation of the compressor with the network during engine's deceleration.

Measurement and recording process of thermal-gas-dynamic parameters is carried out with the use of special analyzers designed and built in the Institute [23].

The problem of model investigations of energy processes occurring in axial compressors of turbine engines of variable geometry of flow passages, has been considered in the doctor thesis of M.Sc. Wirkowski, P. [23]. Complex metrological aspects associated first of all with necessity of mounting many gauges for measuring pressure and temperature of flowing medium, seriously limit possible applications of the method to operation process of engine on board a ship. In the engines subjected to the diagnostic survey, accessible places for fitting additional measuring gauges of low inertia are very limited in number. For this reason further work on the problem will be carried out by using laboratory stand for testing GTD350 aircraft engine. The results have been achieved so far encourage to carry out experimental research in the area of influence of regulation of the fuel supply and starting-up systems of the engine, as well as influence of changes in compressor's design structure (by simulation of contamination of blade passages and guide vane angle changes) on the diagnostic measures defined for engine dynamic behaviour.

## RESEARCH ON VIBRATIONS

Turbine engine vibrations result from loss of stability of its mechanical system, which means that resonance of global character appears, i.e. the whole engine vibrates, - in this case it is a designer's problem, or that of local character when one of the fundamental vibration frequencies of engine subsystem,  $f_{0j}$ , approaches the frequencies of periodically changeable forces exciting vibrations,  $f_{wym}$ .

The loss of stability of the mechanical system results from the following unfavourable phenomena which can occur and develop in the engine: the slow worsening of unbalance state of rotor systems caused by sedimentation of contaminations, erosion and corrosion of blade passages, as well as bent shafts, sudden increasing of unbalance of rotor systems caused by loss of a part of a rotating element, e.g. blade, exceedance of allowable load exerted on bearings, occurrence of friction between rotors and engine casing elements in labyrinth seals, occurrence of self-excited vibrations due to pulsatory flow of working medium (resulting from non-uniform distribution of temperature and flow velocity along flow passage circumference).

The phenomenon of resonance is of a great impact on reliability and durability of engine as it results in material fatigue and consequently – cracks in its structural elements. There are two ways leading to elimination of resonance vibrations:

◊ Making constructional improvements in order to change fundamental frequency of vibrations or that of exciting forces (a change of stiffness and mass of rotating elements),

◊ Removal - from engine operation range – of that rotational speed at which the resonance occurs.

In ship engine operation the basic method to eliminate vibrations is the systematic cleansing (washing) of its flow part and adjusting of gas temperature field in the control cut behind the combustion chamber (usually – behind gas generator turbines). In Fig. 12 the example results of measurements of transverse vibrations of DR76 turbine engine are presented together with results of harmonic analysis of excitations from the side of the engine's rotors.

The research on vibration of gas turbine engines has constituted the subject of scientific considerations of Dr. Grządziela, A., who has extended range of his interest onto vibrations generated by any arbitrary structural node of ship propulsion system of any arbitrary configuration including also the systems driven by piston combustion engines. The

passive experimental research on the problem, which has been continuously carried out since 1997, is aimed at permanent improving the methods of diagnostic use of acoustic vibrational signal for assessment of state of co-axiality of engines and remaining elements of ship propulsion system and power consumer [5].

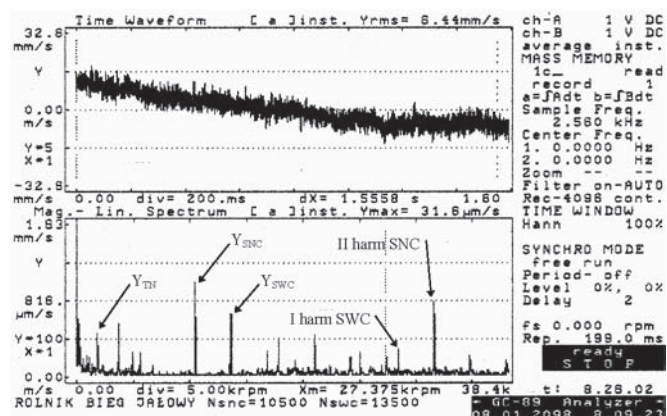


Fig. 12. Linear run and harmonic analysis of vibration signal [23]

## RESEARCH ON BEARING SYSTEMS

Lubrication conditions of bearing units of gas turbine engine decide on its reliability and durability. From service experience of aircraft engines it results that most serious catastrophes of aircrafts are caused by primary, not detected in a proper time, defects of shafts and their rolling bearings. Especially, multi-shaft constructions of a complex kinematic system show the greatest unreliability of the bearing system, resulting from an insufficient fatigue strength.

In heavy waves, due to detrimental action of cyclic loads (impacts and shocks), the rolling bearings of ship gas turbine engines are exposed to failures. From available literature sources it results that most of the occurred defects was always preceded by accelerated wear of the most loaded elements of friction pairs, i.e. raceways of outer and inner rings, rolling elements in the form of balls and rollers as well as distance rings and sleeves and labyrinth seals. Such situation is demonstrated by increased temperature of bearing's structural elements, elevated noisiness during operation, changes in physical and chemical features of lubricating oil, as well as occurrence of metallic particles in it [16].

Hence the lubricating oil parameters can be considered carriers of diagnostic information about technical state of oil-lubricated friction elements of gas turbine engine. The necessary information can be obtained from results of measurements of the following items:

- *Temperature and pressure* in lubricating system (lubricating oil rate of flow)
- *Lubricating oil consumption*
- *Physical and chemical features of of lubricating oil* (viscosity, flash point, acid and base numbers, water content)
- *Concentration of metallic contamination in the oil.*

The tests make it possible to control wear process of a given friction node and to localize – by means of quantitative and qualitative analysis - its friction-dependent elements (such as the above mentioned) during gas turbine engine service. The following means and methods of diagnostic action are used:

- ✦ *Magnetic stoppers and electronic devices signalling metallic filings, mounted in lubricating oil outlet piping – possible detection of large ferromagnetic particles up to 1000 μm in size*

- ✦ Method of radioisotope fluorescence – chemical composition of metallic contaminations (small particles up to  $30\ \mu\text{m}$  in size) is analyzed on the basis of excitation and measurement of intensity of a characteristic X-radiation of a given sample. Leading producers of gas turbines apply specific codes to indicate the sensitive structural elements covered by thin layer of noble metals, that greatly increases engine susceptibility to control in service
- ✦ Optical methods – optical and electronic microscopes used for qualitative assessment, providing sample enlargement of 160-times (and more)
- ✦ Detection of water content and metallic impurities of 2,5– $30\ \mu\text{m}$  in size.

The mechanical tests on contaminations (apart from metallic also graphite ones) contained in lubricating oil of ship engines and reduction gears, have been carried out by the diagnostic team of the Institute since 1992.

The example results of the tests on Fe and Cu content in lubricating oil in function of the operation time  $t$  of LM-2500 engine are presented in Fig. 13.

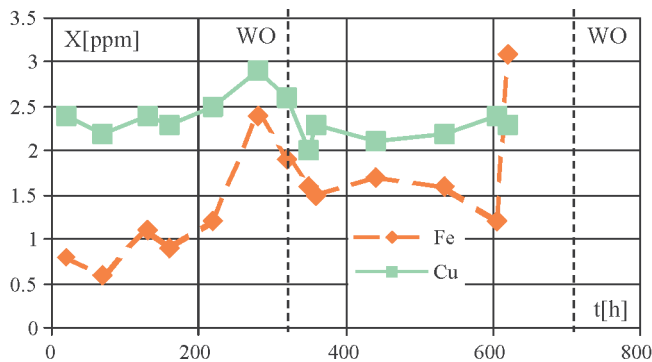


Fig. 13. Runs of changes in Fe and Cu contamination of lubricating oil in function of operation time of LM-2500 engine, WO – oil replacement [13]

On the basis of multi-year tests carried out both by the Institute and the engines' producer, as well as relevant experience of aeronautics, the limits of operational tolerance field were established: for Fe concentration – 6.0 ppm, for Cu concentration – 9.0 ppm. Also, trend functions which make it possible to predict friction wear intensity process in engines and reduction gears, were elaborated. With their use the scheduling of lubricating oil replacement and maintenance intervals is made. As a result of the research work has been carried out so far by the diagnostic team the operational manual of diagnostic tests of bearing systems for all the types of propulsion engines and reduction gears used on board Polish Navy ships, was elaborated; the achievement is based on the doctor thesis of Dr Mironiuk W. [16].

## RESEARCH ON FUEL OIL INJECTORS

The basic task of fuel supply system of ship gas turbine engine is to ensure – in all possible load ranges – an adequate (qualitatively and quantitatively) fuel flux delivered to combustion chamber. Irrespective of an applied design solution, fuel oil injectors take crucial place in the system regarding reliability considerations. They ensure a high effectiveness of fuel combustion process after sufficient spraying the fuel in advance. As a result, a fuel aerosol consisted of drops of 10-20  $\mu\text{m}$  in diameter, is produced [1]. Such atomization of fuel makes its whole vaporization and effective combustion during flow through engine combustion chamber, possible. The greater dispersion of drops the shorter time interval necessary

for vaporization and production of uniform fuel – air mixture, that determines inertance of combustion process.

In engine operation process in shipboard conditions certain disturbances can occur in correct work of particular injectors. They result from continuous process of contamination and wear of flow passages as well as deformations of characteristics of ageing control elements [23,24]. As a consequence, flow rate, quality of fuel atomization and geometry of its outflow from injector also become changed. Unfavourable deformations occur of gas flux temperature field behind combustion chamber, which can lead to a local overheating of its construction. Also, turbine subsystems, especially their guide vanes being under large thermal-gas-dynamic loads of pulsatory flow of working medium, are exposed to failures.

Control of technical state of injectors is necessary in order to prevent possible engine failures and the lowering of operational effectiveness of injectors. The most popular become disassembling-free control methods based on the measuring of selected parameters of thermal cycle of engine, possible to be taken in shipboard conditions. Fuel flow rate measurements, apart from the measurements of selected thermal-gas-dynamic parameters characterizing engine load, can be also a valuable source of diagnostic information on technical state of injectors [1].

In ship gas turbine engines the two-passage swirl injectors are commonly used, Fig. 14. They ensure a high effectiveness of fuel atomization over whole range of engine load changes.

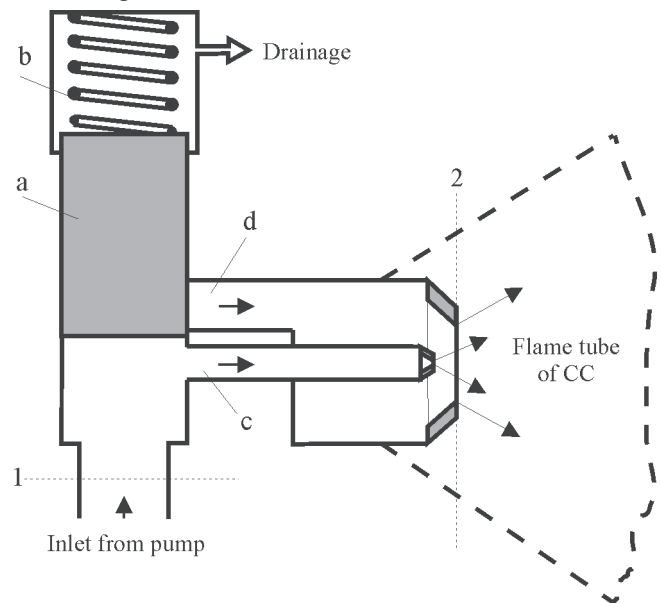


Fig. 14. Schematic diagram of fuel flow through two-passage swirl injector [1]: a – fuel distributor, b – spring, c – 1st passage of injector, d – 2nd passage of injector, 1 and 2 – control cuts

The below given formula (2) for determination of mass flow rate of the fuel delivered to gas turbine engine injector is the most often used way of mathematical description of its work in steady states of engine operation [1]:

$$\dot{m}_{\text{pal}} = \sqrt{2\rho_{(T)}\Delta p_w} \left[ \sum_{k=1}^n (\mu_{\text{wyp}} A_{\text{wyp}})_k \right] \quad (2)$$

where:

- $k$  – number of injectors
- $\Delta p = p_1 - p_2$  – drop of pressure in injectors
- $\mu_{\text{wyp}}$  – fuel outflow coefficient
- $A_{\text{wyp}}$  – area of spayer nozzle cross-section in fuel outflow plane.

In the process of assessment (calculation) of rate of fuel flow into engine combustion chamber under operation, an important difficulty constitutes determination of the outflow coefficient  $\mu_{\text{wyp}}$  for particular injectors. It is a function of flow character defined by Reynolds number, as well as of a form and dimensions of sprayer nozzle [23].

For this reason it is usually determined on the basis of results of experimental tests. For the analyzed type of injector the value of  $\mu_{\text{wyp}} = 0.92 \pm 0.02$ , as determined on a laboratory stand of "cool combustion chamber", is provided by its producer [24]. The value should be considered only as a preliminary estimation. In real operation conditions of injector installed in engine, its elements are subjected to direct action of fuel combustion zone and they are heated up to high temperature (500-600K). Their flow passages become "deformed" and achieve a new, real value of the fuel outflow coefficient. Another service problem, as well as manufacturing one, is the necessity of selecting individual sets of injectors for each of the engine, to match similar values of mass flow rate for 1<sup>st</sup> and 2<sup>nd</sup> flow passage. Unrepeatability of their production results in a substantial scatter of flow rate values even up to 5-7% for one set of injectors [24].

The diagnostic tests of ship engine injectors are aimed at determination of an averaged value of fuel outflow coefficient for one set of injectors on the basis of measurements of gas-dynamic parameters of working medium, as well as fuel combustion.

The so elaborated loading characteristics represent a relation between flow rate and mean fuel outflow coefficient in function of changes of the load determined on the basis of rotational speed of gas generator rotor coupled with fuel pump – Fig. 15.

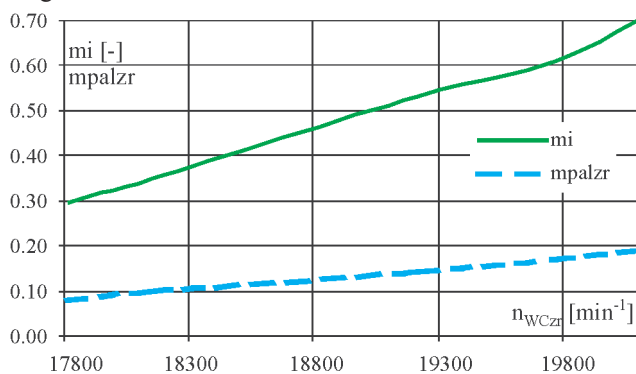


Fig. 15. Changes of mass flow rate and mean fuel outflow coefficient in function of rotational speed of rotor of HP engine DR76 [1]

Comparative analysis of the so elaborated characteristics related to the reference values recorded during the initial phase of operation makes it possible to formulate a diagnosis on technical state of flow passages of set of injectors of an engine in service.

## SUMMARY

- The Institute of Ship Construction and Operation, Polish Naval Academy, carries out diagnostic tests of piston and turbine engines of all kinds, installed on Polish Navy ships. On the basis of currently performed investigations it is possible to carry out operation of more than 150 engines of the total power output close to 500 MW, in accordance with their technical state.
- The test stands, data base as well as diagnostic programs are successively amended and extended regarding workshop repair and changes of characteristics of engines during service.

- Until now over 1000 expertises of ship propulsion systems fitted with piston and turbine combustion engines have been prepared.
- Presently carried out research projects are focused on development and modernization of the basic diagnostics system to the extent which will make it possible to carry out diagnostic control of ship piston and turbine engines installed on board American-origin frigates (fitted with Detroit Diesel 16V149 TI engines and General Electric LM-2500 engines), which have been lately incorporated into Polish Navy.

## BIBLIOGRAPHY

1. Białomyzy A., Korczewski Z.: „A method of experimental determination of fuel outflow coefficient for a set of injectors of ship gas turbine engine” (in Polish). 12<sup>th</sup> Symposium on Fluid Fuels and Lubricating Products used in Maritime Economy. Ministry of Transport and Maritime Economy, Szczyrk, 6-8 May 1997
2. Bruski S., Korczewski Z.: „Results of stand tests of influence of selected defects of fuel system of ship piston combustion engine on shaftline torsional vibration spectrum” (in Polish). Scientific Bulletin of Polish Naval Academy (Zeszyty Naukowe AMW), no. 2/2003
3. Charchalis A.: „Diagnostics of ship gas turbine engines” (in Polish). Publishing House of Polish Naval Academy (Wydawnictwo AMW), Gdynia 1991
4. Charchalis A., Korczewski Z.: „Diagnostic methods for ship gas turbine engines” (in Polish). Mechanical Review (Przegląd Mechaniczny), no. 3,4, Warszawa 1997
5. Grządziela A.: „A method for control of co-axiality of elements of ship propulsion systems fitted with gas turbine engines” (in Polish), Doctor thesis, Polish Naval Academy, Gdynia 1998
6. Hemingway B.E.: “A new British naval gas turbine”. The Oil Engine and Gas Turbine, October, England 1959
7. Hemingway B.E.: “Surge and its implications in gas turbines”, The Oil Engine and Gas Turbine, October, England 1961
8. Korczewski Z.: “Application of endoscopic methods in diagnosing the marine engines”, 2<sup>nd</sup> International Scientific Technical Conference „EXPLO-DIESEL & GAS TURBINE’01”, Gdańsk–Międzyzdroje–Kopenhaga, 23-27 April 2001
9. Korczewski Z.: “An approach to modeling of gas-dynamic processes in turbo-charging system of marine four-stroke diesel engine”, Polish Maritime Research no. 3/2002
10. Korczewski Z.: “Preliminary identification of gas-dynamic processes in exhaust gas channel of pulsatory supercharging system of a marine diesel engine”, Polish Maritime Research no. 4/2002
11. Korczewski Z.: „A method for diagnosing the ship turbo-charged engines, based on results of testing gas-dynamic processes occurring in exhaust gas systems” (in Polish), Diagnostyka, Vol. 25/2003
12. Korczewski Z.: „A method for diagnosing the flow part of gas turbine engine in service” (in Polish). Doctor thesis, Polish Naval Academy, Gdynia 1992
13. Korczewski Z.: „Identification of gas-dynamic processes in compressor unit of gas turbine engine, for diagnostic purposes” (in Polish), Assistant-professorship dissertation (a monograph), Scientific Bulletin of Polish Naval Academy (Zeszyty Naukowe AMW) no. 138A, Gdynia 1999
14. Korczewski Z., Pojawa B.: „Endoscopic diagnostics of ship engines” (in Polish). Scientific Bulletin of Polish Naval Academy (Zeszyty Naukowe AMW), no. 3/2004
15. Kniaziewicz T., Zadrag R.: „Possibility of testing and lowering content of toxic compounds contained in exhaust gas emitted from piston combustion engines installed on board Polish Navy ships”, (in Polish) 22<sup>nd</sup> Symposium on Ship Power Plants. Gdynia Maritime University, 14-15 November 2002

16. Mironiuk W.: „Assessment of failure states of bearing systems of ship gas turbine engine” (in Polish), Doctor thesis, Polish Naval Academy, Gdynia 1995
17. Piaseczny L., Kafar I., Zadrag R., Bergier T., Kniaziewicz T.: „Report on realization of the research project no. 9T12D00613” (in Polish), Polish Naval Academy, Gdynia 1998
18. Piaseczny L., Zadrag R., Kniaziewicz T.: „A system for measuring emission of toxic compounds contained in exhaust gas from ship combustion engines” (in Polish), 23rd Symposium on Ship Power Plants, Gdynia Maritime University, Gdynia, 14–15 November 2002
19. Pojawa B.: „A method for diagnosing start-up system of ship gas turbine engine” (in Polish), Doctor thesis, Polish Naval Academy, Gdynia 2002
20. Polanowski S.: „A novel type of analyzer for measuring and diagnosing ship engines” (in Polish), Journal of KONES, Warszawa-Poznań 1995
21. Polanowski S. et al. „Reports on diagnostic tests of piston combustion engines operating on board Polish Navy ships” (in Polish), Research reports of Polish Naval Academy (Prace badawcze AMW), Gdynia 1992–1999
22. Włoch J.: „Diagnosing ship gas turbine engines on the basis of quantities which characterize run of starting-up and stopping operations” (in Polish), Doctor thesis, Polish Naval Academy, Gdynia 1995
23. Various authors: „Reports on realization of R&D projects and expertises concerning diagnostics of piston and gas turbine engines operating on board Polish Navy ships” (in Polish), Research reports of Polish Naval Academy, Gdynia, 1982–2005
24. „Technical and operational documentation of the ship gas turbine engines of LM2500, DR76 and DR77 types” (in Polish).

---

**CONTACT WITH THE AUTHOR**

\*\*\*\*Zbigniew Korczewski.\*\*\*Rj 0F 0  
 Mechanic-Electric Faculty,  
 Polish Naval University  
 Śmidowicza 69  
 81-103 Gdynia POLAND  
 e-mail: zkorczewski@wp.pl



Photo: C. Spigarski

# Determination of location of Top Dead Centre and compression ratio value on the basis of ship engine indicator diagram

Stanisław Polanowski  
Polish Naval University

## ABSTRACT



*In the polytropic model of compression process, exponent of polytropic compression curve was replaced with a power polynomial in which the piston travel was used as its argument. It was shown that 3<sup>rd</sup> order polynomial is optimum one. In the model were taken into account the following: design parameters of cylinder, influence of cylinder wear and gas blow-by on compression process, error in determining the piston's Top Dead Centre (TDC) location, measurement error due to indicator diagram's truncation. The presented solution of the non-linear model is based on its partial linearization, use of the least squares method as well as on application of the optimum determination methods known in the theory of experiment. The model makes it possible to determine TDC location on indicator diagram dealing with combustion, determination of total compression ratio, pressure value of indicator diagram truncation, as well as determination of maximum values of compression pressure on the diagrams in which self-ignition occurs before reaching the TDC.*

**Keywords:** Top Dead Centre, compression ratio, ship engine indicator diagram

## INTRODUCTION

Indication of ship engines has been used for regulating and diagnosing purposes since the beginning of their use in shipbuilding. Mechanical indicators used for that purpose make it possible only to determine maximum pressure values of combustion and compression and to roughly assess run of working processes in cylinders on the basis of developed indicator diagrams.

Appearance, in the 1970s, of electronic pressure analyzers often called also MIP (mean indicated pressure) calculators and application of computer technique generally have not changed situation in the area of gaining information from indicator diagrams.

In the presently offered pressure analyzers no important progress has been done as compared with processing capabilities of NK-5 pressure analyzers of Autronica, a Norwegian firm, which have been the first and most commonly applied instruments of the kind in shipbuilding. In many cases, especially as far as portable pressure analyzers are concerned, one can speak about a regress in comparison with their prototype, i.e. NK-5 model. Most of them is not even capable of determining the mean indicated pressure. In any of them no advanced processing of indicator diagrams can be carried out e.g. in the form of analyzing indicator diagram within pressure range as well as determining heat emission characteristics which can serve as a basic source of diagnostic information. Such situation results from met difficulties in indicating ship engines in the domain of crankshaft rotation angle and from lack of mathematical models applicable to pressure analyzers

for automatic analyzing the indicator diagrams. However a main abstacle is the difficulty in determining TDC location on indicator diagrams with a sufficient accuracy, i.e. not lower than  $\pm 0.3^\circ\text{OWK}$  (degree of Crankshaft Rotation Angle). The task is especially difficult in the case of measurements carried out on indicator valves because of deformations of pressure runs, introduced by gas passages and indicator valves themselves.

In the case of low-speed engines when self-ignition occurs after reaching the TDC, peaks of pure compression can be often observed, such as shown in the indicator diagram for RTA52 engine (Fig. 1).

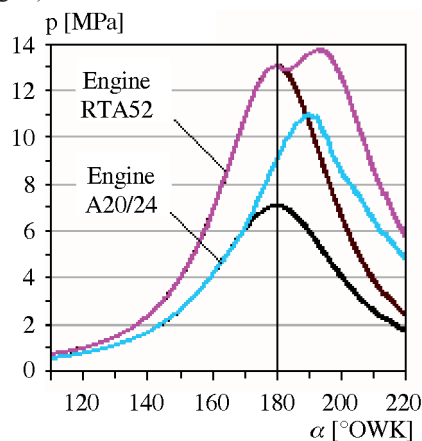


**Fig. 1.** Typical indicator diagrams of ship engines: - for RTA52 engine of  $p_e = 1,8 \text{ MPa}$ ,  $n = 137 \text{ rpm}$ , for A120/24 engine of  $p_e = 1,8 \text{ MPa}$ ,  $n = 750 \text{ rpm}$ .

The pure decompression runs on the right from the self-ignition points were determined by means of extrapolation technique. In such case one assumes that the piston's TDC occurs in the maximum compression pressure point or the point of the first derivative's transition through zero. Location of the TDC by using this method may be burdened with large values of errors. Determination of the TDC is connected with specific difficulties when self-ignition occurs just in the TDC or earlier as in the case of medium-speed engines (see Fig. 1 – A20/24 engine). Large difficulties in measuring and analyzing are introduced by the problem of assessment of cylinder tightness, which is usually performed on the basis of maximum compression pressure values. If self-ignition events occur before reaching the TDC then it is necessary to stop delivering the fuel oil to the tested cylinders, that can be allowed in service conditions only in special cases because of possible loss of tightness of fuel system. Large variability of load is often observed, e.g. in electric generating set driving engines, that can make obtaining comparable measurement results of compression pressure in particular cylinders, difficult.

### MODEL OF COMPRESSION CURVE APPROXIMATION

The simplest model of compression process is polytropic one which is usually presented in the following form:

$$pV^m = \text{const} = c \quad (1)$$

where:

$V$  – gas volume

$m$  – exponent of polytropic curve,  $m = \text{const}$ .

The maximum compression pressure values applied in contemporary ship engines, exceed 5 MPa, and in the case of highly supercharged ones – 10 MPa. For this reason the assumption of  $m = \text{const}$  will usually lead to excessive errors in determining the thermodynamic parameters [1]. For the highly supercharged engines values of the mentioned errors can even exceed 5%.

Having replaced – in the polytropic model – the compression curve exponent  $m = \text{const}$  with the exponent  $m_x = \text{var}$ , finding the logarithm and differentiating the model (1), one obtains a non-uniform differential equation of the compression process in piston engine, e.g. that in the domain of the piston travel  $S_x$ , (2):

$$p^{-1} \frac{dp}{dS_x} + \frac{dm_x}{dS_x} \ln V + m_x V^{-1} \frac{dV}{dS_x} = 0 \quad (2)$$

It should be added that the above presented model is that of polytropic process. Its equation does not possess any solutions in the domain of elementary functions. The known solutions of the differential equations of the compression process [2, 3] are of a cognitive character only and thus they are not applicable to diagnostic problems. The main limitations are: that TDC location is a priori assumed known, lack of association of the mathematical model with technical state of piston-cylinder system, as well as the not taking into account the disturbances introduced by gas passages, indicator valves and measuring gauges.

If the exponent of compression curve cannot be assumed constant and form of its function is unknown then it is natural to assume that the exponent  $m_x$  can be approximated by the power polynomial of  $a$ -order [7, 8, 10,], e.g. that in the domain of the piston travel  $S_x$ :

$$m_x = m_0 + m_1 S_x + \dots + m_a S_x^a \quad (3)$$

where:

$m_0, m_1, \dots, m_a$  – polynomial coefficients.

The earlier attempts to express the exponent  $m_x$  as well as the thermodynamical model directly in the domain of crankshaft rotation angle were abandoned due to a high complexity of the model and associated computational difficulties [5, 9, 11].

Results of analyses of approximation quality of compression curves by using the least squares method, obtained for ship engines of various types for the values of  $a$  within the range of 0 ÷ 4 show that the least values of sums of squares of deviations were obtained for  $a = 3$  (see Tab. 1) [7, 8, 10].

Tab. 1. Influence of the order of power polynomial,  $a$ , on percentage increase of the sums of squares of deviations as compared with the approximation based on  $a = 3$ ;  $\alpha_c$  – approximation interval

No.	Type of engine	a					$\alpha_c$ °OWK	Number of samples
		0	1	2	3	4		
1	6AL20/24	15900	98	21	0	20	70-168	981
2	40DM	2940	840	54	0	54	80-175	951
3	5RTA52	13900	1340	21	0	21	100-175	751
4	6RTA58	6820	790	3	0	3	80-175	951

The above given results justified to assume the 3<sup>rd</sup> order polynomial to be the model of  $m_x$  exponent in the domain of piston travel [8, 10].

The instantaneous volume of gas within cylinder,  $V$ , which appears in Eq. (1), can be expressed as follows:

$$V = V_s - V_{sx} + V_\epsilon + V_z + V_{bx} \quad (4)$$

where:

$V_s$  – piston displacement volume,

$V_{sx}$  – piston volume corresponding with the piston travel done starting from the BDC (Bottom Dead Centre),

$V_\epsilon$  – geometrical volume of compression chamber,

$V_z$  – change of cylinder volume due to wear of elements and influence of assembling process,

$V_{bx}$  – apparent change of cylinder volume due to blow-by of gases.

The quantity  $V_{bx}$  constitutes the volume by which the cylinder volume  $V$  should be increased to obtain changes of gas parameters resulting from gas losses due to blow-by effects. It is a function of piston travel.

By dividing Eq. (4) by the displacement volume  $V_s$ , the particular volumes in Eq. (4) can be transformed to the following dimensionless form [8]:

$$v = 1 - v_{sx} + v_\epsilon + v_z + v_{bx} \quad (5)$$

The value  $v_{sx}$  is equal to the dimensionless piston travel  $s_x$  done starting from the BDC, which is expressed by the known formula for central crank system:

$$s_x = \frac{1}{2} (1 - \lambda^{-1} + \sqrt{\lambda^{-2} - \sin^2 \alpha} - \cos \alpha) \quad (6)$$

where:

$\alpha$  – crankshaft rotation angle counted from the BDC

$\lambda$  – crank radius/connecting-rod-length ratio

To crank systems of articulated connecting-rods appropriate kinematic relations should be applied.

By introducing the notation:

$$v_{xs} = 1 - v_{sx} = 1 - s_x \quad (7)$$

and

$$v_{cx} = v_\epsilon + v_z + v_{bx} \quad (8)$$

the basic model of compression process can be expressed as follows:

$$p(v_{xs} + v_{cx})^{m_x} = \text{const} = c \quad (9)$$

for which – according to the made assumptions – the following is valid:

$$m_x = m_0 + m_1 s_x + m_2 s_x^2 + m_3 s_x^3 \quad (10)$$

For diagnostic purposes the notion of the total compression ratio  $\varepsilon_c$  determinable from the below given expression, is introduced:

$$\varepsilon_c = \frac{1 + v_c}{v_c} \quad (11)$$

where:

$$v_c = v_{cx} (s_x = 1)$$

The volume  $v_c$  characterizes influence of gas blow-by and changes of compression chamber volume on compression ratio value.

The notion „total compression ratio” was attributed to the quantity  $\varepsilon_c$  to distinguish it from the notion of the real compression ratio defined as the ratio of the working space volume at the instant of closing the ports or valves during compression stroke and the compression chamber volume.

In the performed calculations the simple linear relationship of apparent increase of cylinder volume due to gas blow-by:  $v_{bx} = 0.01 s_x$ , was assumed. Assumption of another form of the blow-by function would not make calculations more difficult.

It should be mentioned that in service conditions indication process is realized in the domain of piston travel or time. Due to influence of gas passages and indicator valves, locations of the dynamic TDC measured on engine and that thermodynamic determined on indicator diagram can significantly differ to each other. For Sulzer A medium-speed engines the differences reach 3,5 °OWK at the rotational speed of 750 rpm [6].

For this reason the angle axis of indicator diagram,  $\alpha_i$ , should be shifted relative to the angle axis of kinematic system,  $\alpha$ , by the TDC location error [7, 8, 10], that is expressed as follows:

$$\alpha = \alpha_i + \Delta\alpha_G \quad (12)$$

where:

$\Delta\alpha_G$  – the TDC location error.

Value of the TDC location error is searched for.

The gauges used for indication of ship engines are generally dynamic ones in which constant component is eliminated. The effect of truncation of indicator diagrams from below occurs, which can be clearly observed on the runs of initial compression process in cylinders of 5RTA52 engine (Fig. 2). In this case measurements were performed by means of a pressure gauge of Kistler firm.

Hence it should be assumed that the real pressure  $p$  in the compression curve model (9) is the following sum [7, 8, 10]:

$$p = p_i + \Delta p_i \quad (13)$$

where:

$p_i$  – recorded pressure run (indicator diagram)

$\Delta p_i$  – error of indicator diagram truncation (offset).

### APPROXIMATION OF COMPRESSION PRESSURE RUN BY MEANS OF GLOBAL MODEL AND DETERMINATION OF VALUES OF PARAMETERS

The global model of approximation of compression curve constitutes the set of Eqs. (6), (9), (10), (11), (12) i (13).

The input quantities and parameters of the model are the following:

- ✦ the recorded indicated pressure  $p_i$
- ✦ the crankshaft rotation angle  $\alpha$ , (6)
- ✦ the design (construction) parameter  $\lambda$ , (6).

The searched-for quantities are the following:

- ✦ values of the constants of compression curve exponent  $m_0 \div m_3$ , (10), and of the constant  $c$ , (9)
- ✦ value of the piston's TDC location error  $\Delta\alpha_G$ , (12)
- ✦ the total compression ratio  $\varepsilon_c$ , (11)
- ✦ error (pressure) of indicator curve truncation,  $\Delta p_i$ , (13).

To determine the above mentioned parameters was used the least squares approximation method whose essence consists in finding the minimum value of the functional:

$$Sp = \text{MIN} \sum_{n_1}^{n_r} (p_n - \hat{p}_{mn})^2 \quad (14)$$

where:

$Sp$  – sum of squares of deviations for approximated run

MIN – operator of minimum

$p_n$  – corrected indicated pressure

$\hat{p}_{mn}$  – pressure obtained from approximation

$n_1$  – sample number at the beginning of the approximation interval  $\alpha_{cl}$

$n_r$  – sample number at the end of the approximation interval  $\alpha_{cr}$

To determine values of the parameters a linearization of the model (9) was applied, realized by finding the logarithms, twofold application of the least squares criterion (14) as well as by using the method of experiment theory [4], in order to obtain optimum values of the parameters  $\Delta\alpha_G$ ,  $\varepsilon_c$  and  $\Delta p_i$  regarding minimization of the sum of squares expressed by the second criterion [7, 8, 10].

A number of calculations and analyses was performed for a few types of medium-speed and slow-speed ship engines, from which mutually confirming results were achieved [7, 8, 10]. The below given presentation of the obtained results is based on the analysis of indicator diagrams of 5RTA52 engine (new one) recorded during sea trials (Fig. 2).

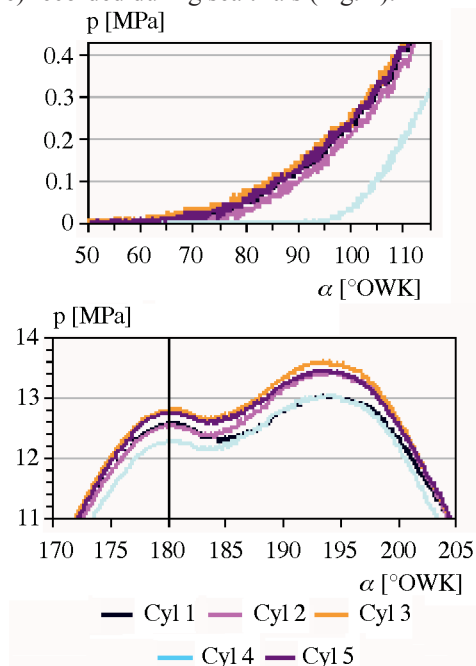


Fig. 2. Runs of compression pressure at the beginning of compression and close to the TDC, for particular cylinders of 5RTA52 engine

It can be observed (Tab. 2) that the determined values of  $\Delta\alpha_G$ ,  $\varepsilon_c$  and  $\Delta p_1$  for particular cylinders are very close to each other for both options of determination, and also in the case of including two different values of the parameter  $\alpha_{cr}$ .

**Tab. 2.** Results of determination of values of the parameters  $\Delta\alpha_G$ ,  $\varepsilon_c$  and  $\Delta p_1$  for cylinders of 5RTA52 engine (Fig. 2), for  $\alpha_{cr} = 100$  °OWK: option no. 1 – simultaneous determination of  $\Delta\alpha_G$ ,  $\varepsilon_c$  and  $\Delta p_1$ ; option no.2 – simultaneous determination of  $\Delta\alpha_G$ ,  $\varepsilon_c$  for the assumed value of  $\Delta p_1 = 0,27$  MPa

Option no.	$\alpha_{cr}$ °OWK	$\Delta\alpha_G$ °OWK				
		Cyl. 1	Cyl. 2	Cyl. 3	Cyl. 4	Cyl. 5
1	180	-0.35	-0.25	-0.25	-0.25	-0.50
1	175	-0.35	-0.25	-0.25	-0.20	-0.50
2	180	-0.40	-0.25	-0.25	-0.30	-0.50
2	175	-0.35	-0.25	-0.25	-0.20	0.50
$\varepsilon_c$						
1	180	13.95	14.65	14.20	13.15	14.05
1	175	13.95	14.80	14.30	13.10	14.00
2	180	13.90	14.65	14.20	13.00	14.05
2	175	13.95	14.80	14.30	13.00	14.05
$\Delta p_1$ MPa						
1	180	0.225	0.270	0.275	0.260	0.265
1	175	0.230	0.270	0.270	0.280	0.260

The observed differences between values of  $\Delta p_1$  for particular cylinders may awake some doubts (Tab. 2). Results of simulation analysis demonstrated that in the case in question the estimation errors of  $\Delta p_1$  values equal to  $\pm 20\%$  lead to the determination errors of  $\varepsilon_c$  values not greater than  $\pm 2\%$ . Therefore it is justified to assume - for calculations - the same  $\Delta p_1$  values for all cylinders, depending on supercharging pressure value.

Analogous results were obtained also from analyses of indicator diagrams for engines of other types [8, 10].

## DETERMINATION OF THE TDC AND ASSESSMENT OF APPROXIMATION MODEL ADEQUACY

For analyzing the problem of determination of piston's TDC were used the indicator diagrams where compression pressure maximum was observed (Fig. 2, Fig. 3).

In the case of 6AL20/24 medium-speed engine the diagrams represented runs of pure compression in tested cylinder (Fig. 3) [8] because self-ignition occurred in the engine before reaching the TDC, under every load.

For measurement performing in cylinder the value of  $\Delta\alpha_G$  is small and equal to about 0.1 °OWK, but for measuring on indicator valve the value of  $\Delta\alpha_G$  is equal to over -0.9 °OWK (Fig. 3). It is caused by disturbances from the side of the gas passage and indicator valve itself. It should be mentioned that on the above presented diagrams (Fig. 3) the angular lag between the run on the indicator valve and that in the cylinder could not be observed, though it was equal to 2.7°OWK.

Identical symptoms as those shown in Fig. 3 take place in the case of slow-speed engines (Fig. 4).

For successive cylinders of 5RTA52 engine the following values of the error  $\Delta\alpha_G$  were achieved: -0.35; -0.25; -0.25; -0.25, -0.5 °OWK. Analyzing indicator diagrams of engines of different types, in some cases one observed  $\Delta\alpha_G$  values reaching even 1 °OWK. Hence when the TDC location is assumed at the compression pressure maximum point or in the point of transition through zero of its 1<sup>st</sup>-order derivative, one should take into account possibility of making large errors in

determining the mean indicated pressure and characteristics of heat emission.

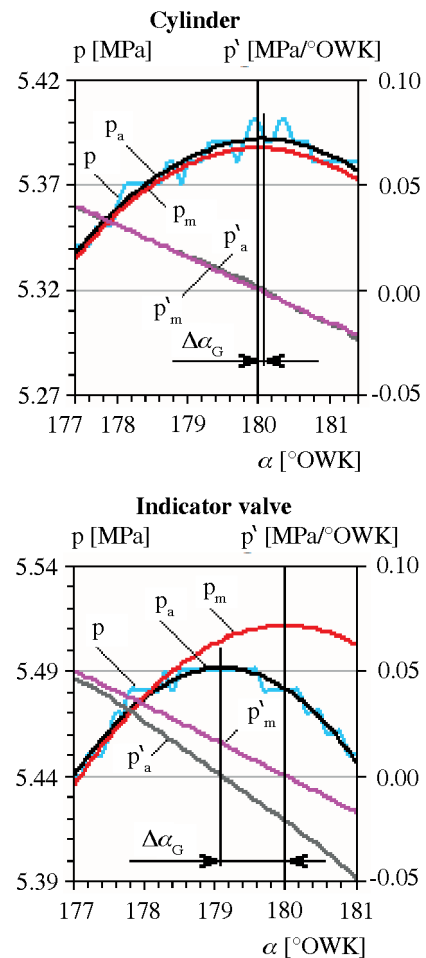


**Fig. 3.** Comparison of determination results of the TDC location on the runs of pure compression in a cylinder and on indicator valve for 6AL20/24 medium-speed engine (50% rated load,  $n = 750$  rpm) for the approximation interval  $\alpha_c = 100 \div 180$  °, and obtained by using the approximation model;  $p'_a$ ,  $p'_m$  – the 1<sup>st</sup>-order derivatives of the runs in question. The value of  $\Delta p_1$  was assumed with taking into account supercharging pressure value.

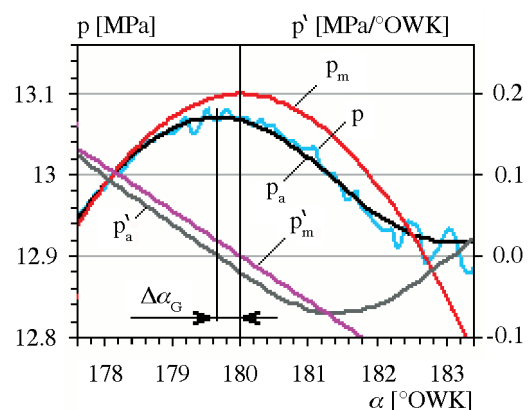


**Fig. 4.** Comparison of determination results of the TDC location on the indicator diagram of 5RTA52 slow-speed engine (100% rated load,  $n = 130.5$  rpm, cylinder no.1) for the approximation interval  $\alpha_c = 100 \div 180$  °OWK. The value of  $\Delta p_1 = 0.27$  MPa was assumed with taking into account supercharging pressure value.

The question arises if the TDC locations determined on the basis of approximation by means of the total model are not erroneous and if the method makes it possible to determine the TDC locations in the case when self-ignition occurs before reaching the TDC. For adequacy of the elaborated model speak the results of the TDC determination for e.g. 5RTA52 engine,

obtained for different values of the ends of the approximation interval  $\alpha_{cr} \geq 173$  °OWK (Fig. 5).

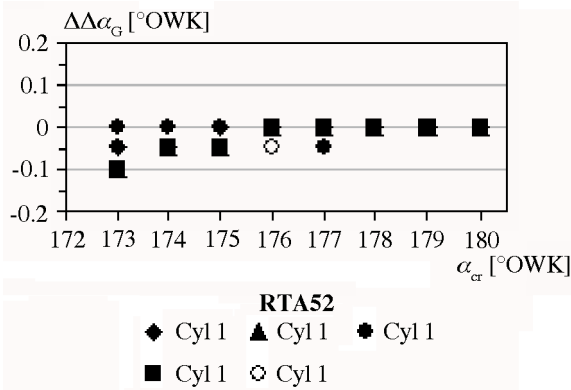


Fig. 5. Influence of end values of the approximation interval  $\alpha_{cr}$  on the increments of error values,  $\Delta\Delta\alpha_G$  for successive cylinders of 5RTA52 engine, at  $\alpha_{cl} = 100$  °OWK.

The value of  $\Delta\Delta\alpha_G$  did not exceed 0,1 °OWK at  $\alpha_{cr} = 173$  °OWK, and at  $\alpha_{cr} \geq 174$  °OWK it did not exceed 0,05 °OWK (Fig. 5). It means that prevailing influence on value of the sum of squares of deviations has location of the angle axis of the kinematic system relative to the angle axis of the indicator diagram. Identical results were obtained for engines of other types including medium-speed ones [8, 10]. However for the values  $\alpha_{cr} < 165$  °OWK the values of  $\Delta\Delta\alpha_G$  can exceed 1°OWK, which is associated with exceedance of the inflection point (i.e. zero value of the 2<sup>nd</sup> order derivative) which – in the case of ship engines- is located close to 167°OWK, counting from the BDC. Correctness of the method in question is confirmed by results of analysis of influence of  $\alpha_{cr}$  location on determination errors of maximum compression pressure values when location of the TDC on indicator diagram is known (Fig. 6).

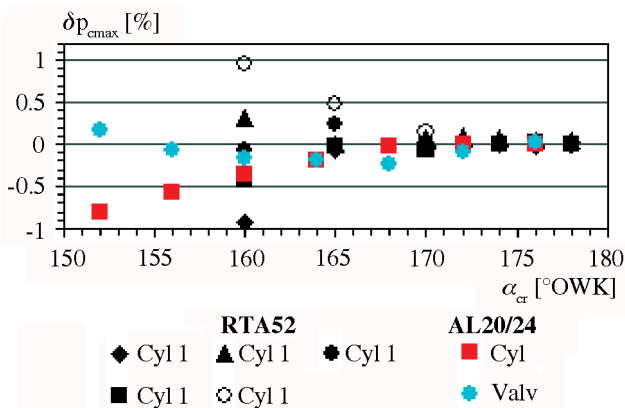


Fig. 6. Influence of value of  $\alpha_{cr}$  on value of the determination error of maximum compression pressure value,  $\delta p_{cmax}$  for successive cylinders of 5RTA52 engines, as well as for pure compression diagrams of 6AL20/24 engine, at  $\alpha_{cl} = 100$  °OWK.

As observed in Fig. 6 the errors of prediction of maximum compression pressure values,  $\delta p_{cmax}$ , do not exceed 1% even for  $\alpha_{cr} = 150$  °OWK, and for  $\alpha_{cr} > 160$  °OWK they drop to 0,5 % and take very small values for  $\alpha_{cr} > 160$  °OWK, that confirms adequacy of the elaborated model and the method of determination of parameters.

Appropriate choice of initial value of the approximation interval  $\alpha_{cl}$  greatly influences obtained results [8, 10]. The values of  $\alpha_{cl}$  should be generally selected in the points where valves or ports are already closed and proper compression is under way and the diagram is only a little disturbed. For ship engines the optimum values of  $\alpha_{cl}$  are contained within the range of 70÷100 °OWK depending on type of such engine [8, 10].

## ASSESSMENT OF DIAGNOSTIC USEFULNESS OF THE PARAMETER $\epsilon_c$

The obtained calculation results showed that for 6AL20/24 engine under various loads, both for measurements performed in cylinder or on indicator valve, the determined values of  $\epsilon_c$  are close to each other as compared with the maximum compression pressure values,  $p_{cmax}$ , (Tab. 3).

Tab. 3. Comparison of the values of  $\epsilon_c$  and  $p_{cmax}$  determined on the basis of indicator diagrams of a 6AL20/24 laboratory engine

Load [%]	Place of measurement	$\epsilon_c$ [°]	$p_{cmax}$ [MPa]
50 - (pure compression)	Cylinder	13.9	5.28
	Indicator valve	14.1	5.48
100	Cylinder	14.1	7.24
	Indicator valve	14.3	7.38

In the case of the measurement performed on indicator valve the increase of the value of  $p_{cmax}$  by about 35 % resulted in the increase of the value of  $\epsilon_c$  by 1,4 % only; and in the case of the measurement in cylinder – the situation was similar. Analyzing the values of  $\epsilon_c$  (Tab. 4), determined on the basis of the indicator diagrams of 5RTA52 engine (Fig. 2), one can observe that the value of  $\epsilon_c$  for cylinder no. 4 is significantly smaller, and for cylinder no. 2 - significantly greater than those for the remaining cylinders.

Tab. 4. Comparison of the deviations of values of the parameters  $\epsilon_c$  and  $p_{cmax}$  from their mean values, for successive cylinders of 5RTA52 engine:  $\delta\epsilon_c$  – percentage deviations of  $\epsilon_c$ ,  $\delta p_{cmax}$  – percentage deviations of  $p_{cmax}$

Cylinder number	1	2	3	4	5
$\delta\epsilon_c$ , %	-0.7	4.6	1.4	-5.7	0.4
$\delta p_{cmax}$ , %	-0.17	-0.40	1.70	-2.35	1.23

If for assessment of tightness of cylinders of 5RTA52 engine one takes into account the values of  $p_{cmax}$  (Fig. 2) then in the case of cylinder no. 4 the value of  $\delta p_{cmax} = -2.35$  % makes it possible to consider the cylinder as that having correct parameters of compression process in spite of that for the cylinder:  $\delta\epsilon_c = -5.7$  %. In the case of cylinder no. 2 attention should be focused on the small value of  $\delta p_{cmax} = -0.40$  %, whereas  $\delta\epsilon_c = 4.6$  %, having opposite sign against that of  $\delta p_{cmax}$ . In the case of cylinder no. 4 a setting error was made and the valve was closed much later than in the remaining cylinders, which can be stated from the pressure run occurring at the beginning of compression process (Fig. 2). It is also possible to demonstrate that the phenomenon was not caused by a greater value of the error  $\Delta p_1$  observed in that case [8, 10].

It should be also observed that the error  $\Delta\alpha_G$  greatly influences the error in determining  $\epsilon_c$  (Tab. 5).

Tab. 5. Influence of the error  $\Delta\alpha_G$  on the error  $\delta\epsilon_c$  in the case of RTA52 engine (for cylinder no. 5)

$\Delta\alpha_G$ , °OWK	-0.3	-0.2	-0.1	0	0.1	0.2	0.3
$\delta\epsilon_c$ , %	-10.9	-7.1	-3.4	0	3.3	6.5	9.5

In view of the so great influence of the error  $\Delta\alpha_G$  on the determination error of total compression ratio,  $\delta\epsilon_c$ , to accurately determine the TDC location becomes especially

important. In the case of slow-speed engines if measurements are performed carefully both in the aspect of pressure and angle axis measurements, to determine the TDC locations burdened with the error values below  $\pm 0.05$  °OWK, will be possible.

## CONCLUSIONS

- The presented model and method of approximation of indicator diagrams in the compression range make it possible to determine the TDC's location on indicator diagrams also in the case if self-ignition occurs before reaching the TDC.
- The so determined TDC is equivalent to that kinematic.
- The TDC's location considered identical with the location of maximum value of compression pressure or with zero point of 1<sup>st</sup> order derivative of pressure run curve is burdened with the error whose value can range from a few decimal parts to 1 °OWK.
- The presented method makes it possible to determine the total compression ratio  $\varepsilon_c$ . This parameter is more suitable for assessing cylinder tightness losses than maximum value of compression pressure in view of a weak dependence of  $\varepsilon_c$  values on engine load level.
- Accuracy of determination of values of the parameter  $\varepsilon_c$  is greatly influenced by value of the error of the TDC's location. Even the values of the error  $\Delta\alpha_G$  equal to  $\pm 0.3$  °OWK will produce the errors in determining  $\varepsilon_c$  values, of the order of  $\pm 10$  %.
- In the case of slow-speed engines, on the basis of the approximation model it can be also possible to determine values of the indicator diagram truncation pressure  $\Delta p_l$ . However it seems that in the case of service measurements it would be better to resign from determination of value of the parameter in question and to assume - for calculations - its value by taking into account supercharging pressure value.

## BIBLIOGRAPHY

1. Baehr H.D.: *Thermodynamik. Eine Einführung in die Grundlagen und ihre technischen Anwendungen*. Springer, 1973 (edition in Russian, 1977)
2. Benson R.S., Whitehouse N. D.: *Internal combustion engines*. Pergamon Press, 1979
3. Cichy M.: *Calculation of compression and decompression processes by means of the finite difference method* (in Polish). Scientific Bulletin of Gdańsk University of Technology (Zeszyty Naukowe Politechniki Gdańskiej), Mechanics (Mechanika), no. 73, Gdańsk 1996
4. Hartman K., Lezki E., Schäfer W.: *Statistische Versuchplanung und-auswertung in der Stoffwirtschaft*. VEB, Leipzig, 1974 (edition in Russian, 1977)

5. Polanowski S.: *Errors arising from relating the piston TDC to zero points of derivatives of ship engine cylinder pressure function* (in Polish, abstract in English). Proceedings of KONES Conference 2000, (saved in Warsaw Institute of Aeronautics)
6. Polanowski S.: *Main sources of measurement errors of mean indicated pressure of ship engines in service conditions* (in Polish, abstract in English). Journal of KONES, 1995, (saved in Warsaw Institute of Aeronautics) Polanowski S., Errors in Toking MIP Measurements by Means of Microcomputer Combustion Pressure Analyzer, Journal of Polish CIMAC, Warsaw, 1992..
7. Polanowski S.: *Gaining diagnostic information from indicator diagrams of ship engines by using advanced methods of data processing* (in Polish, abstract in English). Scientific Bulletin of Polish Naval University, no. 162 K/2, Gdynia 2005
8. Polanowski S.: *A study of analysis methods of indicator diagrams in the aspect of diagnostics of ship engines* (in Polish). Scientific Bulletin of Polish Naval University, no. 169 A, Gdynia 2007
9. Polanowski S.: *TDC determination on combustion indicator diagram*. Journal of KONES, 1999, Vol. 6, No 1-2, (saved in Warsaw Institute of Aeronautics)
10. Polanowski S.: *Wieloparametrowy model przebiegu ciśnienia sprężania w cylindrze silnika okrętowego*. Scientific booklet Akademii Marynarki Wojennej, 1 (160), Gdynia 2005 (abstract in English)
11. Polanowski S.: *Wyznaczanie wykładników politropy sprężania dla pozyskania informacji diagnostycznej z wykresu indykatorowego silnika okrętowego*. Conference materials KONES 2001.

## NOMENCLATURE

$\alpha$	– crankshaft rotation angle counted from BDC
$\alpha_c$	– approximation interval
$\alpha_{cl}$	– beginning of approximation interval
$\alpha_{cr}$	– end of approximation interval
$\delta\varepsilon_c$	– error, i.e. percentage deviation of $\varepsilon_c$
$\delta p_{cmax}$	– error, i.e. percentage deviation of $p_{cmax}$
$\Delta p_l$	– error of indicator diagram truncation (offset)
$\Delta\alpha_G$	– error in TDC location
$\varepsilon_c$	– total compression ratio
$p$	– pressure, given on corrected indicator diagram
$p_a$	– smoothed run of indicator diagram
$p_{acmax}$	– maximum value of compression pressure
$p_m$	– run of pressure obtained from approximation by means of a model
$p'_a$	– 1 <sup>st</sup> order derivative of run curve of $p_a$
$p'_m$	– 1 <sup>st</sup> order derivative of run curve of $p_m$

## CONTACT WITH THE AUTHOR

\*\*\*\*\*Stanisław Polanowski, RtqH0  
Mechanic-Electric Faculty,  
Polish Naval University  
Śmidowicza 69  
81-103 Gdynia, POLAND  
e-mail: SPolanowski@o2.pl

# A probabilistic concept of load assessment of self-ignition engines

Jerzy Girtler, Prof.  
Gdańsk University of Technology

## ABSTRACT



*A proposal of probabilistic interpretation of loading process of self-ignition combustion engines, was presented. Probabilistic description of loading the engines was proposed with taking into account known parameters (indices) of their operation. It was demonstrated that instantaneous load of such engines can be considered a random variable. Attention was paid to the fact that the load can be taken as a multi-dimensional random variable. Engine load changes during its operation were considered as the loading process and presented in the form of a multi-dimensional stochastic process whose states are loads considered to be random variables. It was demonstrated that the loading process can be taken as the stochastic one of asymptotically independent increments, stationary and ergodic. Justification of the above mentioned features of the loading process is contained in the presented hypotheses. It was also demonstrated that in testing the load process of self-ignition engines stochastic relation between thermal and mechanical loading should be taken into account.*

**Keywords:** hypothesis, load, self-ignition engine, stochastic process

## INTRODUCTION

Loads belong to the crucial causes of wear both surface (linear) and volumetric one, that results in failures of self-ignition engines. Especially unfavourable influence on wear of the engines is due to excessive thermal loads in the elements which form their working spaces (combustion chambers). Though mechanical loads of the engines have not so important influence on their wear but if they are excessive (especially those exerted on main and crankshaft bearings) they can also lead to serious failures called breakdowns [3, 7, 8, 15].

It is possible to predict such failures in the case of application of suitable diagnostic systems so designed as to generate full diagnoses, i.e. these capable of predicting their technical state. To elaborate such prediction it is necessary to determine a.o. loads which can appear during operation of engines. In present, loads of combustion engines have been generally analyzed deterministically [7, 9, 16, 17, 18]. Such analyses based on a probabilistic approach have been performed as a rule in a simplified way. However loads of the combustion engines should be modeled in time and space as random variables attributed to random events in which loads of an appropriate value are measured. The fact that a given load measurement is a random event, means that to which an appropriate probability should be attributed. Moreover the loads should be analyzed in successive instants of operation of combustion engines. The so considered loads form the process of data. Hence it is necessary to elaborate a concept of analyzing and assessing such loads in the probabilistic aspect with taking into account the fact that the load changes successively occurring one by one in the above mentioned instants form a stochastic process. However the instants are not random variables but parameters of the process.

In order to elaborate such concept, probabilistic features of the loading process of combustion engines should be first determined beginning from analysis of states of the process, i.e. the engine loads considered to be random variables.

## ENGINE LOADING CONSIDERED AS A RANDOM VARIABLE

In Introduction it was demonstrated that engine load values can not be precisely predicted. Therefore the following hypothesis  $H_1$  can be formulated: „Engine load is a random variable therefore during successively performed measurements its values can be predicted only with a certain probability”.

Qualitative interpretation of combustion engine load in an arbitrary instant  $t$  can be presented in the following form:

$$Q_D(t) = Q_C(t) + Q_M(t) \quad (1)$$

where:

$$Q_C(t) = \Delta U(t) + Q_O(t)$$

and

$Q_D(t)$  – thermal energy (EC) delivered to engine in the instant  $t$

$Q_C(t)$  – thermal energy transferred by engine elements during its operation (thermal loading) in the instant  $t$

$Q_M(t)$  – mechanical energy associated with presence of gravity and formation of gas forces, friction and inertia forces (mechanical loading) in the instant  $t$

$\Delta U(t)$  – internal material energy increments, in the instant  $t$ , of elements through which a part of the thermal energy  $Q_C(t)$ , denoted  $Q_O(t)$ , penetrates

$Q_O(t)$  – energy emitted to environment in the instant  $t$ , by walls of engine elements, e.g. those forming working spaces (combustion chambers) and other.

The above mentioned engine loads can be considered random variables. They result first from transformation of chemical energy contained in fuel into thermal energy, and next - the latter into mechanical one (Fig. 1). In the interpretation of the transformations it was taken into account that the heat is a form of transformation of chemical energy into thermal one, and the work – that of thermal energy into mechanical one.

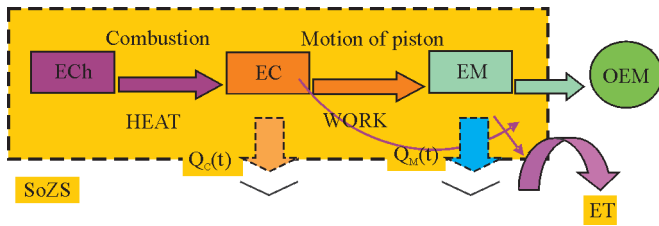


**Fig. 1.** Example schematic diagram of energy transformation in self-ignition engine: ECh – chemical energy; EC – thermal energy; EM – mechanical energy; ET – thermal and mechanical energy losses; SoZS – self-ignition engine; OEM – mechanical energy consumer (e.g. ship propeller, electric generator, compressor, pump);  $Q_c(t)$  – thermal load in the instant  $t$ ;  $Q_s(t)$  – mechanical load in the instant  $t$ .

In the case when only one parameter (one random quantity) is used for load description then the load (value of the loading process) is one-dimensional random variable. And, if many parameters are used to describe the load (i.e. value of loading process) then it is a multi-dimensional variable. The load is then described by a set of many (generally  $n$  in number) random variables. In such case it can be considered to be a  $n$ -dimensional random function, i.e. a set of many ( $n$ ) real functions which attribute unambiguously many numerical values to each random event, which load measurement constitutes too [1, 3, 4, 10, 14].

In service practice the self-ignition engine load is usually defined by means of the following parameters:  $p_{max}$  – maximum combustion pressure,  $t_{max}$  – maximum combustion temperature,  $p_e$  – mean effective pressure,  $c_{sr}$  – mean piston speed,  $\Delta\phi_{psr}$  – mean pressure rate velocity. The specified parameters can be considered to be values of random variables which can be denoted respectively as follows:  $P_{max}$ ,  $T_{max}$ ,  $P_e$ ,  $C_{sr}$  and  $\Delta\Phi_{psr}$ .

If the load is determined by means of such random variables as: maximum pressure ( $P_{max}$ ) and maximum temperature ( $T_{max}$ ), the two random variables ( $P_{max}$ ,  $T_{max}$ ) can be considered simultaneously. The variables can be taken stepwise. Then the quantities  $p_{imax}$  and  $t_{jmax}$  are arbitrary realizations of the variables. Hence the pair ( $p_{imax}$ ,  $t_{jmax}$ ) is realization of the two-dimensional random variable ( $P_{max}$ ,  $T_{max}$ ). Simultaneous occurrence of the events:  $P_{max} = p_{imax}$  and  $T_{max} = t_{jmax}$  is determined by the probability  $q(p_{imax}, t_{jmax})$ . In this case all the values  $p_{imax}$  and  $t_{jmax}$  which can occur, must follow the relation [1, 10]:

$$\sum_{i=1}^r \sum_{j=1}^r q(p_{imax}, t_{jmax}) = 1 \quad (2)$$

The set of the probabilities  $q(p_{imax}, t_{jmax})$  constitutes a two-dimensional distribution of the random variable ( $P_{max}$ ,  $T_{max}$ ).

The probability  $p(p_{imax})$  of the random event  $P_{max} = p_{imax}$  without taking into account value of the random variable  $T_{max}$  is equal to the sum of the probabilities  $q(p_{imax}, t_{jmax})$ , which contains all possible values  $t_{jmax}$ , therefore:

$$q(p_{imax}) = \sum_{j=1}^r q(p_{imax}, t_{jmax}) \quad (3)$$

The set of the probabilities  $q(p_{imax})$  determined according to Eq. (3), is a boundary distribution of the random variable  $P_{max}$ .

In practice it is necessary to determine the conditional probability  $q(p_{imax}/t_{jmax})$  of the random event  $P_{max} = p_{imax}$  under

the condition (assumption):  $T_{max} = t_{jmax}$ . This implies that an engine is most loaded mechanically and thermally when in its working spaces (cylinders) maximum pressure and temperature values occur. The probability can be determined by using the formula:

$$q(p_{imax}/t_{jmax}) = \frac{q(p_{imax}, t_{jmax})}{q(t_{jmax})} \quad (4)$$

The set of the conditional probabilities  $q(p_{imax}/t_{jmax})$  under the same condition (assumption):  $T_{max} = t_{jmax}$ , is a conditional distribution of the random variable  $P_{max}$  under the condition:  $T_{max} = t_{jmax}$ . The sum of the conditional probabilities  $q(p_{imax}/t_{jmax})$  containing all the possible values  $p_{imax}$  equals one, i.e.:

$$\sum_{i=1}^r q(p_{imax}/t_{jmax}) = 1 \quad (5)$$

In practice it may so happen that the random variables  $P_{max}$  and  $T_{max}$  are independent, e.g. as a result of an incorrectly performed regulation of engine. Then the following relations are valid:

$$q(p_{imax}/t_{jmax}) = q(p_{imax}) \quad (6)$$

$$q(t_{jmax}/p_{imax}) = q(t_{jmax}) \quad (7)$$

By taking into account Eq. (6) and (7) in Eq. (4) the following is obtained:

$$q(p_{imax}/t_{jmax}) = q(p_{imax}) q(t_{jmax}) \quad (8)$$

The random variables  $P_{max}$ ,  $T_{max}$  which satisfy the condition (8), are stochastically independent. In the case if the condition is not satisfied the random variables  $P_{max}$ ,  $T_{max}$  are stochastically dependent (correlated) random variables. As results from Eq. (8), in investigations should be taken into account the fact that in the case of the independent random variables  $P_{max}$ ,  $T_{max}$  their conditional distributions do not differ from their boundary distributions.

The load described by three parameters, for instance the maximum pressure  $P_{max}$ , maximum temperature  $T_{max}$  and mean effective pressure  $p_e$ , can be considered in the same way. Then the three stepwise random variables ( $P_{max}$ ,  $T_{max}$ ,  $P_e$ ) should be considered. The three quantities:  $p_{imax}$ ,  $t_{jmax}$  and  $p_{ekmax}$  constitute realizations of the random variables. Hence the three ( $p_{imax}$ ,  $t_{jmax}$ ,  $p_{ek}$ ) is realization of the three-dimensional random variable. The probability of simultaneous occurrence of the events:  $P_{max} = p_{imax}$ ,  $T_{max} = t_{jmax}$  and  $P_e = p_{ek}$ , constitutes the probability  $q(p_{imax}, t_{jmax}, p_{ek})$ .

In the case of the taking into account of all the values:  $p_{imax}$ ,  $t_{jmax}$  and  $p_{ek}$ , which can occur, the following is valid:

$$\sum_{i=1}^r \sum_{j=1}^r \sum_{k=1}^r q(p_{imax}, t_{jmax}, p_{ek}) = 1 \quad (9)$$

The set of the probabilities  $q(p_{imax}, t_{jmax}, p_{ek})$  is a three-dimensional distribution of the random variable ( $P_{max}$ ,  $T_{max}$ ,  $P_e$ ).

The probabilities  $q(p_{imax})$  of the random variable:  $P_{max} = p_{imax}$  without taking into account value of the random variable  $T_{max}$  as well as the random variable  $P_e$ , is equal to the sum of the probabilities  $q(p_{imax}, t_{jmax}, p_{ek})$  which covers all the possible values of  $t_{jmax}$  and  $p_{ek}$ , hence:

$$q(p_{imax}) = \sum_{j=1}^r \sum_{k=1}^r q(p_{imax}, t_{jmax}, p_{ek}) \quad (10)$$

The set of the probabilities  $q(p_{imax})$  which follow Eq. (10), is a boundary distribution of the random variable  $P_{max}$ .

The presented proposal of description of the load of combustion engines is important as the load impacts wear of their elements. For this reason, the wear in a given instant of operation time of the engines is also a random variable, and when analyzed in successive instants of the operation, their values should be considered as those following a random process.

## ENGINE LOADING CONSIDERED AS A STOCHASTIC PROCESS

As commonly known, in trying to maintain engine's continuous power rate or its rated power, in successive instants engine's mechanical load values are rather close to each other, depending on operational conditions. And, engine's thermal load values can, in presence of the mechanical loads, vary and even exceed to a great extent their limit values. It results from the dependence of thermal load not only on mechanical one but also on a state of engine's cooling system, lubricating oil quality, pressure in lubricating system of bearings, oil quantity delivered to lubricate cylinder liners, etc [4, 7, 8, 12].

The loading (mechanical and thermal) of engines can be considered in a dynamic (short) time interval measured in [ms] (i.e. that in which one or at most a few thermodynamic cycles of engine occur), or in that quasi-static (long) which is equivalent to a correct engine operation time interval usually measured in [h].

By comparing the loads which occur during successive thermodynamic cycles, i.e. during the short time interval ( $t_d$ ), one can state that they are different because different causes [7, 8, 16, 17, 18]. Along with increasing values of the engine operation time  $t_d$  the differences are also increasing. Hence at a given value of the dynamical time interval and in investigating the loads during particular cycles in the instants  $t_{d1}$ ,  $t_{d2}$ , ..., one can obtain different engine load values. The event of obtaining a given value of the load is random one. It means that to each instant of the time  $t_d$  a random variable equivalent to the engine load in that instant, can be attributed. In the same way to each instant of the quasi-static time ( $t_q$ ) a random variable equivalent to the engine load in that instant, can be attributed.

The engine load taken as a random variable in a given instant  $t$ , constitutes value of the loading process. In turn, the process constitutes a run of consecutive load changes causally inter-connected in function of time, and possible to be described by different random parameters (quantities) whose values can be predicted only with a certain probability. Hence the loading process is stochastic, i.e. a function whose values for a given time instant of engine operation,  $t$ , are randomly variable. Therefore the following hypothesis  $H_2$  can be formulated: „The engine loading process is stochastic because values of the engine loading in a given time instant (which is not a random variable) are randomly variable”.

As results from the theory of stochastic processes the set of such instants is that of parameters of the process [6, 14].

The engine loading process is stochastic one of continuous realizations. However by its discretization the stochastic process of constant realizations within particular time intervals of engine operation, can be achieved. The so modified loading process (process of load changes) can be described in the form of a semi- Markovian model which has a strictly determined set of loading states, [4, 6, 14].

The engine loading can be characterized by means of various quantities (parameters, indices). Generally, it can be expressed in the following form (11):

$$Q(t) = f[Q_M(t), Q_C(t)] \quad (11)$$

where:

$Q$  – engine's loading

$Q_M$  – engine's mechanical loading

$Q_C$  – engine's thermal loading

$t$  – engine's operation time interval.

In empirical loading investigations at least two stochastic processes:  $\{Q_M(t): t \geq 0\}$  and  $\{Q_C(t): t \geq 0\}$  can be considered. They are components of the vectorial process  $\{Q(t): t \geq 0\}$ , [4, 9, 16, 17, 18].

In the case of the loads  $Q_M$  and  $Q_C$  it can be possible to write that they are vectors of the following components in a given instant  $t$ :

$$Q_M : [p_{max}, p_z, p_e, c_{sr}, \varphi, \varphi_p, n, P_g, P_b, \dots] \quad (12)$$

$$Q_C : [\dot{q}, \nabla T, \rho, p_e, c_{sr}, T_{max}, T_z, T_{sw}, \dot{Q}, \dots] \quad (13)$$

where:

$p_{max}$  – maximum combustion pressure;  $p_z$  – combustion pressure;  $p_e$  – mean effective pressure ( $p_e = \eta_m p_i$ ;  $\eta_m$  – mechanical efficiency;  $p_i$  – mean indicated pressure)

$c_{sr}$  – mean piston speed;  $\varphi$  – degree of isochoric pressure increment;  $\varphi_p$  – instantaneous pressure increase rate;  $n$  – engine crankshaft rotational speed;  $P_g$  – gas pressure force;  $P_b$  – inertia force;  $\dot{q}$  – thermal flux (energy) density;  $\nabla T$  – temperature gradient;  $\rho$  – degree of initial isobaric decompression;  $T_{max}$  – maximum combustion temperature;  $T_z$  – combustion pressure;  $T_{sw}$  – exhaust gas temperature;  $Q$  – heat flux;  $T_{ol}$  – oil temperature;  $T_w$  – cooling water temperature.

As results from Eqs. (11) ÷ (13), the engine loading depends on many quantities (parameters, indices), hence it can be considered a stochastic process which contains superposition (composition) of particular individual processes (in the simplest case – that of  $Q_M$  and  $Q_C$ ). Such interpretation of the loading is suitable for general considerations but it may be rather not useful for practical purposes.

The loading can be also considered to be a vectorial process whose components are random variables which characterize load values in particular instants of engine operation time, described in the form of Eqs. (12) and (13).

Generally, the loading can be understood as a process whose states can be taken into account in the form of random variables. The process, as observed from Eqs. (12) and (13), is multi-dimensional because it can be determined only when load parameters which form a complete set of parameters, are measured and probabilities of obtaining their values - determined.

The complete set of load parameters (indices) can be interpreted as that which contains all the parameters necessary to determine engine's loading.

In every instant  $t_{dl}$  ( $l = 1, 2, \dots, n$ ), of the dynamic time interval  $t_d$ ,  $n$  following random variables:  $Q_{t_{dl1}}, Q_{t_{dl2}}, \dots, Q_{t_{dln}}$ , can be considered. The variables have been further denoted:  $Q_1, Q_2, \dots, Q_n$ . They can stand for  $n$  different quantities (parameters, indices) of investigated loading (e.g.  $Q_1 = p_{max}$ ,  $Q_2 = T_{max}$ ,  $Q_3 = p_e$ ,  $Q_4 = \dot{q}$ , etc).

If particular load features are simultaneously considered (the load can be characterized by an excessive combustion pressure, excessive combustion temperature, excessive heat flux, etc) the set of  $n$  random variables, being a  $n$ - dimensional random variable, is obtained. Hence at a distinguished instant  $t$  the loading  $Q(t)$  can be considered to be a  $n$ - dimensional random variable  $Q_t$  (further marked  $Q$ ). Therefore the so considered loading can be determined by a set of  $n$  real unambiguous functions which attribute numerical values to every random event (i.e. occurrence of a given load value).

Generally, in order to simplify further considerations, they can be limited by assuming that the random variable  $Q$  will be a two-dimensional random function  $(Q_M, Q_C)$ . For the reason that measurements are periodically executed it can be assumed that the random variables  $Q_M$  and  $Q_C$  are stepwise (non-continuous) random ones. Realizations of the variables are respectively the quantities:  $q_{M_i}$  and  $q_{C_i}$ . Hence the pair  $(q_{M_j}, q_{C_j})$  is realization of the random variable  $(Q_M, Q_C)$ . The variable takes the values  $(q_{M_j}, q_{C_j})$  with a determined probability  $p(q_{M_j}, q_{C_j})$  which is that of simultaneous occurrence of the events:

$$Q_M = q_{M_i} \text{ and } Q_C = q_{C_i}$$

The set of the above mentioned probabilities  $p(q_{M_j}, q_{C_j})$  constitutes the two-dimensional distribution of the random variable  $(Q_M, Q_C)$ . In a similar way as in the preceding considerations which have made it possible to formulate Eqs. (2) and (3), the mentioned distribution  $p(q_{M_j}, q_{C_j})$  satisfies the following condition:

$$\sum_{i=1}^r \sum_{j=1}^r p(q_{M_i}, q_{C_j}) = 1 \quad (14)$$

The boundary distribution of the random variable  $Q_M$  is as follows:

$$p(q_{M_i}) = \sum_{j=1}^r p(q_{M_i}, q_{C_j}) \quad (15)$$

and, the distribution of the random variable  $Q_C$  has the following form:

$$p(q_{C_j}) = \sum_{i=1}^r p(q_{M_i}, q_{C_j}) \quad (16)$$

From the investigations have been performed so far it results that some quantities which characterize the loading, e.g.  $p_e, c_{sr}$  [3, 16, 17, 18] characterize both mechanical and thermal one. Therefore it is obvious that there are relations between the mechanical and thermal load. For the reason that they constitute random processes a stochastic relationship between them should be expected. Hence to explain the relationship the following hypothesis  $H_3$  can be formulated: „Between the mechanical load  $Q_M(t)$  and the thermal load  $Q_C(t)$  a stochastic relationship occurs because determined variants of one of the variables are accompanied by different variants of the other.”

Therefore it yields that the relationship between the loads:  $(Q_M(t)$  and  $Q_C(t)$ ) cannot be described by using the common method of algebraic equations. This seems true as the loading depends on a large number of factors including those non-measurable [2, 3, 12, 14]:

During the main energy transformation process in combustion engine (Fig. 1) thermal energy is transformed into mechanical one, but not inversely. Hence the thermal load  $(Q_C)$  can be conventionally assumed an independent variable, and the mechanical load  $(Q_M)$  – a dependent variable. Analogously, it can be assumed that  $Q_{C_1}, Q_{C_2}, \dots, Q_{C_n}$  are independent variables, but  $Q_{M_1}, Q_{M_2}, \dots, Q_{M_n}$  – dependent ones.

A degree in which the load  $Q_M$  is determined - either by the load  $Q_C$ , or  $Q_{C_j}$  ( $j=1, 2, \dots, n$ ) considered to be independent variables, may be very different. In practice it may happen that one independent variable ( $Q_C$ ) almost fully determines the dependent variable ( $Q_M$ ). However it may also happen that a few independent variables ( $Q_{C_j}$ ) only to a small extent influence the dependent variable ( $Q_M$ ). From the above said it results that there is a necessity of taking into account an intensity (force) of the stochastic relationship between  $Q_C$  and  $Q_M$ .

The intensity (force) of the stochastic relationship between  $Q_M(t)$  and  $Q_C(t)$  can be determined, during empirical investigations, by using the relationship [10]:

$$T_{MC}^2 = T_{CM}^2 = \frac{\chi^2}{N\sqrt{(k-1)(l-1)}} \quad (17)$$

where:

- $k$  – number of variants of the variable  $Q_M$
- $l$  – number of variants of the variable  $Q_C$
- $N$  – boundary number of the variable  $Q_M$  or  $Q_C$
- $\chi^2$  – value calculated from chi- square formula
- $T_{(c)}$  – Czuprow's convergence coefficient.

It can be proved [10] that  $T_{MC}$  takes values from the interval  $[0, 1]$ . The coefficient equals zero ( $T_{MC} = 0$ ) if no relationship between values of the process  $(Q_M$  and  $Q_C)$  occurs, and if it is equal to 1 ( $T_{MC} = 1$ ) a functional relationship takes place. Hence from the hypothesis  $H_3$  on the relationship between the loads  $Q_M$  and  $Q_C$  the following consequence  $K$  can be derived:  $T_{MC} = T_{CM} \neq 0 = T_{MC} \neq 1$ .

Assuming that the syntactic implication  $H \Rightarrow K$  is true, to verify the hypothesis the following methods can be applied [11, 13]:

- ☛ the reductive reasoning which proceeds according to the scheme:

$$(K, H \Rightarrow K) \vdash H \quad (18)$$

- ☛ the „modus tollens” rule which proceeds in line with the scheme:

$$(\sim K, H \Rightarrow K) \vdash \sim H \quad (19)$$

where: the symbols  $\vdash$  – sign that the hypothesis  $H$  is true.

In this case, application of the reductive reasoning can be justified by the following:

- ☆ Mechanical load increasing as a rule always results in thermal load increasing as an increase of the torque  $M_o$  requires an increase of the fuel charge  $\Delta G_p$ , i.e. that of the chemical energy contained in the charge. The charge increase makes it possible to develop a greater thermal energy inside the engine combustion chamber (working space). A part of the energy is transformed into the mechanical energy (EM) in the form of work (Fig.1) and the remaining part, the lost energy (ET), is transferred by the chamber walls to cooling medium and - together with exhaust gas - to the environment.
- ☆ Despite the mechanical load does not undergo large changes, the thermal load can be significantly increased due to worsening the cooling conditions, e.g. due to sedimentation of mineral deposits on cooling space surface, air penetration to the space, etc.

Despite the reductive reasoning does not guarantee that the conclusion that  $q_M$  has increased is true, the relation:  $(q_M \Rightarrow q_C) \cap q_C$  is true. However it does not mean that, if the implication:  $(q_M \Rightarrow q_C)$  on the interpretation that if the mechanical load  $q_M$  increases the thermal load  $q_C$ ” also increases, it can not be assumed true that if  $q_C$  increases then also  $q_M$  increases, i.e.:

$$[(q_M \Rightarrow q_C) \cap q_C] \Rightarrow q_M \quad (20)$$

And, application of the „modus tollens” rule results from that the scheme of reasoning on the hypothesis  $H_3$  is reliable and leads to its falsification. However it is so only in the case if empirical investigations are truly capable of undeniable contradicting the hypothesis  $H_3$ , i.e. that the mechanical load will increase.

It is possible to state generally whether the random variables  $Q_M$  and  $Q_C$  are mutually dependent, by investigating the probabilities determined with the use of the general equations: (14)  $\div$  (16) or those detailed: (6)  $\div$  (8).

In the case when - as in the detailed considerations – the conditional distributions of the variables do not differ from their boundary distributions, the following is valid:

$$p(q_{M_i}, q_{C_j}) = p(q_{M_i}) p(q_{C_j}) \quad (21)$$

It means that the random variables  $Q_M$  and  $Q_C$  are independent. And, if Eq. (21) is not satisfied they are stochastically dependent. In this case verification of the hypothesis H can follow the schemes similar to those presented in the form of Eqs. (18) and (19).

Investigation of stochastic relationship between the random variables  $Q_M$  and  $Q_C$  is difficult because distributions of the investigated loads (including conditional distributions) can differ in many features (variability, concentration, asymmetry etc). Hence it is much easier to examine statistical relationship between the mentioned random variables  $Q_M$  and  $Q_C$ .

It should be observed that if no stochastic relationship between the random variables  $Q_M$  and  $Q_C$  takes place then any statistical relationship does not take place between them too. However reverse implication is not true. It directly results from that the same conditional mean values are related to the same conditional distributions, whereas to the same conditional mean values the same distributions are not to be related [1, 10].

The statistical relationship is distinguished by that to particular mechanical load values to attribute a mean value of thermal load, or reversely, is possible.

Investigation of statistical relationship between any random variables is realized by means of statistical ordered series or appropriate regression equations which make it possible to determine whether a correlation takes place between the mentioned loads and - if it does - whether it is positive or negative. In practice particular realizations of self-ignition engine loads are observed. In the case if realizations of load for a given time instant  $t$  differ only a little, i.e. if its particular values for a given time instant  $t$  constitute (for increasing  $n$ , i.e. number of load measurements) the series of random variables  $Q_n$  ( $n = 1, 2, \dots$ ), then the series is stochastically convergent to zero under the following condition, [1, 10]:

$$\lim_{n \rightarrow \infty} P\{|Q_n| > \varepsilon\} = 0 \quad (22)$$

for an arbitrary number  $\varepsilon > 0$ .

The above is equivalent to the statistical convergence of the series of random variables  $\{Q_n\}$  toward the constant value  $q \neq 0$ , hence – to the statistical convergence of the random variables  $\{Q_n - q\}$  toward zero, that can be expressed as follows [1, 10]:

$$\lim_{n \rightarrow \infty} P\{|Q_n - q| > \varepsilon\} = 0 \quad (23)$$

or

$$\lim_{n \rightarrow \infty}^{(st)} Q_n = q \quad (24)$$

The relation (24) makes it possible to consider loads as a deterministic process, i.e. that statistical having prediction error equal to zero. In such process the past fully determines the future. The simplification consisting in the assumption that “the loading constitutes a deterministic process” is commonly applied in investigating the engine loads. However it makes load assessment to be fully adequate to reality both as regards to its features, especially to be capable of rational forming its run, i.e. its rational steering, and - if possible - its optimal control, difficult.

Comparing the loads occurring in successive cycles (number of cycles  $n \geq 4$ ), hence within the time interval  $t_d$  (short), one can state that they are different. The differences are increasing along with increasing  $n$ , i.e. when considering the load within the time interval  $t_q$  (long). For this reason

different load values are obtained at a determined value of the time interval  $t_d$  and during investigation of the load in particular cycles at the instants  $t_{d1}, t_{d2}, \dots$ . The fact of obtaining a given (expected) load value is a random event. This is such event because as a result of determination of the same empirical conditions the expected load value can occur, but it can also not occur. It means that a random variable can be attributed to every instant  $t_d$ . Similarly, to every instant  $t_q$  a relevant random variable can be attributed.

From the above presented considerations it results that the following hypothesis  $H_4$  can be formulated: „*The loading is a process of asymptotically independent increments because along with increasing partition between the time intervals within which the load is investigated (load measurements are made) its values are less and less mutually dependent*”.

Another feature which characterizes load changes consists in that observed load values do not show any monotonic changes both in the dynamic time ( $t_d$ ), i.e. that necessary to realize one engine cycle and in the quasi-static time ( $t_q$ ) in which the engine delivers power to a consumer, e.g. screw propeller. Hence it can be assumed that peak values of the quantities which characterize the loading, appear at random. Therefore to unambiguously (precisely) predict an instant of its occurrence, is not possible. The lack of monotony feature of engine load changeability makes it possible to formulate the hypothesis  $H_5$  as follows: „*The loading is a stationary process because in a longer time the monotony feature of engine load changes is lacking*”.

The load stationarity (in a broader sense) means that in each case all multi-dimensional probability density functions depend only on the mutual distance of the instants  $\tau_1, \tau_2, \dots, \tau_n$ , and do not depend on themselves [2, 5, 12, 14]. Hence one-dimensional probability density function of load values does not depend on the instant which the value corresponds with, and two-dimensional one depends only on difference of the instants in which observed load values have appeared. And, in a narrower sense, the stationary loading (fully stationary) is understood as that whose all statistical moments of higher orders as well as total moments of the loading (considered as a process) does not depend on time. In the case of the stationary process (in a narrower sense) the expected value  $m(t)$ , variance  $V(t)$ , auto-correlation  $A(\tau_1, \tau_2)$  and auto-covariance  $K(\tau_1, \tau_2)$  do not change. And, the stationary process in a broader sense is characterized by that  $m(t) = m = \text{const}$  as well as  $A(\tau_1, \tau_2) = A^*(\tau_2 - \tau_1) = A^*(r)$ . In practice, the stationarity of the loading in a broader sense is of importance.

To confirm the presented features of the stochastic process which the engine loading constitutes, it is necessary to perform relevant empirical investigations. From the tests of self-ignition engines, have been carried out so far, it results that their loading is changing continuously so that its particular values measured after passing very short time intervals, are strongly correlated to each other. However, if the time partition between measurements increases, correlation between the loads decreases. Hence the loading values measured within time intervals (or instants) very distant from each other, can be assumed independent. The feature is called the asymptotic independence of the load value measured e.g. in the instant  $\tau_{i+1}$  and the value measured in the instant  $\tau_i$  i.e. when the partition (time distance)  $\Delta\tau = \tau_{i+1} - \tau_i$  is sufficiently long. The so considered asymptotic independence between load values measured or calculated in the instants  $\tau_i$  and  $\tau_{i+1}$  illustrates the fact that along with increasing  $\Delta\tau$  dependence between them is decreasing. And, from the self-ignition engine work principle results also that within a longer time of its correct operation there is no (and can not be) monotonously increasing or

decreasing changes. Hence it can be assumed that maximum load values appear at random in determined instants, therefore they can be predicted only with a certain probability. This lack of monotony feature is called the load stationarity.

Therefore it can be assumed that verification of the presented hypothesis can be performed by checking the following consequences which result from it:

- $K_1: m_1(t) = m_1 = \text{const}$
- $K_2: A(t_1, t_2) = A^*(t_2 - t_1) = A^*(\Delta t)$

To verify the hypothesis in question the reductive reasoning in accordance with Eq. (18) can be used.

Hence the hypothesis  $H_6$  of the following content can be formed: „The loading of every engine is an ergodic process because the loading values do not depend on its initial state”.

The hypothesis is of practical importance as it implies that the loading can be considered to be a stochastic process in which observation probability of the value  $q(t)$  belonging to the strictly determined set  $A \subset R$ , can be estimated by means of the mean time of presence of each of its realizations in the set at a long time of observation (measurements). This hypothesis - together with the preceding one - explains why vibro-acoustic diagnostics of machines in which vibro-acoustic signal is assumed stationary and ergodic, is useful in practice. As results from the just presented hypotheses, this is an obvious assumption as the loading (cause) generates vibro-acoustic signal (consequence).

The statement whether the loading (taken as a stationary process) is ergodic, consists in comparing its statistical characteristics (expected value, auto-correlation, variance etc) achieved as a result of averaging the realization set  $\{q_k(t)\}$ , with the statistical characteristics obtained as a result of averaging a single, sufficiently long realization of the loading.

As results from the hypotheses (from the 3<sup>rd</sup> to the 5<sup>th</sup>, inclusive), the loading investigated in the instants very distant from each other, can be considered a purely random process, i.e. such stochastic process in which all the random variables  $q_k(t \in R_+)$ , in the discrete time  $(t_d)$ , are mutually independent.

The presented opinion on engine load features may lead to new possibilities in empirical determining wear- to- load relationships. Probabilistic approach to engine load is presented in some publications, e.g. [2, 4, 12], where it has been assumed that load realization is normal process and its values are random variables following the Moivre – Gauss distribution.

## FINAL REMARKS AND CONCLUSIONS

○ In the presented analysis and synthesis of events it was demonstrated that the loading of every self-ignition engine considered in a given instant of its time of operation (work), can be taken as a multi-dimensional random variable. The loading analyzed in successive instants of operational time of such engines can be considered to be realizations of the loading process. Hence the loading process of every engine should be investigated under assumption that it is a multi-dimensional stochastic process. The hypotheses have been proposed why it is possible to assume that the loading process of any self-ignition engine can be taken as a stochastic process of asymptotically independent increments, and stationary and ergodic one, as well as that there is stochastic independence between its mechanical and thermal loads. Intensity of the stochastic relationship can be stated by using the Czuprow's test of convergence [10] during investigations.

- For verification of the presented hypotheses the method of non-deductive (inductive) reasoning called the reductive reasoning, as well as the deductive reasoning method called the „modus tollens” rule, have been proposed.
- To recognize features of the processes it is necessary to form relevant mathematical models by using the system modeling and by performing suitable empirical investigations.
- From the preliminary considerations it results that the loading processes of combustion engines are the processes whose features can be analyzed by applying the theories of decision (controlled) semi-Markov processes [4, 5].

## BIBLIOGRAPHY

1. Firkowicz S.: *Statistical assessment of quality and reliability of electronic lamps* (in Polish). Scientific Technical Publishers (WNT), Warszawa 1963
2. Gercbach I.B., Kordonski Ch.B.: *Reliability models of technical objects* (in Polish). Scientific Technical Publishers (WNT), Warszawa 1968
3. Girtler J.: *Control of the operation process of ship combustion engines on the basis of diagnostic decision making model* (in Polish). Scientific Bulletins of AMW, no. 100A, Gdynia 1989
4. Girtler J.: *Stochastic model of load spectrum of self-ignition engine* (in Polish). Problems of Operation of Machines (Zagadnienia Eksploatacji Maszyn). Quarterly of Polish Academy of Sciences (Kwartalnik PAN), no. 1/97, 1994
5. Girtler J.: *Physical aspects of application and usefulness of semi-Markov processes for modeling the processes occurring in operational phase of technical objects*. Polish Maritime Research, Vol. 11, No 3, September 2004
6. Grabski F.: *Theory of semi-Markov operational processes of technical objects* (in Polish). Scientific Bulletins of AMW (Zeszyty Naukowe AMW), no. 75A, Gdynia 1982
7. Gurbin I.B., Syrkin P.E.: *Ekspluatatsionnaya nadezhnost' avtomobilnykh dvigatelej* (in Russian). Moscow, Transport 1984
8. Karpov L.N.: *Nadezhnost' i kaczestwo sudovych dizelej* (in Russian). Moscow, Transport 1985
9. Kozłowiecki H.: *Bearings of piston combustion engines* (in Polish). Warszawa, Telecommunication and Transport Publishers (WKiŁ) 1982
10. Krzysztofiak M., Urbaneck D.: *Statistical methods* (in Polish). Polish Scientific Publishers (PWN), Warszawa 1979
11. Leszek W.: *Empirical investigations* (in Polish). ITE, Radom 1997
12. Niewczas A.: *Foundations of stochastic model of frictional wear in durability problems of machine elements* (in Polish). Scientific Bulletins (Zeszyty Naukowe), Mechanics (Mechanika) no. 19, Radom University of Technology (Politechnika Radomska), 1989
13. Pabis S.: *Methodology and methods of empirical sciences* (in Polish). Polish Scientific Publishers (PWN), Warszawa 1985
14. Rozanov Ju.A.: *Stacionarnyje sluchajnye processy* (in Russian). Fizmatgiz, Moscow 1963
15. Spiridonov Ju.N., Rukavišnikov N.F.: *Remont sudovych dizelej* (in Russian). Transport, Moscow 1989
16. Wajand J.A.: *Self-ignition engines* (in Polish). Scientific Technical Publishers (WNT), Warszawa 1980
17. Włodarski J.K.: *Piston combustion engines. Tribological Processes* (in Polish). Telecommunication and Transport Publishers (WKiŁ), Warszawa 1981
18. Voinov A.N.: *Sgoranie v bystrochodnykh poršnevnykh dvigateljach* (in Russian). Mašinostroenie, Moscow 1977.

## CONTACT WITH THE AUTHOR

Jerzy Girtler, Prof., D.Sc.  
 Faculty of Ocean Engineering  
 and Ship Technology  
 Gdansk University of Technology  
 Narutowicza 11/12  
 80-952 Gdansk, POLAND  
 e-mail : jgirtl@pg.gda.pl

# A discrete model of the plate heat exchanger

Andrzej Mielewczyk, Ph.D.  
 Gdynia Maritime University

## ABSTRACT



*Developing numerical control methods requires precise models of technical machines. The article presents a discrete model of a plate heat exchanger. The model was worked out based on differential equations to secure high accuracy. Correctness of the model was verified using the data for the M10 – MFM cooler produced by Alfa-Laval.*

**Keywords:** simulation, dynamic model, Z transform, plate cooler, ship facilities

## INTRODUCTION

Heat exchangers are used in all types of power plants for heating or cooling the working medium having the liquid or gaseous form. The operation of heat exchangers is crucial for keeping accurate temperature of the process.

In marine power plants three-step main engine cooling systems have been introduced, which increased the number of coolers and control systems. Plate heat exchangers are in common use here. Moreover, the plate construction is also used in the designs of condensers, evaporators, and fuel heaters.

Marine power plant simulators require fast algorithms simulating the operation of plate heat exchangers to determine new control points for numerous installations. At the same time, the simulation is expected to model properly static and dynamic properties of the heat transfer process [7, 13, 15].

The principles applicable when working out the simulation algorithm have been formulated in [10]. The there presented procedure is used for working out equations for the fresh water/sea water heat exchanger model.

## MODEL OF THE PLATE HEAT EXCHANGER

The plate heat exchanger consists of plates arranged parallel to each other, between which the first and second working medium flows alternately. The heat transfer process is repeated between successive plates. Each plate takes the working medium from the main collector and generates repeatable heat transfer conditions, including constant medium flow velocity and heat transfer conditions represented by the overall heat transfer coefficient. In order to develop a mathematical model of

the plate heat exchanger, a two-plate system with co-current or counter-current flow is to be analysed, Fig. 1. When modelling the heat transfer, the following simplifying assumptions were adopted [2, 3, 4, 12, 14]:

- ☆ physical parameters of the working media do not depend on temperature within the range of temperature changes taking place in the exchanger,
- ☆ the averaged profile of the working medium flow velocity is characteristic for the plug flow (turbulent flow),
- ☆ temperature gradients in y and z directions are equal to zero,
- ☆ thermal capacity of the plate membrane is neglected due to its small thickness ( $g = 0.4 \text{ mm}$ ).

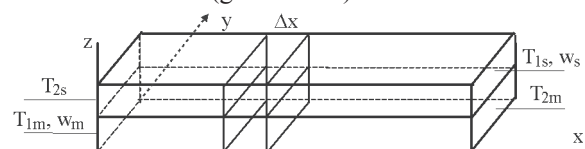


Fig. 1. Scheme of the plate heat exchanger segment for the counter-current flow

Taking into account the above assumptions we can write the energy balance for an element having length  $\Delta x$  [11, 13]. The heat transfer process in the plate heat exchanger is described by a system of differential equations (1) and (2):

$$\begin{cases} \frac{\partial T_s(x, \tau)}{\partial \tau} + w_s \frac{\partial T_s(x, \tau)}{\partial x} = -a [T_s(x, \tau) - T_m(x, \tau)] & (1) \\ \frac{\partial T_m(x, \tau)}{\partial \tau} + w_m \frac{\partial T_m(x, \tau)}{\partial x} = b [T_s(x, \tau) - T_m(x, \tau)] & (2) \end{cases}$$

where:

$$a = \frac{2k}{z c_s \rho_s} \quad (3)$$

$$b = \frac{2k}{z c_m \rho_m} \quad (4)$$

The basic variable is the temperature of the liquid  $T_s$  and  $T_m$  with respect to plate length  $x$  and time  $\tau$ . The system of equations (1) and (2) was solved using the  $Z$  transform, and its solution was:

$$\left\{ \begin{array}{l} \bar{T}_s(x, z) \left( a + \frac{z-1}{T} \right) + w_s \frac{d\bar{T}_s(x, z)}{dx} - \frac{z}{T} \bar{T}_s(x, 0) = a \cdot T_m(x, z) \end{array} \right. \quad (5)$$

$$\left\{ \begin{array}{l} \bar{T}_m(x, z) \left( b + \frac{z-1}{T} \right) + w_m \frac{d\bar{T}_m(x, z)}{dx} - \frac{z}{T} \bar{T}_m(x, 0) = b \cdot \bar{T}_s(x, z) \end{array} \right. \quad (6)$$

The process is nonlinear due to the flow velocity  $w$  and heat transfer conditions  $k$ . However, their changes are slower than temperature changes in a given discretisation step, and are assumed constant in a single iteration step. This way we arrive at a system of first-order differential equations (5) and (6) with constant coefficients.

To solve the system of equations (5) and (6) we assume a constant non-zero value of the temperature along plate length in time  $\tau = 0$ :

$$T_s(x, 0) = T_{s0}(x) = \text{const} \quad T_m(x, 0) = T_{m0}(x) = \text{const} \quad (7)$$

The general solution of the system of equations (5) and (6) for non-zero initial conditions (7) is a composition of functions:

$$\left\{ \begin{array}{l} \bar{T}_s(x, z) = Ae^{r_1 x} + Be^{r_2 x} + \bar{T}_{ss}(x, z) \\ \bar{T}_m(x, z) = \left( 1 + \frac{z-1}{aT} + \frac{w_s}{a} r_1 \right) Ae^{r_1 x} + \left( 1 + \frac{z-1}{aT} + \frac{w_s}{a} r_2 \right) Be^{r_2 x} + \bar{T}_{mm}(x, z) \end{array} \right. \quad (8)$$

where:

$$r_1 = \alpha \left[ z + \beta - \sqrt{(z + \beta)^2 + \gamma} \right] - \frac{z-1}{Tw_s} x - \frac{a}{w_s} x \quad (10)$$

$$r_2 = -\alpha \left[ z + \beta - \sqrt{(z + \beta)^2 + \gamma} \right] - \frac{z-1}{Tw_m} x - \frac{b}{w_m} x \quad (11)$$

$$\bar{T}_{ss}(x, z) = \frac{z \frac{z-1}{T} + bz}{Tw_s w_m r_1 r_2} T_{s0} + \frac{az}{Tw_s w_m r_1 r_2} T_{m0} = \frac{z(z-1)T_{s0} + zT(bT_{s0} + aT_{m0})}{(z-1)^2 + (z-1)T(a+b)} \quad (12)$$

$$\bar{T}_{mm}(x, z) = \frac{bz}{Tw_s w_m r_1 r_2} T_{s0} + \frac{z \frac{z-1}{T} + az}{Tw_s w_m r_1 r_2} T_{m0} = \frac{z(z-1)T_{m0} + zT(bT_{s0} + aT_{m0})}{(z-1)^2 + (z-1)T(a+b)} \quad (13)$$

and

$$\alpha = \frac{w_m - w_s}{2Tw_m w_s} x \quad (14)$$

$$\beta = T \frac{aw_m - bw_s}{w_m - w_s} - 1 \quad (15)$$

$$\gamma = 4abT^2 \frac{w_m w_s}{(w_m - w_s)^2} \quad (16)$$

The complete solution will be obtained for known initial conditions. The most typical flow arrangement used in plate coolers bases on the counter-flow. The assumed initial conditions include a step temperature change at plate cooler inlet, recorded simultaneously on the cooled and cooling medium sides, Fig. 1:

$$\bar{T}_s(x = 1, z) = Ae^{r_1} + Be^{r_2} + \bar{T}_{ss}(1, z) = \bar{T}_{s1}(1, z) \quad (17)$$

$$\bar{T}_m(x = 0, z) = \left(1 + \frac{z-1}{aT} + \frac{w_s}{a}r_1\right)A + \left(1 + \frac{z-1}{aT} + \frac{w_s}{a}r_2\right)B + \bar{T}_{mm}(0, z) = \bar{T}_{m1}(0, z) \quad (18)$$

After calculating the integration constants A and B from equations (17) and (18), and placing them to the system of equations (8) and (9) we get the solution:

$$\begin{aligned} \bar{T}_{s2}(0, z) = & \left[ \bar{T}_{s1}(1, z) - \bar{T}_{ss}(1, z) \right] \frac{\left(1 + \frac{\gamma}{\left(z + \beta + \sqrt{(z + \beta)^2 + \gamma}\right)^2}\right) e^{-\alpha \left[z + \beta - \sqrt{(z + \beta)^2 + \gamma}\right]} e^{\frac{z-1}{T w_s}} e^{\frac{a}{w_s}}}{1 + \frac{\gamma}{\left(z + \beta + \sqrt{(z + \beta)^2 + \gamma}\right)^2} e^{-2\alpha \left[z + \beta - \sqrt{(z + \beta)^2 + \gamma}\right]} e^{\frac{(z-1)w_m - w_{s1}}{T w_m w_s}} e^{\frac{a w_m - b w_{s1}}{w_m w_s}}} + \\ & + \left[ \bar{T}_{m1}(0, z) - \bar{T}_{mm}(0, z) \right] \frac{2T a w_m}{(w_m - w_s)} \frac{z + \beta + \sqrt{(z + \beta)^2 + \gamma}}{1 + \frac{\gamma}{\left(z + \beta + \sqrt{(z + \beta)^2 + \gamma}\right)^2} e^{-2\alpha \left[z + \beta - \sqrt{(z + \beta)^2 + \gamma}\right]} e^{\frac{(z-1)w_m - w_{s1}}{T w_m w_s}} e^{\frac{a w_m - b w_{s1}}{w_m w_s}}} + \\ & + \bar{T}_{ss}(0, z) \\ & \text{---} \\ \bar{T}_{m2}(1, z) = & - \frac{1}{z + \beta + \sqrt{(z + \beta)^2 + \gamma}} + \frac{e^{-2\alpha \left[z + \beta - \sqrt{(z + \beta)^2 + \gamma}\right]} e^{\frac{(z-1)w_m - w_{s1}}{T w_m w_s}} e^{\frac{a w_m - b w_{s1}}{w_m w_s}}}{z + \beta + \sqrt{(z + \beta)^2 + \gamma}} + \\ = & \left[ \bar{T}_{s1}(1, z) - \bar{T}_{ss}(1, z) \right] \frac{2b T w_s}{(w_m - w_s)} \frac{z + \beta + \sqrt{(z + \beta)^2 + \gamma}}{1 + \frac{\gamma}{\left(z + \beta + \sqrt{(z + \beta)^2 + \gamma}\right)^2} e^{-2\alpha \left[z + \beta - \sqrt{(z + \beta)^2 + \gamma}\right]} e^{\frac{(z-1)w_m - w_{s1}}{T w_m w_s}} e^{\frac{a w_m - b w_{s1}}{w_m w_s}}} + \\ & + \left[ \bar{T}_{m1}(0, z) - \bar{T}_{mm}(0, z) \right] \frac{\left(1 + \frac{\gamma}{\left(z + \beta + \sqrt{(z + \beta)^2 + \gamma}\right)^2}\right) e^{-\alpha \left[z + \beta - \sqrt{(z + \beta)^2 + \gamma}\right]} e^{-\frac{z-1}{T w_m}} e^{-\frac{b}{w_m}}}{1 + \frac{\gamma}{\left(z + \beta + \sqrt{(z + \beta)^2 + \gamma}\right)^2} e^{-2\alpha \left[z + \beta - \sqrt{(z + \beta)^2 + \gamma}\right]} e^{\frac{(z-1)w_m - w_{s1}}{T w_m w_s}} e^{\frac{a w_m - b w_{s1}}{w_m w_s}}} + \\ & + \bar{T}_{mm}(1, z) \end{aligned} \quad (20)$$

The original form of functions  $T_{s2}$   $T_{m2}$  is obtained after applying the definition [6]:

$$f_n = \lim_{p \rightarrow 0} \frac{1}{n!} \frac{d^n F \left( z = \frac{1}{p} \right)}{dp^n} \quad (21)$$

$$F_a(z) = \frac{1}{z + \beta + \sqrt{(z + \beta)^2 + \gamma}}$$

$$f_a(nT) = 0, \sum_{m=0}^S (-1)^{n-1} (-1)^m \frac{(n-1)!}{2^{2m+1} m! (m+1)! (n-1-2m)!} \beta^{n-1-2m} \gamma^m$$
(22)

where:

$$S = \begin{cases} \frac{n-1}{2} & \text{for odd } n \\ \frac{n-2}{2} & \text{for even } n \end{cases}$$

$$F_b(z) = \frac{1}{z + \beta + \sqrt{(z + \beta)^2 + \gamma}} e^{-2\alpha [z + \beta - \sqrt{(z + \beta)^2 + \gamma}]}$$

$$f_b(nT) = 0, \sum_{k=0}^{n-1} \sum_{m=0}^S (-1)^{n-1} (-1)^k (-1)^m \frac{(k+1)(n-1)!}{2^{2m+1} k! m! (m+k+1)! (n-k-1-2m)!} \beta^{n-1-k-2m} \gamma^m (\alpha\gamma)^k$$
(23)

where:

$$S = \begin{cases} \frac{n-k-1}{2} & \text{for odd } n \text{ and even } k \text{ or even } n \text{ and odd } k \\ \frac{n-k-2}{2} & \text{for even } n \text{ and even } k \text{ or odd } n \text{ and odd } k \end{cases}$$

$$F_c(z) = \frac{\gamma}{\left(z + \beta + \sqrt{(z + \beta)^2 + \gamma}\right)^2} e^{-\alpha [z + \beta - \sqrt{(z + \beta)^2 + \gamma}]}$$

$$f_c(nT) = 0, \sum_{k=0}^{n-2} \sum_{m=0}^S (-1)^n (-1)^k (-1)^m \frac{(k+2)(n-1)!}{2^{2m+k+2} k! m! (m+k+2)! (n-k-2-2m)!} \beta^{n-2-k-2m} \gamma^{m+1} (\alpha\gamma)^k$$
(24)

$$S = \begin{cases} \frac{n-k-3}{2} & \text{for odd } n \text{ and even } k \text{ or even } n \text{ and odd } k \\ \frac{n-k-2}{2} & \text{for even } n \text{ and even } k \text{ or odd } n \text{ and odd } k \end{cases}$$

$$F_d(z) = \frac{\gamma}{\left(z + \beta + \sqrt{(z + \beta)^2 + \gamma}\right)^2} e^{-2\alpha [z + \beta - \sqrt{(z + \beta)^2 + \gamma}]}$$

$$f_d(nT) = 0, \sum_{k=0}^{n-2} \sum_{m=0}^S (-1)^n (-1)^k (-1)^m \frac{(k+2)(n-1)!}{2^{2m+2} k! m! (m+k+2)! (n-k-2-2m)!} \beta^{n-2-k-2m} \gamma^{m+1} (\alpha\gamma)^k$$
(25)

where:

$$S = \begin{cases} \frac{n-k-3}{2} & \text{for odd } n \text{ and even } k \text{ or even } n \text{ and odd } k \\ \frac{n-k-2}{2} & \text{for even } n \text{ and even } k \text{ or odd } n \text{ and odd } k \end{cases}$$

$$F_e(z) = e^{-\alpha [z + \beta - \sqrt{(z + \beta)^2 + \gamma}]}$$

$$f_e(nT) = 1, \sum_{k=0}^{n-1} \sum_{m=0}^S (-1)^n (-1)^k (-1)^m \frac{(n-1)!}{2^{2m+k+1} k! m! (m+k+1)! (n-k-1-2m)!} \beta^{n-1-k-2m} \gamma^m (\alpha\gamma)^{k+1}$$
(26)

where:

$$S = \begin{cases} \frac{n-k-1}{2} & \text{for odd } n \text{ and even } k \text{ or even } n \text{ and odd } k \\ \frac{n-k-2}{2} & \text{for even } n \text{ and even } k \text{ or odd } n \text{ and odd } k \end{cases}$$

After dividing numerically by series we arrive at the response in discrete time instants:

$$T_{m2}(l, nT) = \sum_n [T_{s1}(nT) - T_{ss}(l, nT)] \frac{2bT_w s}{(w_m - w_s)} \frac{f_b \left[ nT - \frac{l}{w_m} + \frac{l}{w_s} \right] e^{\frac{aw_m - bw_s}{w_m w_s}} - f_a(nT)}{1 + f_d \left[ nT - \frac{l}{w_m} + \frac{l}{w_s} \right] e^{\frac{aw_m - bw_s}{w_m w_s}}} +$$

$$+ \sum_n [T_{m1}(nT) - T_{mm}(0, nT)] \frac{f_e \left[ nT - \frac{l}{w_m} \right] e^{\frac{b}{w_m}} + f_c \left[ nT + \frac{l}{w_m} \right] e^{\frac{b}{w_m}}}{1 + f_d \left[ nT - \frac{l}{w_m} + \frac{l}{w_s} \right] e^{\frac{aw_m - bw_s}{w_m w_s}}} + T_{mm}(l, nT)$$

$$T_{s2}(0, nT) = \sum_n [T_{s1}(nT) - T_{ss}(l, nT)] \frac{f_e \left[ nT + \frac{l}{w_s} \right] e^{\frac{a}{w_s}} + f_c \left[ nT + \frac{l}{w_s} \right] e^{\frac{a}{w_s}}}{1 + f_d \left[ nT - \frac{l}{w_m} + \frac{l}{w_s} \right] e^{\frac{aw_m - bw_s}{w_m w_s}}} +$$

$$+ \sum_n [T_{m1}(nT) - T_{mm}(0, nT)] \frac{2Taw_m}{(w_m - w_s)} \frac{f_a(nT) - f_b \left[ nT - \frac{l}{w_m} + \frac{l}{w_s} \right] e^{\frac{aw_m - bw_s}{w_m w_s}}}{1 + f_d \left[ nT - \frac{l}{w_m} + \frac{l}{w_s} \right] e^{\frac{aw_m - bw_s}{w_m w_s}}} + T_{ss}(0, nT)$$

The excitation functions  $T_{s1}$  and  $T_{m1}$  can be arbitrary, but this requires the use of the function convolution operation. For the step excitation function, its response is the sum of terms of a given series. In case of another function, its approximation by a staircase function is recommended. Such approximation is used in numerical control algorithms.

The final solution includes all process variables and the time in a discrete form. In one discretisation step the process variables take constant values and can be only changed in the next discretisation step. Thus we reduce the model to a linear form. By modifying parameters in successive steps we arrive as a quasi-linear solution to a nonlinear system. If the parameters do not have to be changed, a series of consecutive process values is calculated.

Sample results of calculations performed using the above-described method are shown in Fig. 2.

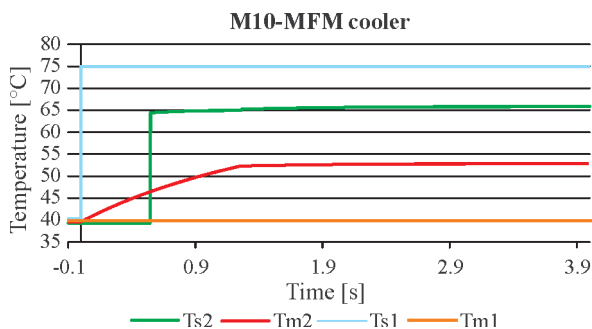


Fig. 20 Interval of the transformed function discretisation

The simulation of cooling plate operation made use of the following input data:

**M10 – MFM cooler**, type: fresh water - sea water

$l = 0.675$  m

$a = 0.75$  [1/s]

$w_s = 1.23$  [m/s]

$b = 0.74$  [1/s]

$w_m = 0.944$  [m/s]

The initial temperature distribution along the plate length:

$$T_{0s}(x) = 39.3^\circ\text{C} \quad T_{0m}(x) = 39.3^\circ\text{C}$$

The signal assumed at cooler input:

$$T_{1s}(\tau) = 75.0^\circ\text{C} \quad T_{1m}(\tau) = 39.3^\circ\text{C}$$

## CONCLUSIONS

The presented model of the plate heat exchanger reveals good agreement with the real results. It can be used in numerical simulations, depending on the available simulation time.

The performed cooler model analyses make the basis for formulating the following conclusions:

- The obtained static and dynamic characteristics are fully compatible within the entire range of loads taking place in operating practice.
- The model correctly reacts to changes of working medium flow velocities and other parameters.
- Detailed analysis of the simulated phenomena and processes is possible. It can refer to both the control processes, and diagnostics of the technical state of the examined cooler.
- Comparing counter-current and co-current flows produces better results, but makes the time in which the steady state is reached longer.

## NOMENCLATURE

- A, B – integration constants  
a, b – heat transfer constant for plate cooler cooled and cooling side, respectively [s<sup>-1</sup>]  
c – specific heat of the liquid [J/kgK]  
k – plate cooler heat transfer coefficient [W/m<sup>2</sup>K]  
l – plate length [m]  
ρ – liquid density [kg/m<sup>3</sup>]  
T<sub>m</sub> – sea water temperature in the plate cooler [K, °C]  
T<sub>s</sub> – fresh water temperature in the plate cooler [K, °C]  
T – interval of the transformed function discretisation [s],  

$$Z(f) = \bar{f}(z) = \sum_{n=0}^{\infty} f(nT)z^{-n}$$
  
τ – time [s]  
x – temperature distribution along plate length  
w<sub>m</sub> – sea water flow velocity [m/s]  
w<sub>s</sub> – fresh water flow velocity [m/s]  
z – distance between plates [m]

## Indices

- 0 – initial value,  
1 – input boundary value,  
2 – output boundary value,  
m – sea water, cooling medium  
s – fresh water, cooled medium

## BIBLIOGRAPHY

1. Douglas J. M.: *Dynamics and control of processes. Analysis of dynamic systems* (in Polish). WNT, Warsaw 1976
2. Friedly J. C.: *Analysis of process dynamics* (in Polish). WNT, Warsaw 1975
3. Gdula S.J.: *Heat transfer, collective work* (in Polish). PWN, Warsaw 1984

4. Hobler T.: *Heat flow and heat exchangers* (in Polish). WNT, Warsaw 1979
5. Kaćki E.: *Partial differential equations in problems of physics and technique* (in Polish). WNT, Warsaw 1992
6. Kudrewicz J.: *Z transform and difference equations* (in Polish). PWN, Warsaw 2000
7. Mielewicz A.: *A simulation model of the process of control of cooling and lubrication installations in a medium-speed combustion engine* (in Polish). Ph.D. thesis, Gdansk University of Technology, Faculty of Ocean Engineering and Ship Technology, Gdansk 1998
8. Mielewicz A.: *Computer simulation of control processes of ship power plant auxiliary systems*. Polish Maritime Research. No 3(25) September 2000 vol. 7
9. Mielewicz A.: *A simulation model of plate cooler*. Polish Maritime Research. No 3(29) September 2001 vol. 8
10. Mielewicz A.: *Numerical simulation of heat flow processes*. Polish Maritime Research. No 4(46) October 2005 vol. 12
11. Mikielewicz J.: *Modelling thermal and flow processes* (in Polish). PAS Institute of Fluid-Flow Machinery, Wrocław 1995
12. Petela R.: *Heat flow* (in Polish). PWN, Warszawa 1983
13. Piekarski M., Poniewski M.: *Dynamics and control of heat and mass transfer processes* (in Polish). WNT Warsaw 1994
14. Taler J., Duda P.: *Solving direct and inverse heat conduction problems* (in Polish). WNT, Warszawa 2003
15. Tarnowski W.: *Modelling of systems* (in Polish). Koszalin University of Technology, Koszalin 2004

## CONTACT WITH THE AUTHOR

Andrzej Mielewicz, 'Rj 0F0  
Department of Basic Engineering Sciences,  
Gdynia Maritime University  
Morska 81-87  
81-225 Gdynia, POLAND  
e-mail: miczyk@am.gdynia.pl

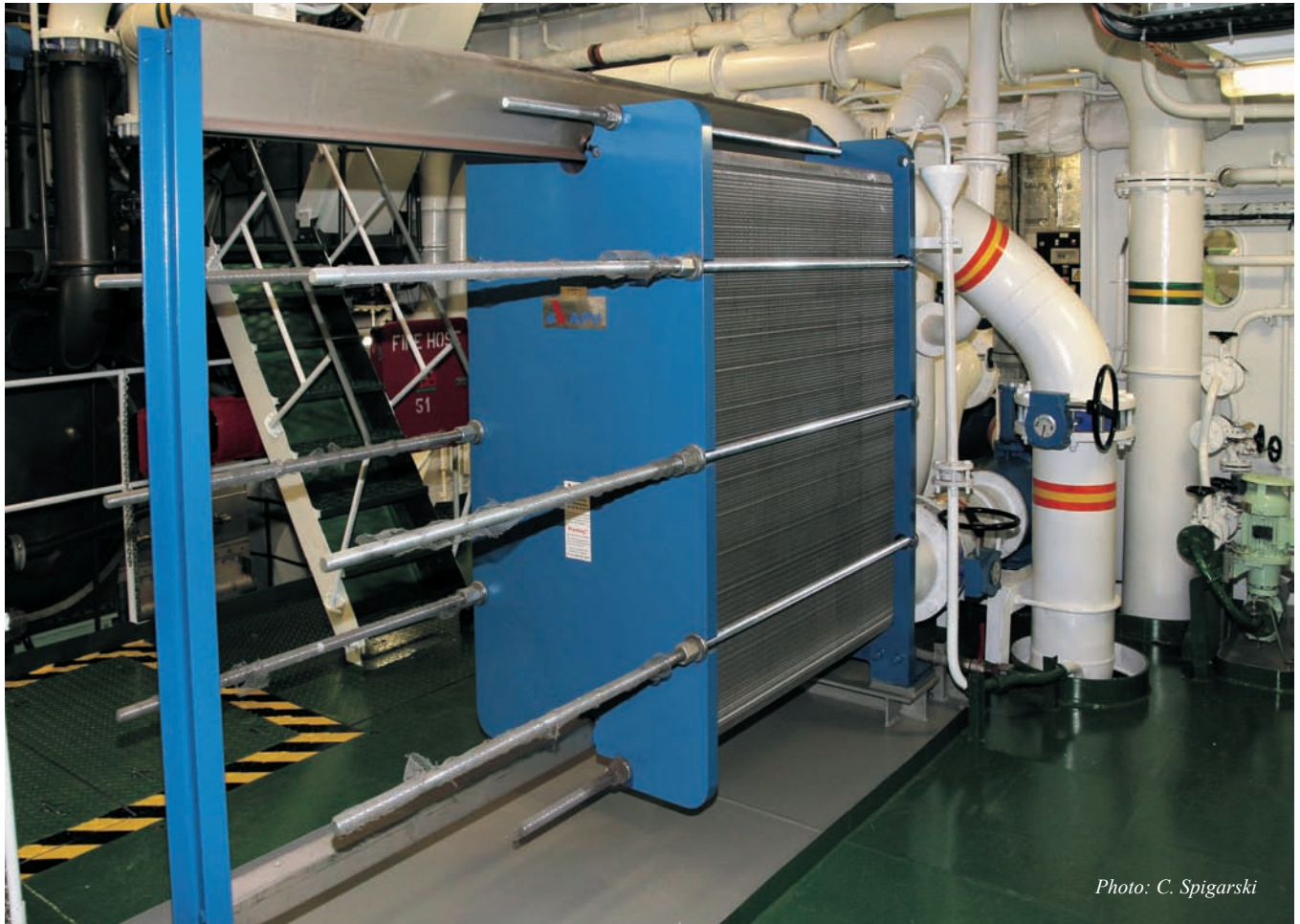


Photo: C. Spigarski

# Detection of ferromagnetic objects in local magnetic anomaly of the Daltic Uea

Mirosław Wołoszyn, Ph. D.  
Gdansk University of Technology

## ABSTRACT



*In geological researches several kinds of methods are applied to discovering the natural resources. Planes, helicopters and UAVs (Unmanned Vehicle) are used in researches in large areas. The gravity, electromagnetic and magnetic methods, which are used in geological researches, are presented in this paper. The special attention was paid to magnetic systems installed on mobile platforms. The magnetic field of the Earth obtained from mathematical model was compared to the real magnetic field in the selected part of the Baltic Sea. The results of the calculations showed that the mathematical model of the Earth's magnetic field does not consider local magnetic anomalies. The strong local magnetic anomalies cause serious problems with detection of underwater objects. Special problems appear in the magnetic system on a helicopter, which are presented in this paper.*

**Keywords:** geological researches, gravity, electromagnetic, magnetic methods

## INTRODUCTION

In geological researches several kinds of methods are applied to discovering the natural resources. Planes, helicopters and UAVs (Unmanned Vehicle) are used in researches in large areas. The gravity, electromagnetic and magnetic methods are applied to researches. In the gravity method the extremely small changes of the Earth's gravity are measured [1]. The sensitivity of contemporary gravimeters is less than 1 mGal ( $1 \text{ Gal} = 10^{-2} \text{ m/s}^2$ ). The gravimeters allow to measure the changes of the Earth's gravity on level close to  $10^{-6} \text{ g}$ . One of a few leading producers of extremely sensitive gravimeters is Gravimetric Technologies Ltd. a company in Moscow [2]. The GT-1A gravimeter installed on the Cessna 404 plane was shown in fig.1 [3].

Deposits of natural resources are discovered also by applying the electromagnetic method. The first electromagnetic systems appeared and were developed in Scandinavia, the USA and Canada in the 20s of XX century. The electromagnetic method is applied to measure the conductivity of the soil. The electromagnetic systems are installed on planes or helicopters. A big coil is towed by a helicopter or carried by a plane. The current impulse in the coil generates strong magnetic field (primary field), which penetrates layers of the Earth (fig. 2). The time-varying field produces eddy currents in the soil. After the switch off of the current in the coil they are only the eddy currents that produce the magnetic field (secondary



Fig. 1. The GT-1A gravimeter installed on Cessna 404 plane [12]

field). The time-varying secondary field produces emf voltage in the measure coil. The induced emf voltage depends on a conductivity of the soil. The analysis of the conductivity of the ground allows to detect natural resources.

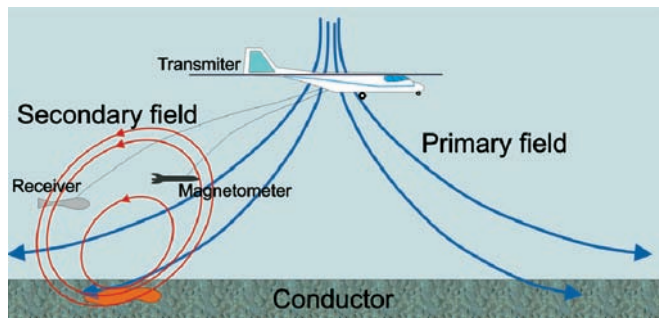


Fig. 2. The electromagnetic method

One of the biggest commercial companies (Fugro) has three electromagnetic systems for geological researches: GEOTEM (fig. 3), MEGATEM and TEMPEST. The biggest MEGATEM system is installed on Dash 7 plane and allows to discover the natural resources up to 300 m. The value of the magnetic moment generated by the system is  $2.2 \cdot 10^6 \text{ Am}^2$ .



Fig. 3. The GEOTEM electromagnetic system on the plane Casa 212 [4]

The magnetic method is also applied to geological researches. Homogeneity of the Earth's magnetic field is disturbed by different properties of the Earth's layers. This method is also applied to detection of ferromagnetic objects (UXO – Unexploded Objects, submarines, wrecks, landmines and marine mines). Each ferromagnetic object disturbs the homogeneity of the Earth's magnetic field (fig. 4). The measures of the magnetic field near the object allow to detect, to localize and to identify it [5].

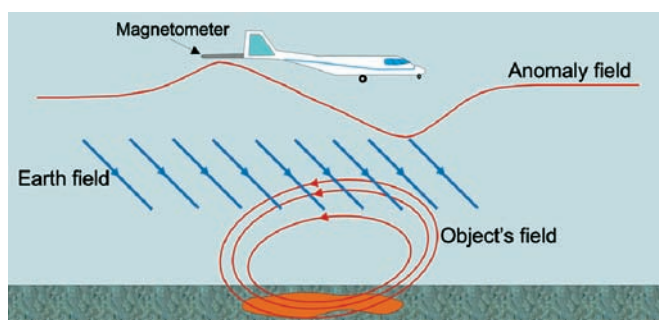


Fig. 4. The disturbance of the homogeneity of the Earth's magnetic field near the ferromagnetic object

The influence of the strong local magnetic anomaly on the magnetic measurements, with systems installed on planes and helicopters, was presented in this paper. The mathematical model of the Earth's magnetic field was described. The magnetic field based on the mathematical model was compared to the real magnetic field of the Baltic Sea. The calculations of the magnetic field were carried out in MathCad [6].

## EARTH MAGNETIC FIELD-MATHEMATICAL MODEL

The magnetic field of the Earth can be described by magnetic scalar potential if  $\mathbf{j} = 0$ :

$$\mathbf{H} = -\nabla\Psi \quad (1)$$

The magnetic flux density over the surface of the Earth is  $\mathbf{B} = \mu_0\mathbf{H}$ . So the equation:

$$\nabla\mathbf{B} = 0 \quad (2)$$

comes down to the form:

$$\nabla\mathbf{H} = 0 \quad (3)$$

On the basis of the equations (2) and (3) the magnetic scalar potential  $\Psi$  satisfies the Laplace's equation:

$$\nabla^2\Psi = 0 \quad (4)$$

The Laplace's equation in spherical coordinate system is:

$$\frac{1}{r^2} \frac{\partial}{\partial r} \left( r^2 \frac{\partial \Psi}{\partial r} \right) + \frac{1}{r^2 \sin \theta} \frac{\partial}{\partial \theta} \left( \sin \theta \frac{\partial \Psi}{\partial \theta} \right) + \frac{1}{r^2 \sin^2 \theta} \frac{\partial^2 \Psi}{\partial \phi^2} = 0 \quad (5)$$

The solution of the Laplace's equation (5) is [7]:

$$\Psi(r, \theta, \phi) = \sum_{l=0}^{\infty} \sum_{m=0}^l (A_{lm} r^l + B_{lm} r^{-(l+1)}) Y_l^m(\theta, \phi) \quad (6)$$

where:  $A_{lm}$  and  $B_{lm}$  – constants and

$$Y_l^m(\theta, \phi) = \left[ \frac{(2l+1)(l-m)!}{4\pi(l+m)!} \right]^{\frac{1}{2}} P_{l,m}(\cos \theta) e^{jm\phi} \quad (7)$$

where:  $P_{l,m}$  – Legendre polynomials [7].

Schmidt developed the formulae describing the magnetic scalar potential in 1939 [7]. These formulae allow to calculate the approximate value of the components of the magnetic flux density at any point of the Earth. The magnetic scalar potential of the Earth is:

$$\Psi(r, \theta, \phi) = \frac{a}{\mu_0} \sum_{l=1}^{\infty} \sum_{m=0}^l P_l^m(\cos \theta) (g_l^m \cos m\phi + h_l^m \sin m\phi) \quad (8)$$

where:  $P_l^m$  – partially normalized Schmidt's functions [7].

The Gauss' coefficients ( $g_l^m$  and  $h_l^m$ ) (8) are obtained by using many sets of observations of the components of the magnetic field at many points of the Earth. The components of the magnetic flux density of the Earth are (for  $\mathbf{1}_x = -\mathbf{1}_\theta$ ,  $\mathbf{1}_y = \mathbf{1}_\phi$ ,  $\mathbf{1}_z = -\mathbf{1}_r$ ):

$$B_{xe} = \frac{1}{r} \frac{\partial \Psi}{\partial \theta} \quad (9)$$

$$B_{ye} = -\frac{1}{r \sin \theta} \frac{\partial \Psi}{\partial \phi} \quad (10)$$

$$B_{ze} = \frac{\partial \Psi}{\partial r} \quad (11)$$

The modulus of the magnetic flux density in the Cartesian coordinate system is (fig. 5):

$$B_e = \sqrt{B_{xe}^2 + B_{ye}^2 + B_{ze}^2} \quad (12)$$

The magnetic inclination is:

$$I = \arctg\left(\frac{B_{ze}}{\sqrt{B_{xe}^2 + B_{ye}^2}}\right) \quad (13)$$

and declination:

$$D = \arctg\left(\frac{B_{ye}}{B_{xe}}\right) \quad (14)$$

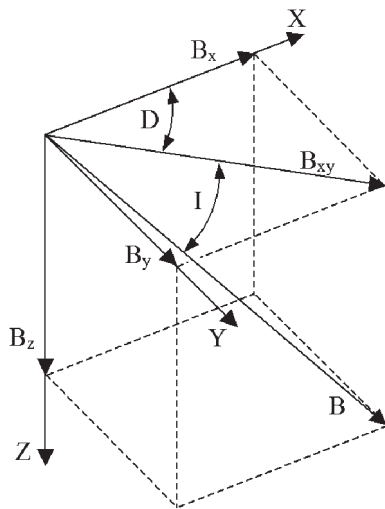


Fig. 5. The components of the Earth's magnetic field

The characteristic components of the Earth's magnetic field were calculated in MathCad for 4-th degree of Gauss coefficients ( $l = 4$ ). The isodynamic chart of the total magnetic flux density was shown in fig. 6. The isoclinic chart of the inclination in degrees was shown in fig. 7.

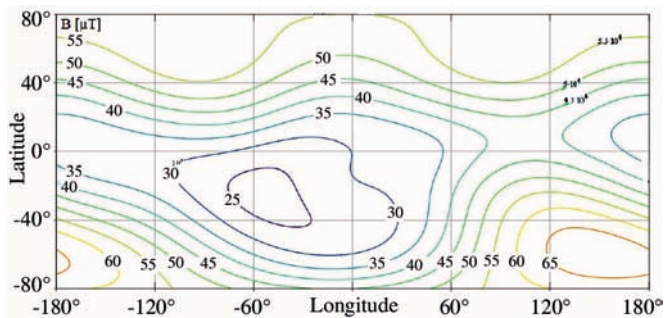


Fig. 6. The isodynamic chart of the total magnetic flux density

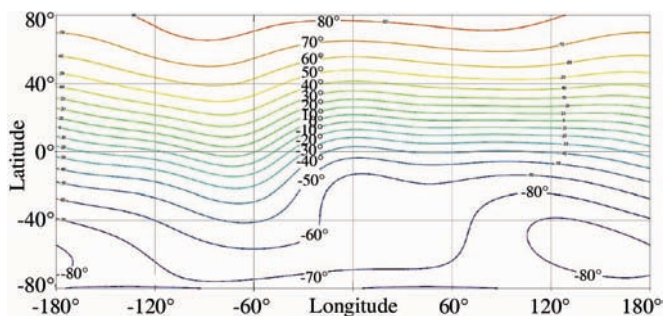


Fig. 7. The isoclinic chart of the inclination in degrees

The distribution of the Earth's magnetic field given by the mathematical model can be used for example in demagnetisation systems of war ships. This distribution has global character and

does not include local magnetic anomaly. It is the consequence of the limited number of observatories at which the components of the magnetic field are measured. The distributions of the local magnetic anomalies are different and depend on "geological history" of the Earth's layers. The most popular magnetic anomalies in the world occur in the surroundings of Kursk. The massive layers of rocks containing the iron ore cause these anomalies. The values of the anomalies are about 27 nT 350 km over the Earth's surface. The relatively strong local anomalies occur above the Baltic Sea. The distribution of the modulus of the magnetic flux density obtained from mathematical model (8-12) of the Baltic Sea area was shown in fig. 8. The distribution of the magnetic field is approximately linear. The real distribution of the magnetic field in the same area of the Baltic Sea was shown in fig. 9.

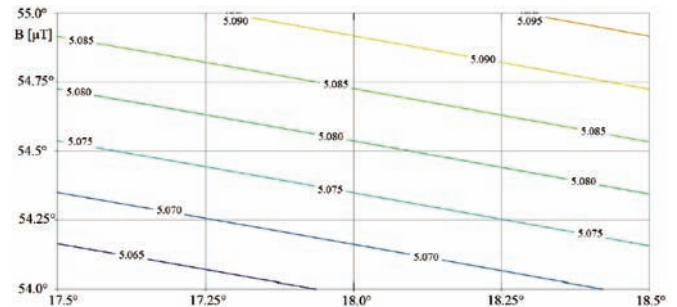


Fig. 8. The isodynamic chart of the total magnetic flux density of the Baltic Sea area

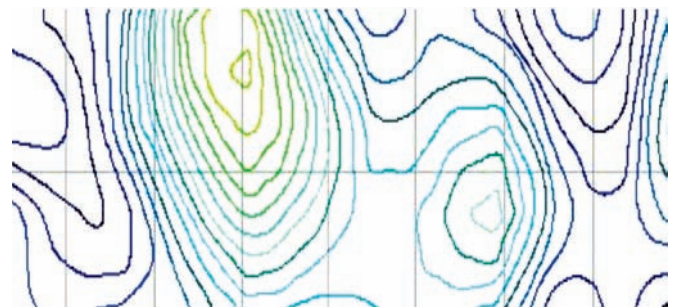


Fig. 9. The real isodynamic chart of the total magnetic flux density of the Baltic Sea area (the same area as in fig.8)

The variations of the magnetic field over the surface of the Baltic Sea are about  $2 \mu\text{T}$  an area of several square kilometres. Such strong anomalies make serious problem in detection of ferromagnetic objects.

## MAGNETOMETERS

The scalar magnetometers are used mainly in geological researches and military magnetic systems. The contemporary optically pumped magnetometers are of high sensitivity  $10^{-12}$  T [8] (fig. 10). The SQUID vector magnetometers of the highest sensitivity (about  $10^{-14}$  T) are also used [8, 9]. The magnetic field of the Earth is about  $5 \cdot 10^{-6}$  T (fig. 6). So, the sensitivity of the magnetometers is more than million fold less than the total magnetic field of the Earth. The magnetometers are installed on mobile platforms: planes, helicopters or UAV.

## MAGNETIC SYSTEMS ON AIR PLATFORMS

The magnetic system installed on a plane has one or a set of magnetometers. The system with one magnetometer measures the total magnetic field (fig.11).

On account of the natural magnetic variations (hundreds pT ÷ several nT) the second magnetometer on the ground is



Fig. 10. The optically pumped magnetometer G-822A of Geometrics Company [13]



Fig. 11. The military magnetic system with one magnetometer (the sensor is in the tail of the plane)

used as the reference magnetometer. The system with a set of magnetometers measures the difference of modulus of the magnetic field [fig.12].



Fig. 12. The magnetic system with a set of magnetometers (the sensors are installed in the tail of the plane and on wings) [14]

The magnetic system on the plane includes the digital compensator of magnetic disturbances [10, 11]. Each change of the position of the plane in respect of the vector of magnetic field of the Earth disturbs the magnetic field surrounding the

plane. These disturbances are caused by constant and induced magnetization of the ferromagnetic elements of the plane and eddy currents induced in the metallic elements of the plane. The mathematical model of the magnetic disturbances is used in the compensator [10]. The linear model is described by the equation:

$$H_T(t) = \sum_{i=1}^{18} k_i \cdot A_i(t) \quad (15)$$

where:

- $k_i$  – the constant factors of the model
- $A_i(t)$  – the functions depend on the position of the plane
- $t$  – time.

The values of the functions  $A_i(t)$  are calculated on the basis of the direction cosines and the derivatives of the direction cosines [10]. The direction and derivative cosines are measured by 3-axis fluxgate magnetometer. The factors  $k_i$  are connected with induced and constant magnetization of the ferromagnetic elements of the plane and with eddy currents. Every plane has some characteristic values of these factors. The digital compensator determines the factors  $k_i$  on the basis of measurements of the magnetic flux density executed in the uniform magnetic field of the Earth with forced banking of the plane (pitch, yaw, roll). The simple magnetic system on a plane consists of a scalar magnetometer, a fluxgate magnetometer and a computer (fig.13).

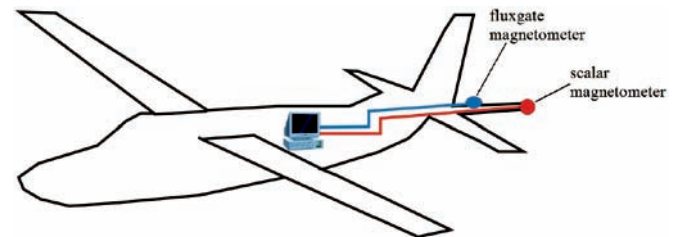


Fig. 13. The structure of the magnetic system on a plane

The example of the compensation of the magnetic disturbances of the plane was shown in fig.14. The magnetic system with a good compensator allows making measurements with sensitivity less than 100 pT.

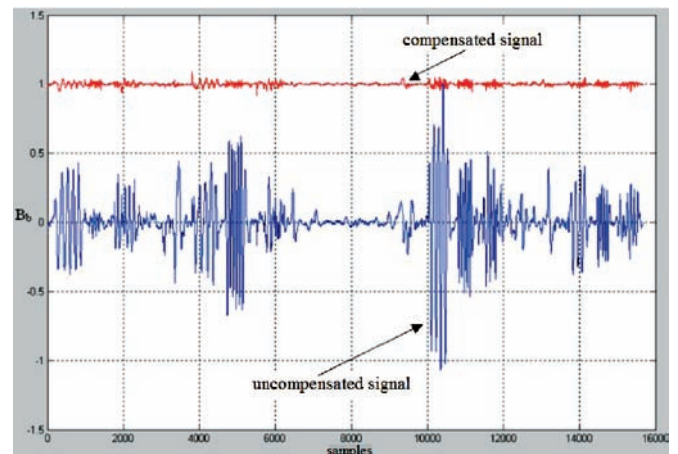


Fig. 14. The results of the compensation of the disturbances of the magnetic field

The first Polish navy aircraft with magnetic system was shown in fig.15.

This patrol-pathfinder navy plane An-28B1R Bis is used for instance in searching and tracking of submarines in the Baltic Sea. The systems installed on a helicopter do not need the

compensator, if the magnetic sensor is in the remote distance from the helicopter. The magnetic sensor is mainly inside the gondola, which is towed by the helicopter (fig.16).



Fig. 15. The Polish navy aircraft with magnetic system (photo by: Mariusz Adamski)



Fig. 16. The magnetic system on a helicopter with the magnetic sensor inside the gondola

The example of the Polish navy helicopter Mi-14Pl with magnetic system was shown in fig.17.



Fig. 17. The Polish navy helicopter Mi-14Pl with magnetic system (photo by: Mariusz Adamski)

## DETECTION OF OBJECTS IN LOCAL ANOMALY AREAS

The magnetic systems installed on planes or helicopters are used in geological researches and submarines or wrecks detection. The strong local magnetic anomalies cause serious problems in detection of small signals connected with ferromagnetic objects. A good example of a special area with

strong local anomalies is the Baltic Sea. The magnetic system should have a sophisticated detection algorithm. Particular problems occur in the system of a helicopter towing a gondola. The trajectory of the gondola's flight is not a straight line. The deviations from the straight line of the gondola occur during the flight. The deviations are bigger during bad meteorological conditions (for example big crosswind). The gondola moves approximately along the trajectory:

$$\begin{aligned} x(t) &= v_o t \cos(\alpha_k) - A \sin(2\pi f_o t) \sin(\alpha_k) \\ y(t) &= v_o t \sin(\alpha_k) + A \sin(2\pi f_o t) \cos(\alpha_k) \end{aligned} \quad (16)$$

where:

- $v_o$  – a constant velocity of a platform
- $A_y$  – amplitude of deviation
- $f_o$  – frequency of deviation of the gondola
- $\alpha_k$  – an angle between direction of a straight line trajectory and x axis.

The frequency of the gondola's deviation depends on the length of the cable, mass and aerodynamics parameters of the gondola and meteorological conditions. The result of the gondola's deviation is the interference signal in measurements of the magnetic flux density. The example of the local magnetic anomalies similar to real anomalies on the Baltic Sea was presented in fig. 18.

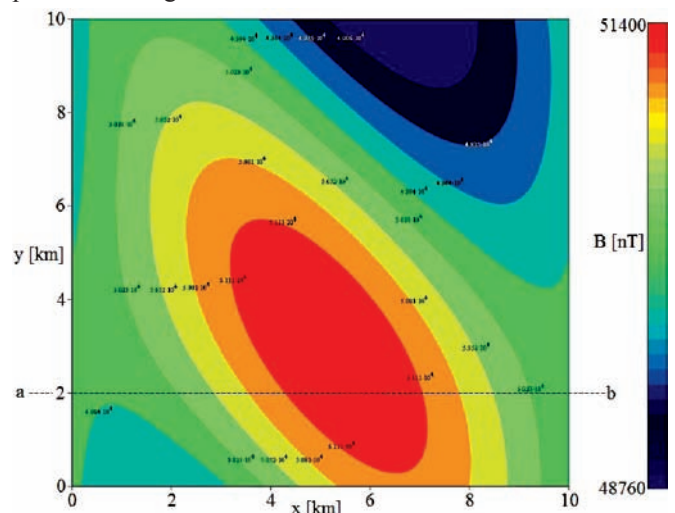


Fig. 18. The distribution of a local magnetic anomaly similar to real anomaly on the Baltic Sea

The interference signal  $\Delta B(t)$  appears in the measure signal with the frequency about  $f_o$  (fig.19):

$$\Delta B(t) = B_{xyk}(t) - B_{xyp}(t) \quad (17)$$

where:

- $B_{xyk}(t)$  – the changes of the magnetic flux density in time along a non-linear trajectory
- $B_{xyp}(t)$  – the changes of the magnetic flux density in time along a linear trajectory.

The amplitude and waveband of the interference signal depend on many factors such as:

- ❖ the distribution and values of the anomalies,
- ❖ the direction of the movements of the magnetic sensor,
- ❖ the mass of the gondola
- ❖ the length of the gondola's cable
- ❖ the meteorological conditions.

The values of these interferences could amount to several nT in extreme cases.

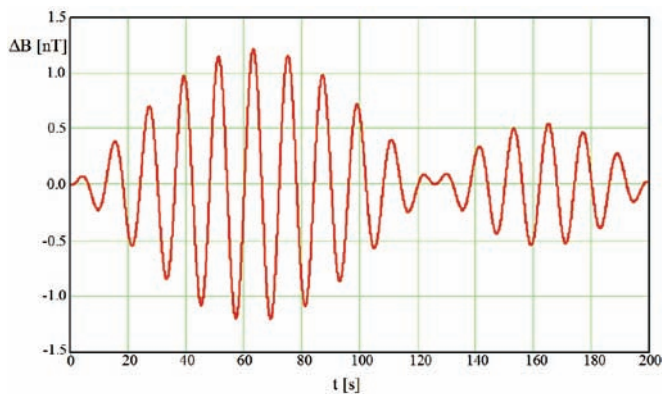


Fig. 19. The changes of the  $\Delta B(t)$  caused by the gondola's deviation  
 ( $A = 4 \text{ m}$ ,  $\alpha_s = 0^\circ$ ,  $v_o = 50 \text{ m/s}$ ,  $f_o = 0.1 \text{ Hz}$ )  
 along a linear trajectory a-b (fig.18)

## CONCLUSIONS

The measure methods, which are used in geological researches, are presented in this paper. The special attention was paid to magnetic systems installed on mobile platforms. The magnetic field of the Earth obtained from mathematical model was compared to the real magnetic field in the selected part of the Baltic Sea. The results of the calculations showed that the mathematical model of the Earth's magnetic field does not consider local magnetic anomalies. The strong local magnetic anomalies cause serious problems with detection of underwater objects. Special problems appear in the magnetic system on a helicopter. The interference signals appear in the measurements of the magnetic flux density when the sensor is towed in the gondola. These signals have to be compensated in order to avoid false detection signals.

## BIBLIOGRAPHY

1. Telford W.M., Geldart L.P., Sheriff R.E.: *Applied Geophysics*. Cambridge University Press, New York 1990

2. [www.canadianmicrogravity.com](http://www.canadianmicrogravity.com)
3. Gabell A., Tuckett H., Olson D.: *The GT-1A mobile gravity system*. Abstract from the ASEG-PESA Airborne Gravity 2004 Workshop, pp.55-62, Sydney 2004
4. [www.fugro.com](http://www.fugro.com)
5. McFee J.E., Das Yogadhish, Ellingson R.O.: *Locating and Identifying Compact Ferrous Objects*. IEEE Transactions on Geoscience and Remote Sensing, vol.28., no.2, pp.182-193, march 1990
6. MathCad 2000 User Guide, MathSoft Inc., 2000
7. Merrill R., McElhinny M., McFadden: *The magnetic field of the Earth*. International Geophysics Series. Volume 63. Academic Press. San Diego, California, USA, 1998
8. Ripka P.: *Magnetic sensors and magnetometers*. Artech House, Norwood 2001
9. Clem T.: *Superconducting magnetic sensors operating from a moving platform*. IEEE Trans. Appl. Supercond., Vol. 5(2), pp.2124-2148, 1995
10. Leliak P.: *Identification and Evaluation of Magnetic Field Sources of Magnetic Airborne Detector Equipped Aircraft*. IRE Trans. Aerospace and Navigational Electronics, vol. 8, September 1961, pp. 95-105
11. Wołoszyn M.: *Symulator kompensatora zakłóceń magnetycznych generowanych przez samolot*. Pomiary Automatyka Kontrola, grudzień 2004
12. [www.canadianmicrogravity.com](http://www.canadianmicrogravity.com)
13. [www.geometrics.com](http://www.geometrics.com)
14. [www.fugro.com](http://www.fugro.com)

---

## CONTACT WITH THE AUTHOR

Mirosław Wołoszyn  
 Gdansk University of Technology  
 Electrical and Control Engineering  
 G. Narutowicza 11/12  
 80-952 Gdańsk POLAND  
 email: [mwołosz@ely.pg.gda.pl](mailto:mwołosz@ely.pg.gda.pl)  
 phone: (+48) 58 347 24 35



Photo: C. Spigarski